A STRUCTURE-PRESERVING PARAMETRIC FINITE ELEMENT METHOD FOR ANISOTROPIC SURFACE DIFFUSION

LI YIFEI

(B.Sc., Peking University, China)

A THESIS SUBMITTED

FOR THE DEGREE OF DOCTOR OF PHILOSOPHY

DEPARTMENT OF MATHEMATICS

NATIONAL UNIVERSITY OF SINGAPORE

2023

Ph.D. Advisor:

Professor BAO Weizhu

Examiners:

Professor REN Weiqing

Professor CAI Zhenning

To my parents

DECLARATION

I hereby declare that the thesis is my original work and it has been written by me in its entirety. I have duly acknowledged all the sources of information which have been used in the thesis.

This thesis has also not been submitted for any degree in any university previously.

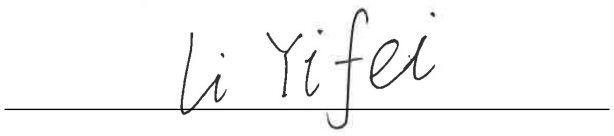

Li Yifei

August 5, 2023

Acknowledgements

First and foremost, I would like to express my deepest appreciation to my supervisor, Prof. Weizhu Bao, for his professional guidance, profound insights, and patient assistance throughout my PhD study. His generous support for both my mental and physical health is invaluable. Besides the direct help from Prof. Bao, he also set me a benchmark for what it means to be a successful and responsible mathematician through his daily behaviors! I am honored to have the opportunity to learn from him.

I am also grateful to my collaborators, Prof. Wei Jiang, Dr. Quan Zhao, Dr. Weijie Huang, Prof. Harald Garcke, Prof. Lifang Pei, and Prof. Meng Li. Their invaluable guidance, open discussions, and willingness to answer my questions have helped me grow as a researcher. Many thanks for the great experience to learn the importance of collaboration with other people.

I would like to extend my sincere thanks to my colleagues in our research group. The engaging mathematical discussions we've shared have greatly enriched my academic experience. I am also grateful for their assistance in various aspects of my life, making my academic life at NUS more enjoyable.

I would like to express my gratitude to my friends in Singapore, Mr. Zichen Zhao, Mr. Yurui Chen, and Mr. Kuangyu Ding, as well as my friends in China,

including Mr. Wuchuan Xu, Mr. Xinan Sun, Mr. Minghe Shi, Prof. Lin Lin, and Mr. Junfu Yao. Their companionship has brought color and joy to my daily life.

Last but not least, I owe a debt of gratitude to my family, my father Dongshuan Li and my mother Jian Li, for their unconditional love and support throughout my life. Although they know little about my research, their unwavering trust in me has been my source of strength and inspiration, and I dedicate this thesis to them.

Contents

Summary

Anisotropic surface diffusion is an important geometric flow that is widely applied in mathematics, physics, computer science, and solid-state materials science for studying interface evolution. It models the motion of atoms or molecules on a solid interface driven by the capillary effect that minimizes anisotropic surface energy while preserving enclosed mass. Nevertheless, anisotropic surface energy $\gamma(\boldsymbol{n})$ determined by the outward normal vector $\boldsymbol{n}$ can induce various instabilities during interface evolution. To comprehend and capture these instabilities, developing a numerical scheme that preserves mass conservation and energy dissipation at the discretized level is essential.

Among various numerical methods for anisotropic surface diffusion, the parametric finite element method (PFEM) achieves the best performance in terms of accuracy, efficiency, and mesh quality, while it can also preserve the two geometric properties of isotropic surface diffusion. The high performance of PFEM has enabled its application to an extensive range of geometric flows and free boundary problems, making its structure-preserving extension to anisotropic surface diffusion essential and highly demanded. However, the previously established state-of-the-art structure-preserving PFEM (SP-PFEM) is specially designed for the Riemannian metric anisotropy. Therefore, it is worthwhile to design a SP-PFEM for anisotropic

surface diffusion with general anisotropies.

This thesis aims to develop a SP-PFEM for anisotropic surface diffusion of curves in two dimensions (2D) with $d = 2$ and of surfaces in three dimensions (3D) with $d = 3$, incorporating a more general anisotropic surface energy function. The key concepts of the SP-PFEM developed here are the *surface energy matrix* $\boldsymbol{Z}_k(\boldsymbol{n})$ or $\boldsymbol{G}_k(\boldsymbol{n})$ and the *minimal stabilizing function* $k_0(\boldsymbol{n})$. The main contribution of this work is the introduction of a novel analytical framework that plays a vital role in establishing energy stability, which significantly contributes to the existing PFEMs. The thesis is composed of three parts.

In the first part, for *symmetric anisotropies* $\gamma(-\boldsymbol{n}) = \gamma(\boldsymbol{n})$, we propose a symmetrized SP-PFEM for anisotropic surface diffusion of curves in 2D based on the arclength parameterization. The new symmetrized SP-PFEM is proven to preserve mass conservation and unconditional energy dissipation at the discretized level. The energy stable condition only requires the regularity of the anisotropy to be at least $C^2(\mathbb{R}^2 \setminus \{\mathbf{0}\})$, which drastically relaxed the previously established state-of-the-art condition. Moreover, we introduce a new framework that reduces the proof of energy stability to the existence of the minimal stabilizing function $k_0(\boldsymbol{n})$. For several commonly-used symmetric anisotropies in 2D, the explicit formulations of $k_0(\boldsymbol{n})$ are also been analyzed. The symmetrized SP-PFEM is further extended to surfaces in 3D by replacing the arclength derivative with the surface gradient. The difference and the essential difficulty between 2D and 3D is proof of energy stability. Although our symmetrized SP-PFEMs are implicit methods, numerical experiments show that only 2 to 3 iterations are required at each time step. Extensive numerical results also show the second-order convergence rate in space, validate the structure-preserving analysis, illustrate the good mesh distribution, and match perfectly with the theoretical equilibrium.

In the second part, *for the general anisotropies with* $\gamma(-\boldsymbol{n}) \neq \gamma(\boldsymbol{n})$ we design a unified SP-PFEM for anisotropic surface diffusion of both curves in 2D and surfaces in 3D with a unified energy stable condition. The unified condition is much more

mild and general, which is not only naturally true for the symmetric anisotropy but also valid for almost arbitrary anisotropies. Therefore, the unified SP-PFEM can work for almost all the anisotropic surface energies used in applications. Moreover, we develop a unified framework for showing the existence of the minimal stabilizing function, that allows us to adopt dimensional-independent techniques to show the semi-positive definiteness of dimensional-dependent matrices instead of handling the dimensional-dependent inequalities. Numerical results indicate the unified SP-PFEM enjoys the same advantages compared to the symmetrized SP-PFEMs. It also works well for anisotropies with a weaker regularity condition as predicted, which is a significant achievement compared with other PFEMs.

In the last part, we apply the unified SP-PFEM for other geometric flows with the anisotropic effect, including the anisotropic curvature flow and the anisotropic mass-conserved curvature flow. The proposed SP-PFEM is proven to preserve unconditional energy dissipation for the two geometric flows. It can preserve volume conservation for anisotropic mass-conserved curvature flow with delicately designed parameters, and preserve volume decay rate for anisotropic curvature flow. Our numerical experiments show most of the desired properties of the unified SP-PFEM for anisotropic surface diffusion also hold when extended to other anisotropic geometric flows. Therefore, it suggests the newly proposed unified SP-PFEM may have broader applications to the interface/surface evolution problems.

List of Tables

List of Figures

List of Symbols and Abbreviations

d ($d = 2$ or 3)	dimension
$\mathbb{R}^d$	d dimensional Euclidean space
$\mathbb{R}^d_*$	$\mathbb{R}^d \setminus \{\mathbf{0}\}$
$\mathbb{S}^d$	d dimensional sphere
2D ($d = 2$)	two dimensions
3D ($d = 3$)	three dimensions
$\mathbb{R}_{\geq 0}$	non-negative number
t	time
$\Gamma := \Gamma(t)$	curve when $d = 2$ or surface when $d = 3$
$\boldsymbol{X}$	global parameterization of Γ
$\boldsymbol{\rho}$	point on Γ
$T_{\boldsymbol{\rho}}\Gamma$	tangent space of Γ at $\boldsymbol{\rho}$
$\{\boldsymbol{e}_1, \ldots, \boldsymbol{e}_{\boldsymbol{d-1}}\}$	orthonormal basis of tangent space $T_{\boldsymbol{\rho}}\Gamma$
$\boldsymbol{\tau}$	unit tangential vector for curves
$\boldsymbol{\tau}_1, \boldsymbol{\tau}_2$	orthonormal basis of $T_{\boldsymbol{\rho}}\Gamma$ of a surface
$\boldsymbol{n}$	outward unit normal vector of Γ at $\boldsymbol{\rho}$
V_n	normal velocity
$\gamma(\boldsymbol{n})$	anisotropic surface energy

$\gamma(\boldsymbol{p})$	one-homogeneous extension of $\gamma(\boldsymbol{n})$
θ	inclination angle between $\boldsymbol{n}$ and the y-axis in 2D
$\bar{\gamma}(\theta) = \gamma(-\sin\theta, \cos\theta)$	anisotropic surface energy in θ-formulation in 2D
$\tilde{\gamma} = \bar{\gamma}(\theta) + \bar{\gamma}''(\theta)$	surface stiffness
$\boldsymbol{\xi}$	Cahn-Hoffman ξ-vector
I_d	$d \times d$ identical matrix
s	arclength parameterization for curves
∂_s	arclength derivative for curves
$\boldsymbol{v}^T$ or $\boldsymbol{V}^T$	transpose of a vector $\boldsymbol{v}$ or a matrix $\boldsymbol{V}$
$\boldsymbol{v}^\perp = (v_2, -v_1)^T$	clockwise rotation by $\frac{\pi}{2}$ for $\boldsymbol{v} \in \mathbb{R}^2$
$\nabla_{\boldsymbol{e}}$	directional derivative with respect to $\boldsymbol{e}$
∇_Γ	surface gradient with respect to Γ
$\underline{D}_i$	i-th component of ∇_Γ
$\nabla_\Gamma \cdot$	surface divergence with respect to Γ
$\Delta_\Gamma = \nabla_\Gamma \cdot \nabla_\Gamma$	surface Laplace-Beltrami operator with respect to Γ
κ	curvature of a curve in 2D
$\mathcal{H}$	mean curvature of a surface in 3D
μ	chemical potential or weighted mean curvature
$W(\Gamma)$	total surface energy of Γ
$M(\Gamma)$	total mass of Γ (area for $d = 2$, volume for $d = 3$)
$\mathcal{F}$	Frank shape
$\mathcal{W}$	Wulff shape
$\boldsymbol{Z}_k(\boldsymbol{n})$	symmetrized surface energy matrix
$\boldsymbol{G}_k(\boldsymbol{n})$	surface energy matrix
$k(\boldsymbol{n})$	stabilizing function
$k_0(\boldsymbol{n})$	minimal stabilizing function
FEM	finite element method
PFEM	parametric finite element method
SP-PFEM	structure-preserving PFEM

ES-PFEM	energy-stable PFEM
ASD	anisotropic surface diffusion

Chapter 1

Introduction

In this chapter, we begin by discussing the motivation for studying surface diffusion. We then introduce the surface energy and the Cahn-Hoffman $\boldsymbol{\xi}$-vector to model the anisotropic effect. Subsequently, thermodynamic variation is employed to formulate the anisotropic surface diffusion. By utilizing an appropriate global parameterization, we derive the partial differential equation formulation for anisotropic surface diffusion. We then review the existing theoretical results and numerical methods. Finally, we conclude the chapter with a discussion of the scope of this thesis.

1.1 Surface diffusion

Surface diffusion is a fundamental phenomenon in various fields, especially in materials science, where it plays a critical role in understanding and simulating the evolution of interfaces in solid-state materials. In 1957, Mullins first introduced surface diffusion as a mathematical model to describe the motion of atoms or molecules on a solid interface driven by the capillary effect [43, 116, 127]. The capillary effect arises from the surface energy, which tends to minimize the total area of the surface but preserves the total mass enclosed by the surface [43, 55, 139]. These two geometric properties make surface diffusion broadly applied in physics [20, 68, 85, 129],

computer science [43, 55, 145], and materials science [93, 137, 142]; including fluid dynamics, image processing [47, 59, 119], crystal growth [92, 114, 143, 152], and solid-state dewetting [10, 142]. For example, Figure 1.1 shows the surface diffusion of solid thin film into isolated spherical islands. Here the sharp edges and facets are smoothing out, which leads to a more uniform equilibrium shape.

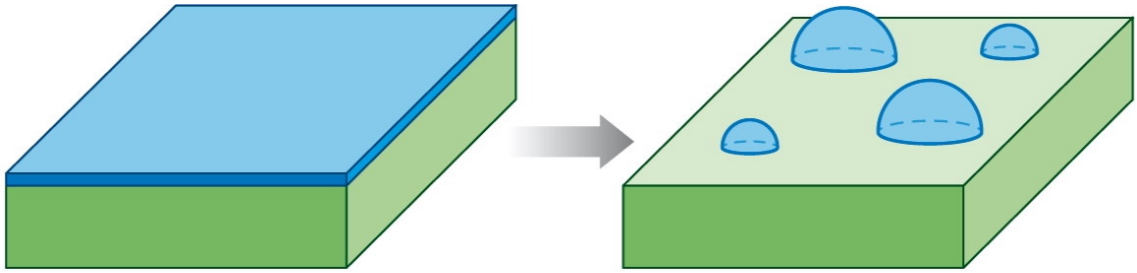

Figure 1.1: Surface diffusion of a solid thin film dewetting into isolated spherical islands. Image credit goes to [142].

Most of the solid-state materials have anisotropic properties, meaning that their surfaces exhibit directional variations in energy. Anisotropic surface diffusion takes into account the anisotropic properties of the surface, rendering the model more accurate and realistic. In fact, anisotropic surface diffusion has been known as important kinetics and mechanism in surface phase formation [34, 45, 82], epitaxial growth [68, 81, 85], heterogeneous catalysis [130], and many other areas in materials science [122, 137]. It has proven significant and broader applications in materials science, and computational geometry as well as solid-state physics, such as growth of nanomaterials [40], morphology development in alloys [45, 79], evolution of voids in microelectronic circuits [110], solid-state dewetting [93, 135, 142, 145, 150], deformation of images [47], and other areas.

However, anisotropic surface energy can lead to various instabilities during the evolution of the interfaces, such as the Rayleigh-Plateau instability [83, 123], fingering instability [99, 100, 120], faceting instability [51, 80, 86, 108, 151], corner instability [150], and pinch-off process [136, 152], which can be observed in figure 1.2.

Furthermore, these instabilities can occur simultaneously. For example, a combination of fingering instabilities and Rayleigh-Plateau instabilities can occur, where the growth of perturbation on a retracting edge creates the fingering shapes, and the cylindrical fingers break up to form small islands due to Rayleigh-Plateau instability, as illustrated in Figure 1.3. In order to accurately capture these instabilities and understand the underlying mechanisms that drive them, a reliable and accurate numerical scheme needs to preserve the geometric properties of anisotropic surface diffusion. As a result, developing a numerical scheme that preserves mass conservation and energy dissipation for anisotropic surface diffusion is important and highly necessary.

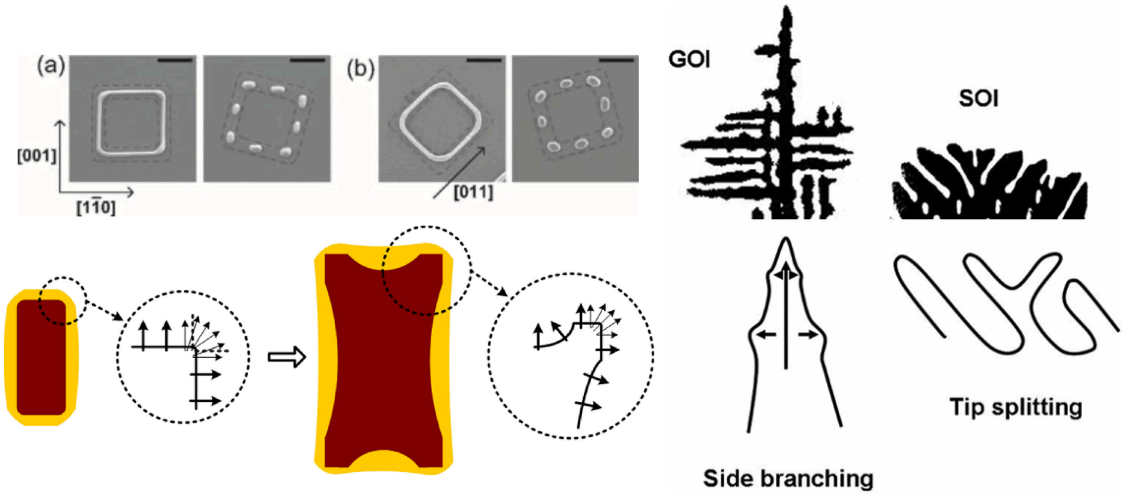

Figure 1.2: Illustration of various instabilities caused by anisotropic surface energy during the evolution of interfaces: pinch-off (top left, adapted from [152]), corner instability (bottom left, adapted from [150]), and faceting instability (right, adapted from [108]).

1.2 Surface energy and Cahn-Hoffman ξ-vector

The anisotropic effect of solid interface is typically governed by the anisotropic surface energy, which is conventionally denoted as γ. In fact, γ may depend on

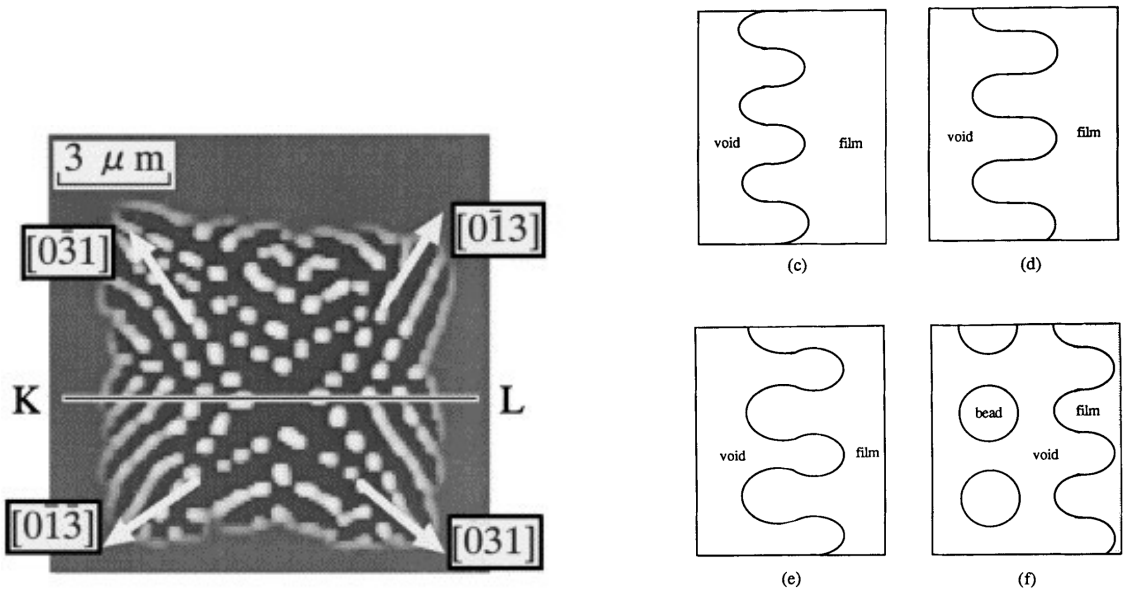

Figure 1.3: Illustration of the combination of fingering and Rayleigh-Plateau instabilities observed in a 7-nm-thick SOI surface after anisotropic surface diffusion (left, adapted from [120]). Schematic representation (right, adapted from [99]): (c)-(d) Growth of perturbation on a retracting edge leading to fingering shapes, and (e)-(f) cylindrical fingers breaking up to form small islands due to Rayleigh-Plateau instability.

factors such as temporature, interface inclination, position, and other factors [88, 124,131]. For simplicity, we only consider the case where $\gamma = \gamma(\boldsymbol{n}) > 0$, meaning γ is a positive function determined by the outward unit normal vector $\boldsymbol{n}$ of the interface Γ. If Γ is a curve in $\mathbb{R}^2$, the outward unit normal vector $\boldsymbol{n} \in \mathbb{S}^1$ is determined by the inclination angle θ between the y-axis, and we have the θ-formulation $\bar{\gamma}(\theta) = \gamma(-\sin\theta, \cos\theta)$; and if Γ is a surface in $\mathbb{R}^3$, $\boldsymbol{n} \in \mathbb{S}^2$. To unify the notation, we denote the dimension of the space as d, with the normal vector in $\mathbb{S}^{d-1}$. Additionally, we assume that $\gamma(\boldsymbol{n})$ is a continuous function with respect to $\boldsymbol{n}$, implying $\gamma(\boldsymbol{n}) \in C(\mathbb{S}^{d-1})$.

To improve the understanding of the behavior of different instabilities driven by the anisotropic effect, it is necessary to classify the anisotropic surface energy. When $\gamma(\boldsymbol{n})$ is uniform in all directions (e.g. $\gamma(\boldsymbol{n}) \equiv 1$) for $\boldsymbol{n} \in \mathbb{S}^{d-1}$, then the anisotropic surface energy collapses to the (isotropic) surface energy. In contrast, when $\gamma(\boldsymbol{n})$ is not a constant, i.e., with anisotropic surface energy: the classification for the anisotropy in θ-formulation in two dimensions (2D) can be given by checking the surface stiffness $\tilde{\gamma}(\theta) = \bar{\gamma}(\theta) + \bar{\gamma}''(\theta)$ [84, 117]. If the surface stiffness is greater than zero for all θ, such anisotropic surface energy is referred to *weakly anisotropic*. On the contrary, the *strongly anisotropic* surface energy gives a negative surface stiffness for some directions. In fact, the classification of the weak and strong anisotropies is rather important in the well-posedness of the anisotropic surface diffusion [3,46,134], the stability of the equilibrium [42, 83, 96], and the numerical analysis [10, 65, 145].

For the general anisotropy $\gamma(\boldsymbol{n})$, the classification can be visualized by the Frank diagram $\mathcal{F}$, which is given as [69]

$$\mathcal{F} := \{\boldsymbol{p} \in \mathbb{R}^d \Big| \gamma(\boldsymbol{p}) \leq 1\}. \tag{1.1}$$

For each direction $\boldsymbol{n} \in \mathbb{S}^{d-1}$, the radius of $\mathcal{F}$ is $\frac{1}{\gamma(\boldsymbol{n})}$, thus the Frank diagram is also called the $\frac{1}{\gamma}$-plot. Figure 1.4 & 1.5 show the Frank diagrams for different anisotropies for curves in 2D and surfaces in three dimensions (3D), respectively. It can be seen that the convexity of $\mathcal{F}$ depends on the anisotropic surface energy $\gamma(\boldsymbol{n})$. In fact, the *weakly anisotropic* surface energy gives a convex Frank diagram, and *strongly*

anisotropic surface energy gives a non-convex Frank diagram [144].

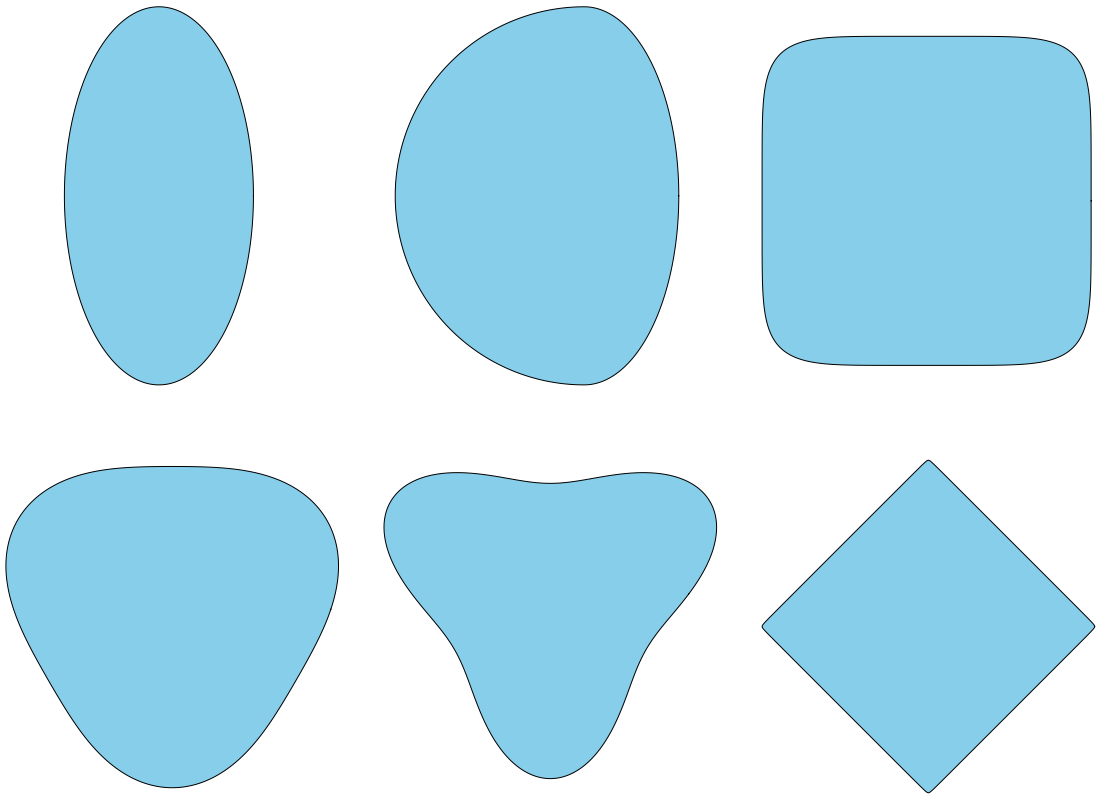

Figure 1.4: Frank diagrams in 2D for various anisotropic surface energies. Left to right, top to bottom: Riemannian metric anisotropy with $G = \mathrm{diag}(4, 1)$; piecewise Riemannian metric anisotropy with $a = \frac{5}{2}, b = \frac{3}{2}$; l^6-norm metric anisotropy; 3-fold anisotropy with $\beta = \frac{1}{9}$; 3-fold anisotropy with $\beta = \frac{1}{4}$; regularized l^1-norm metric anisotropy with $\varepsilon = 0.01$.

For testing the convexity of the Frank diagram $\mathcal{F}$ and further discussion, it is useful to examine the differentiability of the surface energy $\gamma(\boldsymbol{n})$. To achieve this, we consider its one-homogeneous extension $\gamma(\boldsymbol{p})$ defined throughout the whole space $\mathbb{R}^d$, which is given as [55, 97, 139]

$$\gamma(\boldsymbol{p}) := \begin{cases} |\boldsymbol{p}|\,\gamma\left(\frac{\boldsymbol{p}}{|\boldsymbol{p}|}\right), & \forall \boldsymbol{p} = (p_1, \ldots, p_d)^T \in \mathbb{R}^d_* := \mathbb{R}^d \setminus \{\boldsymbol{0}\}, \\ 0, & \boldsymbol{p} = \boldsymbol{0}, \end{cases} \tag{1.2}$$

where $|\boldsymbol{p}| = \sqrt{p_1^2 + \ldots + p_d^2}$.

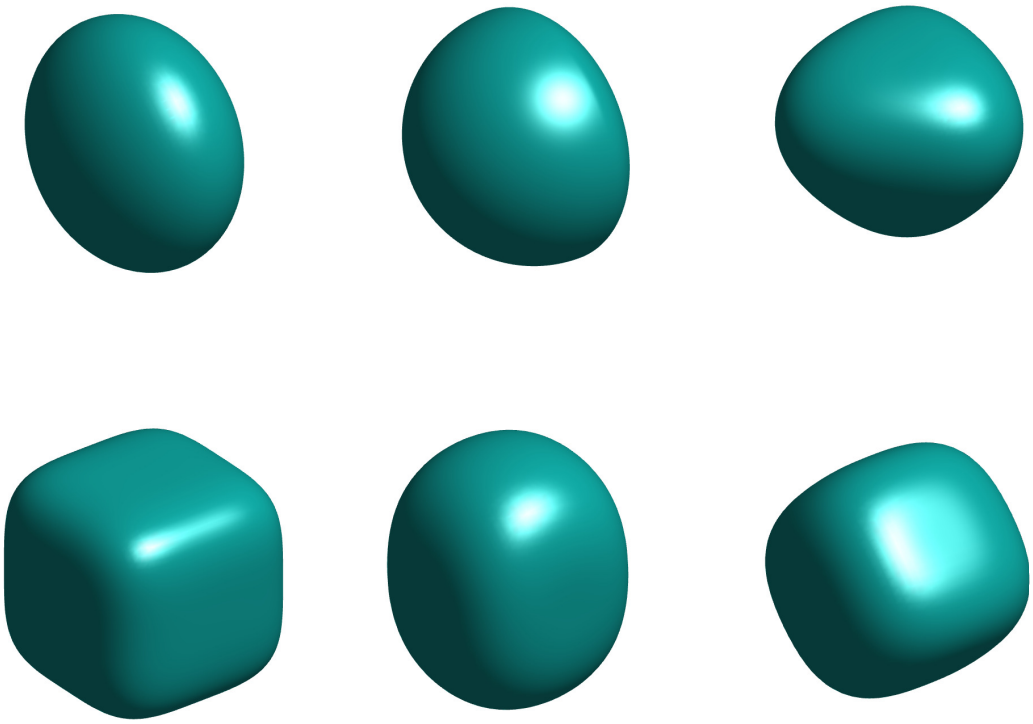

Figure 1.5: Frank diagrams in 3D for various anisotropic surface energies. Left to right, top to bottom: Riemannian metric anisotropy with $G = \mathrm{diag}(2, 1, 1)$; piecewise Riemannian metric anisotropy with $a = \frac{5}{2}, b = \frac{3}{2}$; 3-fold anisotropy with $\beta = \frac{1}{4}$; l^4-norm metric anisotropy; [001] orientation and the [011] orientation with $\beta = \frac{1}{3}$.

We observe that (1.2) establishes a one-to-one correspondence between $\gamma(\boldsymbol{n})$ and $\gamma(\boldsymbol{p})$. Thus it suffices to discuss the differentiability of $\gamma(\boldsymbol{p})$. Clearly, for $0 < \gamma(\boldsymbol{n})$, we have $\gamma(\boldsymbol{p}) \geq 0$. And for $\boldsymbol{p} \in \mathbb{R}^d_*$, the differentability of $\gamma(\boldsymbol{p})$ is well defined. We assume that $\gamma(\boldsymbol{p})$ is at least C^2 in $\mathbb{R}^d_*$. Therefore, when $\gamma(\boldsymbol{p}) \in C(\mathbb{R}^d) \cap C^2(\mathbb{R}^d_*)$, we can introduce the widely used Cahn-Hoffman $\boldsymbol{\xi}$-vector and the Hessian matrix $\mathbf{H}_\gamma$ as [42, 89, 97]

$$\boldsymbol{\xi} = (\xi_1, \ldots, \xi_d)^T := \boldsymbol{\xi}(\boldsymbol{n}) = \nabla\gamma(\boldsymbol{p})|_{\boldsymbol{p}=\boldsymbol{n}}, \qquad \mathbf{H}_\gamma(\boldsymbol{p}) := \nabla\nabla\gamma(\boldsymbol{p}),\ \forall \boldsymbol{p} \in \mathbb{R}^d_*. \tag{1.3}$$

By one-homogeneity, it can be easily verified that the $\boldsymbol{\xi}$ vector as well as the Hessian matrix $\mathbf{H}_\gamma$ satisfy the following properties [7, 55]

$$\boldsymbol{\xi} \cdot \boldsymbol{n} = \gamma(\boldsymbol{n}), \quad (\mathbf{H}_\gamma(\boldsymbol{p})\boldsymbol{p}) \cdot \boldsymbol{q} = 0, \quad \mathbf{H}_\gamma(\lambda\boldsymbol{p}) = \frac{1}{\lambda}\mathbf{H}_\gamma(\boldsymbol{p}), \quad \forall \boldsymbol{p}, \boldsymbol{q} \in \mathbb{R}^d_*, \lambda \neq 0. \tag{1.4}$$

From (1.4), we observe that $\mathbf{H}_\gamma(\boldsymbol{n})\boldsymbol{n} = \mathbf{0}$ for all $\boldsymbol{n} \in \mathbb{S}^{d-1}$. Therefore 0 is an eigenvalue of $\mathbf{H}_\gamma(\boldsymbol{n})$ and $\boldsymbol{n}$ is a corresponding eigenvector. We denote the other $d-1$ eigenvalues of $\mathbf{H}_\gamma(\boldsymbol{n})$ as $\lambda_1(\boldsymbol{n}) \leq \ldots \leq \lambda_{d-1}(\boldsymbol{n}) \in \mathbb{R}$. In fact, the classification of anisotropic surface energies also relies on the Hessian matrix $\mathbf{H}$. When $\boldsymbol{\tau}^T\mathbf{H}_\gamma(\boldsymbol{n})\boldsymbol{\tau} \geq 0$ for all $\boldsymbol{n}, \boldsymbol{\tau} \in \mathbb{S}^{d-1}$ satisfying $\boldsymbol{\tau} \cdot \boldsymbol{n} := \boldsymbol{\tau}^T\boldsymbol{n} = 0$ ($\Leftrightarrow \lambda_1(\boldsymbol{n}) \geq 0$ for all $\boldsymbol{n} \in \mathbb{S}^{d-1}$), it is referred to *weakly anisotropic*; and when $\boldsymbol{\tau}^T\mathbf{H}_\gamma(\boldsymbol{n})\boldsymbol{\tau}$ changes sign for $\boldsymbol{n}, \boldsymbol{\tau} \in \mathbb{S}^{d-1}$ satisfying $\boldsymbol{\tau} \cdot \boldsymbol{n} = 0$ ($\Leftrightarrow \lambda_1(\boldsymbol{n}) < 0$ for some $\boldsymbol{n} \in \mathbb{S}^{d-1}$), it is referred to *strongly anisotropic*.

For the curve Γ in 2D, the $\boldsymbol{\xi}$-vector can also be represented by the θ-formulation, which provides an alternative perspective for understanding it. The equation for the θ-formulation is as follows (c. f. Figure 1.6):

$$\boldsymbol{\xi} = \bar{\gamma}(\theta)\boldsymbol{n} - \bar{\gamma}'(\theta)\boldsymbol{\tau}. \tag{1.5}$$

This equation can be regarded as the vector decomposition of $\boldsymbol{\xi}$-vector into a fixed value $\gamma(\theta)$ in the normal direction $\boldsymbol{n}$ and the derivative of the θ-formulation $\bar{\gamma}'(\theta)$ in the tangent direction $\boldsymbol{\tau}$. We can observe that for the isotropic surface energy $\bar{\gamma}(\theta) \equiv 1$, the tangent component $\bar{\gamma}'(\theta) = 0$, thus the $\boldsymbol{\xi}$-vector collapses to the normal vector $\boldsymbol{n}$.

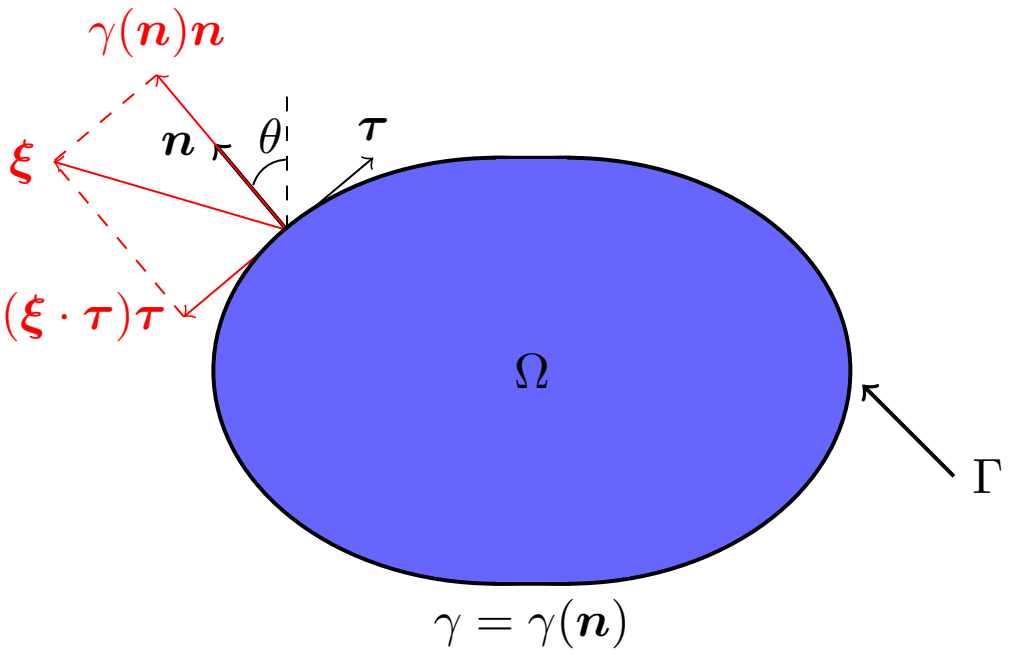

Figure 1.6: An illustration of a closed curve Γ in $\mathbb{R}^2$ with an anisotropic surface energy $\gamma(\boldsymbol{n})$, where $\boldsymbol{n}$ is the outward unit normal vector, $\boldsymbol{\tau}$ is the unit tangential vector, $\boldsymbol{\xi}$ is the Cahn-Hoffman vector in (1.3), and θ is the angle between $\boldsymbol{n}$ and y-axis such that $\boldsymbol{n} = (-\sin\theta, \cos\theta)^T$ with $\theta \in [-\pi, \pi]$.

1.3 Thermodynamic variation

Thermodynamic variation is an essential tool for deriving and understanding anisotropic surface diffusion. Let the interface be $\Gamma \subset \mathbb{R}^d$ parameterized by the function $\boldsymbol{X}(\cdot)$, where $\boldsymbol{X}(\boldsymbol{\rho}) = \boldsymbol{\rho}, \forall \boldsymbol{\rho} \in \Gamma$. For a given anisotropic surface energy $\gamma(\boldsymbol{n})$, the total surface energy function W is given as [35, 75, 141, 145]

$$W(\Gamma) := \int_\Gamma \gamma(\boldsymbol{n})\, dA. \tag{1.6}$$

Here dA is the area element. Let $\boldsymbol{V} \in [C^\infty(\Gamma)]^d$ be a test function on Γ, ε is a small parameter. The small perturbation Γ^ε of Γ is thus given as

$$\Gamma^\varepsilon := \{\boldsymbol{\rho}^\varepsilon \in \mathbb{R}^d | \boldsymbol{\rho}^\varepsilon = \boldsymbol{X}(\boldsymbol{\rho}) + \varepsilon \boldsymbol{V}(\boldsymbol{\rho})\}. \tag{1.7}$$

For any test function $\boldsymbol{V}$, the limit $\lim\limits_{\varepsilon \to 0} \frac{W(\Gamma^\varepsilon) - W(\Gamma)}{\varepsilon}$ is well defined. Thus we can define the first variation of W with respect to the test function $\boldsymbol{V}$ as

$$\delta W(\Gamma)(\boldsymbol{V}) := \lim_{\varepsilon \to 0} \frac{W(\Gamma^\varepsilon) - W(\Gamma)}{\varepsilon}. \tag{1.8}$$

From [4, 35, 55, 97], we know that the first variation $\delta W(\Gamma)$ has the following formulation

$$\delta W(\Gamma)(\boldsymbol{V}) = \int_\Gamma \mu(\boldsymbol{V} \cdot \boldsymbol{n})\, dA. \tag{1.9}$$

where $\mu := \mu(\boldsymbol{\rho})$ is the chemical potential.

(1.9) gives a variational formulation for the chemical potential μ. To get an alternative local formulation, we need to introduce several surface calculus operators. Let f be a C^1 function defined in an open neighborhood of Γ, then the surface gradient operator $\nabla_\Gamma f$ at $\boldsymbol{\rho} \in \Gamma$ is given as [58, 74, 77]

$$\nabla_\Gamma f(\boldsymbol{\rho}) := \nabla f(\boldsymbol{\rho}) - (\nabla f(\boldsymbol{\rho}) \cdot \boldsymbol{n})\boldsymbol{n} = (\underline{D}_1 f, \underline{D}_2 f, \ldots, \underline{D}_d f)^T, \tag{1.10}$$

where ∇ stands for the usual gradient operator, see Figure 1.7 for the illustration. Similarly, the surface divergence operator $\nabla_\Gamma \cdot$ for a vector-valued $[C^1]^d$ function $\boldsymbol{f} = (f_1, \ldots, f_d)^T$ and the surface Laplace-Beltrami operator Δ_Γ for a scalar-valued

C^2 function f are given as [107]

$$\nabla_\Gamma \cdot \boldsymbol{f} := \sum_{i=1}^{d} \underline{D}_i f_i \,, \quad \Delta_\Gamma f := \nabla_\Gamma \cdot \nabla_\Gamma f = \sum_{i=1}^{d} \underline{D}_i \underline{D}_i f. \tag{1.11}$$

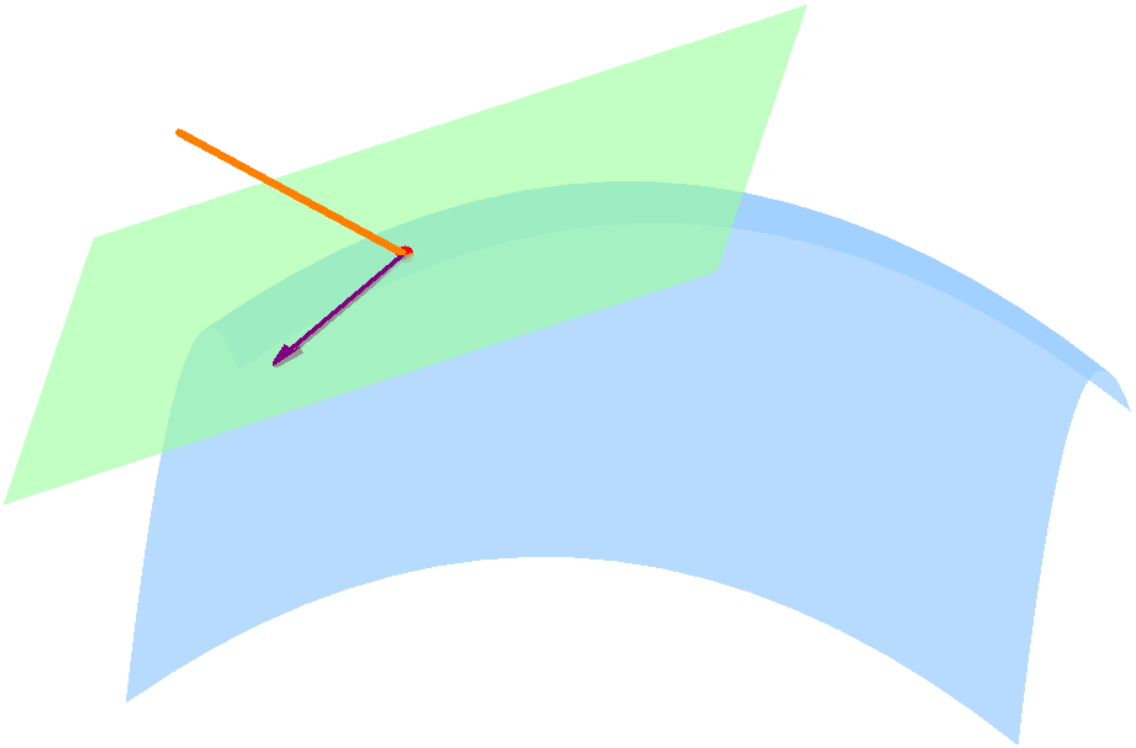

Figure 1.7: Illustration of the surface gradient operator for a surface in 3D. The surface is represented in a light blue color, while the tangent plane is depicted in light green. The usual gradient is displayed in orange, and its surface gradient is shown in purple, which is the projection of the usual gradient onto the tangent plane.

By adopting the surface divergence operator $\nabla_\Gamma \cdot$, the chemical potential can be represented by the $\boldsymbol{\xi}$ vector as follows [55, 89]

$$\mu(\boldsymbol{\rho}) = \nabla_\Gamma \cdot \boldsymbol{\xi}(\boldsymbol{n}). \tag{1.12}$$

If there is no anisotropic effect, the $\boldsymbol{\xi}$ vector collapses to the unit normal vector $\boldsymbol{n}$, and the chemical potential μ goes to the mean curvature $\mathcal{H}$ by the fact $\mathcal{H} = \nabla_\Gamma \cdot \boldsymbol{n}$

in [16,116]. Thus the chemical potential μ is also called the weighted mean curvature $\mathcal{H}_\gamma$ in some literature [52,62,139].

In 2D, the curve $\Gamma = \boldsymbol{X}(\cdot)$ can be parametrized by the arc-length s, and the arc-length parameter induces the arc-length derivative ∂_s [10,109,145]. By adopting the arc-length parameterization, the chemical potential μ can also be represented as [42,97,116]

$$\mu = -\partial_s(\boldsymbol{\xi}^\perp) \cdot \boldsymbol{n}, \tag{1.13}$$

here $\perp$ means the counterclockwise rotation by $\frac{\pi}{2}$ in $\mathbb{R}^2$, that is, if $\boldsymbol{u} = (u_1, u_2)^T$, $\boldsymbol{u}^\perp = (u_2, -u_1)^T$. And for the θ-formulation, besides using the $\boldsymbol{\xi}$-vector, we can apply the stifness $\tilde{\gamma}(\theta)$ to formulate the chemical potential μ as:

$$\mu = \tilde{\gamma}(\theta)\kappa = (\bar{\gamma}(\theta) + \bar{\gamma}''(\theta))\kappa, \tag{1.14}$$

here κ is the curvature for curves.

The anisotropic surface diffusion can be regarded as the H^{-1} gradient flow of the total surface energy function $W(\Gamma)$ [43]. By utilizing the chemical potential μ derived from the thermodynamic variation, the anisotropic surface diffusion is as follows

$$V_n = \Delta_\Gamma \mu, \tag{1.15}$$

where V_n represents the normal velocity. Specifically, for the isotropic case $\gamma(\boldsymbol{n}) \equiv 1$, the weighted mean curvature μ collapses to the mean curvature κ; and the anisotropic surface diffusion (1.15) also collapses to the (isotropic) surface diffusion $V_n = \Delta_\Gamma \kappa$.

The equilibrium shape of the anisotropic surface diffusion (1.15) is called the Wulff shape $\mathcal{W}$, which was first described by Wulff using a geometric construction [148]. The mathematical description for the Wulff shape $\mathcal{W}$ is given as [38,72,138]

$$\mathcal{W} := \{\boldsymbol{p} \in \mathbb{R}^d | \, \boldsymbol{p} \cdot \boldsymbol{n} \leq \gamma(\boldsymbol{n}), \, \forall \boldsymbol{n} \in \mathbb{S}^{d-1}\}. \tag{1.16}$$

In Figure 1.8 we show the Wulff shape for several commonly used anisotropies for surfaces.

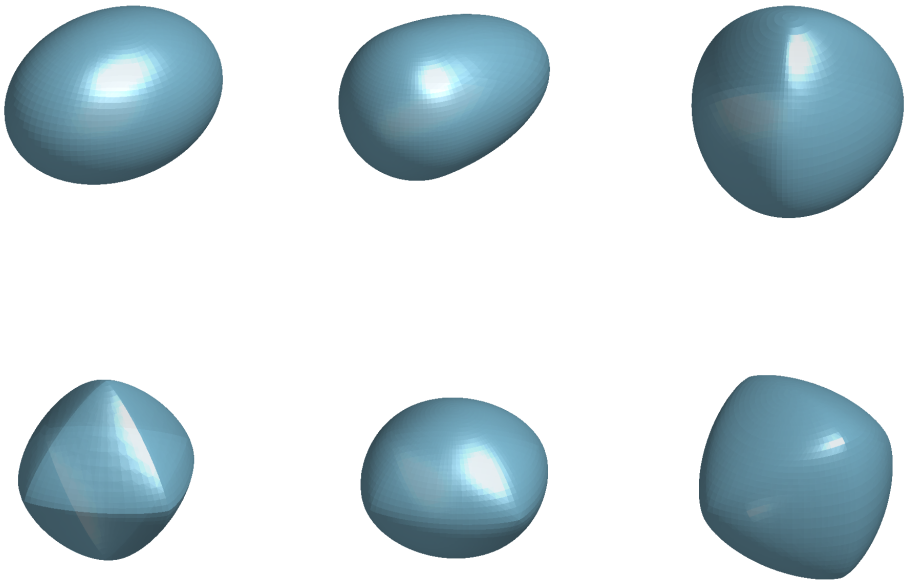

Figure 1.8: Wulff shapes in 3D for various anisotropic surface energies, corresponding to the anisotropic surface energies in the Frank diagrams in 3D (Figure 1.5).

For a curve in 2D, we can adopt the θ-formulation to give its Wulff shape analytically by the so-called Wulff envelope as [41]

$$\mathcal{W} := \{(x(\theta), y(\theta))^T | x(\theta) = -\bar{\gamma}(\theta)\sin\theta - \bar{\gamma}'(\theta)\cos\theta,\ y(\theta) = \bar{\gamma}(\theta)\cos\theta - \bar{\gamma}'(\theta)\sin\theta\}. \tag{1.17}$$

The Wulff envelope given by the parametrized curve may have possible "ears", and the Wulff shape is derived by removing these "ears" from the Wulff envelope [84, 117]. We illustrate the construction of the Wulff shape from the corresponding Wulff envelopes for selected $\gamma(\boldsymbol{n})$ in Figure 1.9. We remark here if $\bar{\gamma}(\theta)$ is weakly anisotropic (or the surface stiffness $\tilde{\gamma}(\theta) \geq 0, \forall\theta$), then there is no such "ears"; otherwise there are "ears" in the Wulff envelope.

1.4 Anisotropic surface diffusion (ASD)

We consider an initial curve or surface, denoted as Γ_0. Its evolution is governed by the anisotropic surface diffusion given by the geometric flow formulation (1.15)

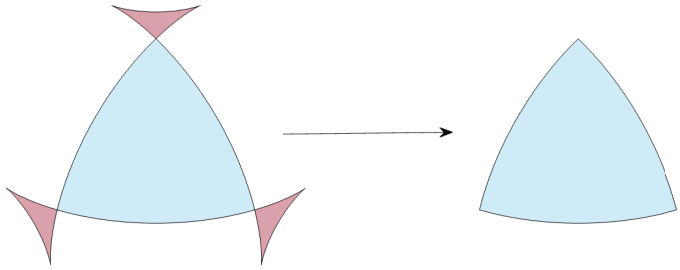

Figure 1.9: Obtaining the 2D Wulff shape from the Wulff envelope. On the left, the Wulff envelope is shown with red "ears". By removing these "ears", we derive the Wulff shape on the right.

resulting in an evolving interface represented by $(\Gamma(t))_{t\geq 0}$, where $\Gamma(0) = \Gamma_0$. An important aspect of modeling and understanding the anisotropic surface diffusion is the employment of global parameterization [33,70], which offers a rigorous approach to analyze the evolving interface $(\Gamma(t))_{t\geq 0}$ and its properties.

Definition 1.1 (Global parameterization)**.** *Let $(\Gamma(t))_{t\geq 0}$ be an evolving interface with the initial interface $\Gamma(0) = \Gamma_0 \subset \mathbb{R}^d$. A global parameterization of $(\Gamma(t))_{t\geq 0}$ is a diffeomorphism $\boldsymbol{X}(\cdot, t)$ from Γ_0 to $\Gamma(t)$ with $\boldsymbol{X}(\boldsymbol{\rho}, 0) = \boldsymbol{X}_0(\boldsymbol{\rho}) := \boldsymbol{\rho}$, $\forall \boldsymbol{\rho} \in \Gamma_0$.*

By establishing a one-to-one correspondence $\boldsymbol{X}(\cdot, t)$ between points on the interface $\Gamma(t)$ and points in the initial interface Γ_0, which is a fixed reference manifold, the global parameterization $\boldsymbol{X}(\cdot, t)$ enables the study of the functions and surface operators defined on $\Gamma(t)$ to be transformed to the initial interface Γ_0. Let $f(\cdot)$ be a function defined on $\Gamma(t)$, the pullback of $f(\cdot)$ by $\boldsymbol{X}(\cdot, t)$ gives a function $\boldsymbol{X}^*(t)f(\cdot)$ on Γ_0 defined by $\boldsymbol{X}^*(t)f(\boldsymbol{\rho}) := f(\boldsymbol{X}(\boldsymbol{\rho}, t))$. Moreover, denote the Jacobian of $\boldsymbol{X}(\cdot, t)$ to be $\mathbf{J}_{\boldsymbol{X}(t)}(\cdot)$. By change of variable, we have

$$\int_{\Gamma(t)} f \, dA = \int_{\Gamma_0} \boldsymbol{X}^*(t) f \det(\mathbf{J}_{\boldsymbol{X}(t)}) \, dA. \tag{1.18}$$

The global parameterization $\boldsymbol{X}(\cdot, t)$ from Γ_0 to $\Gamma(t)$ also gives a pushforward $d\boldsymbol{X}(\cdot, t)$ from $T_{\boldsymbol{\rho}}\Gamma_0$ the tangent space of Γ_0 at $\boldsymbol{\rho}$ to $T_{\boldsymbol{X}(\boldsymbol{\rho},t)}\Gamma(t)$ the tangent space of $\Gamma(t)$ at $\boldsymbol{X}(\boldsymbol{\rho}, t)$. Thus suppose $\{\boldsymbol{e}_1, \boldsymbol{e}_2, \ldots, \boldsymbol{e}_{d-1}\}$ forms a orthonormal basis of $T_{\boldsymbol{\rho}}\Gamma_0$ with

$\boldsymbol{n} = \boldsymbol{e}_1 \wedge \ldots \wedge \boldsymbol{e}_{d-1}$, then the outward unit vector $\boldsymbol{n}$ at $\boldsymbol{X}(\boldsymbol{\rho}, t)$ is

$$\boldsymbol{n}(\boldsymbol{\rho}, t) := \boldsymbol{n}(\boldsymbol{X}(\boldsymbol{\rho}, t)) = \frac{\hat{\boldsymbol{e}}_1 \wedge \ldots \wedge \hat{\boldsymbol{e}}_{d-1}}{|\hat{\boldsymbol{e}}_1 \wedge \ldots \wedge \hat{\boldsymbol{e}}_{d-1}|}, \tag{1.19}$$

which is determined by the global parameterization $\boldsymbol{X}(\boldsymbol{\rho}, t)$ with $\hat{\boldsymbol{e}}_j = d\boldsymbol{X}(\cdot, t)\boldsymbol{e}_j$, $j = 1, \ldots, d-1$. Also, by the change of variable and the chain rule, we know that the gradient operator

$$\nabla \boldsymbol{f}|_{\boldsymbol{p}=\boldsymbol{X}(\boldsymbol{\rho},t)} = \mathbf{J}^{-1}_{\boldsymbol{X}(t)}(\boldsymbol{\rho}) \nabla (\boldsymbol{X}^*(t) f(\boldsymbol{\rho})) \tag{1.20}$$

is also determined by $\boldsymbol{X}(\boldsymbol{\rho}, t)$. Therefore, by (1.10) and (1.11), the surface gradient, the surface divergence, and the surface Laplace-Beltrami operator on $\Gamma(t)$ are also determined by the global parameterization $\boldsymbol{X}(\boldsymbol{\rho}, t)$. Thus global parameterization provides a solid foundation for subsequent theoretical and numerical investigations. In the following discussion, we do not discriminate the function with its pullback and pushforward.

By adopting the global parameterization $\boldsymbol{X}$, the normal velocity can be written as $V_n(\boldsymbol{\rho}, t) = \boldsymbol{n}(\boldsymbol{\rho}, t) \cdot \partial_t \boldsymbol{X}(\boldsymbol{\rho}, t)$. Thus the geometric description of the anisotropic surface diffusion can be represented as the following geometric partial differential equations

$$\begin{cases} \partial_t \boldsymbol{X} = (\Delta_\Gamma \mu)\, \boldsymbol{n}, \quad \boldsymbol{\rho} \in \Gamma_0, \quad t > 0, & \text{(1.21a)} \\ \mu = \nabla_\Gamma \cdot \boldsymbol{\xi}, \quad \boldsymbol{\xi} = \nabla \gamma(\boldsymbol{p})\big|_{\boldsymbol{p}=\boldsymbol{n}}. & \text{(1.21b)} \end{cases}$$

Here the surface divergence and surface Laplace-Beltrami operator are varying with respect to the evolving interface $\Gamma(t)$ rather than Γ_0.

For the 2D curve with arc-length parameter s, the surface Laplace-Beltrami operator collapses to the second-order arc-length derivative ∂_{ss}. This, together with the chemical potential μ given by (1.13), gives the following formulation for anisotropic surface diffusion in 2D

$$\begin{cases} \partial_t \boldsymbol{X} = (\partial_{ss} \mu)\, \boldsymbol{n}, \quad \boldsymbol{\rho} \in \Gamma_0, \quad t > 0, & \text{(1.22a)} \\ \mu = -\partial_s(\boldsymbol{\xi}^\perp) \cdot \boldsymbol{n}, \quad \boldsymbol{\xi} = \nabla \gamma(\boldsymbol{p})\big|_{\boldsymbol{p}=\boldsymbol{n}}. & \text{(1.22b)} \end{cases}$$

Moreover, if we adopt the θ-formulation, the chemical potential μ is $\mu = \tilde{\gamma}(\theta)\kappa = (\bar{\gamma}(\theta) + \bar{\gamma}''(\theta))\kappa$, see (1.14). Thus the anisotropic surface diffusion in 2D can also be

written as

$$\begin{cases} \partial_t \boldsymbol{X} = (\partial_{ss}\,\mu)\,\boldsymbol{n}, \quad \boldsymbol{\rho} \in \Gamma_0, \quad t > 0, & (1.23a) \\ \mu = \tilde{\gamma}(\theta)\kappa = (\bar{\gamma}(\theta) + \bar{\gamma}''(\theta))\kappa. & (1.23b) \end{cases}$$

We note that for the isotropic case $\bar{\gamma}(\theta) \equiv 1$, the surface stiffness $\tilde{\gamma}(\theta) \equiv 1$ and the anisotropic surface diffusion goes to the (isotropic) surface diffusion.

The partial differential equation formulation for anisotropic surface diffusion, as presented in (1.21) or (1.22), also adheres to the two geometric properties: conservation of the total mass $M(t)$ and dissipation of the surface energy $W(t)$.

In a 2D curve, the total mass corresponds to the area enclosed by $\Gamma(t)$, which is also referred to as the enclosed area and denoted by $A(t)$. Conversely, in a 3D surface, the total mass corresponds to the volume enclosed by $\Gamma(t)$, also known as the enclosed volume and denoted by $V(t)$. From the Reynolds transport theorem [33], it is easy to see that the two geometric laws are well preserved during the evolution.

1.5 Literature review

Surface diffusion has been extensively studied mathematically. For isotropic surface diffusion of two-dimensional curves, the local existence and regularity were first established by Elliott and Garcke [66] for C^4-initial curves and then extended for H^4-initial curves by Giga and Ito [76]. If the initial curve is close to a circle, the solution is globally existed and will converge exponentially fast [66]. These results are later extended to higher dimensions by Escher, Mayer, and Simonett [67]. Moreover, it is proved to have topological changes such as pinch-off [76]. For anisotropic surface diffusion with crystalline formulation, the local existence is recently developed in [73].

Different numerical methods have been developed for isotropic surface diffusion, and each of the numerical methods requires different parameterizations and assumptions for the evolving surface. For the surfaces that can be represented as graphs over a fixed domain, several methods are available, including the finite difference

method [50], the finite element method [5, 55, 56], and the discontinuous Galerkin method [149]. We refer to [5,54,56] for the error analysis of the finite element method for the semi-discretization and full-discretization. However, the surface may lose its graph property during evolution [76, 112]. The aforementioned methods can also be applied to axisymmetric surfaces [32, 49, 118]. The level set method represents the surface implicitly as the zero level set of a d dimensional function, making it suitable for handling complex geometries and topological changes but increasing computational cost [74, 121], we refer to [39, 48, 125]. The marker-particle method represents the surface with discrete particles and tracks their motion [60, 147]. It requires a severe restriction on numerical stability, and the particles need to be re-distributed frequently. The θ-L formulation method employs the tangential angle θ and total length L to represent 2D curves [90] and axisymmetric 3D surfaces [91]. The evolving surface finite element method [94, 105] is a specialized finite element technique, which tracks the evolution of the normal vector $\boldsymbol{n}$ and the mean curvature κ. It allows for convergence analysis in the case of continuous finite elements with a polynomial degree of at least two [106]. Nevertheless, due to the high nonlinearity of surface diffusion, the aforementioned numerical schemes must introduce artificial tangential velocity or implement mesh regularization to avoid mesh coalescence. Additionally, most of these methods cannot preserve energy dissipation and mass conservation in full discretization.

In contrast to many other methods for surface diffusion, the parametric finite element method (PFEM) [10,16,19,87,97,109] performs the best in terms of accuracy and efficiency as well as mesh quality in practical computations. By adopting Dziuk's formulation $\kappa\boldsymbol{n} = -\partial_{ss}\boldsymbol{X}$ with the polygon curves in 2D [61], Barrett, Garcke and Nürnberg first proposed the PFEM in [16] for simulating the surface diffusion of curves in 2D based on the following weak formulation for the mean curvature κ

$$\int_\Gamma \kappa\boldsymbol{n}\cdot\boldsymbol{\omega}\,dA = \int_\Gamma \partial_s\boldsymbol{X}\cdot\partial_s\boldsymbol{\omega}\,dA. \tag{1.24}$$

The derived PFEM is semi-implicit, unconditionally energy-stable, and enjoys asymptotic equal mesh distribution [16] and thus there is no need to re-mesh during time

evolution. It is then generalized to the surfaces in 3D [19] with the surface gradient ∇_Γ, and most of its desired properties including the energy dissipation are also preserved in full discretization. Very recently, by introducing a smart approximation of the normal vector $\boldsymbol{n}$, a structure-preserving PFEM (SP-PFEM) was proposed for the surface diffusion [6,13] that can further preserve the conservation of total mass. As a result, the PFEM and its extension to the SP-PFEM, provide highly accurate, efficient, and robust numerical schemes for surface diffusion.

Moreover, the high performance of the PFEM enables its application to a wide range of geometric flows with isotropic surface energy other than surface diffusion, including mean curvature flow [15–17,21,71], Willmore flow [16,18,27,53,63], Mullins-Sekerka problem [22], Stefan problem [22,25], and so on. In addition to geometric flows, PFEM also has broad applications in two-phase fluid flow [24,26,28], solid-state dewetting problems [10,14,95,96,98,145,154,155], biomembranes [28–31], and other research areas. Due to the success of PFEM in surface diffusion and various other applications, the extension of PFEM to anisotropic surface diffusion becomes increasingly important and highly demanded.

However, due to the high nonlinearity of the weighted mean curvature μ, designing a structure-preserving PFEM for anisotropic surface diffusion with arbitrary surface energy $\gamma(\boldsymbol{n})$ is a notoriously difficult task. For the curves in 2D, Zhao and Jiang developed a PFEM that represents the weighted mean curvature, μ, with the $\boldsymbol{\xi}$-vector through the weak formulation [97]

$$\int_\Gamma \mu \boldsymbol{n} \cdot \boldsymbol{\omega}\, dA = -\int_\Gamma \partial_s \boldsymbol{\xi}^\perp \cdot \partial_s \boldsymbol{\omega}\, dA. \tag{1.25}$$

In addition, Bao, Jiang, Wang and Zhao proposed a PFEM by utilizing the $\bar{\gamma}(\theta)$ formulation to represent the weighted mean curvature μ with κ as $\mu = (\bar{\gamma}(\theta)+\bar{\gamma}(\theta)'')\kappa$ [10]. While for the surfaces in 3D, Bao, Jiang and Zhao identified a weak formulation of μ by coupling the $\boldsymbol{\xi}$-vector with $\gamma(\boldsymbol{n})$ [154]:

$$\int_\Gamma \mu \boldsymbol{n} \cdot \boldsymbol{\omega}\, dA = \int_\Gamma \gamma(\boldsymbol{n}) \nabla_\Gamma \boldsymbol{X} : \nabla_\Gamma \boldsymbol{\omega}\, dA + \sum_{i,l=1}^{3} \int_\Gamma \xi_i n_l \nabla_\Gamma x_i \cdot \nabla_\Gamma \omega_l\, dA. \tag{1.26}$$

This leads to a novel PFEM for arbitrary surface energy $\gamma(\boldsymbol{n})$, which was further extended to simulate the solid-state dewetting. Although it can be observed that the energy is decreasing at the discretized level for all of the above-mentioned PFEMs, their energy dissipation laws have not yet been established. For other numerical schemes related to anisotropic surface diffusion, we refer to [44, 60, 64, 78, 103, 104, 128, 133, 146, 147] and references therein.

Rather than dealing with the general anisotropic surface energies, it is possible to design an energy-stable PFEM for specific anisotropies. Barrett, Garcke and Nürnberg observed that for the Riemannian matric surface energy, there is a one-to-one correspondence between an anisotropic surface diffusion of curves with a special anisotropy and an isotropic surface diffusion of curves on a special manifold [57]. Consequently, they proposed an energy-stable PFEM for evolving curves driven by the Riemannian metric surface energy [17]. Based on that idea, Zhao and Bao then proposed an energy-stable PFEM for axis-symmetric surfaces in 3D [6, 153]. In [19], the energy-stable PFEM was extended for anisotropic surface diffusion on 3D surfaces, and the anisotropic surface energies were generalized to the regularized Riemannian metric surface energy. On the other hand, by incorporating a surface energy matrix $\boldsymbol{G}(\theta)$ using the θ-formulation [109],

$$\int_\Gamma \mu \boldsymbol{n} \cdot \boldsymbol{\omega}\, dA = \int_\Gamma (\boldsymbol{G}(\theta)\partial_s \boldsymbol{X}) \cdot \partial_s \boldsymbol{\omega}\, dA, \tag{1.27}$$

Li and Bao introduced an energy-stable PFEM for general surface energy with a strong condition on $\bar{\gamma}(\theta)$. Given that the energy-stable conditions on $\gamma(\boldsymbol{n})$ in the aforementioned ES-PFEMs are strict, they are not applicable for all commonly used anisotropic surface energies. Therefore, it is important to develop ES-PFEMs with milder energy-stable conditions for wider applicability.

1.6 Scope of this thesis

The goal of this work is to design a structure-preserving parametric finite element method (SP-PFEM) for anisotropic surface diffusion of 2D curves and of 3D surfaces,

with a more general anisotropic surface energy $\gamma(\boldsymbol{n})$. Firstly, we start with the symmetrized SP-PFEM of 2D curves with the symmetric anisotropy, i.e., $\gamma(-\boldsymbol{n}) = \gamma(\boldsymbol{n})$. We establish the energy stability which only requires the regularity of $\gamma(\boldsymbol{p}) \in C^2(\mathbb{R}^d \setminus \{\boldsymbol{0}\})$. Then we extend the symmetrized SP-PFEM as well as the energy stability condition to 3D surfaces. After that, we introduce a unified SP-PFEM for both 2D curves and 3D surfaces. By proposing a novel analysis framework, we then drastically extend the energy-stable condition from $\gamma(-\boldsymbol{n}) = \gamma(\boldsymbol{n})$ to $\gamma(-\boldsymbol{n}) > (5-d)\gamma(\boldsymbol{n})$, and the regularity requirement on $\gamma(\boldsymbol{p})$ is reduced to piecewise-$C^2(\mathbb{R}^d \setminus \{\boldsymbol{0}\})$.

In Chapter 2, we consider the anisotropic surface diffusion of 2D curves with symmetric $\gamma(-\boldsymbol{n}) = \gamma(\boldsymbol{n})$. By introducing a novel symmetric positive definite surface energy matrix $\boldsymbol{Z}_k(\boldsymbol{n})$ depending on the Cahn-Hoffman $\boldsymbol{\xi}$-vector and a stabilizing function $k(\boldsymbol{n})$, we first reformulate the anisotropic surface diffusion into a conservative form and then derive a new symmetrized variational formulation for the anisotropic surface diffusion with both weakly and strongly anisotropic surface energies. A semi-discretization by PFEM in space for the symmetrized variational formulation is proposed and its area (or mass) conservation and energy dissipation are proved. It is further discretized in time by the implicit-explicit Euler method, which preserves the mass conservation in the discretized level. After that, we prove that the symmetrized SP-PFEM is energy dissipative and thus is unconditionally energy-stable for almost all anisotropic surface energies $\gamma(\boldsymbol{n})$ arising in practical applications. Specifically, for several commonly-used anisotropic surface energies, we construct $\boldsymbol{Z}_k(\boldsymbol{n})$ explicitly. Finally, extensive numerical results are reported to demonstrate the efficiency and accuracy as well as the unconditional energy-stability of the proposed symmetrized parametric finite element method.

In Chapter 3, we extend the symmetrized SP-PFEM to 3D. By generalizing the novel symmetric positive definite surface energy matrix $\boldsymbol{Z}_k(\boldsymbol{n})$ to 3D, we present a new symmetrized variational formulation for anisotropic surface diffusion in 3D. Then we propose the symmetrized SP-PFEM to discretize the symmetrized variational problem in space via PFEM and in time via the implicit-explicit Euler method.

We prove the unconditional energy stability of the proposed symmetrized SP-PFEM for 3D surfaces under the same condition as 2D. Extensive numerical results are reported to demonstrate the efficiency and accuracy as well as structure-preserving properties of the proposed symmetrized SP-PFEM for solving anisotropic surface diffusion in 3D.

In Chapter 4, for the arbitrary anisotropic surface energy $\gamma(\boldsymbol{n})$, we propose a unified SP-PFEM for anisotropic surface diffusion in both two and three dimensions. The proposed unified SP-PFEM is based on a unified surface energy matrix $\boldsymbol{G}_k(\boldsymbol{n})$ and a unified weak formulation of the chemical potential μ. The main challenge and contribution are establishing a unified framework to prove energy stability under the simple conditions $\gamma(\boldsymbol{p}) \in C^2(\mathbb{R}^d \setminus \{\boldsymbol{0}\})$ and $\gamma(-\boldsymbol{n}) < (5-d)\gamma(\boldsymbol{n})$ for $\boldsymbol{n} \in \mathbb{S}^{d-1}$. The structure-preserving properties of the proposed method are also verified through numerical experiments.

In Chapter 5, we apply the unified SP-PFEM to simulate the evolution of a close 2D curve under other anisotropic geometric flows including anisotropic curvature flow and anisotropic mass-conserved curvature flow. Extensive numerical results are reported to demonstrate the efficiency and unconditional energy stability as well as the good mesh quality property of the proposed SP-PFEM for simulating anisotropic geometric flows.

In Chapter 6, we conclude the results of this thesis and suggest some possible future works.

Chapter 2

A SP-PFEM for curves with symmetric surface energy

To develop a structure-preserving parametric FEM (SP-PFEM) for anisotropic surface diffusion, we start with the *symmetric anisotropic surface energy*, i.e.,

$$\gamma(-\boldsymbol{n}) = \gamma(\boldsymbol{n}), \quad \forall \boldsymbol{n} = (n_1, n_2)^T \in \mathbb{S}^1. \tag{2.1}$$

The first step and the most simple case is to consider the motion of a *planar curve* Γ in 2D – that instead of applying the general global parameterization, we can adapt the arc-length parameterization s. Let $\mathbb{T} = \mathbb{R}/\mathbb{Z} = [0,1]$ be the periodic unit interval and we parameterize the evolution curves $\Gamma(t)$ as

$$\Gamma(t) := \boldsymbol{X}(\rho, t) = (x(\rho, t),\ y(\rho, t))^T :\ \mathbb{T} \times \mathbb{R}^+ \ \to\ \mathbb{R}^2. \tag{2.2}$$

The arc-length parameter s is given by $s(\rho, t) = \int_0^\rho |\partial_q \boldsymbol{X}|\ \mathrm{d}q$ with its derivative $\partial_\rho s = |\partial_\rho \boldsymbol{X}|$. By the introduced time-independent variable ρ, the evolving curve $\Gamma(t)$ can then be parameterized over a fixed domain $\rho \in \mathbb{T} = [0,1]$. Based on the arc-length parameterization, the unit tangent vector $\boldsymbol{\tau}$ is $\partial_s \boldsymbol{X}$, and the outward normal vector $\boldsymbol{n} = -\boldsymbol{\tau}^\perp$. Moreover, the weighted mean curvature μ has an elegant formulation $\mu = -\partial_s \boldsymbol{\xi}^\perp \cdot \boldsymbol{n}$ in 2D, see (1.13). Thus, the anisotropic surface diffusion

(1.22) is given as

$$\begin{cases} \boldsymbol{n} \cdot \partial_t \boldsymbol{X} = \partial_{ss}\, \mu, \quad \boldsymbol{\rho} \in \Gamma_0, \quad t > 0, & \text{(2.3a)} \\ \mu = -\partial_s(\boldsymbol{\xi}^{\perp}) \cdot \boldsymbol{n}, \quad \boldsymbol{\xi} = \nabla\gamma(\boldsymbol{p})\big|_{\boldsymbol{p}=\boldsymbol{n}}. & \text{(2.3b)} \end{cases}$$

In this Chapter, for the symmetric anisotropic surface energy, we introduce a symmetrized SP-PFEM for anisotropic surface diffusion and prove its energy stability. We first summarize the commonly-used symmetric anisotropic surface energies and introduce the functional space. Then we introduce the symmetrized surface energy matrix $\boldsymbol{Z}_k(\boldsymbol{n})$ to derive a symmetrized conservative weak formulation for (2.3). After that, we employ the PFEM to derive the full discretization. We then prove the energy stability and discuss the minimal value of the stabilizing term $k(\boldsymbol{n})$. Finally, extensive numerical results are shown to demonstrate the desired property of our symmetrized SP-PFEM.

2.1 Mathematical formulation for ASD in two dimensions

2.1.1 Some anisotropic surface energies and their $\boldsymbol{\xi}$-vectors

Here we list the commonly used symmetric $\gamma(\boldsymbol{n})$ with their $\boldsymbol{\xi}$-vector, eigenvalues of the Hessian and Hessian as follows:

- the Riemannian metric anisotropic surface energy [17, 33]

$$\gamma(\boldsymbol{n}) = \sqrt{\boldsymbol{n}^T G \boldsymbol{n}}, \qquad \forall \boldsymbol{n} = (n_1, n_2)^T \in \mathbb{S}^1, \tag{2.4}$$

where $G \in \mathbb{R}^{2\times 2}$ is a symmetric positive definite matrix. We have

$$\gamma(\boldsymbol{p}) = \sqrt{\boldsymbol{p}^T G \boldsymbol{p}}, \qquad \forall \boldsymbol{p} \in \mathbb{R}^2_* := \mathbb{R}^2 \setminus \{\boldsymbol{0}\}, \tag{2.5}$$

$$\boldsymbol{\xi} = \boldsymbol{\xi}(\boldsymbol{n}) = \gamma(\boldsymbol{n})^{-1} G\, \boldsymbol{n}, \qquad \lambda(\boldsymbol{n}) = \gamma(\boldsymbol{n})^{-3} \det(G) > 0, \tag{2.6}$$

which indicates the Riemannian metric anisotropy is always weakly anisotropic.

- the l^r-norm ($r \geq 2$) metric anisotropic surface energy [36, 55]

$$\gamma(\boldsymbol{n}) = \|\boldsymbol{n}\|_{l^r} = (|n_1|^r + |n_2|^r)^{\frac{1}{r}}, \qquad \forall \boldsymbol{n} = (n_1, n_2)^T \in \mathbb{S}^1, \tag{2.7}$$

where $1 < r < \infty$. We have

$$\gamma(\boldsymbol{p}) = \|\boldsymbol{p}\|_{l^r} = (|p_1|^r + |p_2|^r)^{\frac{1}{r}}, \qquad \forall \boldsymbol{p} = (p_1, p_2)^T \in \mathbb{R}^2_*, \tag{2.8}$$

$$\boldsymbol{\xi} = \boldsymbol{\xi}(\boldsymbol{n}) = \gamma(\boldsymbol{n})^{1-r} \begin{pmatrix} |n_1|^{r-2} n_1 \\ |n_2|^{r-2} n_2 \end{pmatrix}, \quad \lambda(\boldsymbol{n}) = (r-1)\frac{|n_1 n_2|^{r-2}}{\gamma(\boldsymbol{n})^{2r-1}}, \quad \forall \boldsymbol{n} \in \mathbb{S}^1, \tag{2.9}$$

which indicates the l^r-norm ($r \geq 2$) metric anisotropy is always weakly anisotropic.

- the m-fold anisotropic surface energy [10, 96, 113, 145]

$$\gamma(\boldsymbol{n}) = 1 + \beta \cos(m(\theta - \theta_0)), \qquad \forall \boldsymbol{n} = (-\sin\theta, \cos\theta)^T \in \mathbb{S}^1, \tag{2.10}$$

where $m = 2, 4, 6$, $\theta_0 \in [-\pi, \pi]$ is a constant, and $\beta \geq 0$ is a dimensionless anisotropic strength constant. When $\theta_0 = 0$, we have

$$\gamma(\boldsymbol{p}) = \left(p_1^2 + p_2^2\right)^{\frac{1}{2}} (1 + \beta \cos(m\theta)), \forall \boldsymbol{p} = |p|(-\sin\theta, \cos\theta)^T \in \mathbb{R}^2_*. \tag{2.11}$$

Plugging (2.11) into (1.3), we get

$$\boldsymbol{\xi} = \boldsymbol{\xi}(\boldsymbol{n}) = \boldsymbol{n} + \beta \cos(m\theta)\boldsymbol{n} + \beta m \sin(m\theta)\boldsymbol{n}^{\perp}, \quad \boldsymbol{n} = (-\sin\theta, \cos\theta), \tag{2.12}$$

$$\lambda(\boldsymbol{n}) = 1 - \beta(m^2 - 1)\cos(m\theta), \tag{2.13}$$

which indicates that it is weakly anisotropic if $0 \leq \beta \leq \frac{1}{m^2-1}$; otherwise, it is strongly anisotropic.

- the regularized l^1-norm metric anisotropic surface energy which can be viewed as a regularization for the non-smooth surface energy $\gamma(\boldsymbol{n}) = |n_1| + |n_2|$ [17, 23]

$$\gamma(\boldsymbol{n}) = \sqrt{n_1^2 + \varepsilon^2 n_2^2} + \sqrt{\varepsilon^2 n_1^2 + n_2^2}, \qquad \forall \boldsymbol{n} = (n_1, n_2)^T \in \mathbb{S}^1, \tag{2.14}$$

where $0 < \varepsilon \ll 1$ is a regularization parameter. This regularization is weakly anisotropic from (2.4).

For all the above $\gamma(\boldsymbol{n})$, their Hessian matrices are of the form:

$$\mathbf{H}_\gamma(\boldsymbol{n}) = \lambda(\boldsymbol{n}) \begin{pmatrix} n_2^2 & -n_1 n_2 \\ -n_1 n_2 & n_1^2 \end{pmatrix}, \qquad \forall\, \boldsymbol{n} = (n_1, n_2)^T \in \mathbb{S}^1. \tag{2.15}$$

2.1.2 A symmetric surface energy matrix

In the following subsections, by defining the symmetrized surface energy matrix $\boldsymbol{Z}_k(\boldsymbol{n})$, we present a new conservative and self-adjoint weak formulation of the weighted mean curvature μ as well as a new symmetrized conservative variational formulation of (2.3). Finally, we prove the area conservation and energy dissipation of the new symmetrized conservative weak formulation.

Introducing a symmetric surface energy matrix $\boldsymbol{Z}_k(\boldsymbol{n})$ as

$$\boldsymbol{Z}_k(\boldsymbol{n}) = \gamma(\boldsymbol{n}) I_2 - \boldsymbol{n}\boldsymbol{\xi}(\boldsymbol{n})^T - \boldsymbol{\xi}(\boldsymbol{n})\boldsymbol{n}^T + k(\boldsymbol{n})\boldsymbol{n}\boldsymbol{n}^T, \qquad \forall \boldsymbol{n} \in \mathbb{S}^1, \tag{2.16}$$

where $k(\boldsymbol{n}) : \mathbb{S}^1 \to \mathbb{R}^+$ is a stabilizing function to be determined later, then we have

Lemma 2.1 (symmetric and conservative form)**.** *With the symmetric surface energy matrix $\boldsymbol{Z}_k(\boldsymbol{n})$ in (2.16), the anisotropic surface diffusion (1.21) can be reformulated as*

$$\begin{cases} \boldsymbol{n} \cdot \partial_t \boldsymbol{X} = \partial_{ss}\mu, & \text{(2.17a)} \\ \mu\, \boldsymbol{n} = -\partial_s(\boldsymbol{Z}_k(\boldsymbol{n})\partial_s \boldsymbol{X}). & \text{(2.17b)} \end{cases}$$

Proof. From (1.3), noting (1.4) and the fact $\boldsymbol{\tau} = \partial_s \boldsymbol{X}, \boldsymbol{n} = \boldsymbol{\tau}^\perp$, we get

$$\boldsymbol{\xi}^\perp = \gamma(\boldsymbol{n})\boldsymbol{n}^\perp + (\boldsymbol{\xi}\cdot\boldsymbol{\tau})\boldsymbol{\tau}^\perp = \gamma(\boldsymbol{n})\boldsymbol{\tau} - (\boldsymbol{\xi}\cdot\boldsymbol{\tau})\boldsymbol{n}. \tag{2.18}$$

From (2.16), noticing (2.18) and $\boldsymbol{n}\cdot\boldsymbol{\tau} = 0$, we get

$$\begin{aligned} \boldsymbol{Z}_k(\boldsymbol{n})\partial_s \boldsymbol{X} = \boldsymbol{Z}_k(\boldsymbol{n})\boldsymbol{\tau} &= (\gamma(\boldsymbol{n}) I_2 - \boldsymbol{n}\boldsymbol{\xi}^T - \boldsymbol{\xi}\boldsymbol{n}^T + k(\boldsymbol{n})\boldsymbol{n}\boldsymbol{n}^T)\boldsymbol{\tau} \\ &= \gamma(\boldsymbol{n})\boldsymbol{\tau} - (\boldsymbol{\xi}\cdot\boldsymbol{\tau})\boldsymbol{n} + (\boldsymbol{n}\cdot\boldsymbol{\tau})\,(k(\boldsymbol{n})\boldsymbol{n} - \boldsymbol{\xi}) = \boldsymbol{\xi}^\perp. \end{aligned} \tag{2.19}$$

Plugging (2.19) into the identity $\mu\boldsymbol{n} = -\partial_s\boldsymbol{\xi}^\perp$ from [97], we obtain (2.17) immediately. □

Remark 2.1. *When $\gamma(\boldsymbol{n}) \equiv 1$ and by taking $k(\boldsymbol{n}) \equiv 2$ in (2.16), we have $\mu = \kappa$ and $\boldsymbol{\xi} = \boldsymbol{n}$, and thus $\boldsymbol{Z}_k(\boldsymbol{n}) \equiv I_2$. Then (2.17) collapses to the standard formulation by PFEM for surface diffusion [16]. Similarly, when $\gamma(\boldsymbol{n})$ is chosen as the Riemannian metric anisotropic surface energy (2.4), by taking $k(\boldsymbol{n}) = \gamma(\boldsymbol{n})^{-1}\, Tr(G)$ with $Tr(G)$ denoting the trace of G, then (2.17) collapses to the formulation used in [17]. A similar formulation but without the symmetrizing term $-\boldsymbol{\xi}(\boldsymbol{n})\boldsymbol{n}^T$ and the stabilizing term $k(\boldsymbol{n})$ can also be found in [19, (1.18)].*

2.1.3 A symmetrized conservative weak formulation

For the closed curve $\Gamma(t)$, we also introduce the Sobolev space defined as

$$L^2(\mathbb{T}) = \left\{ u : \mathbb{T} \to \mathbb{R} \mid \int_{\Gamma(t)} |u(s)|^2 ds = \int_{\mathbb{T}} |u(s(\rho,t))|^2 \partial_\rho s \, d\rho < +\infty \right\}, \tag{2.20}$$

equipped with the L^2-inner product

$$\big(u, v\big)_{\Gamma(t)} := \int_{\Gamma(t)} u(s) v(s)\, ds = \int_{\mathbb{T}} u(s(\rho,t)) v(s(\rho,t)) \partial_\rho s \, d\rho, \quad \forall\, u, v \in L^2(\mathbb{T}), \tag{2.21}$$

which can be easily extended to $[L^2(\mathbb{T})]^2$.

Moreover, we define the Sobolev space

$$H^1(\mathbb{T}) := \left\{ u : \mathbb{T} \to \mathbb{R},\ \text{and } u \in L^2(\mathbb{T}),\ \partial_\rho u \in L^2(\mathbb{T}) \right\}. \tag{2.22}$$

Multiplying a test function $\varphi(\rho) \in H^1(\mathbb{T})$ to (2.17a), and then integrating over $\Gamma(t)$ and taking integration by parts, we have

$$\Big(\boldsymbol{n} \cdot \partial_t \boldsymbol{X}, \varphi\Big)_{\Gamma(t)} = \Big(\partial_{ss}\mu, \varphi\Big)_{\Gamma(t)} = -\Big(\partial_s \mu, \partial_s \varphi\Big)_{\Gamma(t)}. \tag{2.23}$$

Similarly, by multiplying a test function $\boldsymbol{\omega} = (\omega_1, \omega_2)^T \in [H^1(\mathbb{T})]^2$ to (2.17b), we obtain

$$\Big(\mu\, \boldsymbol{n}, \boldsymbol{\omega}\Big)_{\Gamma(t)} = \Big(-\partial_s(\boldsymbol{Z}_k(\boldsymbol{n})\partial_s \boldsymbol{X}), \boldsymbol{\omega}\Big)_{\Gamma(t)} = \Big(\boldsymbol{Z}_k(\boldsymbol{n})\partial_s \boldsymbol{X}, \partial_s \boldsymbol{\omega}\Big)_{\Gamma(t)}. \tag{2.24}$$

By combining the two weak formulations (2.23) and (2.24), we now get the novel symmetrized variational formulation for the anisotropic surface diffusion (2.17) (or

(1.21)) with the initial condition $\Gamma(0) = \Gamma_0$. More precisely, for a given initial curve $\Gamma_0 := \Gamma(0) = \boldsymbol{X}(\mathbb{T}, 0)$ with $\boldsymbol{X}(\rho, 0) = \boldsymbol{X}_0(L_0\rho) \in [H^1(\mathbb{T})]^2$, find the solution $\Gamma(t) := \boldsymbol{X}(\mathbb{T}, t)$, $\boldsymbol{X}(\cdot, t) \in [H^1(\mathbb{T})]^2$ and $\mu(\cdot, t) \in H^1(\mathbb{T})$ such that:

$$\Big(\boldsymbol{n} \cdot \partial_t \boldsymbol{X}, \varphi\Big)_{\Gamma(t)} + \Big(\partial_s \mu, \partial_s \varphi\Big)_{\Gamma(t)} = 0, \qquad \forall \varphi \in H^1(\mathbb{T}), \tag{2.25a}$$

$$\Big(\mu, \boldsymbol{n} \cdot \boldsymbol{\omega}\Big)_{\Gamma(t)} - \Big(\boldsymbol{Z}_k(\boldsymbol{n}) \partial_s \boldsymbol{X}, \partial_s \boldsymbol{\omega}\Big)_{\Gamma(t)} = 0, \quad \forall \boldsymbol{\omega} \in [H^1(\mathbb{T})]^2. \tag{2.25b}$$

2.1.4 Structure-preserving properties

Let $A(t)$ denote the area (i.e., the region $\Omega(t)$ enclosed by the curve $\Gamma(t)$) and $W(t)$ denote the free energy (or weighted length), which are defined as

$$A(t) := \int_{\Omega(t)} 1 \, d\mathbf{x} = \int_0^{L(t)} y(s,t) \partial_s x(s,t) \, ds, \quad W(t) := \int_{\Gamma(t)} \gamma(\boldsymbol{n}) \, ds, \quad t \geq 0. \tag{2.26}$$

For the above variational problem (2.25), we have

Proposition 2.1 (area conservation and energy dissipation)**.** *The area $A(t)$ of the solution $\Big(\boldsymbol{X}(\cdot,\ t),\ \mu(\cdot,\ t)\Big) \in [H^1(\mathbb{T})]^2 \times H^1(\mathbb{T})$ defined by the variational problem (2.25) is conserved, and the energy $W(t)$ is dissipative, i.e.*

$$A(t) \equiv A(0), \quad W(t) \leq W(t_1) \leq W(0), \quad t \geq t_1 \geq 0. \tag{2.27}$$

Proof. The proof of area conservation is similar to the Proposition 2.1 in [109], thus we omit the details for brevity.

To prove the energy dissipation in (2.27), taking the derivative of $W(t)$ with respect to t, noting (1.3), (2.19), (2.25b) with $\boldsymbol{\omega} = \partial_t \boldsymbol{X}$, and (2.25a) with $\varphi = \mu$, and $\partial_t \boldsymbol{n} = (\boldsymbol{\tau} \cdot \partial_t \boldsymbol{n})\boldsymbol{\tau} = -(\boldsymbol{n} \cdot \partial_s \partial_t \boldsymbol{X})\boldsymbol{\tau}$, we have

$$\begin{aligned}
\dot{W}(t) &= \frac{d}{dt} \int_0^{L(t)} \gamma(\boldsymbol{n}) ds = \frac{d}{dt} \int_0^1 \gamma(\boldsymbol{n}) \partial_\rho s d\rho = \int_0^1 (\gamma(\boldsymbol{n}) \partial_t \partial_\rho s + \nabla \gamma(\boldsymbol{n}) \cdot \partial_t \boldsymbol{n} \partial_\rho s) d\rho \\
&= \int_0^1 (\gamma(\boldsymbol{n})\boldsymbol{\tau} - (\boldsymbol{\xi} \cdot \boldsymbol{\tau})\boldsymbol{n}) \cdot \partial_s \partial_t \boldsymbol{X} \partial_\rho s \, d\rho = \Big(\boldsymbol{Z}_k(\boldsymbol{n}) \partial_s \boldsymbol{X}, \partial_s \partial_t \boldsymbol{X}\Big)_{\Gamma(t)} \\
&= -\Big(\partial_s \mu, \partial_s \mu\Big)_{\Gamma(t)} \leq 0,
\end{aligned}$$

which implies the energy dissipation in (2.27). □

2.2 The SP-PFEM discretization

2.2.1 Semi-discretization and its properties

Let $N > 0$ be an integer, the mesh size $h = 1/N$, the grid points $\rho_j = jh$ for $j = 0, 1, \ldots, N$, and the subintervals $I_j = [\rho_{j-1}, \rho_j]$ for $j = 1, 2, \ldots, N$. Then we can give a uniform partition of the torus $\mathbb{T}$ by $\mathbb{T} = [0, 1] = \bigcup_{j=1}^{N} I_j$. Moreover, the finite element subspace of $H^1(\mathbb{T})$ is given by

$$\mathbb{K}^h = \mathbb{K}^h(\mathbb{T}) := \{u^h \in C(\mathbb{T}) \mid u^h \mid_{I_j} \in \mathcal{P}_1,\ \forall j = 1, 2, \ldots, N\},$$

where $\mathcal{P}_1$ stands for the space of polynomials of degree at most 1.

Let the piecewise linear curve $\Gamma^h(t) := \boldsymbol{X}^h(\mathbb{T}, t)$, $\boldsymbol{X}^h(\cdot, t) = (x^h(\cdot, t), y^h(\cdot, t))^T \in [\mathbb{K}^h]^2$ be the numerical approximation of $\Gamma(t) := \boldsymbol{X}(\mathbb{T}, t)$, $\boldsymbol{X}(\cdot, t) \in [H^1(\mathbb{T})]^2$ and the piecewise linear function $\mu^h(\cdot, t) \in \mathbb{K}^h$ be the numerical approximation of $\mu(\cdot, t) \in H^1(\mathbb{T})$, where $(\boldsymbol{X}(\cdot, t), \mu(\cdot, t)) \in [H^1(\mathbb{T})]^2 \times H^1(\mathbb{T})$ is given by the variational problem (2.25). Then $\Gamma^h(t)$ is formed by ordered vectors $\{\boldsymbol{h}_j(t)\}_{j=1}^{N}$ and we assume that for $t \geq 0$, these vectors $\boldsymbol{h}_j(t)$ satisfy

$$h_{\min}(t) := \min_{1 \leq j \leq N} |\boldsymbol{h}_j(t)| > 0,\ \boldsymbol{h}_j(t) := \boldsymbol{X}^h(\rho_j, t) - \boldsymbol{X}^h(\rho_{j-1}, t),\ \forall j, \tag{2.28}$$

where $|\boldsymbol{h}_j(t)|$ is the length of the vector $\boldsymbol{h}_j(t)$ for $j = 1, 2, \ldots, N$.

The outward unit normal vector $\boldsymbol{n}^h$, the unit tangential vector $\boldsymbol{\tau}^h$, and the Cahn-Hoffman $\boldsymbol{\xi}$-vector $\boldsymbol{\xi}^h$ of the curve $\Gamma^h(t)$ are constant vectors in the interior of each interval I_j which can be computed by $\boldsymbol{h}_j(t)$ as

$$\boldsymbol{n}^h|_{I_j} = -\frac{(\boldsymbol{h}_j)^\perp}{|\boldsymbol{h}_j|} := \boldsymbol{n}_j^h, \quad \boldsymbol{\tau}^h|_{I_j} = \frac{\boldsymbol{h}_j}{|\boldsymbol{h}_j|} := \boldsymbol{\tau}_j^h, \quad \boldsymbol{\xi}^h|_{I_j} = \boldsymbol{\xi}(\boldsymbol{n}_j^h) := \boldsymbol{\xi}_j^h. \tag{2.29}$$

Furthermore, for two scalar-/vector-valued functions u and v in $\mathbb{K}^h$ or $[\mathbb{K}^h]^2$ respectively, the mass lumped inner product $\big(\cdot, \cdot\big)_{\Gamma^h}^h$ over Γ^h is defined as

$$\big(u,\ v\big)_{\Gamma^h}^h := \frac{1}{2} \sum_{j=1}^{N} |\boldsymbol{h}_j| \Big[\big(u \cdot v\big)(\rho_j^-) + \big(u \cdot v\big)(\rho_{j-1}^+)\Big], \tag{2.30}$$

where $u(\rho_j^\pm) = \lim\limits_{\rho \to \rho_j^\pm} u(\rho)$ for $0 \leq j \leq N$.

Suppose $\Gamma^h(0) := \boldsymbol{X}^h(\mathbb{T},0)$, $\boldsymbol{X}^h(\cdot,0) \in [\mathbb{K}^h]^2$ is the piecewise linear interpolation of $\boldsymbol{X}_0(s)$, where $\boldsymbol{X}^h(\rho=\rho_j,0) = \boldsymbol{X}_0(s=s_j^0)$ with $s_j^0 = L_0\rho_j$ for $j=0,1,\ldots,N$. Now we can state the following spatial semi-discretization of the symmetrized variational formulation (2.25): for a given initial curve $\Gamma^h(0) := \boldsymbol{X}^h(\mathbb{T},0)$, $\boldsymbol{X}^h(\cdot,0) \in [\mathbb{K}^h]^2$, find the solution $\Gamma^h(t) := \boldsymbol{X}^h(\mathbb{T},t)$, $\boldsymbol{X}^h(\cdot,t) = (x^h(\cdot,t), y^h(\cdot,t))^T \in [\mathbb{K}^h]^2$ and $\mu^h(\cdot,t) \in \mathbb{K}^h$, such that

$$\Big(\boldsymbol{n}^h \cdot \partial_t \boldsymbol{X}^h, \varphi^h\Big)_{\Gamma^h}^h + \Big(\partial_s \mu^h, \partial_s \varphi^h\Big)_{\Gamma^h}^h = 0, \qquad \forall \varphi^h \in \mathbb{K}^h, \tag{2.31a}$$

$$\Big(\mu^h, \boldsymbol{n}^h \cdot \boldsymbol{\omega}^h\Big)_{\Gamma^h}^h - \Big(\boldsymbol{Z}_k(\boldsymbol{n}^h)\partial_s \boldsymbol{X}^h, \partial_s \boldsymbol{\omega}^h\Big)_{\Gamma^h}^h = 0, \quad \forall \boldsymbol{\omega}^h \in [\mathbb{K}^h]^2, \tag{2.31b}$$

where

$$\begin{aligned} \boldsymbol{Z}_k(\boldsymbol{n}^h) &= \gamma(\boldsymbol{n}^h) I_2 - \boldsymbol{n}^h \boldsymbol{\xi}(\boldsymbol{n}^h)^T - \boldsymbol{\xi}(\boldsymbol{n}^h)(\boldsymbol{n}^h)^T + k(\boldsymbol{n}^h)\, \boldsymbol{n}^h (\boldsymbol{n}^h)^T \\ &= \gamma(\boldsymbol{n}^h) I_2 - \boldsymbol{n}^h (\boldsymbol{\xi}^h)^T - \boldsymbol{\xi}^h (\boldsymbol{n}^h)^T + k(\boldsymbol{n}^h)\, \boldsymbol{n}^h (\boldsymbol{n}^h)^T. \end{aligned}$$

Let $A^h(t)$ be the area/mass of the interior region of the piecewise linear closed curve $\Gamma^h(t)$, and $W^h(t)$ be its energy, which are defined as

$$A^h(t) = \frac{1}{2}\sum_{j=1}^{N} [x_j^h(t) - x_{j-1}^h(t)][y_j^h(t) + y_{j-1}^h(t)], \quad W^h(t) = \sum_{j=1}^{N} |\boldsymbol{h}_j(t)| \gamma(\boldsymbol{n}_j^h). \tag{2.32}$$

For the spatial semi-discretization (2.31), we also have

Proposition 2.2 (area/mass conservation and energy dissipation)**.** *Let* $\Big(\boldsymbol{X}^h(\cdot,\ t),\ \mu^h(\cdot,\ t)\Big) \in [\mathbb{K}^h]^2 \times \mathbb{K}^h$ *be a solution of the spatial semi-dicsretization* (2.31)*, then the area/mass* $A^h(t)$ *is conserved and the energy* $W^h(t)$ *is dissipative, i.e.*

$$A^h(t) \equiv A^h(0) = \frac{1}{2}\sum_{j=1}^{N} [x_0(s_j) - x_0(s_{j-1})][y_0(s_j) + y_0(s_{j-1})], \quad t \geq 0, \tag{2.33}$$

$$W^h(t) \leq W^h(t_1) \leq W^h(0) = \sum_{j=1}^{N} |\boldsymbol{h}_j(0)|\, \gamma(\boldsymbol{n}_j^h), \qquad t \geq t_1 \geq 0. \tag{2.34}$$

Proof. The proof of area/mass conservation is similar to the Proposition 3.1 in [109], thus we omit the details for brevity.

To prove the energy dissipation (2.34), noticing $\boldsymbol{n}_j^h \cdot \boldsymbol{n}_j^h = 1$ and $\boldsymbol{n}_j^h \cdot \boldsymbol{\tau}_j^h = 0$, we have

$$2\dot{\boldsymbol{n}}_j^h \cdot \boldsymbol{n}_j^h = 0, \qquad \dot{\boldsymbol{n}}_j^h \cdot \boldsymbol{\tau}_j^h + \dot{\boldsymbol{\tau}}_j^h \cdot \boldsymbol{n}_j^h = 0; \qquad\qquad 1 \le j \le N, \tag{2.35}$$

which immediately implies

$$\dot{\boldsymbol{n}}_j^h = (\dot{\boldsymbol{n}}_j^h \cdot \boldsymbol{n}_j^h)\boldsymbol{n}_j^h + (\dot{\boldsymbol{n}}_j^h \cdot \boldsymbol{\tau}_j^h)\boldsymbol{\tau}_j^h = -(\dot{\boldsymbol{\tau}}_j^h \cdot \boldsymbol{n}_j^h)\boldsymbol{\tau}_j^h = -\frac{\dot{\boldsymbol{h}}_j \cdot \boldsymbol{n}_j^h}{|\boldsymbol{h}_j|}\boldsymbol{\tau}_j^h, \ 1 \le j \le N. \tag{2.36}$$

Differentiating $W^h(t)$ in (2.32) with respect to t, noticing (2.35) and (2.36), we obtain

$$\begin{aligned}
\dot{W}^h(t) &= \frac{d}{dt}\left(\sum_{j=1}^{N} |\boldsymbol{h}_j(t)|\, \gamma(\boldsymbol{n}_j^h)\right) = \sum_{j=1}^{N}\left(\gamma(\boldsymbol{n}_j^h)\frac{d}{dt}|\boldsymbol{h}_j(t)| + \nabla\gamma(\boldsymbol{n}_j^h)\cdot\dot{\boldsymbol{n}}_j^h\,|\boldsymbol{h}_j(t)|\right)\\
&= \sum_{j=1}^{N}\Big(\gamma(\boldsymbol{n}_j^h)\boldsymbol{\tau}_j^h\cdot\dot{\boldsymbol{h}}_j(t) - \nabla\gamma(\boldsymbol{n}_j^h)\cdot\boldsymbol{\tau}_j^h\,\boldsymbol{n}_j^h\cdot\dot{\boldsymbol{h}}_j(t)\Big)\\
&= \sum_{j=1}^{N}|\boldsymbol{h}_j(t)|\left(\gamma(\boldsymbol{n}_j^h)\boldsymbol{\tau}_j^h - \nabla\gamma(\boldsymbol{n}_j^h)\cdot\boldsymbol{\tau}_j^h\,\boldsymbol{n}_j^h\right)\cdot\frac{\dot{\boldsymbol{h}}_j(t)}{|\boldsymbol{h}_j(t)|}.
\end{aligned} \tag{2.37}$$

Noting

$$\partial_s\boldsymbol{X}^h\big|_{I_j} = \frac{\boldsymbol{h}_j(t)}{|\boldsymbol{h}_j(t)|}, \quad \partial_s\partial_t\boldsymbol{X}^h\big|_{I_j} = \frac{1}{|\boldsymbol{h}_j(t)|}\,\partial_t\boldsymbol{X}^h\big|_{I_j} = \frac{\dot{\boldsymbol{h}}_j(t)}{|\boldsymbol{h}_j(t)|}, \quad 1 \le j \le N, \tag{2.38}$$

and using (2.31b) with $\boldsymbol{\omega}^h = \partial_t\boldsymbol{X}^h$ and (2.31a) with $\varphi^h = \mu^h$, we get

$$\begin{aligned}
\dot{W}^h(t) &= \sum_{j=1}^{N}|\boldsymbol{h}_j(t)|\,\left(Z_k(\boldsymbol{n}_j^h)\boldsymbol{\tau}_j^h\right)\cdot\frac{\dot{\boldsymbol{h}}_j(t)}{|\boldsymbol{h}_j(t)|}\\
&= \sum_{j=1}^{N}|\boldsymbol{h}_j(t)|\,\left(Z_k(\boldsymbol{n}_j^h)\,\partial_s\boldsymbol{X}^h\big|_{I_j}\right)\cdot\left(\partial_s\partial_t\boldsymbol{X}^h\right)\big|_{I_j}\\
&= \left(Z_k(\boldsymbol{n}_j^h)\partial_s\boldsymbol{X}^h, \partial_s\partial_t\boldsymbol{X}^h\right)_{\Gamma^h}^h = \left(\mu^h, \boldsymbol{n}^h\cdot\partial_t\boldsymbol{X}^h\right)_{\Gamma^h}^h\\
&= -\left(\partial_s\mu^h,\ \partial_s\mu^h\right)_{\Gamma^h}^h \le 0, \qquad t \ge 0,
\end{aligned} \tag{2.39}$$

which implies the energy dissipation in (2.34). □

2.2.2 Full-discretization

Let $\tau > 0$ be the time step size, and $t_m = m\tau$ be the discrete time levels for each $m \geq 0$. Let $\Gamma^m \triangleq \Gamma^{h,m} = \boldsymbol{X}^m(\mathbb{T})$, $\boldsymbol{X}^m(\cdot) = (x^m(\cdot), y^m(\cdot))^T \in [\mathbb{K}^h]^2$ is the numerical approximation of $\Gamma^h(t_m) = \boldsymbol{X}^h(\mathbb{T}, t_m)$, $\boldsymbol{X}^h(\cdot, t_m) \in [\mathbb{K}^h]^2$ and $\mu^m(\cdot) \in \mathbb{K}^h$ be the numerical approximation of $\mu^h(\cdot, t_m) \in \mathbb{K}^h$ for each $m \geq 0$, where $(\boldsymbol{X}^h(\cdot, t), \mu^h(\cdot, t))$ is the solution of the semi-discretization (2.31). Similarly, Γ^m is formed by the ordered vectors $\{\boldsymbol{h}_j^m\}_{j=1}^N$ defined by

$$\boldsymbol{h}_j^m := \boldsymbol{X}^m(\rho_j) - \boldsymbol{X}^m(\rho_{j-1}), \qquad j = 1, 2, \ldots, N. \tag{2.40}$$

Again, for each $m \geq 0$, the outward unit normal vector $\boldsymbol{n}^m$, the unit tangential vector $\boldsymbol{\tau}^m$, and the Cahn-Hoffman $\boldsymbol{\xi}$-vector $\boldsymbol{\xi}^m$ of the curve Γ^m are constant vectors in the interior of each interval I_j which can be computed as

$$\boldsymbol{n}^m|_{I_j} = -\frac{(\boldsymbol{h}_j^m)^\perp}{|\boldsymbol{h}_j^m|} := \boldsymbol{n}_j^m, \quad \boldsymbol{\tau}^m|_{I_j} = \frac{\boldsymbol{h}_j^m}{|\boldsymbol{h}_j^m|} := \boldsymbol{\tau}_j^m, \quad \boldsymbol{\xi}^m|_{I_j} = \boldsymbol{\xi}(\boldsymbol{n}_j^m) := \boldsymbol{\xi}_j^m. \tag{2.41}$$

Following the idea in [13, 94] to design a symmetrized SP-PFEM for surface diffusion, i.e., using the backward Euler method in time and the information of the curve at current time step and next time step to linearly interpolate the normal vector, a symmetrized SP-PFEM discretization of (2.31) is given as: for a given initial curve $\Gamma^0 := \boldsymbol{X}^0(\mathbb{T})$, $\boldsymbol{X}^0(\cdot) \in [\mathbb{K}^h]^2$, for $m \geq 0$, find the curve $\Gamma^{m+1} := \boldsymbol{X}^{m+1}(\mathbb{T})$, $\boldsymbol{X}^{m+1}(\cdot) \in [\mathbb{K}^h]^2$ and the chemical potential $\mu^{m+1}(\cdot) \in \mathbb{K}^h$, such that

$$\left(\frac{\boldsymbol{X}^{m+1} - \boldsymbol{X}^m}{\tau} \cdot \boldsymbol{n}^{m+\frac{1}{2}}, \varphi^h\right)_{\Gamma^m}^h + \left(\partial_s \mu^{m+1}, \partial_s \varphi^h\right)_{\Gamma^m}^h = 0, \ \forall \varphi^h \in \mathbb{K}^h, \tag{2.42a}$$

$$\left(\mu^{m+1}, \boldsymbol{n}^{m+\frac{1}{2}} \cdot \boldsymbol{\omega}^h\right)_{\Gamma^m}^h - \left(\boldsymbol{Z}_k(\boldsymbol{n}^m)\partial_s \boldsymbol{X}^{m+1}, \partial_s \boldsymbol{\omega}^h\right)_{\Gamma^m}^h = 0, \ \forall \boldsymbol{\omega}^h \in [\mathbb{K}^h]^2, \tag{2.42b}$$

where s is the arclength parameter of Γ^m, and $\boldsymbol{n}^{m+\frac{1}{2}}$ and $\boldsymbol{Z}_k(\boldsymbol{n}^m)$ are defined as

$$\boldsymbol{n}^{m+\frac{1}{2}} := -\frac{1}{2}\left(\partial_s \boldsymbol{X}^m + \partial_s \boldsymbol{X}^{m+1}\right)^\perp = -\frac{1}{2}\frac{1}{|\partial_\rho \boldsymbol{X}^m|}\left(\partial_\rho \boldsymbol{X}^m + \partial_\rho \boldsymbol{X}^{m+1}\right)^\perp \tag{2.43}$$

$$\begin{aligned} \boldsymbol{Z}_k(\boldsymbol{n}^m) &= \gamma(\boldsymbol{n}^m) I_2 - \boldsymbol{n}^m \boldsymbol{\xi}(\boldsymbol{n}^m)^T - \boldsymbol{\xi}(\boldsymbol{n}^m)(\boldsymbol{n}^m)^T + k(\boldsymbol{n}^m)\, \boldsymbol{n}^m (\boldsymbol{n}^m)^T \\ &= \gamma(\boldsymbol{n}^m) I_2 - \boldsymbol{n}^m (\boldsymbol{\xi}^m)^T - \boldsymbol{\xi}^m (\boldsymbol{n}^m)^T + k(\boldsymbol{n}^m)\, \boldsymbol{n}^m (\boldsymbol{n}^m)^T, \end{aligned} \tag{2.44}$$

and for any scalar-/vector-valued function $f \in \mathbb{K}^h$ or $[\mathbb{K}^h]^2$ respectively, we compute its derivative with respect to the arclength parameter on Γ^m as $\partial_s f = |\partial_\rho \boldsymbol{X}^m|^{-1}\partial_\rho f$.

The above scheme is "weakly implicit" with only one nonlinear term introduced in (2.42a) and (2.42b), respectively. In particular, the nonlinear term is a polynomial function of degree at most two with respect to the components of $\boldsymbol{X}^{m+1}$ and μ^{m+1}. Again, similar to [13] for surface diffusion, the symmetrized fully-implicit SP-PFEM (2.42) can be efficiently and accurately solved by the Newton's iterative method in practical computations.

Remark 2.2. *The choice of $\boldsymbol{n}^{m+\frac{1}{2}}$ in (2.42) plays an essential role in the proof of the area conservation, but it makes the numerical scheme fully-implicit, i.e. a nonlinear system has to be solved at each time step. By replacing $\boldsymbol{n}^{m+\frac{1}{2}}$ with $\boldsymbol{n}^m$, we can easily construct a semi-implicit PFEM, where only a linear system has to be solved at each time step. Similar to the symmetrized fully-implicit SP-PFEM (2.42), the symmetrized semi-implicit PFEM can also be proved to be unconditionally energy-stable if $\gamma(\boldsymbol{n})$ satisfies the condition (2.48). Of course, the symmetrized semi-implicit PFEM does not conserve the area at the fully-discrete level.*

2.2.3 Structure-preserving properties

Let A^m be the area of the interior region of the piecewise linear closed curve Γ^m, and W^m $(m \geq 0)$ be its energy, which are defined as

$$A^m := \frac{1}{2}\sum_{j=1}^{N}\left(x_j^m - x_{j-1}^m\right)\left(y_j^m + y_{j-1}^m\right), \quad W^m := W(\Gamma^m) = \sum_{j=1}^{N}|\boldsymbol{h}_j^m|\gamma(\boldsymbol{n}_j^m). \tag{2.45}$$

Denote

$$F(\boldsymbol{n},\hat{\boldsymbol{n}}) = \frac{\gamma(\hat{\boldsymbol{n}})^2 - \gamma(\boldsymbol{n})^2 + 2\gamma(\boldsymbol{n})(\boldsymbol{\xi}\cdot\hat{\boldsymbol{n}}^\perp)(\boldsymbol{n}\cdot\hat{\boldsymbol{n}}^\perp)}{\gamma(\boldsymbol{n})(\boldsymbol{n}\cdot\hat{\boldsymbol{n}}^\perp)^2}, \qquad \forall \boldsymbol{n} \neq \pm\hat{\boldsymbol{n}} \in \mathbb{S}^1. \tag{2.46}$$

The minimal stabilizing function $k_0(\boldsymbol{n}):\ \mathbb{S}^1 \to \mathbb{R}^+$ is given as

$$k_0(\boldsymbol{n}) := \max_{\hat{\boldsymbol{n}}\in\mathbb{S}^1_{\boldsymbol{n}}} F(\boldsymbol{n},\hat{\boldsymbol{n}}), \qquad \text{with} \quad \mathbb{S}^1_{\boldsymbol{n}} := \left\{\hat{\boldsymbol{n}} \in \mathbb{S}^1 \mid \hat{\boldsymbol{n}}\cdot\boldsymbol{n} \geq 0\right\}, \qquad \boldsymbol{n} \in \mathbb{S}^1. \tag{2.47}$$

And our main result is the area conservation and unconditional energy stability in the fully-discrete level, which is stated as follows

Theorem 2.1 (area conservation and energy stablility)**.** *Suppose $\gamma(\boldsymbol{n})$ is an even function that satisfies the following energy-stable condition:*

$$\gamma(-\boldsymbol{n}) = \gamma(\boldsymbol{n}), \quad \forall \boldsymbol{n} \in \mathbb{S}^1, \qquad \gamma(\boldsymbol{p}) \in C^2(\mathbb{R}^2_*). \tag{2.48}$$

Then we can choose $k(\boldsymbol{n}) \geq k_0(\boldsymbol{n})$ in (2.42). Let $(\boldsymbol{X}^m(\cdot), \mu^m(\cdot)) \in [\mathbb{K}^h]^2 \times \mathbb{K}^h$ be a solution of the symmetrized SP-PFEM (2.42), then the area A^m in (2.45) is conserved and the surface energy W^m is decreasing, i.e.

$$A^m \equiv A^0 = \frac{1}{2}\sum_{j=1}^{N} \left(x_j^0 - x_{j-1}^0\right)\left(y_j^0 + y_{j-1}^0\right), \qquad m \geq 0. \tag{2.49}$$

$$W^{m+1} \leq W^m \leq \ldots \leq W^0 = \sum_{j=1}^{N} |\boldsymbol{h}_j^0|\, \gamma(\boldsymbol{n}_j^0), \qquad \forall m \geq 0. \tag{2.50}$$

Proof of area conservation

Define $\Gamma^h(\alpha) = \boldsymbol{X}^h(\cdot, \alpha)$ as the linear conbination of $\boldsymbol{X}^m$ and $\boldsymbol{X}^{m+1}$ as

$$\boldsymbol{X}^h(\cdot, \alpha) := (1-\alpha)\boldsymbol{X}^m(\cdot) + \alpha \boldsymbol{X}^{m+1}(\cdot),$$

when $\alpha = 0$, $\Gamma^h(\alpha)$ goes to Γ^m; and $\Gamma^h(\alpha)$ goes to Γ^{m+1} if $\alpha = 1$.

Denote the enclosed area by $\Gamma^h(\alpha)$ as $A(\alpha)$. By applying the Reynolds transport theorem to $A(\alpha)$ ([13, Theorem 2.1]), we obtain that

$$\begin{aligned}\frac{dA(\alpha)}{d\alpha} &= \int_{\Gamma^h(\alpha)} \partial_\alpha \boldsymbol{X}^h \cdot \boldsymbol{n}^h \, ds \\ &= \int_{\Gamma^m} (\boldsymbol{X}^{m+1} - \boldsymbol{X}^m) \cdot (-[(1-\alpha)\partial_s \boldsymbol{X}^m + \alpha \partial_s \boldsymbol{X}^{m+1}]^\perp) \, ds\end{aligned}$$

Integrate $\frac{dA(\alpha)}{d\alpha}$ from $\alpha = 0$ to $\alpha = 1$, we obtain

$$A(1) - A(0) = \left((\boldsymbol{X}^{m+1} - \boldsymbol{X}^m) \cdot \boldsymbol{n}^{m+\frac{1}{2}}, 1\right)_{\Gamma^m}^h$$

By taking $\varphi^h = 1$ in (2.42a), we obtain $A^{m+1} = A^m$, which leads to the area conservation. □

We leave the proof of the existence of $k_0(\boldsymbol{n})$ as well as the energy stability to the next section.

Remark 2.3. *In practical computations, if one does not want to solve a nonlinear coupled system at every time step, we also propose the following semi-implicit symmetrized energy-stable PFEM (ES-PFEM) discretization of (2.31) : for a given* $\Gamma^0 := \Gamma^h(0) \in [\mathbb{K}^h]^2$*, for* $m \geq 0$*, find the closed curve* $\Gamma^{m+1} := \boldsymbol{X}^{m+1}(\cdot) = (x^{m+1}(\cdot), y^{m+1}(\cdot))^T \in [\mathbb{K}^h]^2$ *and a chemical potential* $\mu^{m+1}(\cdot) \in \mathbb{K}^h$*, such that*

$$\Big(\frac{\boldsymbol{X}^{m+1}-\boldsymbol{X}^m}{\tau}\cdot\boldsymbol{n}^m,\ \varphi^h\Big)^h_{\Gamma^m} + \Big(\partial_s\mu^{m+1},\ \partial_s\varphi^h\Big)^h_{\Gamma^m} = 0, \qquad \forall\varphi^h\in\mathbb{K}^h, \tag{2.51a}$$

$$\Big(\mu^{m+1}, \boldsymbol{n}^m\cdot\boldsymbol{\omega}^h\Big)^h_{\Gamma^m} - \Big(\boldsymbol{Z}_k(\boldsymbol{n}^m)\partial_s\boldsymbol{X}^{m+1},\ \partial_s\boldsymbol{\omega}^h\Big)^h_{\Gamma^m} = 0, \quad \forall\boldsymbol{\omega}^h\in[\mathbb{K}^h]^2. \tag{2.51b}$$

Similar to the Theorem 4.1 in [109], we can prove the well-posedness result of the symmetrized ES-PFEM (2.51) under the same assumptions in [109, Theorem 4.1]. The only difference is here we use the positive definiteness of $\boldsymbol{Z}_k(\boldsymbol{n})$ *instead of the* $\boldsymbol{G}(\theta)$ *in [109].*

2.3 Proof of energy dissipation

In this section, we show first show under the condition (2.48) on $\gamma(\boldsymbol{n})$ is satisfied, the minimal stabilizing function $k_0(\boldsymbol{n})$ (2.47) is well defined, then prove the energy dissipation of the symmetrized SP-PFEM (2.42).

2.3.1 The stabilizing function

The function $F(\boldsymbol{n},\hat{\boldsymbol{n}})$ is continuous for $\boldsymbol{n}\neq\pm\hat{\boldsymbol{n}}$. Thus to show the maximum in (2.47) is finite, it suffices to extent the definition of $F(\boldsymbol{n},\hat{\boldsymbol{n}})$ to $\boldsymbol{n}=\pm\hat{\boldsymbol{n}}$.

Theorem 2.2 (existence of limit)**.** *For* $\gamma(\boldsymbol{p})\in C^2(\mathbb{R}^2_*)$*, we have*

$$\lim_{\substack{\hat{\boldsymbol{n}}\to\boldsymbol{n}\\ \hat{\boldsymbol{n}}\in\mathbb{S}^1}} F(\boldsymbol{n},\hat{\boldsymbol{n}}) = (\boldsymbol{n}^\perp)^T\mathbf{H}_\gamma(\boldsymbol{n})\boldsymbol{n}^\perp + \frac{|\boldsymbol{\xi}|^2}{\gamma(\boldsymbol{n})}, \qquad \forall\boldsymbol{n}\in\mathbb{S}^1. \tag{2.52}$$

Proof. Plugging the vector decomposition $\gamma(\boldsymbol{n}) = \boldsymbol{\xi}\cdot\boldsymbol{n} = (\boldsymbol{\xi}\cdot\hat{\boldsymbol{n}}^\perp)(\boldsymbol{n}\cdot\hat{\boldsymbol{n}}^\perp)+(\boldsymbol{\xi}\cdot\hat{\boldsymbol{n}})(\boldsymbol{n}\cdot\hat{\boldsymbol{n}})$

and $1 = \boldsymbol{n}\cdot\boldsymbol{n} = (\boldsymbol{n}\cdot\hat{\boldsymbol{n}}^{\perp})^2 + (\boldsymbol{n}\cdot\hat{\boldsymbol{n}})^2$ into (2.46), we get

$$\begin{aligned} F(\boldsymbol{n},\hat{\boldsymbol{n}}) &= \frac{\gamma(\hat{\boldsymbol{n}})^2 - \gamma(\boldsymbol{n})^2 + 2\gamma(\boldsymbol{n})^2 - 2\gamma(\boldsymbol{n})(\boldsymbol{\xi}\cdot\hat{\boldsymbol{n}})(\boldsymbol{n}\cdot\hat{\boldsymbol{n}})}{\gamma(\boldsymbol{n})|\boldsymbol{n}-\hat{\boldsymbol{n}}|^2(1-|\boldsymbol{n}-\hat{\boldsymbol{n}}|^2/4)} \\ &= \frac{\gamma(\hat{\boldsymbol{n}})^2 + \gamma(\boldsymbol{n})^2 - 2\gamma(\boldsymbol{n})(\boldsymbol{\xi}\cdot\hat{\boldsymbol{n}})(1-|\boldsymbol{n}-\hat{\boldsymbol{n}}|^2/2)}{\gamma(\boldsymbol{n})|\boldsymbol{n}-\hat{\boldsymbol{n}}|^2(1-|\boldsymbol{n}-\hat{\boldsymbol{n}}|^2/4)} \\ &= \frac{1}{1-|\boldsymbol{n}-\hat{\boldsymbol{n}}|^2/4}\left[\frac{\gamma(\hat{\boldsymbol{n}})^2 - \gamma(\boldsymbol{n})^2 - 2\gamma(\boldsymbol{n})(\boldsymbol{\xi}\cdot(\hat{\boldsymbol{n}}-\boldsymbol{n}))}{\gamma(\boldsymbol{n})|\boldsymbol{n}-\hat{\boldsymbol{n}}|^2} + \boldsymbol{\xi}\cdot\hat{\boldsymbol{n}}\right]. \end{aligned} \tag{2.53}$$

Here we use the following equality

$$\boldsymbol{n}\cdot\hat{\boldsymbol{n}} = \frac{|\boldsymbol{n}|^2 + |\hat{\boldsymbol{n}}|^2 - |\boldsymbol{n}-\hat{\boldsymbol{n}}|^2}{2} = 1 - \frac{|\boldsymbol{n}-\hat{\boldsymbol{n}}|^2}{2}.$$

Under the condition $\gamma(\boldsymbol{p}) \in C^2(\mathbb{R}^2_*)$, using Taylor expansion and noting $\nabla\gamma(\boldsymbol{p})^2 = 2\gamma(\boldsymbol{p})\nabla\gamma(\boldsymbol{p})$ and $\boldsymbol{\xi} = \nabla\gamma(\boldsymbol{p})|_{\boldsymbol{p}=\boldsymbol{n}}$, we obtain

$$\gamma(\boldsymbol{p})^2 - \gamma(\boldsymbol{n})^2 - 2\gamma(\boldsymbol{n})\boldsymbol{\xi}\cdot(\boldsymbol{p}-\boldsymbol{n}) = (\boldsymbol{p}-\boldsymbol{n})^T\left[\gamma(\boldsymbol{n})\mathbf{H}_\gamma(\boldsymbol{n}) + \boldsymbol{\xi}\boldsymbol{\xi}^T\right](\boldsymbol{p}-\boldsymbol{n}) + o(|\boldsymbol{p}-\boldsymbol{n}|^2).$$

For any $\boldsymbol{n} \in \mathbb{S}^1$, noting that

$$\lim_{\substack{\boldsymbol{p}\to\boldsymbol{n}^+ \\ \boldsymbol{p}\in\mathbb{S}^1}} \frac{\boldsymbol{p}-\boldsymbol{n}}{|\boldsymbol{p}-\boldsymbol{n}|} = \boldsymbol{n}^{\perp}, \quad \lim_{\substack{\boldsymbol{p}\to\boldsymbol{n}^- \\ \boldsymbol{p}\in\mathbb{S}^1}} \frac{\boldsymbol{p}-\boldsymbol{n}}{|\boldsymbol{p}-\boldsymbol{n}|} = -\boldsymbol{n}^{\perp},$$

where $\boldsymbol{p} \to \boldsymbol{n}^+/\boldsymbol{n}^-$ means $\boldsymbol{p}\cdot\boldsymbol{n}^{\perp} \geq 0/\leq 0$, respectively. We then get

$$\begin{aligned} \lim_{\substack{\boldsymbol{p}\to\boldsymbol{n}^+ \\ \boldsymbol{p}\in\mathbb{S}^1}} \frac{(\boldsymbol{p}-\boldsymbol{n})^T\left[\gamma(\boldsymbol{n})\mathbf{H}_\gamma(\boldsymbol{n}) + \boldsymbol{\xi}\boldsymbol{\xi}^T\right](\boldsymbol{p}-\boldsymbol{n})}{|\boldsymbol{p}-\boldsymbol{n}|^2} &= (\boldsymbol{n}^{\perp})^T\left[\gamma(\boldsymbol{n})\mathbf{H}_\gamma(\boldsymbol{n}) + \boldsymbol{\xi}\boldsymbol{\xi}^T\right]\boldsymbol{n}^{\perp}, \\ \lim_{\substack{\boldsymbol{p}\to\boldsymbol{n}^- \\ \boldsymbol{p}\in\mathbb{S}^1}} \frac{(\boldsymbol{p}-\boldsymbol{n})^T\left[\gamma(\boldsymbol{n})\mathbf{H}_\gamma(\boldsymbol{n}) + \boldsymbol{\xi}\boldsymbol{\xi}^T\right](\boldsymbol{p}-\boldsymbol{n})}{|\boldsymbol{p}-\boldsymbol{n}|^2} &= -(\boldsymbol{n}^{\perp})^T\left[\gamma(\boldsymbol{n})\mathbf{H}_\gamma(\boldsymbol{n}) + \boldsymbol{\xi}\boldsymbol{\xi}^T\right](-\boldsymbol{n}^{\perp}) \\ &= (\boldsymbol{n}^{\perp})^T\left[\gamma(\boldsymbol{n})\mathbf{H}_\gamma(\boldsymbol{n}) + \boldsymbol{\xi}\boldsymbol{\xi}^T\right]\boldsymbol{n}^{\perp}, \end{aligned}$$

thus we have

$$\begin{aligned} \lim_{\substack{\boldsymbol{p}\to\boldsymbol{n} \\ \boldsymbol{p}\in\mathbb{S}^1}} \frac{\gamma(\boldsymbol{p})^2 - \gamma(\boldsymbol{n})^2 - 2\gamma(\boldsymbol{n})\boldsymbol{\xi}\cdot(\boldsymbol{p}-\boldsymbol{n})}{|\boldsymbol{p}-\boldsymbol{n}|^2} &= (\boldsymbol{n}^{\perp})^T\left[\gamma(\boldsymbol{n})\mathbf{H}_\gamma(\boldsymbol{n}) + \boldsymbol{\xi}\boldsymbol{\xi}^T\right]\boldsymbol{n}^{\perp} \\ &= \gamma(\boldsymbol{n})\,(\boldsymbol{n}^{\perp})^T\mathbf{H}_\gamma(\boldsymbol{n})\boldsymbol{n}^{\perp} + (\boldsymbol{\xi}\cdot\boldsymbol{n}^{\perp})^{\mathbf{2}}. \end{aligned} \tag{2.54}$$

Combining (2.53) and (2.54), noting (1.3) to get $\gamma(\boldsymbol{n}) = \boldsymbol{\xi}\cdot\boldsymbol{n}$, we obtain

$$\begin{aligned}\lim_{\substack{\hat{\boldsymbol{n}}\to\boldsymbol{n}\\ \hat{\boldsymbol{n}}\in\mathbb{S}^1}} F(\boldsymbol{n},\hat{\boldsymbol{n}}) &= \frac{1}{\gamma(\boldsymbol{n})}\lim_{\substack{\boldsymbol{p}\to\boldsymbol{n}\\ \boldsymbol{p}\in\mathbb{S}^1}} \frac{\gamma(\boldsymbol{p})^2-\gamma(\boldsymbol{n})^2-2\gamma(\boldsymbol{n})\boldsymbol{\xi}\cdot(\boldsymbol{p}-\boldsymbol{n})}{|\boldsymbol{p}-\boldsymbol{n}|^2}+\boldsymbol{\xi}\cdot\boldsymbol{n}\\ &= (\boldsymbol{n}^\perp)^T\mathbf{H}_\gamma(\boldsymbol{n})\boldsymbol{n}^\perp+\frac{(\boldsymbol{\xi}\cdot\boldsymbol{n}^\perp)^2}{\gamma(\boldsymbol{n})}+\boldsymbol{\xi}\cdot\boldsymbol{n}\\ &= (\boldsymbol{n}^\perp)^T\mathbf{H}_\gamma(\boldsymbol{n})\boldsymbol{n}^\perp+\frac{|\boldsymbol{\xi}|^2}{\gamma(\boldsymbol{n})}. \end{aligned}\tag{2.55}$$

The proof is completed. □

Under the condition (2.48), for any $\boldsymbol{n}\in\mathbb{S}^1$, it is easy to see that $F(\boldsymbol{n},\hat{\boldsymbol{n}})$ is a continuous function for $\hat{\boldsymbol{n}}\in\mathbb{S}^1$ with $\hat{\boldsymbol{n}}\neq-\boldsymbol{n}$. Furthermore, if $\gamma(\boldsymbol{n})=\gamma(-\boldsymbol{n})$, then we know $F(\boldsymbol{n},\hat{\boldsymbol{n}})\in C^1(\mathbb{S}^1\times\mathbb{S}^1)$. This, together with the above Theorem, suggests us to define the following

Theorem 2.3 (existence of stabilizing function)**.** *Under the condition* (2.48) *on* $\gamma(\boldsymbol{n})$ *and assume* $k(\boldsymbol{n})\geq k_0(\boldsymbol{n})$ *for* $\boldsymbol{n}\in\mathbb{S}^1$ *in* (2.16)*, we have*

$$\gamma(\boldsymbol{n})[(\hat{\boldsymbol{n}}^\perp)^T\boldsymbol{Z}_k(\boldsymbol{n})\hat{\boldsymbol{n}}^\perp]\geq\gamma(\hat{\boldsymbol{n}})^2,\qquad\forall\boldsymbol{n},\,\hat{\boldsymbol{n}}\in\mathbb{S}^1.\tag{2.56}$$

In addition, we have an alternative definition of $k_0(\boldsymbol{n})$ *in* (2.47) *as*

$$k_0(\boldsymbol{n})=\inf\left\{k(\boldsymbol{n})\mid\gamma(\boldsymbol{n})[(\hat{\boldsymbol{n}}^\perp)^T\boldsymbol{Z}_k(\boldsymbol{n})\hat{\boldsymbol{n}}^\perp]\geq\gamma(\hat{\boldsymbol{n}})^2,\quad\forall\hat{\boldsymbol{n}}\in\mathbb{S}^1\right\},\quad\boldsymbol{n}\in\mathbb{S}^1.\tag{2.57}$$

Proof. Assume $k(\boldsymbol{n})\geq k_0(\boldsymbol{n})$ for $\boldsymbol{n}\in\mathbb{S}^1$. For any $\boldsymbol{n}\in\mathbb{S}^1$, when $\hat{\boldsymbol{n}}\in\mathbb{S}^1_{\boldsymbol{n}}$, i.e. $\hat{\boldsymbol{n}}\cdot\boldsymbol{n}\geq0$, plugging (2.16) into the left hand of (2.56), noting (2.46) and (2.47), we have

$$\begin{aligned}\gamma(\boldsymbol{n})[(\hat{\boldsymbol{n}}^\perp)^T\boldsymbol{Z}_k(\boldsymbol{n})\hat{\boldsymbol{n}}^\perp] &= \gamma(\boldsymbol{n})^2-2\gamma(\boldsymbol{n})(\boldsymbol{\xi}\cdot\hat{\boldsymbol{n}}^\perp)(\boldsymbol{n}\cdot\hat{\boldsymbol{n}}^\perp)+\gamma(\boldsymbol{n})k(\boldsymbol{n})(\boldsymbol{n}\cdot\hat{\boldsymbol{n}}^\perp)^2\\ &\geq \gamma(\boldsymbol{n})^2-2\gamma(\boldsymbol{n})(\boldsymbol{\xi}\cdot\hat{\boldsymbol{n}}^\perp)(\boldsymbol{n}\cdot\hat{\boldsymbol{n}}^\perp)+\gamma(\boldsymbol{n})k_0(\boldsymbol{n})(\boldsymbol{n}\cdot\hat{\boldsymbol{n}}^\perp)^2\\ &\geq \gamma(\boldsymbol{n})^2-2\gamma(\boldsymbol{n})(\boldsymbol{\xi}\cdot\hat{\boldsymbol{n}}^\perp)(\boldsymbol{n}\cdot\hat{\boldsymbol{n}}^\perp)+\gamma(\boldsymbol{n})F(\boldsymbol{n},\hat{\boldsymbol{n}})(\boldsymbol{n}\cdot\hat{\boldsymbol{n}}^\perp)^2\\ &= \gamma(\hat{\boldsymbol{n}})^2. \end{aligned}\tag{2.58}$$

On the other hand, when $\hat{\boldsymbol{n}}\cdot\boldsymbol{n}<0$, then $-\hat{\boldsymbol{n}}\cdot\boldsymbol{n}>0$, from (2.58) by replacing $\hat{\boldsymbol{n}}$ by $-\hat{\boldsymbol{n}}$ and noting $\gamma(-\hat{\boldsymbol{n}})=\gamma(\hat{\boldsymbol{n}})$, we have

$$\gamma(\boldsymbol{n})[(\hat{\boldsymbol{n}}^\perp)^T\boldsymbol{Z}_k(\boldsymbol{n})\hat{\boldsymbol{n}}^\perp]=\gamma(\boldsymbol{n})[(-\hat{\boldsymbol{n}}^\perp)^T\boldsymbol{Z}_k(\boldsymbol{n})(-\hat{\boldsymbol{n}}^\perp)]\geq\gamma(-\hat{\boldsymbol{n}})^2=\gamma(\hat{\boldsymbol{n}})^2.\tag{2.59}$$

Combining (2.58) and (2.59), we get (2.56) immediately.

From the above proof, it is easy to see that

$$\gamma(\boldsymbol{n})[(\hat{\boldsymbol{n}}^{\perp})^T \boldsymbol{Z}_{k_0}(\boldsymbol{n})\hat{\boldsymbol{n}}^{\perp}] \geq \gamma(\hat{\boldsymbol{n}})^2, \qquad \forall \boldsymbol{n},\, \hat{\boldsymbol{n}} \in \mathbb{S}^1,$$

which implies

$$k_0(\boldsymbol{n}) \geq \inf\left\{k(\boldsymbol{n}) \mid \gamma(\boldsymbol{n})[(\hat{\boldsymbol{n}}^{\perp})^T \boldsymbol{Z}_k(\boldsymbol{n})\hat{\boldsymbol{n}}^{\perp}] \geq \gamma(\hat{\boldsymbol{n}})^2, \quad \forall \hat{\boldsymbol{n}} \in \mathbb{S}^1\right\}, \quad \forall \boldsymbol{n} \in \mathbb{S}^1. \tag{2.60}$$

On the other hand, suppose $\boldsymbol{Z}_k(\boldsymbol{n})$ satisfies (2.56), then we have

$$\gamma(\boldsymbol{n})\left(\gamma(\boldsymbol{n}) - 2(\boldsymbol{\xi}\cdot\hat{\boldsymbol{n}}^{\perp})(\boldsymbol{n}\cdot\hat{\boldsymbol{n}}^{\perp}) + k(\boldsymbol{n})(\boldsymbol{n}\cdot\hat{\boldsymbol{n}}^{\perp})^2\right) \geq \gamma(\hat{\boldsymbol{n}})^2, \qquad \forall \hat{\boldsymbol{n}} \in \mathbb{S}^1_{\boldsymbol{n}}, \tag{2.61}$$

which implies

$$k(\boldsymbol{n}) \geq \frac{\gamma(\hat{\boldsymbol{n}})^2 - \gamma(\boldsymbol{n})^2 + 2\gamma(\boldsymbol{n})(\boldsymbol{\xi}\cdot\hat{\boldsymbol{n}}^{\perp})(\boldsymbol{n}\cdot\hat{\boldsymbol{n}}^{\perp})}{\gamma(\boldsymbol{n})(\boldsymbol{n}\cdot\hat{\boldsymbol{n}}^{\perp})^2} = F(\boldsymbol{n},\hat{\boldsymbol{n}}), \quad \forall \hat{\boldsymbol{n}} \in \mathbb{S}^1_{\boldsymbol{n}}. \tag{2.62}$$

By condition (2.48), this inequality holds for all $\hat{\boldsymbol{n}} \in \mathbb{S}^1$. Thus we get $k(\boldsymbol{n}) \geq k_0(\boldsymbol{n})$, which implies

$$k_0(\boldsymbol{n}) \leq \inf\left\{k(\boldsymbol{n}) \mid \gamma(\boldsymbol{n})[(\hat{\boldsymbol{n}}^{\perp})^T \boldsymbol{Z}_k(\boldsymbol{n})\hat{\boldsymbol{n}}^{\perp}] \geq \gamma(\hat{\boldsymbol{n}})^2, \quad \forall \hat{\boldsymbol{n}} \in \mathbb{S}^1\right\}, \quad \forall \boldsymbol{n} \in \mathbb{S}^1. \tag{2.63}$$

Combining (2.60) and (2.63), we obtain (2.57) immediately. □

Remark 2.4. *Assume* $\boldsymbol{n} = (-\sin\theta, \cos\theta)^T$ *(*$\theta \in [-\pi, \pi]$*) and* $\hat{\boldsymbol{n}} = (-\sin\hat{\theta}, \cos\hat{\theta})^T$*, then the problem to find the minimal stabilizing function* $k_0(\boldsymbol{n})$ *defined in* (2.47) *can be reformulated as an optimization problem in term of the single variable* $\hat{\theta}$*, i.e.,*

$$\tilde{k}_0(\theta) := k_0(\boldsymbol{n}) = k_0(-\sin\theta, \cos\theta) = \max_{\hat{\theta}\in[\theta-\frac{\pi}{2},\theta+\frac{\pi}{2}]} \tilde{F}^{\theta}(\hat{\theta}), \qquad -\pi \leq \theta \leq \pi, \tag{2.64}$$

where

$$\tilde{F}^{\theta}(\hat{\theta}) := F(\boldsymbol{n},\hat{\boldsymbol{n}}) = \frac{\bar{\gamma}(\hat{\theta})^2 - \bar{\gamma}(\theta)^2 - 2\bar{\gamma}(\theta)\bar{\gamma}'(\theta)\cos(\hat{\theta}-\theta)\sin(\hat{\theta}-\theta)}{\bar{\gamma}(\theta)\sin^2(\hat{\theta}-\theta)} + 2\bar{\gamma}(\theta), \tag{2.65}$$

with $\bar{\gamma}(\theta) := \gamma(\boldsymbol{n}) = \gamma(-\sin\theta, \cos\theta)$ *and* $\bar{\gamma}(\hat{\theta}) := \gamma(\hat{\boldsymbol{n}}) = \gamma(-\sin\hat{\theta}, \cos\hat{\theta})$ *by noting* $\boldsymbol{\xi} = \boldsymbol{\xi}(\boldsymbol{n}) = \bar{\gamma}(\theta)\boldsymbol{n} - \bar{\gamma}'(\theta)\boldsymbol{n}^{\perp}$*. Thus for a given* $\boldsymbol{n}$ *(or* θ*), we can obtain* $k_0(\boldsymbol{n})$ *(or* $\tilde{k}_0(\theta)$*) by numerically solving the above single-variable optimization problem* (2.64)*.*

Corollary 2.1 (positivity of the minimal stabilizing function)**.** *Assume* (2.56) *is satisfied, then* $\boldsymbol{Z}_k(\boldsymbol{n})$ *is a symmetric positive definite matrix and*

$$\gamma(-\boldsymbol{n}) = \gamma(\boldsymbol{n}), \qquad k_0(\boldsymbol{n}) > 0, \qquad \forall \boldsymbol{n} \in \mathbb{S}^1. \tag{2.66}$$

Proof. Taking $\hat{\boldsymbol{n}} = -\boldsymbol{n}$ in (2.56), noting the first equality in (2.58), we get $\gamma(\boldsymbol{n})^2 \geq \gamma(-\boldsymbol{n})^2$ which suggests $\gamma(-\boldsymbol{n})^2 \geq \gamma(-(-\boldsymbol{n}))^2 = \gamma(\boldsymbol{n})^2$, and thus we obtain the first equality in (2.66) since $\gamma(\boldsymbol{n}) > 0$. From (2.56), we get $\boldsymbol{Z}_k(\boldsymbol{n})$ is symmetric positive definite, which implies $k(\boldsymbol{n}) = \mathrm{Tr}(\boldsymbol{Z}_k(\boldsymbol{n})) \geq k_0(\boldsymbol{n}) = \mathrm{Tr}(\boldsymbol{Z}_{k_0}(\boldsymbol{n})) > 0$ for $\boldsymbol{n} \in \mathbb{S}^1$. □

If we consider from the anisotropic surface energy $\gamma(\boldsymbol{n})$ to its corresponding minimal stabilizing function $k_0(\boldsymbol{n})$ defined in (2.57) (or (2.47)) as a mapping, then it is a sub-linear mapping, i.e., positively homogeneous and subadditive.

Lemma 2.2 (positive homogeneity and subadditivity)**.** *Assume* $k_0(\boldsymbol{n})$*,* $k_1(\boldsymbol{n})$ *and* $k_2(\boldsymbol{n})$ *be the minimal stabilizing functions for the anisotropic surface energies* $\gamma(\boldsymbol{n})$*,* $\gamma_1(\boldsymbol{n})$ *and* $\gamma_2(\boldsymbol{n})$*, respectively, then we have*

(i) if $\gamma_1(\boldsymbol{n}) = c\,\gamma(\boldsymbol{n})$ *with* $c > 0$*, then* $k_1(\boldsymbol{n}) = c\,k_0(\boldsymbol{n})$ *for* $\boldsymbol{n} \in \mathbb{S}^1$*, and*

(ii) if $\gamma(\boldsymbol{n}) = \gamma_1(\boldsymbol{n}) + \gamma_2(\boldsymbol{n})$*, then* $k_0(\boldsymbol{n}) \leq k_1(\boldsymbol{n}) + k_2(\boldsymbol{n})$ *for* $\boldsymbol{n} \in \mathbb{S}^1$*.*

Proof. From (1.3), we get

$$\boldsymbol{\xi} = \nabla\gamma(\boldsymbol{p})\big|_{\boldsymbol{p}=\boldsymbol{n}}, \qquad \boldsymbol{\xi}_1 = \nabla\gamma_1(\boldsymbol{p})\big|_{\boldsymbol{p}=\boldsymbol{n}}, \qquad \boldsymbol{\xi}_2 = \nabla\gamma_2(\boldsymbol{p})\big|_{\boldsymbol{p}=\boldsymbol{n}}. \tag{2.67}$$

(i) If $\gamma_1(\boldsymbol{n}) = c\,\gamma(\boldsymbol{n})$, we get $\boldsymbol{\xi}_1 = c\,\boldsymbol{\xi}$. This, together with (2.46), implies

$$F_1(\boldsymbol{n}, \hat{\boldsymbol{n}}) = \frac{\gamma_1(\hat{\boldsymbol{n}})^2 - \gamma_1(\boldsymbol{n})^2 + 2\gamma_1(\boldsymbol{n})(\boldsymbol{\xi}_1 \cdot \hat{\boldsymbol{n}}^\perp)(\boldsymbol{n} \cdot \hat{\boldsymbol{n}}^\perp)}{\gamma_1(\boldsymbol{n})(\boldsymbol{n} \cdot \hat{\boldsymbol{n}}^\perp)^2} = c\,F(\boldsymbol{n}, \hat{\boldsymbol{n}}). \tag{2.68}$$

Combining (2.68) and (2.47), we obtain the positive homogeneity immediately.

(ii) If $\gamma(\boldsymbol{n}) = \gamma_1(\boldsymbol{n}) + \gamma_2(\boldsymbol{n})$, then $\boldsymbol{\xi} = \boldsymbol{\xi}_1 + \boldsymbol{\xi}_2$, thus we have

$$\begin{aligned} \boldsymbol{Z}_{k_1+k_2}(\boldsymbol{n}) &= \gamma(\boldsymbol{n})I_2 - \boldsymbol{\xi}\boldsymbol{n}^T - \boldsymbol{n}\boldsymbol{\xi}^T + (k_1(\boldsymbol{n}) + k_2(\boldsymbol{n}))\boldsymbol{n}\boldsymbol{n}^T \\ &= \boldsymbol{Z}^{(1)}_{k_1}(\boldsymbol{n}) + \boldsymbol{Z}^{(2)}_{k_2}(\boldsymbol{n}), \end{aligned}$$

where

$$\boldsymbol{Z}_{k_1}^{(1)}(\boldsymbol{n}) = \gamma_1(\boldsymbol{n})I_2 - \boldsymbol{\xi}_1\boldsymbol{n}^T - \boldsymbol{n}(\boldsymbol{\xi}_1)^T + k_1(\boldsymbol{n})\boldsymbol{n}\boldsymbol{n}^T,$$
$$\boldsymbol{Z}_{k_2}^{(2)}(\boldsymbol{n}) = \gamma_2(\boldsymbol{n})I_2 - \boldsymbol{\xi}_2\boldsymbol{n}^T - \boldsymbol{n}(\boldsymbol{\xi}_2)^T + k_2(\boldsymbol{n})\boldsymbol{n}\boldsymbol{n}^T.$$

By using Cauchy inequality, we get

$$\begin{aligned}
&\gamma(\boldsymbol{n})[(\hat{\boldsymbol{n}}^\perp)^T\boldsymbol{Z}_{k_1+k_2}(\boldsymbol{n})\hat{\boldsymbol{n}}^\perp] \\
&\geq \left(\sqrt{\gamma_1(\boldsymbol{n})[(\hat{\boldsymbol{n}}^\perp)^T\boldsymbol{Z}_{k_1}^{(1)}(\boldsymbol{n})\hat{\boldsymbol{n}}^\perp]} + \sqrt{\gamma_2(\boldsymbol{n})[(\hat{\boldsymbol{n}}^\perp)^T\boldsymbol{Z}_{k_2}^{(2)}(\boldsymbol{n})\hat{\boldsymbol{n}}^\perp]}\right)^2 \\
&\geq (\gamma_1(\hat{\boldsymbol{n}}) + \gamma_2(\hat{\boldsymbol{n}}))^2 = \gamma(\hat{\boldsymbol{n}})^2. \qquad (2.69)
\end{aligned}$$

Combining (2.69) and (2.57), we get $k_0(\boldsymbol{n}) \leq k_1(\boldsymbol{n}) + k_2(\boldsymbol{n})$ for $\boldsymbol{n} \in \mathbb{S}^1$. □

2.3.2 The proof

For the symmetrized SP-PFEM (2.42) , we have:

Theorem 2.4 (energy dissipation)**.** *Assume the surface energy matrix $\boldsymbol{Z}_k(\boldsymbol{n})$ satisfies (2.56), then the symmetrized SP-PFEM (2.42) is unconditionally energy stable, i.e. for any $\tau > 0$, we have*

$$W^{m+1} \leq W^m \leq \ldots \leq W^0 = \sum_{j=1}^{N} |\boldsymbol{h}_j^0|\,\gamma(\boldsymbol{n}_j^0), \qquad \forall m \geq 0. \qquad (2.70)$$

Proof. Under (2.56), we know that $\boldsymbol{Z}_k(\boldsymbol{n})$ is symmetric positive definite. Thus we have

$$\Big(\boldsymbol{Z}_k(\boldsymbol{n})\boldsymbol{u}, \boldsymbol{u} - \boldsymbol{v}\Big) \geq \frac{1}{2}\Big(\boldsymbol{Z}_k(\boldsymbol{n})\boldsymbol{u}, \boldsymbol{u}\Big) - \frac{1}{2}\Big(\boldsymbol{Z}_k(\boldsymbol{n})\boldsymbol{v}, \boldsymbol{v}\Big), \quad \forall \boldsymbol{u}, \boldsymbol{v} \in \mathbb{R}^2. \qquad (2.71)$$

Using (2.19) and $\boldsymbol{\xi} \cdot \boldsymbol{n} = \gamma(\boldsymbol{n})$, we get

$$(\partial_s \boldsymbol{X}^m)^T\boldsymbol{Z}_k(\boldsymbol{n}^m)\partial_s\boldsymbol{X}^m = \boldsymbol{\tau}^m \cdot (\boldsymbol{\xi}^m)^\perp = \gamma(\boldsymbol{n}^m). \qquad (2.72)$$

Combining (2.72) and (2.71), noting $\boldsymbol{Z}_k(\boldsymbol{n})$ satisfies (2.56), we obtain

$$\begin{aligned}
&\Big(\boldsymbol{Z}_k(\boldsymbol{n}^m)\partial_s\boldsymbol{X}^{m+1},\ \partial_s\boldsymbol{X}^{m+1}-\partial_s\boldsymbol{X}^m\Big)_{\Gamma^m}^h+\int_{\Gamma^m}\gamma(\boldsymbol{n}^m)ds\\
&\geq\frac{1}{2}\Big(\boldsymbol{Z}_k(\boldsymbol{n}^m)\partial_s\boldsymbol{X}^{m+1},\ \partial_s\boldsymbol{X}^{m+1}\Big)_{\Gamma^m}^h+\frac{1}{2}\int_{\Gamma^m}\gamma(\boldsymbol{n}^m)ds\\
&=\sum_{j=1}^N\frac{\left(\boldsymbol{h}_j^{m+1}\right)^T\boldsymbol{Z}_k(\boldsymbol{n}_j^m)\boldsymbol{h}_j^{m+1}+\gamma(\boldsymbol{n}_j^m)|\boldsymbol{h}_j^m|^2}{2|\boldsymbol{h}_j^m|}\\
&\geq\sum_{j=1}^N|\boldsymbol{h}_j^{m+1}|\sqrt{\left(\left(\boldsymbol{n}_j^{m+1}\right)^\perp\right)^T\boldsymbol{Z}_k(\boldsymbol{n}_j^m)\left(\boldsymbol{n}_j^{m+1}\right)^\perp\gamma(\boldsymbol{n}_j^m)}\\
&\geq\sum_{j=1}^N|\boldsymbol{h}_j^{m+1}|\sqrt{\frac{\gamma^2(\boldsymbol{n}_j^{m+1})}{\gamma(\boldsymbol{n}_j^m)}\gamma(\boldsymbol{n}_j^m)}=\sum_{j=1}^N|\boldsymbol{h}_j^{m+1}|\gamma(\boldsymbol{n}_j^{m+1})=\int_{\Gamma^{m+1}}\gamma(\boldsymbol{n}^{m+1})ds.
\end{aligned}\tag{2.73}$$

Taking $\varphi^h=\mu^{m+1}$ in (2.42a) and $\boldsymbol{\omega}^h=\boldsymbol{X}^{m+1}-\boldsymbol{X}^m$ in (2.42b) and combining the inequality (2.73), we get

$$\begin{aligned}
W^{m+1}-W^m&=\int_{\Gamma^{m+1}}\gamma(\boldsymbol{n}^{m+1})ds-\int_{\Gamma^m}\gamma(\boldsymbol{n}^m)ds\\
&\leq\Big(\boldsymbol{Z}_k(\boldsymbol{n}^m)\partial_s\boldsymbol{X}^{m+1},\ \partial_s\boldsymbol{X}^{m+1}-\partial_s\boldsymbol{X}^m\Big)_{\Gamma^m}^h\\
&=-\tau\Big(\partial_s\mu^{m+1},\ \partial_s\mu^{m+1}\Big)_{\Gamma^m}^h\leq 0,\quad\forall m\geq 0,
\end{aligned}\tag{2.74}$$

which implies the energy dissipation (2.70) for the symmetrized SP-PFEM (2.42). □

Combining Theorems 2.3 and 2.4, finally we have

Corollary 2.2 (energy dissipation). *Assume $\gamma(\boldsymbol{n})$ satisfies (2.48) and taking $k(\boldsymbol{n})\geq k_0(\boldsymbol{n})$ in (2.16), then the symmetrized SP-PFEM (2.42) is unconditionally energy stable.*

2.3.3 Explicit formulas for the minimal stabilizing function

Here we give explicit formulas of the minimal stabilizing function $k_0(\boldsymbol{n})$ for several popular anisotropic surface energies $\gamma(\boldsymbol{n})$ in applications. Denote

$$\boldsymbol{J}=\begin{pmatrix}0&-1\\1&0\end{pmatrix},\qquad\boldsymbol{Z}_0(\boldsymbol{n})=\begin{pmatrix}1&n_1n_2\\n_1n_2&1\end{pmatrix},\qquad\forall\,\boldsymbol{n}=\begin{pmatrix}n_1\\n_2\end{pmatrix}\in\mathbb{S}^1.$$

Lemma 2.3 (Riemannian metric)**.** *When $\gamma(\boldsymbol{n})$ is taken as the Riemannian metric anisotropic surface energy (2.4), we have*

$$k_0(\boldsymbol{n}) = \gamma(\boldsymbol{n})^{-1} Tr(G), \qquad \boldsymbol{Z}_{k_0}(\boldsymbol{n}) = \gamma(\boldsymbol{n})^{-1} \boldsymbol{J}^T G \boldsymbol{J}, \qquad \forall \boldsymbol{n} \in \mathbb{S}^1. \tag{2.75}$$

Proof. First we assume $G = \left(\begin{smallmatrix} a & b \\ b & c \end{smallmatrix}\right)$ with $a > 0$ and $ac - b^2 > 0$, then the minimal stabilizing function $k_0(\boldsymbol{n})$ becomes

$$\gamma(\boldsymbol{n})^{-1}\mathrm{Tr}(G) = \gamma(\boldsymbol{n})^{-1}(a + c) := k_1(\boldsymbol{n}). \tag{2.76}$$

By using $\boldsymbol{\xi}$ in (2.5), the corresponding surface energy matrix with respect to $k_1(\boldsymbol{n})$ can be given as

$$\begin{aligned}
\boldsymbol{Z}_{k_1}(\boldsymbol{n}) &= \gamma(\boldsymbol{n}) I_2 - \boldsymbol{\xi}\boldsymbol{n}^T - \boldsymbol{n}\boldsymbol{\xi}^T + k_1(\boldsymbol{n})\boldsymbol{n}\boldsymbol{n}^T \\
&= \gamma(\boldsymbol{n}) I_2 - \gamma(\boldsymbol{n})^{-1} G\boldsymbol{n}\boldsymbol{n}^T - \gamma(\boldsymbol{n})^{-1}\boldsymbol{n}\boldsymbol{n}^T G + \gamma(\boldsymbol{n})^{-1}(a+c)\boldsymbol{n}\boldsymbol{n}^T \\
&= \gamma(\boldsymbol{n})^{-1} \begin{pmatrix} \gamma(\boldsymbol{n})^2 - 2(an_1^2 + bn_1n_2) + (a+c)n_1^2 & * \\ -(an_1n_2 + bn_2^2) - (bn_1^2 + cn_1n_2) + (a+c)n_1n_2 & * \end{pmatrix} \\
&= \gamma(\boldsymbol{n})^{-1} \begin{pmatrix} c & -b \\ -b & a \end{pmatrix} = \gamma(\boldsymbol{n})^{-1} \boldsymbol{J}^T G \boldsymbol{J},
\end{aligned} \tag{2.77}$$

where the $*$ means the entry can be deduced in the same way. By direct computations, we obtain

$$\begin{aligned}
\gamma(\boldsymbol{n})\,(\hat{\boldsymbol{n}}^\perp)^T \boldsymbol{Z}_{k_1}(\boldsymbol{n})\hat{\boldsymbol{n}}^\perp - \gamma(\hat{\boldsymbol{n}})^2 &= (\hat{\boldsymbol{n}}^\perp)^T \boldsymbol{J}^T G \boldsymbol{J}\hat{\boldsymbol{n}}^\perp - \gamma(\hat{\boldsymbol{n}})^2 \\
&= \hat{\boldsymbol{n}}^T G\hat{\boldsymbol{n}} - \gamma(\hat{\boldsymbol{n}})^2 = 0.
\end{aligned}$$

From the alternative definition of $k_0(\boldsymbol{n})$ in (2.57), we obtain $k_0(\boldsymbol{n}) \le k_1(\boldsymbol{n}) = \gamma(\boldsymbol{n})^{-1}(a + c)$.

On the other hand, we take $\hat{\boldsymbol{n}} \to \boldsymbol{n}$ in $F(\boldsymbol{n}, \hat{\boldsymbol{n}})$. By applying (2.52) and the

Hessian matrix derived in (2.5) and (2.15), we then have

$$
\begin{aligned}
&(\boldsymbol{n}^{\perp})^T\mathbf{H}_\gamma\boldsymbol{n}^{\perp}+\frac{|\boldsymbol{\xi}|^2}{\gamma(\boldsymbol{n})}\\
&=\gamma(\boldsymbol{n})^{-3}\left((ac-b^2)(n_2^4+2n_1^2n_2^2+n_1^4)+(an_1+bn_2)^2+(bn_1+cn_2)^2\right)\\
&=\gamma(\boldsymbol{n})^{-3}(ac+a^2n_1^2+2abn_1n_2+2acn_1n_2+c^2n_2^2)\\
&=\gamma(\boldsymbol{n})^{-3}(an_1^2+2bn_1n_2+cn_2^2)(a+c)\\
&=\gamma(\boldsymbol{n})^{-1}(a+c)=k_1(\boldsymbol{n}),
\end{aligned}
$$

which means $k_0(\boldsymbol{n})\geq k_1(\boldsymbol{n})=\gamma(\boldsymbol{n})^{-1}(a+c)$ by (2.47), hence $k_0(\boldsymbol{n})=\gamma(\boldsymbol{n})^{-1}\mathrm{Tr}(\boldsymbol{G})$.

□

Remark 2.5. *By taking $k(\boldsymbol{n})=k_0(\boldsymbol{n})$ in (2.16) and using the semi-implicit discretization $\boldsymbol{n}^m$ instead of $\boldsymbol{n}^{m+\frac{1}{2}}$, the SP-PFEM (2.42) collapses to the BGN formulation used in [17].*

Lemma 2.4 (l^r-norm metric)**.** *When $\gamma(\boldsymbol{n})$ is taken as the l^r-norm metric anisotropic surface energy (2.7), we have*

(i) when $r=4$, $k_0(\boldsymbol{n})=2\gamma(\boldsymbol{n})^{-3}$ and $\boldsymbol{Z}_{k_0}(\boldsymbol{n})=\gamma(\boldsymbol{n})^{-3}\boldsymbol{Z}_0(\boldsymbol{n})$, and

(ii) when $r=6$, $k_0(\boldsymbol{n})=2\gamma(\boldsymbol{n})^{-5}(n_1^4+n_1^2n_2^2+n_2^4)$.

Proof. (i) When $r=4$, a direct computation shows

$$
\begin{aligned}
&\gamma(\boldsymbol{n})\,(\hat{\boldsymbol{n}}^{\perp})^T\boldsymbol{Z}_{k_0}(\boldsymbol{n})\hat{\boldsymbol{n}}^{\perp}-\gamma(\hat{\boldsymbol{n}})^2\\
&=\frac{1-2n_1n_2\hat{n}_1\hat{n}_2}{\sqrt{n_1^4+n_2^4}}-\sqrt{\hat{n}_1^4+\hat{n}_2^4}\\
&=\frac{(n_1^2+n_2^2)^2+(\hat{n}_1^2+\hat{n}_2^2)^2-4n_1n_2\hat{n}_1\hat{n}_2-2\sqrt{\hat{n}_1^4+\hat{n}_2^4}\sqrt{n_1^4+n_2^4}}{2\sqrt{n_1^4+n_2^4}}\\
&\geq\frac{(n_1^2+n_2^2)^2+(\hat{n}_1^2+\hat{n}_2^2)^2-4n_1n_2\hat{n}_1\hat{n}_2-n_1^4-n_2^4-\hat{n}_1^4-\hat{n}_2^4}{2\sqrt{n_1^4+n_2^4}}\\
&=\frac{(n_1n_2-\hat{n}_1\hat{n}_2)^2}{\sqrt{n_1^4+n_2^4}}\geq 0,\qquad\forall\boldsymbol{n},\hat{\boldsymbol{n}}\in\mathbb{S}^1.
\end{aligned}
$$

By Theorem 2.3, we get $k_0(\boldsymbol{n}) \le 2\gamma(\boldsymbol{n})^{-3}$. On the other hand, by taking $\hat{\boldsymbol{n}} = (n_2, n_1)^T \in \mathbb{S}^1$ in (2.46) and the $\boldsymbol{\xi}$ vector given in (2.9), we obtain

$$\begin{aligned} F(\boldsymbol{n}, \hat{\boldsymbol{n}}) &= \frac{2\gamma(\boldsymbol{n})(\gamma(\boldsymbol{n})^{-3}(n_1^3, n_2^3)\cdot(-n_1, n_2))(-n_1^2+n_2^2)}{\gamma(\boldsymbol{n})(-n_1^2+n_2^2)^2} \\ &= 2\gamma(\boldsymbol{n})^{-3}\frac{(-n_1^2+n_2^2)^2(n_2^2+n_1^2)}{(-n_1^2+n_2^2)^2} = k_0(\boldsymbol{n}). \end{aligned}$$

By (2.47), we know that $k_0(\boldsymbol{n}) \ge 2\gamma(\boldsymbol{n})^{-3}$, hence $k_0(\boldsymbol{n}) = 2\gamma(\boldsymbol{n})^{-3}$.

(ii) When $r = 6$, a direct computation shows

$$\begin{aligned} &\gamma(\boldsymbol{n})\,(\hat{\boldsymbol{n}}^\perp)^T Z_{k_0}(\boldsymbol{n})\hat{\boldsymbol{n}}^\perp - \gamma(\hat{\boldsymbol{n}})^2 \\ &= \gamma(\boldsymbol{n})^{-4}\,(1 - n_1^2n_2^2 - 2n_1n_2\hat{n}_1\hat{n}_2) - \sqrt[3]{\hat{n}_1^6+\hat{n}_2^6} \\ &= \gamma(\boldsymbol{n})^{-4}\left(1 - n_1^2n_2^2 - 2n_1n_2\hat{n}_1\hat{n}_2 - \sqrt[3]{(n_1^6+n_2^6)^2(\hat{n}_1^6+\hat{n}_2^6)}\right) \\ &\ge \gamma(\boldsymbol{n})^{-4}\left(\frac{2(n_1^2+n_2^2)^3+(\hat{n}_1^2+\hat{n}_2^2)^3}{3} - n_1^2n_2^2 - 2n_1n_2\hat{n}_1\hat{n}_2 - \frac{2(n_1^6+n_2^6)+(\hat{n}_1^6+\hat{n}_2^6)}{3}\right) \\ &= \gamma(\boldsymbol{n})^{-4}\left(\frac{6n_1^4n_2^2+6n_1^2n_2^4+3\hat{n}_1^4\hat{n}_2^2+3\hat{n}_1^2\hat{n}_2^4}{3} - n_1^2n_2^2 - 2n_1n_2\hat{n}_1\hat{n}_2\right) \\ &= \gamma(\boldsymbol{n})^{-4}\left(2n_1^2n_2^2(n_1^2+n_2^2) + \hat{n}_1^2\hat{n}_2^2(\hat{n}_1^2+\hat{n}_2^2) - n_1^2n_2^2 - 2n_1n_2\hat{n}_1\hat{n}_2\right) \\ &= \gamma(\boldsymbol{n})^{-4}(n_1n_2 - \hat{n}_1\hat{n}_2)^2 \ge 0, \qquad \forall \boldsymbol{n}, \hat{\boldsymbol{n}} \in \mathbb{S}^1. \end{aligned}$$

By Theorem 2.3, we get $k_0(\boldsymbol{n}) \le 2\gamma(\boldsymbol{n})^{-5}(n_2^4 + n_2^2n_1^2 + n_1^4)$. On the other hand, by taking $\hat{\boldsymbol{n}} = (n_2, n_1)^T \in \mathbb{S}^1$ in (2.46) and the $\boldsymbol{\xi}$ vector given in (2.9), we obtain

$$\begin{aligned} F(\boldsymbol{n}, \hat{\boldsymbol{n}}) &= \frac{2\gamma(\boldsymbol{n})(\gamma(\boldsymbol{n})^{-5}(n_1^5, n_2^5)\cdot(-n_1, n_2))(-n_1^2+n_2^2)}{\gamma(\boldsymbol{n})(-n_1^2+n_2^2)^2} \\ &= 2\gamma(\boldsymbol{n})^{-5}\frac{(-n_1^2+n_2^2)^2(n_2^4+n_2^2n_1^2+n_1^4)}{(-n_1^2+n_2^2)^2} = k_0(\boldsymbol{n}). \end{aligned}$$

By (2.47), we know that $k_0(\boldsymbol{n}) \ge 2\gamma(\boldsymbol{n})^{-5}(n_2^4 + n_2^2n_1^2 + n_1^4)$, hence $k_0(\boldsymbol{n}) = 2\gamma(\boldsymbol{n})^{-5}(n_2^4 + n_2^2n_1^2 + n_1^4)$. □

Lemma 2.5 (m-fold)**.** *When $\gamma(\boldsymbol{n})$ is taken as the m-fold anisotropy (2.10), we have*

(i) when $\gamma(\boldsymbol{n}) = 1 + \beta\cos 2\theta$, then

$$k_0(\boldsymbol{n}) = 4 - 2\gamma(\boldsymbol{n}) + \frac{4\beta^2}{\gamma(\boldsymbol{n})}; \text{ and} \tag{2.78}$$

(ii) when $\gamma(\boldsymbol{n}) = 1 + \beta\cos 4\theta$, *then*

$$k_0(\boldsymbol{n}) \le 2\gamma(\boldsymbol{n}) + \frac{16\beta + 16\beta^2}{\gamma(\boldsymbol{n})} : k_1(\boldsymbol{n}). \tag{2.79}$$

Proof. For the m-fold anisotropy $\bar{\gamma}(\theta) = \gamma(\boldsymbol{n}) = 1 + \beta\cos m\theta$, we know that $\bar{\gamma}'(\theta) = -m\beta\sin m\theta$. The $\tilde{F}^\theta(\hat{\theta})$ given in (2.65) is

$$\begin{aligned}\tilde{F}^\theta(\hat{\theta}) =& 2(1+\beta\cos m\theta) \\ &+ \frac{(1+\beta\cos m\hat{\theta})^2 - (1+\beta\cos m\theta)^2}{(1+\beta\cos m\theta)\sin^2(\hat{\theta}-\theta)} + \frac{m\beta\sin m\theta\ \sin(2(\hat{\theta}-\theta))}{\sin^2(\hat{\theta}-\theta)}.\end{aligned} \tag{2.80}$$

(i) For the 2-fold anisotropy, i.e. $m = 2$, by applying Mathematica to (2.80), we get

$$\tilde{F}^\theta(\hat{\theta}) = 4 - 2(1+\beta\cos 2\theta) + \frac{2\beta^2(1-\cos 2(\hat{\theta}+\theta))}{1+\beta\cos 2\theta}. \tag{2.81}$$

Thus by (2.64) in Remark 2.4, we obtain

$$k_0(\boldsymbol{n}) = \max_{\hat{\theta}\in[\theta-\frac{\pi}{2},\theta+\frac{\pi}{2}]} \tilde{F}^\theta(\hat{\theta}) \le 4 - 2\gamma(\boldsymbol{n}) + \frac{4\beta^2}{\gamma(\boldsymbol{n})}. \tag{2.82}$$

On the other hand, by taking $\hat{\theta} = \frac{\pi}{2} - \theta$ in (2.81), we obtain

$$\tilde{F}^\theta(\frac{\pi}{2} - \theta) = 4 - 2\gamma(\boldsymbol{n}) + \frac{4\beta^2}{\gamma(\boldsymbol{n})} \le k_0(\boldsymbol{n}). \tag{2.83}$$

By combining (2.82) and (2.83), we know $k_0(\boldsymbol{n}) = 4 - 2\gamma(\boldsymbol{n}) + \frac{4\beta^2}{\gamma(\boldsymbol{n})}$, which valids (2.78).

(ii) For the 4-fold anisotropy, i.e. $m = 4$, by applying Mathematica to (2.80), we get

$$\begin{aligned}\tilde{F}^\theta(\hat{\theta}) =& 2\gamma(\boldsymbol{n}) - \frac{16\beta\cos(\hat{\theta}-\theta)\cos(\hat{\theta}+3\theta)}{\gamma(\boldsymbol{n})} \\ &- \frac{4\beta^2\cos(\hat{\theta}-\theta)(2\cos(\hat{\theta}+7\theta) + \cos(3\hat{\theta}+5\theta) + \cos(5\hat{\theta}+3\theta))}{\gamma(\boldsymbol{n})}.\end{aligned} \tag{2.84}$$

Thus by (2.64) in Remark 2.4, we obtain

$$k_0(\boldsymbol{n}) = \max_{\hat{\theta}\in[\theta-\frac{\pi}{2},\theta+\frac{\pi}{2}]} \tilde{F}^\theta(\hat{\theta}) \le 2\gamma(\boldsymbol{n}) + \frac{16\beta + 16\beta^2}{\gamma(\boldsymbol{n})} = k_1(\boldsymbol{n}), \tag{2.85}$$

which valids (2.79). □

2.4 Numerical results

In this section, we numerically implement the symmetrized SP-PFEM (2.42) for simulating the evolution of closed curves under anisotropic surface diffusion. Numerical results demonstrate the high performance of the proposed scheme, e.g., the spatial/temporal convergence rates, energy dissipation, area conservation, and asymptotic quasi-uniform mesh distribution. Here, the distance between two closed curves Γ_1 and Γ_2 is measured by the manifold distance $M(\Gamma_1, \Gamma_2)$ which was introduced in the reference [155].

Since formally the scheme is first-order accurate in time and second-order accurate in space, the mesh size h and the time step τ are chosen as $\tau = \mathcal{O}(h^2)$, e.g. $\tau = h^2$, except where noted. Let Γ^m be the numerical approximation of $\Gamma^h(t = t_m = m\tau)$ with mesh size h and time step τ, the numerical error is then measured as

$$e^h(t_m) := M(\Gamma^m, \Gamma(t = t_m)), \qquad m \geq 0. \tag{2.86}$$

Because the exact solution can not be obtained analytically, we choose fine meshes $h = h_e$, $\tau = \tau_e$ to obtain $\Gamma(t = t_m)$ numerically, e.g. $h_e = 2^{-8}$ and $\tau_e = 2^{-16}$.

The normalized area loss and the mesh ratio $R^h(t_m)$, which indicates the mesh quality during evolution, are defined as

$$\frac{\Delta A^h(t_m)}{A^h(0)} := \frac{A^h(t_m) - A^h(0)}{A^h(0)}, \quad R^h(t_m) := \frac{\max_{1\leq j\leq N} |\boldsymbol{h}_j^m|}{\min_{1\leq j\leq N} |\boldsymbol{h}_j^m|}, \quad m \geq 0, \tag{2.87}$$

where $A^h(t_m)$ is the area of the inner region enclosed by Γ^m.

In the following simulations, the initial shape is always chosen as an ellipse with length 4 and width 1 except where noted, and the tolerance of the Newton iteration in the SP-PFEM (2.42) is chosen as 10^{-12}.

2.4.1 Convergence rates and energy dissipation

In order to test convergence rates of the symmetrized SP-PFEM (2.42), without loss of generality, we choose the following two kinds of anisotropic surface energies:

- Case I: the Riemannian metric anisotropic surface energy (2.4) with $G = \mathrm{diag}(1, 2)$, and the corresponding minimal stabilizing function $k_0(\boldsymbol{n})$ is given explicitly in (2.75);
- Case II: the l^r-norm metric anisotropic surface energy (2.7) with $r = 4$ and the corresponding minimal stabilizing function $k_0(\boldsymbol{n})$ is given explicitly in Lemma 2.4.

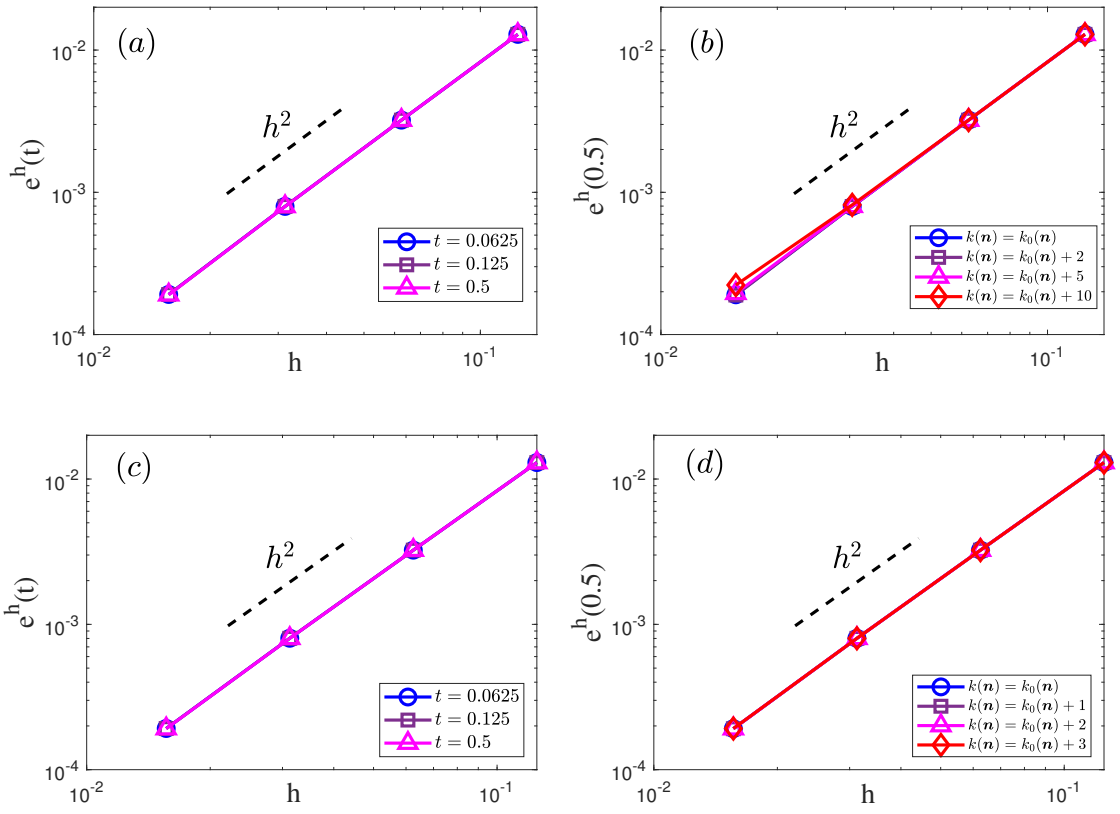

Figure 2.1: Spatial convergence rates of the symmetrized SP-PFEM (2.42) for: Case I at different times with $k(\boldsymbol{n}) = k_0(\boldsymbol{n})$ in (2.75) (a), and at time $t = 0.5$ for different $k(\boldsymbol{n})$ (b); and Case II at different times with $k(\boldsymbol{n}) = k_0(\boldsymbol{n})$ in Lemma 2.4 (c), and at time $t = 0.5$ for different $k(\boldsymbol{n})$ (d).

Fig. 2.1 plots spatial convergence rates of the symmetrized SP-PFEM at different times under a fixed value $k(\boldsymbol{n})$ in (2.16) or different values of $k(\boldsymbol{n})$ under a fixed

time $t = 0.5$. Fig. 2.2 depicts time evolution of the normalized area loss and the normalized energy under different parameters. Fig. 2.3 depicts time evolution of the mesh ratio $R^h(t)$ under different mesh sizes h, time steps τ and $k(\boldsymbol{n})$ for the above two cases.

From Figs. 2.1–2.3, we can obtain the following results for the symmetrized SP-PFEM (2.42) for simulating anisotropic surface diffusion of closed curves:

(i) The symmetrized SP-PFEM is second-order accurate in space (cf. Fig. 2.1);

(ii) The area is conserved numerically up to the round-off error around 10^{-16} (cf. Fig. 2.2(a)&(d));

(iii) The number of Newton iteration at each time step is around 2 to 4, thus it is very efficient (cf. Fig. 2.2(a)&(d));

(iv) The symmetrized SP-PFEM is unconditionally energy-stable when $k(\boldsymbol{n})$ satisfies the energy dissipation condition in Theorem 4.5 (cf. Fig. 2.2(b)-(c)&(e)-(f));

(v) The mesh ratio $R^h(t = t_m)$ approaches a constant C when $t \gg 1$ for each case, which indicates asymptotic quasi-uniform mesh distribution, no matter what kind of anisotropic surface energy is used as long as it is weakly anisotropic.

2.4.2 Application for morphological evolutions

Here, we use the symmetrized SP-PFEM (2.42) to simulate the morphological evolution under different anisotropic surface energies, i.e., morphological evolutions of closed curves from a 4×1 rectangle towards their corresponding equilibrium shapes. Fig. 2.4 depicts morphological evolutions for the four different weakly anisotropic surface energies including (a) the regularized l^1-norm metric (2.14) with $\varepsilon = 0.1$ by taking $k(\boldsymbol{n}) = k_1(\boldsymbol{n}) := \frac{1.01}{\sqrt{n_1^2+0.01n_2^2}} + \frac{1.01}{\sqrt{0.01n_1^2+n_2^2}}$, (b) the l^4-norm metric (2.7) with $r = 4$ and $k(\boldsymbol{n}) = k_0(\boldsymbol{n})$ given in Lemma 2.4, (c) 2-fold anisotropic energy (2.10) with $m = 2$, $\theta_0 = \frac{\pi}{2}$ and $\beta = \frac{1}{3}$ and $k(\boldsymbol{n}) = k_0(\boldsymbol{n})$ given in (2.78), and (d) the Riemannian metric (2.4) with $G = \mathrm{diag}(1, 2)$ and $k(\boldsymbol{n}) = k_0(\boldsymbol{n})$ given in (2.75). Figs. 2.5 and 2.6 show morphological evolutions and the normalized energy $\frac{W^h(t)}{W^h(0)}$ under

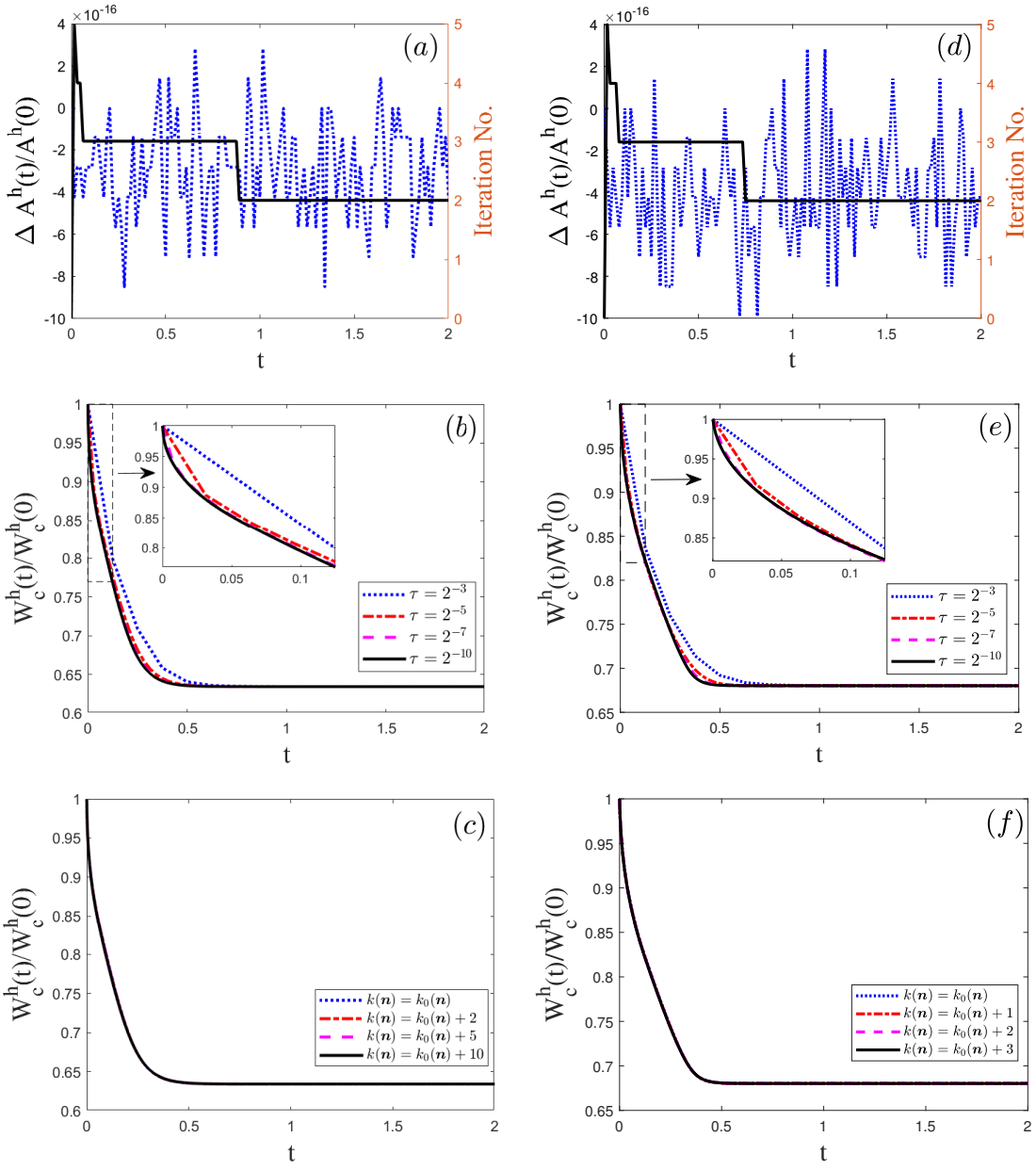

Figure 2.2: Time evolution of the normalized area loss $\frac{\Delta A^h(t)}{A^h(0)}$ (first row, blue dashed line) and iteration number (first row, black line) and the normalized energy $\frac{W^h(t)}{W^h(0)}$ (second and third rows) for: Case I with $k(\boldsymbol{n}) = k_0(\boldsymbol{n})$ in (2.75) for $h = 2^{-3}$ (a), and with $h = 2^{-3}$ for different τ (b), and with $h = 2^{-3}$ for different $k(\boldsymbol{n})$ (c); and Case II with $k(\boldsymbol{n}) = k_0(\boldsymbol{n})$ in Lemma 2.4 for $h = 2^{-3}$ (d), and with $h = 2^{-3}$ for different τ (e), and with $h = 2^{-3}$ for different $k(\boldsymbol{n})$ (f).

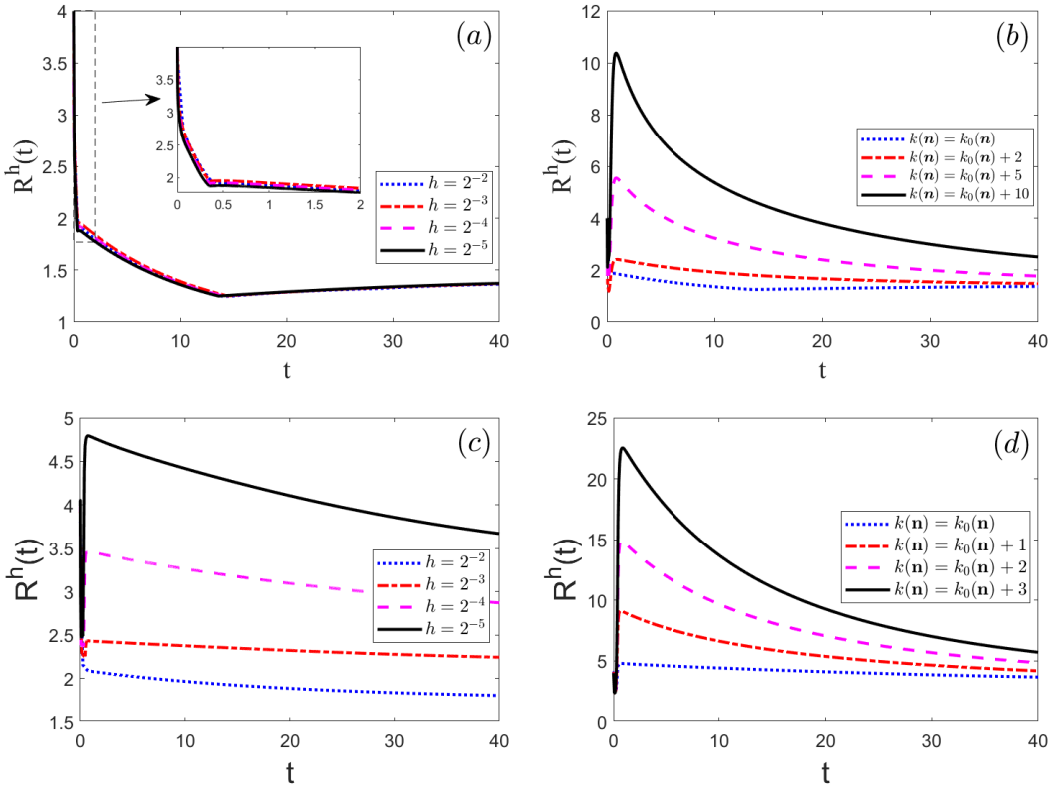

Figure 2.3: Time evolution of the mesh ratio $R^h(t)$ for: Case I with $k(\boldsymbol{n}) = k_0(\boldsymbol{n})$ in (2.75) for different h (a), and with $h = 2^{-5}$ for different $k(\boldsymbol{n})$ (b); and Case II with $k(\boldsymbol{n}) = k_0(\boldsymbol{n})$ in Lemma 2.4 for different h (c), and with $h = 2^{-5}$ for different $k(\boldsymbol{n})$ (d).

the 2-fold $\gamma(\boldsymbol{n}) = 1 + \frac{3}{5}\cos(2\theta)$ and the 4-fold $\gamma(\boldsymbol{n}) = 1 + \frac{3}{10}\cos(4\theta)$, with $k(\boldsymbol{n})$ given in (2.78), (2.79), respectively, which are both strongly anisotropic surface energies. The Frank diagrams of the above anisotropic energies are all shown in Fig. 2.7.

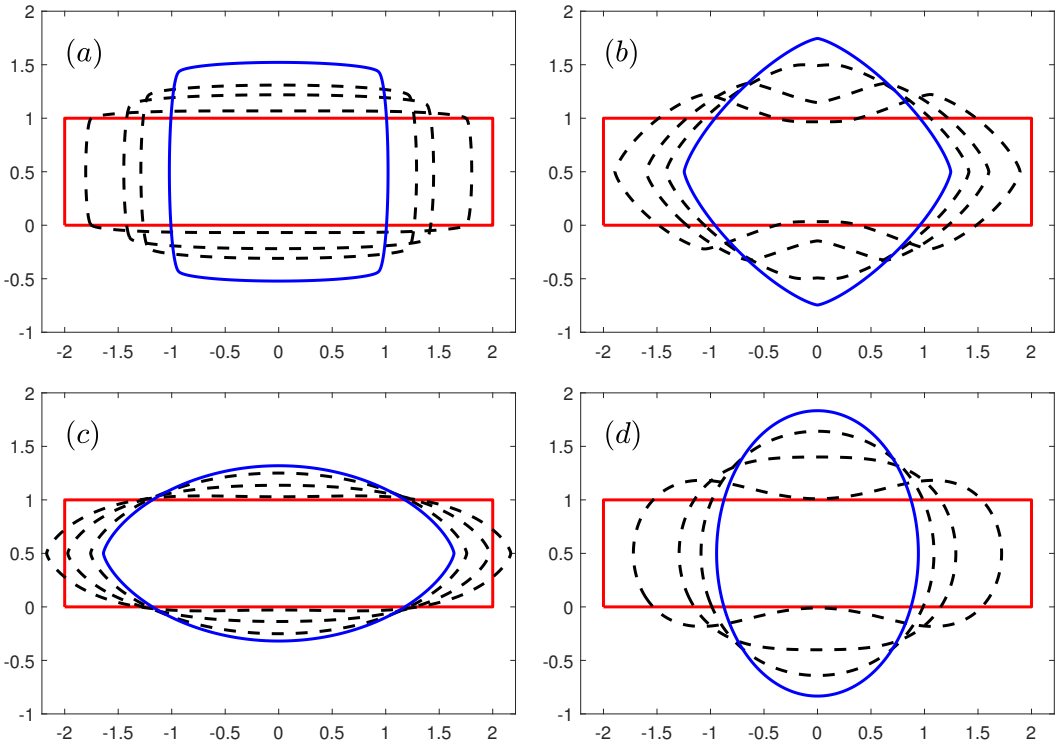

Figure 2.4: Morphological evolutions of a close rectangular curve under anisotropic surface diffusion with different anisotropic surface energies: (a) regularized l^1-norm metric $\gamma(\boldsymbol{n}) = \sqrt{n_1^2 + 0.01n_2^2} + \sqrt{0.01n_1^2 + n_2^2}$; (b) l^4-norm metric $\gamma(\boldsymbol{n}) = \sqrt[4]{n_1^4 + n_2^4}$; (c) 2-fold $\gamma(\boldsymbol{n}) = 1 + \frac{1}{3}\cos(2(\theta - \frac{\pi}{2}))$; and (d) Riemannian metric $\gamma(\boldsymbol{n}) = \sqrt{\boldsymbol{n}^T G \boldsymbol{n}}$, where $G = \mathrm{diag}(1, 2)$ and the parameters $h = 2^{-6}, \tau = h^2$, and the red line, black dashed line and blue line represent the initial shape, intermediate shape and equilibrium shape, respectively.

As shown in Fig. 2.4(a)–(b), if we choose the anisotropy as the regularized l^1-norm metric or the l^4-norm metric, the equilibrium shapes are almost "faceting" squares; for 2-fold anisotropy (c.f. 2.4(c)), the number of edges in its equilibrium shape is exactly two; and for the Riemannian metric anisotropic energy (c.f. 2.4(d)),

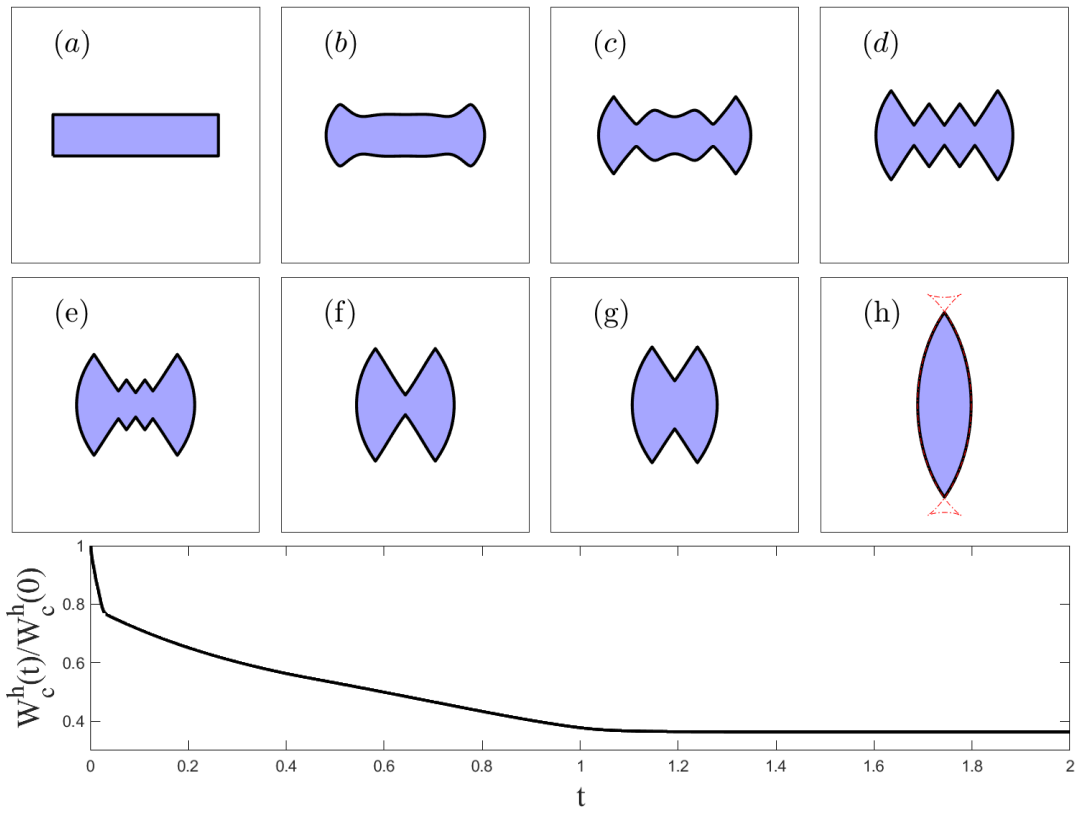

Figure 2.5: Morphological evolutions and the normalized energy of a close rectangular curve under anisotropic surface diffusion with the strongly 2-fold anisotropic surface energy $\gamma(\boldsymbol{n}) = 1 + \frac{3}{5}\cos(2\theta)$ towards its equilibrium at different times: (a) $t = 0$; (b) $t = 10\tau$; (c) $t = 20\tau$; (d) $t = 100\tau$; (e) $t = 250\tau$; (f) $t = 500\tau$; (g) $t = 700\tau$; and (h) $t = 5000\tau$, the other parameters are chosen the same as Fig. 2.4.

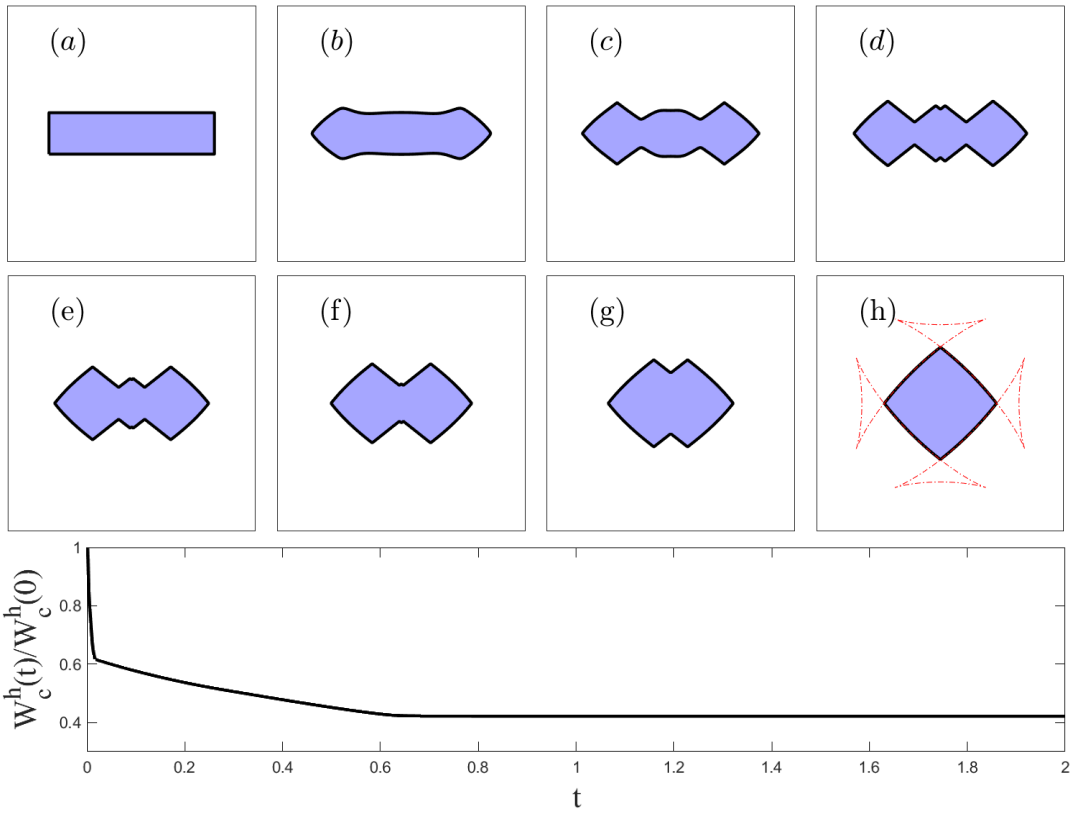

Figure 2.6: Morphological evolutions and the normalized energy of a close rectangular curve under anisotropic surface diffusion with the strongly 4-fold anisotropic surface energy $\gamma(\boldsymbol{n}) = 1 + \frac{3}{10}\cos(4\theta)$ towards its equilibrium at different times: (a) $t = 0$; (b) $t = 5\tau$; (c) $t = 10\tau$; (d) $t = 20\tau$; (e) $t = 160\tau$; (f) $t = 300\tau$; (g) $t = 500\tau$; and (h) $t = 5000\tau$, where the parameters are chosen as $h = 2^{-5}, \tau = h^2$, and the red dashed line in (h) is the Wulff envelope.

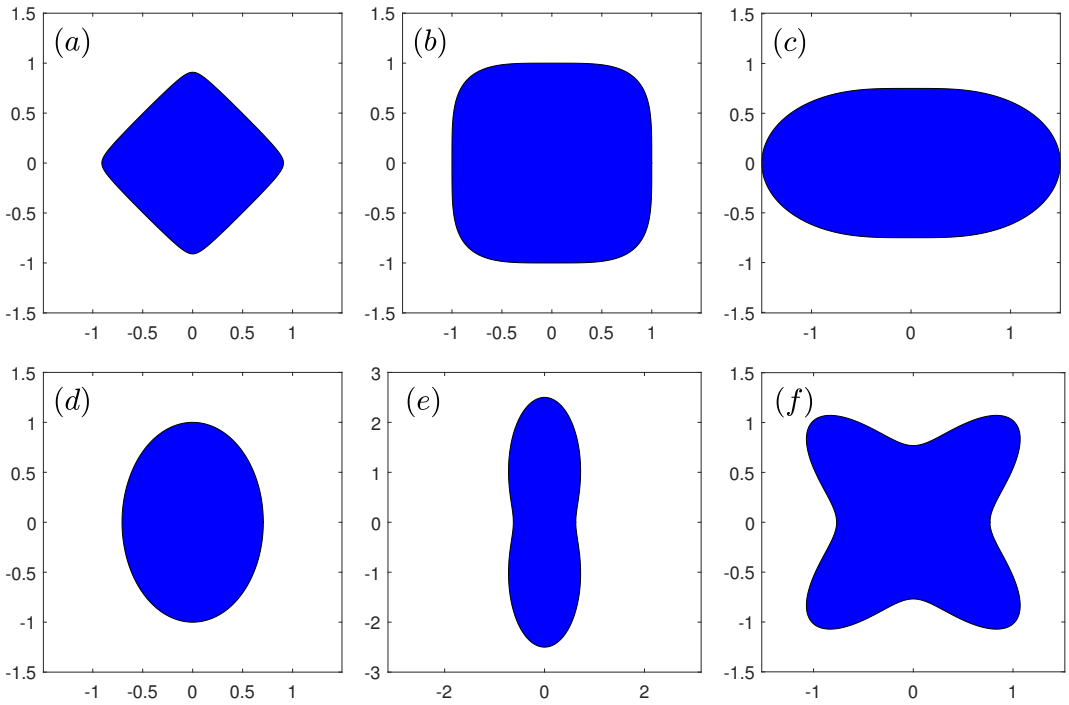

Figure 2.7: The Frank diagrams of the weakly anisotropic energies: (a)-(d) anisotropic energies used in Fig. 2.4; and the strongly anisotropic energies: (e) $\gamma(\boldsymbol{n}) = 1 + \frac{3}{5}\cos(2\theta)$ in Fig. 2.5, and (f) $\gamma(\boldsymbol{n}) = 1 + \frac{3}{10}\cos(4\theta)$ in Fig. 2.6.

the equilibrium shape is an ellipse. The numerical results are perfectly consistent with the theoretical predictions by the well-known Wulff construction [9, 17, 148]. Because the anisotropic surface diffusion is area preserving during the evolution, we can easily obtain its theoretical equilibrium shape (or Wulff shape) by using the expression in [9, 96]. As shown in Figs. 2.5(h)&2.6(h), the numerical equilibrium shapes are again perfectly consistent with the theoretical predictions by the Wulff construction in the strongly anisotropic cases. Meanwhile, we can clearly see that the normalized energy is monotonically decreasing during the evolution for the strongly anisotropic cases. Furthermore, we observe that the numerical equilibrium has several "cusps", which result from the self intersection of the Wulff envelope [9].

Chapter 3

Extension to surfaces with symmetric surface energy

In this Chapter, our goal is to extend the symmetrized SP-PFEM for planer curves (2.42) to surfaces Γ in 3D. Similar to Chapter 2, we focus on the symmetric anisotropy as

$$\gamma(-\boldsymbol{n}) = \gamma(\boldsymbol{n}), \quad \forall \boldsymbol{n} = (n_1, n_2, n_3)^T \in \mathbb{S}^2. \tag{3.1}$$

Our goal is to establish a symmetrized SP-PFEM with the symmetric surface energy $\gamma(\boldsymbol{n})$ satisfies the following relatively mild regularity condition as

$$\gamma(\boldsymbol{p}) \in C^2(\mathbb{R}^3 \setminus \{\boldsymbol{0}\}). \tag{3.2}$$

Which is a direct generalization of the energy-stable condition (2.48) as in the 2D case. To achieve this goal, although the symmetrized surface energy matrix $\boldsymbol{Z}_k(\boldsymbol{n})$ can be easily generalized by $\boldsymbol{\xi}$, there are still several difficulties that need to be solved. The first is we must take the surface gradient ∇_Γ, which is more complicated compared to the arc-length derivative ∂_s. The second is the symmetrized strong formulation (2.17b) for μ relies on ∂_s, and we should design a proper generalization of it with ∇_Γ. Finally, the key concept in the analysis of energy stability – the definition of the minimal stabilizing function $k_0(\boldsymbol{n})$ is dimensional dependent, which means we need to develop a new approach for proving energy stability.

Therefore, this Chapter is organized to answer these three questions one by one. We first list the commonly-used symmetric anisotropic surface energies and introduce the definition of surface gradient operators as well as the functional spaces. Then we extend the symmetrized surface energy matrix $\boldsymbol{Z}_k(\boldsymbol{n})$ in 3D and adopt it to establish the weak formulation for μ, instead of a strong formulation in 2D. After that, we derive the symmetrized conservative weak formulation and apply the PFEM to get the full discretization. Next, the righteous energy stability is established by generalizing the minimal stabilizing function $k_0(\boldsymbol{n})$. Finally, we provide numerous numerical results to illustrate the efficiency and the unconditional energy stability of the 3D extension of the symmetrized SP-PFEM.

3.1 Mathematical formulation

3.1.1 Some anisotropic surface energies and their $\boldsymbol{\xi}$-vectors

Here we list the commonly used symmetric $\gamma(\boldsymbol{n})$ with their $\boldsymbol{\xi}$-vector and Hessian as follows:

- the Riemannian metric anisotropic surface energy [17]

$$\gamma(\boldsymbol{n}) = \sqrt{\boldsymbol{n}^T \boldsymbol{G} \boldsymbol{n}}, \qquad \boldsymbol{n} \in \mathbb{S}^2, \tag{3.3}$$

  where $\boldsymbol{G} \in \mathbb{R}^{3\times 3}$ is a symmetric positive definite matrix. We have

$$\gamma(\boldsymbol{p}) = \sqrt{\boldsymbol{p}^T G \boldsymbol{p}}, \qquad \forall \boldsymbol{p} \in \mathbb{R}^3_* := \mathbb{R}^3 \setminus \{\boldsymbol{0}\}, \tag{3.4}$$

$$\boldsymbol{\xi} = \boldsymbol{\xi}(\boldsymbol{n}) = \gamma(\boldsymbol{n})^{-1} G\, \boldsymbol{n}, \quad \forall \boldsymbol{n} \in \mathbb{S}^2, \tag{3.5}$$

$$\mathbf{H}_\gamma(\boldsymbol{n}) = \gamma(\boldsymbol{n})^{-3/2} \left[\gamma(\boldsymbol{n})^2 G - (G\boldsymbol{n})(G\boldsymbol{n})^T\right]. \tag{3.6}$$

  It is easy to check that $\mathbf{H}_\gamma(\boldsymbol{n})$ is semi-positive definite by using the Cauchy inequality, which indicates the Riemannian metric anisotropy is weakly anisotropic.

- the l^r-norm ($r \geq 2$) metric anisotropic surface energy [12, 36]

$$\gamma(\boldsymbol{n}) = (|n_1|^r + |n_2|^r + |n_3|^r)^{1/r}, \qquad \boldsymbol{n} = (n_1, n_2, n_3)^T \in \mathbb{S}^2, \tag{3.7}$$

where $1 < r < \infty$. We have

$$\gamma(\boldsymbol{p}) = \|\boldsymbol{p}\|_{l^r} = (|p_1|^r + |p_2|^r + |p_3|^r)^{\frac{1}{r}}, \qquad \forall \boldsymbol{p} = (p_1, p_2, p_3)^T \in \mathbb{R}^3_*, \tag{3.8}$$

$$\boldsymbol{\xi} = \boldsymbol{\xi}(\boldsymbol{n}) = \gamma(\boldsymbol{n})^{1-r} \begin{pmatrix} |n_1|^{r-2} n_1 \\ |n_2|^{r-2} n_2 \\ |n_3|^{r-2} n_3 \end{pmatrix}, \qquad \forall \boldsymbol{n} = (n_1, n_2, n_3)^T \in \mathbb{S}^2, \tag{3.9}$$

$$\mathbf{H}_\gamma(\boldsymbol{n}) = (r-1)\gamma(\boldsymbol{n})^{1-2r} \begin{pmatrix} |n_1|^{r-2}(|n_2|^r + |n_3|^r) & * & * \\ -|n_1 n_2|^{r-2} n_1 n_2 & * & * \\ -|n_1 n_3|^{r-2} n_1 n_3 & * & * \end{pmatrix}, \tag{3.10}$$

where the $*$ entries can be deduced from other entries. By checking leading principal minors, we know that $\mathbf{H}_\gamma(\boldsymbol{n})$ is semi-positive definite. Thus the l^r-norm anisotropy is weakly anisotropic.

- the cubic anisotropic surface energy [55, 83, 113]

$$\gamma(\boldsymbol{n}) = 1 + \beta(n_1^4 + n_2^4 + n_3^4), \qquad \boldsymbol{n} = (n_1, n_2, n_3)^T \in \mathbb{S}^2, \tag{3.11}$$

where $m = 2, 3, 4, 6$, and β is a dimensionless anisotropic strength constant. We have

$$\gamma(\boldsymbol{p}) = \left(p_1^2 + p_2^2 + p_3^2\right)^{\frac{1}{2}} + \beta(p_1^4 + p_2^4 + p_3^4)\left(p_1^2 + p_2^2 + p_3^2\right)^{-\frac{3}{2}}, \tag{3.12}$$

$$\boldsymbol{\xi} = \boldsymbol{\xi}(\boldsymbol{n}) = \boldsymbol{n} + \beta\left(4n_1^3 - 3n_1(n_1^4 + n_2^4 + n_3^4), *, *\right)^T, \tag{3.13}$$

$$\lambda_1(\boldsymbol{n}) + \lambda_2(\boldsymbol{n}) = 2(1 - 3\beta) + 36\beta(n_1^2 n_2^2 + n_2^2 n_3^2 + n_3^2 n_1^2), \tag{3.14}$$

$$\lambda_1(\boldsymbol{n})\lambda_2(\boldsymbol{n}) = 20(n_1^4 n_2^4 + n_2^4 n_3^4 + n_3^4 n_1^4) + 72 n_1^2 n_2^2 n_3^2) \geq 0. \tag{3.15}$$

Thus when $\beta = 0$, it is isotropic; when $-1 < \beta < 0$ or $0 < \beta \leq \frac{1}{3}$, it is weakly anisotropic; and when $\beta > \frac{1}{3}$, it is strongly anisotropic.

- the [001], [011], [111] orientation [101, 102, 113, 126]

$$\gamma(\boldsymbol{n}) = 1 + \beta(n_1^4 + n_2^4), \quad \text{[001] orientation,} \tag{3.16a}$$

$$\gamma(\boldsymbol{n}) = 1 + \beta(n_1^4 + \frac{n_2^4 + n_3^4}{2} + 3n_2^2 n_3^2), \quad \text{[011] orientation,} \tag{3.16b}$$

$$\gamma(\boldsymbol{n}) = 1 + \beta\left(\frac{n_1^4 + n_2^4}{2} + \frac{n_3^4}{3} + n_1^2 n_2^2 + 2n_3^2(n_1^2 + n_2^2) + \frac{2\sqrt{2}}{3} n_1^3 n_3 - 2\sqrt{2} n_1 n_2^2 n_3\right), \quad \text{[111] orientation.} \tag{3.16c}$$

here β is a dimensionless anisotropic strength constant;

- the regularized Riemannian metric anisotropic surface energy [19]

$$\gamma(\boldsymbol{n}) = \left(\sum_{l=1}^{L} (\boldsymbol{n}^T G_l \boldsymbol{n})^{r/2}\right)^{1/r}, \tag{3.17}$$

where $r \geq 1$ and $G_1, G_2, \ldots, G_L$ are symmetric positive definite matrices. For the regularized Riemannian metric anisotropic surface energy (3.17)

$$\gamma(\boldsymbol{n}) = \left(\sum_{l=1}^{L} (\boldsymbol{n}^T G_l \boldsymbol{n})^{r/2}\right)^{1/r}, \tag{3.18}$$

where $r \geq 1$ and $G_1, G_2, \ldots, G_L$ are symmetric positive definite matrices, we get

$$\gamma(\boldsymbol{p}) = \left(\sum_{l=1}^{L} (\boldsymbol{p}^T G_l \boldsymbol{p})^{r/2}\right)^{1/r}, \qquad \forall \boldsymbol{p} \in \mathbb{R}^3_*, \tag{3.19}$$

$$\boldsymbol{\xi} = \boldsymbol{\xi}(\boldsymbol{n}) = \gamma(\boldsymbol{n})^{1-r} \sum_{l=1}^{L} \gamma_l^{r-2}(\boldsymbol{n}) G_l \boldsymbol{n} \quad \forall \boldsymbol{n} \in \mathbb{S}^1, \tag{3.20}$$

$$\mathbf{H}_\gamma(\boldsymbol{n}) = \gamma(\boldsymbol{n})^{1-2r}(\boldsymbol{M}_1 + (r-1)\boldsymbol{M}_2). \tag{3.21}$$

where $\gamma_l(\boldsymbol{n}) := \sqrt{\boldsymbol{n}^T G_l \boldsymbol{n}}$ for $l = 1, 2, \ldots, L$, and

$$\boldsymbol{M}_1 = \gamma(\boldsymbol{n})^r \sum_{l=1}^{L} \gamma_l(\boldsymbol{n})^{r-4}(\gamma_l(\boldsymbol{n})^2 G_l - (G_l\boldsymbol{n})(G_l\boldsymbol{n})^T),$$

$$\boldsymbol{M}_2 = \gamma(\boldsymbol{n})^r \sum_{l=1}^{L} (G_l\boldsymbol{n})(G_l\boldsymbol{n})^T \gamma_l^{r-4}(\boldsymbol{n}) - (\sum_{l=1}^{L} \gamma_l^{r-2}(\boldsymbol{n}) G_l\boldsymbol{n})(\sum_{l=1}^{L} \gamma_l^{r-2}(\boldsymbol{n}) G_l\boldsymbol{n})^T.$$

By the Cauchy inequality, we obtain that $\boldsymbol{M}_1$ and $\boldsymbol{M}_2$ are semi-positive definite. Thus the regularized Riemannian metric anisotropy is weakly anisotropic when $r \geq 1$.

3.1.2 Global parameterization and functional spaces

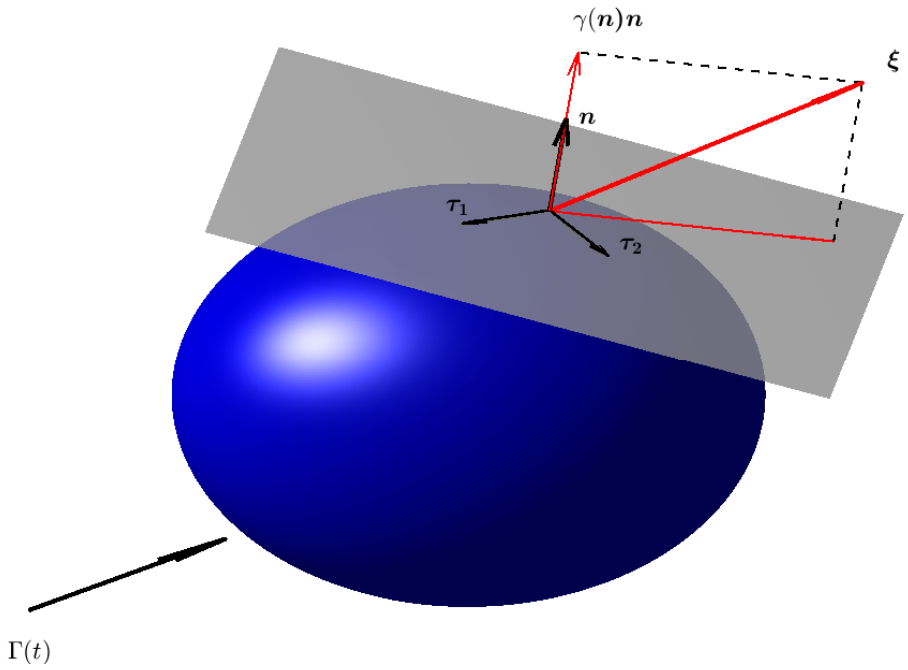

Figure 3.1: An illustration of a closed and orientable surface $\Gamma(t)$ in $\mathbb{R}^3$ under anisotropic surface diffusion with an anisotropic surface energy $\gamma(\boldsymbol{n})$, where $\boldsymbol{n}$ is the outward unit normal vector, $\boldsymbol{\xi}$ is the Cahn-Hoffman $\boldsymbol{\xi}$-vector in (1.3), and $\boldsymbol{\tau}_1$ and $\boldsymbol{\tau}_2$ form a basis of the local tangential space.

Let the closed and orientable surface $\Gamma := \Gamma(t)$ illustrated in Fig. 3.1 be globally parameterized by $\boldsymbol{X}(\boldsymbol{\rho}, t)$ in Definition 1.1 as

$$\boldsymbol{X}(t): \ \Gamma_0 \to \mathbb{R}^3, \boldsymbol{\rho} \mapsto \boldsymbol{X}(\boldsymbol{\rho}, t) = (x_1(\boldsymbol{\rho}, t), x_2(\boldsymbol{\rho}, t), x_3(\boldsymbol{\rho}, t))^T, \tag{3.22}$$

where $\Gamma_0 \subset \mathbb{R}^3$ is the initial surface. Recall that the motion of $\Gamma(t)$ under the anisotropic surface diffusion (1.21) can be mathematically described by the following geometric partial differential equations (PDEs) via the Cahn-Hoffman $\boldsymbol{\xi}$-vector [55]

$$\begin{cases} \boldsymbol{n} \cdot \partial_t \boldsymbol{X}(\boldsymbol{\rho}, t) = \Delta_\Gamma \mu, & \boldsymbol{\rho} \in \Gamma_0, \quad t > 0, \qquad (3.23a) \\ \mu = \nabla_\Gamma \cdot \boldsymbol{\xi}, & \boldsymbol{\xi} = \nabla \gamma(\boldsymbol{p})\big|_{\boldsymbol{p}=\boldsymbol{n}}. \qquad (3.23b) \end{cases}$$

The anisotropic surface diffusion (3.23) can also be regarded as a geometric flow from the given initial closed and orientable surface $\Gamma_0 := \Gamma(0) \subset \mathbb{R}^3$ to the surface $\Gamma(t) \subset \mathbb{R}^3$. We define the function spaces over the evolving surface $\Gamma(t) = \boldsymbol{X}(\boldsymbol{\rho}, t)$.

$$L^2(\Gamma(t)) := \Big\{ u : \Gamma(t) \to \mathbb{R} \,\Big|\, \int_{\Gamma(t)} |u|^2 dA < \infty \Big\}, \tag{3.24}$$

equipped with the L^2-inner product

$$(u, v)_{\Gamma(t)} := \int_{\Gamma(t)} u\, v dA, \quad \forall u, v \in L^2(\Gamma(t)). \tag{3.25}$$

Here the integration over $\Gamma(t)$ can be interpreted by (1.18). The above inner product can be extend to $[L^2(\Gamma(t))]^3$ by replacing the scalar product $u\, v$ by the vector inner product $\boldsymbol{u} \cdot \boldsymbol{v}$. And we adopt the angle bracket to emphasize the inner product for two matrix-valued functions $\boldsymbol{U}, \boldsymbol{V}$ in $[L^2(\Gamma(t))]^{3\times 3}$,

$$\langle \boldsymbol{U}, \boldsymbol{V} \rangle_{\Gamma(t)} := \int_{\Gamma(t)} \boldsymbol{U} : \boldsymbol{V}\, dA, \quad \forall \boldsymbol{U}, \boldsymbol{V} \in [L^2(\Gamma(t))]^{3\times 3}, \tag{3.26}$$

here $\boldsymbol{U} : \boldsymbol{V} = \mathrm{Tr}(\boldsymbol{V}^T \boldsymbol{U})$ is the Frobenius inner product with $\mathrm{Tr}(\boldsymbol{U})$ denoting the trace of a matrix $\boldsymbol{U} \in \mathbb{R}^{3\times 3}$. Furthermore, we introduce the Sobolev space

$$H^1(\Gamma(t)) := \Big\{ u : \Gamma(t) \to \mathbb{R} \,\Big|\, u \in L^2(\Gamma(t)),\, \nabla u \in [L^2(\Gamma(t))]^3 \Big\}. \tag{3.27}$$

And this definition can be extended easily to $[H^1(\Gamma(t))]^3$. We adopt the notation $\nabla_\Gamma f = (\underline{D}_1 f, \underline{D}_2 f, \underline{D}_3 f)^T$ for a scalar-valued function f [55], and the surface gradient for a vector-valued function $\boldsymbol{F} = (f_1, f_2, f_3)^T$ is defined as

$$\nabla_\Gamma \boldsymbol{F} := (\nabla_\Gamma f_1,\, \nabla_\Gamma f_2,\, \nabla_\Gamma f_3)^T \in \mathbb{R}^{3\times 3}. \tag{3.28}$$

3.2 Surface energy matrix and weak formulation

3.2.1 A symmetric surface energy matrix

Introducing the symmetric surface energy matrix $\boldsymbol{Z}_k(\boldsymbol{n})$

$$\begin{aligned}\boldsymbol{Z}_k(\boldsymbol{n}) &= \gamma(\boldsymbol{n})I_3 - \boldsymbol{n}\boldsymbol{\xi}^T(\boldsymbol{n}) - \boldsymbol{\xi}(\boldsymbol{n})\boldsymbol{n}^T + k(\boldsymbol{n})\boldsymbol{n}\boldsymbol{n}^T \\ &= \gamma(\boldsymbol{n})I_3 - \boldsymbol{n}\boldsymbol{\xi}^T - \boldsymbol{\xi}\boldsymbol{n}^T + k(\boldsymbol{n})\boldsymbol{n}\boldsymbol{n}^T, \quad \forall \boldsymbol{n} \in \mathbb{S}^2, \end{aligned} \tag{3.29}$$

where $k(\boldsymbol{n}) : \mathbb{S}^2 \to \mathbb{R}^+$ is a stabilizing function which ensures $\boldsymbol{Z}_k(\boldsymbol{n})$ is positive definite, it is easy to see that the above matrix is a direct generalization from 2D to 3D as proposed in Chapter 2 (2.16). Then we obtain a symmetric and conservative variational (weak) formulation for the chemical potential (or weighted mean curvature) μ via the matrix $\boldsymbol{Z}_k(\boldsymbol{n})$. We remark here that, in 2D case, we can obtain both strong (PDE) and weak (variational) formulations for the chemical potential (or weighted curvature) μ; however, in 3D case, it is not easy to write a simple strong (PDE) formulation for the chemical potential (or weighted mean curvature) μ via the matrix $\boldsymbol{Z}_k(\boldsymbol{n})$.

Lemma 3.1 (The weak formulation for μ)**.** *The weighted mean curvature μ satisfies the following weak formulation.*

$$(\mu, \boldsymbol{n}\cdot\boldsymbol{\omega})_\Gamma = \left\langle \boldsymbol{Z}_k(\boldsymbol{n})\nabla_\Gamma \boldsymbol{X}, \nabla_\Gamma \boldsymbol{\omega}\right\rangle_\Gamma, \quad \forall \boldsymbol{\omega} = (\omega_1, \omega_2, \omega_3)^T \in [H^1(\Gamma(t))]^3. \tag{3.30}$$

Proof. Noticing the fact $\underline{D}_i x_k = \delta_{i,k} - n_k n_i$ and $\nabla_\Gamma f \cdot \boldsymbol{n} = 0$ [55], we obtain

$$\nabla_\Gamma x_k \cdot \nabla_\Gamma \omega_l = \sum_{i=1}^{3} (\delta_{i,k} - n_k n_i)\underline{D}_i \omega_l = \underline{D}_k \omega_l - n_k \nabla_\Gamma \omega_l \cdot \boldsymbol{n} = \underline{D}_k \omega_l. \tag{3.31}$$

From [55, equation (8.18)], we know that

$$\int_{\Gamma(t)} \mu \boldsymbol{n}\cdot\boldsymbol{\omega}\, dA = -\sum_{k,l=1}^{3} \int_\Gamma \xi_k n_l \underline{D}_k \omega_l \, dA + \sum_{k,l=1}^{3} \int_\Gamma \gamma(\boldsymbol{n})\underline{D}_k x_l \underline{D}_k \omega_l \, dA. \tag{3.32}$$

Substituting the identity (3.31) into [55, equation (8.18)] yields the following identity

$$(\mu, \boldsymbol{n}\cdot\boldsymbol{\omega})_\Gamma = \gamma(\boldsymbol{n})\sum_{l=1}^{3}\int_{\Gamma(t)} \nabla_\Gamma x_l \cdot \nabla_\Gamma \omega_l \, d\Gamma - \sum_{k,l=1}^{3}\int_{\Gamma(t)} \xi_k n_l \nabla_\Gamma x_k \cdot \nabla_\Gamma \omega_l \, d\Gamma. \quad (3.33)$$

Obviously, the second term $\langle \gamma(\boldsymbol{n})\nabla_\Gamma \boldsymbol{X}, \nabla_\Gamma \boldsymbol{\omega}\rangle_\Gamma$ corresponds to $\gamma(\boldsymbol{n})I_3$ in $\boldsymbol{Z}_k(\boldsymbol{n})$. Now by simplifying the last term, we have

$$\begin{aligned}
\sum_{k,l=1}^{3}\int_\Gamma \xi_k n_l \nabla_\Gamma x_k \cdot \nabla_\Gamma \omega_l \, dA &= \int_\Gamma \left(\sum_{k=1}^{3} \xi_k (\nabla_\Gamma x_k)\right) \cdot \left(\sum_{l=1}^{3} n_l (\nabla_\Gamma \omega_l)\right) dA \\
&= \int_\Gamma \left((\nabla_\Gamma \boldsymbol{X})^T \boldsymbol{\xi}\right) \cdot \left((\nabla_\Gamma \boldsymbol{\omega})^T \boldsymbol{n}\right) dA \\
&= \int_\Gamma \mathrm{Tr}\left((\nabla_\Gamma \boldsymbol{\omega})^T \boldsymbol{n}\boldsymbol{\xi}^T (\nabla_\Gamma \boldsymbol{X})\right) dA \\
&= \int_\Gamma \left(\boldsymbol{n}\boldsymbol{\xi}^T (\nabla_\Gamma \boldsymbol{X})\right) : \Big(\nabla_\Gamma \boldsymbol{\omega}\Big) dA \\
&= \langle \boldsymbol{n}\boldsymbol{\xi}^T \nabla_\Gamma \boldsymbol{X}, \nabla_\Gamma \boldsymbol{\omega}\rangle_\Gamma, \qquad (3.34)
\end{aligned}$$

which is the $\boldsymbol{n}\boldsymbol{\xi}^T(\boldsymbol{n})$ part in $\boldsymbol{Z}_k(\boldsymbol{n})$.

Finally, recalling the identity $\nabla_\Gamma \boldsymbol{X} = I_3 - \boldsymbol{n}\boldsymbol{n}^T$ and combining the two identities (3.33) and (3.34) yields

$$\begin{aligned}
(\mu, \boldsymbol{n}\cdot\boldsymbol{\omega})_\Gamma &= \langle (\gamma(\boldsymbol{n})I_3 - \boldsymbol{n}\boldsymbol{\xi}^T)\nabla_\Gamma \boldsymbol{X}, \nabla_\Gamma \boldsymbol{\omega}\rangle_\Gamma \\
&= \langle \boldsymbol{Z}_k(\boldsymbol{n})\nabla_\Gamma \boldsymbol{X}, \nabla_\Gamma \boldsymbol{\omega}\rangle_\Gamma + \langle (\boldsymbol{\xi}\boldsymbol{n}^T - k(\boldsymbol{n})\boldsymbol{n}\boldsymbol{n}^T)(I_3 - \boldsymbol{n}\boldsymbol{n}^T), \nabla_\Gamma \boldsymbol{\omega}\rangle_\Gamma \\
&= \langle \boldsymbol{Z}_k(\boldsymbol{n})\nabla_\Gamma \boldsymbol{X}, \nabla_\Gamma \boldsymbol{\omega}\rangle_\Gamma, \qquad (3.35)
\end{aligned}$$

which is the desired result. □

3.2.2 A symmetrized conservative weak formulation

With the weak formulation of μ (3.30) given in lemma 3.1, by taking integration by parts, we can easily derive the following variational formulation for the anisotropic surface diffusion (3.23) (or (1.21)): For a given closed and orientable initial surface

$\Gamma(0) := \Gamma_0$, find the solution $(\boldsymbol{X}(\cdot,t), \mu(\cdot,t)) \in [H^1(\Gamma(t))]^3 \times H^1(\Gamma(t))$ such that

$$(\boldsymbol{n} \cdot \partial_t \boldsymbol{X}, \psi)_{\Gamma(t)} + (\nabla_\Gamma \mu, \nabla_\Gamma \psi)_{\Gamma(t)} = 0 \qquad \forall \psi \in H^1(\Gamma(t)), \tag{3.36a}$$

$$(\mu \boldsymbol{n}, \boldsymbol{\omega})_{\Gamma(t)} - \langle \boldsymbol{Z}_k(\boldsymbol{n}) \nabla_\Gamma \boldsymbol{X}, \nabla_\Gamma \boldsymbol{\omega} \rangle_{\Gamma(t)} = 0 \qquad \forall \boldsymbol{\omega} \in [H^1(\Gamma(t))]^3, \tag{3.36b}$$

3.2.3 Structure-preserving properties

Denote the enclosed volume and the free energy of $\Gamma(t)$ as $V(t)$ and $W(t)$, respectively, which are defined by

$$V(t) := \frac{1}{3} \int_{\Gamma(t)} \boldsymbol{X} \cdot \boldsymbol{n} \, dA, \qquad W(t) := \int_{\Gamma(t)} \gamma(\boldsymbol{n}) \, dA. \tag{3.37}$$

We then show the two geometric properties still hold for the variational formulation (3.36).

Theorem 3.1. *The enclosed volume $V(t)$ and the free energy $W(t)$ of the solution $\Gamma(t)$ of the variational formulation (3.36) are conserved and dissipative, respectively, i.e.*

$$V(t) \equiv V(0), \qquad W(t) \le W(t') \le W(0), \quad t \ge t' \ge 0. \tag{3.38}$$

Proof. Taking the derivative of $V(t)$ with respect to t. From [140], we know that

$$\frac{dV(t)}{dt} = \int_{\Gamma(t)} \boldsymbol{n} \cdot \partial_t \boldsymbol{X} \, dA = (\boldsymbol{n} \cdot \partial_t \boldsymbol{X}, 1)_{\Gamma(t)} = 0, \quad t \ge 0, \tag{3.39}$$

which implies the volume conservation in the left of (3.38).

Similarly, the derivative of $W(t)$ with respect to t is

$$\frac{dW(t)}{dt} = \int_{\Gamma(t)} \boldsymbol{n} \cdot \partial_t \boldsymbol{X} \mu \, dA = (\boldsymbol{n} \cdot \partial_t \boldsymbol{X}, \mu)_{\Gamma(t)} = -(\nabla_\Gamma \mu, \nabla_\Gamma \mu)_{\Gamma(t)} \le 0, \quad t \ge 0, \tag{3.40}$$

which implies the energy dissipation in the right of (3.38). □

3.3 The SP-PFEM discretization

3.3.1 The discretization

We take $\tau > 0$ to be the time step size, and the discrete time levels are $t_m = m\tau$ for each $m \geq 0$. For spatial discretization, as illustrated in figure 3.2, the orientable surface $\Gamma(t_m)$ is approximated by an orientable polyhedron $\Gamma^m = \cup_{j=1}^{J} \bar{\sigma}_j^m$ with J mutually disjoint non-degenerated triangles surfaces σ_j^m and I vertices $\boldsymbol{q}_i^m$. We further denote $\{\boldsymbol{q}_{j_1}^m, \boldsymbol{q}_{j_2}^m, \boldsymbol{q}_{j_3}^m\}$ as the three ordered vertices of the triangle σ_j^m, the induced orientation vector $\mathcal{J}\{\sigma_j^m\} := (\boldsymbol{q}_{j_2}^m - \boldsymbol{q}_{j_1}^m) \times (\boldsymbol{q}_{j_3}^m - \boldsymbol{q}_{j_2}^m)$, and the outward unit normal vector $\boldsymbol{n}_j^m$ of σ_j^m is thus given by $\boldsymbol{n}_j^m = \frac{\mathcal{J}\{\sigma_j^m\}}{|\mathcal{J}\{\sigma_j^m\}|}$. We refer the definition of the orientable polyhedron to Definition 47 in [33].

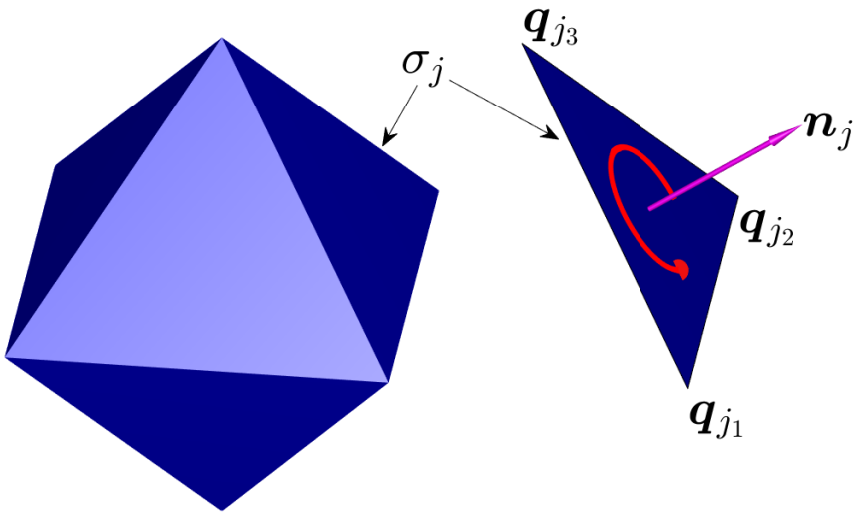

Figure 3.2: An illustration of the approximation polyhedron Γ^0. The vertices $\{\boldsymbol{q}_{j_1}, \boldsymbol{q}_{j_2}, \boldsymbol{q}_{j_3}\}$ of the triangle σ_j is oriented counterclockwise, see the red circular arrow. And the direction of the normal vector $\boldsymbol{n}_j$ is determined by the right-hand rule.

The finite element space with respect to the orientable surface $\Gamma^m = \cup_{j=1}^{J} \bar{\sigma}_j^m$ is

defined as follows

$$\mathbb{K}^m := \left\{ u \in C(\Gamma^m) \,\middle|\, u|_{\sigma_j^m} \in \mathcal{P}^1(\sigma_j^m),\ \forall 1 \le j \le J \right\}, \tag{3.41}$$

which is equipped with the mass lumped inner product $(\cdot,\cdot)^h_{\Gamma^m}$ with h denoting the mesh size of Γ^m as

$$(f,g)^h_{\Gamma^m} := \frac{1}{3}\sum_{j=1}^{J}\sum_{i=1}^{3} |\sigma_j^m| f\left((\boldsymbol{q}_{j_i}^m)^-\right) g\left((\boldsymbol{q}_{j_i}^m)^-\right), \tag{3.42}$$

where $\mathcal{P}^1(\sigma_j^m)$ is the space of polynomials on σ_j^m with degree at most 1, $|\sigma_j^m| := \frac{1}{2}|\mathcal{J}\{\sigma_j^m\}|$ denotes the area of σ_j^m, and $f\left((\boldsymbol{q}_{j_i}^m)^-\right)$ means the one-sided limit of $f(\mathbf{x})$ at $\boldsymbol{q}_{j_i}^m$ inside σ_j^m. This definition is also valid for vector- and matrix-valued function, and the mass lumped inner product of the matrix-valued functions $\boldsymbol{U}$ and $\boldsymbol{V}$ is also emphsized by the angle bracket as

$$\langle \boldsymbol{U}, \boldsymbol{V} \rangle^h_{\Gamma^m} := \frac{1}{3}\sum_{j=1}^{J}\sum_{i=1}^{3} |\sigma_j^m| \boldsymbol{U}((\boldsymbol{q}_{j_i}^m)^-) : \boldsymbol{V}((\boldsymbol{q}_{j_i}^m)^-). \tag{3.43}$$

We remark here that $(f,g)^h_{\Gamma^m}$ and $\langle \boldsymbol{U}, \boldsymbol{V} \rangle^h_{\Gamma^m}$ can be viewed as approximations of $(f,g)_{\Gamma^m}$ and $\langle \boldsymbol{U}, \boldsymbol{V} \rangle_{\Gamma^m}$, respectively. Finally, the discretized surface gradient operator ∇_Γ for $f \in \mathbb{K}^m$ is given by

$$\nabla_\Gamma f|_{\sigma_j^m} := \left(f(\boldsymbol{q}_{j_1}^m)(\boldsymbol{q}_{j_2}^m - \boldsymbol{q}_{j_3}^m) + f(\boldsymbol{q}_{j_2}^m)(\boldsymbol{q}_{j_3}^m - \boldsymbol{q}_{j_1}^m) + f(\boldsymbol{q}_{j_3}^m)(\boldsymbol{q}_{j_1}^m - \boldsymbol{q}_{j_2}^m) \right) \times \frac{\boldsymbol{n}_j^m}{|\mathcal{J}\{\sigma_j^m\}|}, \tag{3.44}$$

and for vector-valued function $\boldsymbol{F} = (f_1, f_2, f_3)^T \in [\mathbb{K}^m]^3$, $\nabla_\Gamma \boldsymbol{F} := (\nabla_\Gamma f_1,\ \nabla_\Gamma f_2,\ \nabla_\Gamma f_3)^T$.

By using the PFEM for spatial discretization and adapting an implicit-explicit (IMEX) Euler method for temporal discretization, i.e. linear parts via backward Euler method and nonlinear part via backward Euler method with proper linearization as well as the integration limits via forward Euler method, an IMEX structural-preserving finite element method (SP-PFEM) for the variational formulation (3.36) can then be stated as follows: Given the initial approximation $\Gamma^0 = \cup_{j=1}^J \overline{\sigma_j^0}$ of $\Gamma(0)$; for each time step $t_m = m\tau$ $(m \ge 0)$, find the solution $\left(\boldsymbol{X}^{m+1}, \mu^{m+1}\right) \in [\mathbb{K}^m]^3 \times \mathbb{K}^m$

such that

$$\left(\boldsymbol{n}^{m+\frac{1}{2}} \cdot \frac{\boldsymbol{X}^{m+1}-\boldsymbol{X}^{m}}{\tau}, \psi\right)_{\Gamma^m} + \left(\nabla_\Gamma \mu^{m+1}, \nabla_\Gamma \psi\right)_{\Gamma^m} = 0, \qquad \forall \psi \in \mathbb{K}^m, \tag{3.45a}$$

$$\left(\mu^{m+1}\boldsymbol{n}^{m+\frac{1}{2}}, \boldsymbol{\omega}\right)_{\Gamma^m} - \langle \boldsymbol{Z}_k(\boldsymbol{n}^m)\nabla_\Gamma \boldsymbol{X}^{m+1}, \nabla_\Gamma \boldsymbol{\omega}\rangle_{\Gamma^m} = 0, \qquad \forall \boldsymbol{\omega} \in [\mathbb{K}^m]^3. \tag{3.45b}$$

Here $\boldsymbol{X}^m(\boldsymbol{q}_i^m) = \boldsymbol{q}_i^m$, $\boldsymbol{X}^{m+1}(\boldsymbol{q}_i^m) = \boldsymbol{q}_i^{m+1}$ for each i, $\boldsymbol{n}^m|_{\sigma_j^m} = \boldsymbol{n}_j^m$, $\sigma_j^{m+1} = \boldsymbol{X}^{m+1}(\sigma_j^m)$ is the triangle with ordered vertices $\{\boldsymbol{q}_{j_1}^{m+1}, \boldsymbol{q}_{j_2}^{m+1}, \boldsymbol{q}_{j_3}^{m+1}\}$ for each j, and $\Gamma^{m+1} = \cup_{j=1}^J \bar{\sigma}_j^{m+1}$ for each m. The semi-implicit approximation $\boldsymbol{n}^{m+\frac{1}{2}}$ of the outward normal vector $\boldsymbol{n}$ at $t = (m+\frac{1}{2})\tau$ is defined as follows

$$\boldsymbol{n}^{m+\frac{1}{2}}|_{\sigma_j^m} := \frac{\mathcal{J}\{\sigma_j^m\} + 4\mathcal{J}\{\sigma_j^{m+\frac{1}{2}}\} + \mathcal{J}\{\sigma_j^{m+1}\}}{6|\mathcal{J}\{\sigma_j^m\}|}, \tag{3.46}$$

where $\sigma_j^{m+\frac{1}{2}} := \frac{1}{2}\left(\sigma_j^m + \sigma_j^{m+1}\right)$.

Remark 3.1. *We note the function $\boldsymbol{X}^{m+1}$ has different meanings at time step t_m (as a function in $[\mathbb{K}^m]^3$) and t_{m+1} (as a function in $[\mathbb{K}^{m+1}]^3$), and we adopt the same notation for simplicity.*

3.3.2 Structure-preserving properties

For the discretized polygon surface $\Gamma^m = \cup_{j=1}^J \bar{\sigma}_j^m$, its enclosed volume and surface energy are denoted as V^m and W^m, respectively, which are defined as

$$V^m := \frac{1}{3}\int_{\Gamma^m} \boldsymbol{X}^m \cdot \boldsymbol{n}^m dA = \frac{1}{9}\sum_{j=1}^{J}\sum_{i=1}^{3} |\sigma_j^m| \boldsymbol{q}_{j_i}^m \cdot \boldsymbol{n}_j^m, \tag{3.47a}$$

$$W^m := \int_{\Gamma^m} \gamma(\boldsymbol{n}^m) dA = \sum_{j=1}^{J} |\sigma_j^m| \gamma(\boldsymbol{n}_j^m), \qquad \forall m \geq 0. \tag{3.47b}$$

Denote the following auxiliary function $F_k(\boldsymbol{n}, \boldsymbol{u}, \boldsymbol{v}) : [\mathbb{S}^2]^3 \to \mathbb{R}$ as

$$F_k(\boldsymbol{n}, \boldsymbol{u}, \boldsymbol{v}) := (\boldsymbol{u}^T \boldsymbol{Z}_k(\boldsymbol{n}) \cdot \boldsymbol{u})(\boldsymbol{v}^T \boldsymbol{Z}_k(\boldsymbol{n}) \cdot \boldsymbol{v}), \tag{3.48}$$

and define the minimal stabilizing function $k_0(\boldsymbol{n}) : \mathbb{S}^2 \to \mathbb{R}$ as (its existence will be given in the next section)

$$k_0(\boldsymbol{n}) = \inf\left\{k(\boldsymbol{n}) \middle| F_k(\boldsymbol{n}, \boldsymbol{u}, \boldsymbol{v}) \geq \gamma^2(\boldsymbol{u} \times \boldsymbol{v}), \quad \forall \boldsymbol{u}, \boldsymbol{v} \in \mathbb{S}^2\right\}. \tag{3.49}$$

Then for the symmetrized SP-PFEM (3.45), we have

Theorem 3.2 (structural-preserving)**.** *Assume $\gamma(\boldsymbol{n})$ satisfies (3.2) and take $k(\boldsymbol{n})$ in (3.29) satisfying $k(\boldsymbol{n}) \geq k_0(\boldsymbol{n})$ for $\boldsymbol{n} \in \mathbb{S}^2$, then the symmetrized SP-PFEM (3.45) is volume conservation and energy dissiption, i.e.*

$$V^{m+1} = V^m = \ldots = V^0, \qquad \forall m \geq 0, \tag{3.50a}$$

$$W^{m+1} \leq W^m \leq \ldots \leq W^0, \qquad \forall m \geq 0. \tag{3.50b}$$

Proof of volume conservation

Define $\Gamma^h(\alpha) = \boldsymbol{X}^h(\cdot, \alpha)$ as the linear conbination of $\boldsymbol{X}^m$ and $\boldsymbol{X}^{m+1}$ as

$$\boldsymbol{X}^h(\cdot, \alpha) := (1-\alpha)\boldsymbol{X}^m(\cdot) + \alpha \boldsymbol{X}^{m+1}(\cdot),$$

and the enclosed volume by $\Gamma^h(\alpha)$ as $V(\alpha)$. By applying the Reynolds transport theorem to $V(\alpha)$ ([13, Theorem 3.1]), we obtain that

$$\begin{aligned} \frac{dV(\alpha)}{d\alpha} &= \int_{\Gamma^h(\alpha)} \partial_\alpha \boldsymbol{X}^h \cdot \boldsymbol{n}^h \, ds \\ &= \int_{\Gamma^m} (\boldsymbol{X}^{m+1} - \boldsymbol{X}^m) \cdot \frac{\mathcal{J}\{\sigma^h(\alpha)\}}{|\mathcal{J}\{\sigma^m\}|} \, ds \end{aligned}$$

Integrate $\frac{dV(\alpha)}{d\alpha}$ from $\alpha = 0$ to $\alpha = 1$, we obtain

$$V(1) - V(0) = \Big((\boldsymbol{X}^{m+1} - \boldsymbol{X}^m) \cdot \boldsymbol{n}^{m+\frac{1}{2}}, 1 \Big)^h_{\Gamma^m}$$

The volume conservation is a direct result by taking $\varphi^h = 1$ in (2.42a). □

The energy dissipation or unconditional energy stability (3.50b) is given in next section.

Remark 3.2. *The symmetrized SP-PFEM (3.45) is 'weakly' implicit, i.e. at each time step, one needs to solve a nonlinear coupled system, which can be solved efficiently by Newton's method. Of course, if we simply replace $\boldsymbol{n}^{m+\frac{1}{2}}$ in (3.45) by $\boldsymbol{n}^m$, we can obtain a semi-implicit energy-stable PFEM (ES-PFEM), where only a linear system needs to be solved at each time. Of course for the semi-implicit ES-PFEM, the volume conservation is no longer valid. Under the same condition as in Theorem 3.2, the ES-PFEM is also unconditionally energy stable.*

Remark 3.3. *The semi-discretization of the variational problem (3.36) in space by the PFEM also preserves the two geometric properties. And the proof is similar to the isotropic case, for details, we refer [13, 16, 154].*

Remark 3.4. *We remark here that all formulations in this section are still valid in 2D. In fact, assume $\Gamma(t)$ be a closed curve in 2D with unit outward normal vector $\boldsymbol{n} \in \mathbb{S}^1$ and tangent vector $\boldsymbol{\tau} = \boldsymbol{n}^\perp$, here $^\perp$ denotes the clockwise rotation by $\frac{\pi}{2}$. And assume $\Gamma(t)$ be globally parameterized by $\boldsymbol{X}(\rho, t) : \mathbb{R}/\mathbb{Z} \to \mathbb{R}^2$ [8]. We further assume s be the arclength parameter of the closed curve $\Gamma(t)$ and thus $\boldsymbol{\tau} = \partial_s \boldsymbol{X}(\rho, t)$ [8]. Notice that*

$$\nabla_\Gamma = \boldsymbol{\tau}\,\partial_s, \qquad \Delta_\Gamma = (\boldsymbol{\tau}\,\partial_s)\cdot(\boldsymbol{\tau}\,\partial_s) = \partial_{ss}, \qquad \nabla_\Gamma \boldsymbol{X} = \partial_s \boldsymbol{X}\boldsymbol{\tau}^T,$$

then we have

$$\Delta_\Gamma\,\mu = \partial_{ss}\mu, \qquad \nabla_\Gamma \cdot \boldsymbol{\xi} = \boldsymbol{\tau}\cdot\partial_s\boldsymbol{\xi} = \boldsymbol{n}^\perp\cdot\partial_s\boldsymbol{\xi} = -\boldsymbol{n}\cdot\partial_s\boldsymbol{\xi}^\perp,$$

$$(\nabla_\Gamma\mu, \nabla_\Gamma\psi)_{\Gamma(t)} = (\boldsymbol{\tau}\partial_s\mu, \boldsymbol{\tau}\partial_s\psi)_{\Gamma(t)} = (\partial_s\mu, \partial_s\psi)_{\Gamma(t)}\,,$$

$$\begin{aligned}\langle \boldsymbol{Z}_k(\boldsymbol{n})\nabla_\Gamma\boldsymbol{X}, \nabla_\Gamma\boldsymbol{\omega}\rangle_{\Gamma(t)} &= \langle \boldsymbol{Z}_k(\boldsymbol{n})\partial_s\boldsymbol{X}\boldsymbol{\tau}^T, \partial_s\boldsymbol{\omega}\boldsymbol{\tau}^T\rangle_{\Gamma(t)}\\ &= \int_{\Gamma(t)} Tr\,(\boldsymbol{\tau}\partial_s\boldsymbol{\omega}^T\boldsymbol{Z}_k(\boldsymbol{n})\partial_s\boldsymbol{X}\boldsymbol{\tau}^T)\,dA\\ &= \int_{\Gamma(t)} Tr\,(\partial_s\boldsymbol{\omega}^T\boldsymbol{Z}_k(\boldsymbol{n})\partial_s\boldsymbol{X}\boldsymbol{\tau}^T\boldsymbol{\tau})\,dA\\ &= (\boldsymbol{Z}_k(\boldsymbol{n})\partial_s\boldsymbol{X}, \partial_s\boldsymbol{\omega})_{\Gamma(t)}\,.\end{aligned}$$

Thus the above equations (3.23) and (3.36) collapse to the equations (1.5) and (2.11) in [8], respectively, in the corresponding 2D setup.

3.4 Proof of energy dissipation

In this section, we first prove the existence of $k_0(\boldsymbol{n})$ and show its sub-linear property as a functional of $\gamma(\boldsymbol{n})$. By utilizing the existence of $k_0(\boldsymbol{n})$ together with several lemmas, we finally prove the energy stability part of our main theorem (3.50b).

3.4.1 Minimal stabilizing function

From (3.49), we know that $F_{k_0}(\boldsymbol{n},\boldsymbol{u},\boldsymbol{v}) \geq 0$. Taking $k = k_0$, $\boldsymbol{u} = \boldsymbol{n}$ and $\boldsymbol{v} = \boldsymbol{\tau} \in \mathbb{S}^2$ satisfying $\boldsymbol{\tau}\cdot\boldsymbol{n} = 0$ in (3.48), noticing $\boldsymbol{\tau}^T \boldsymbol{Z}_{k_0}(\boldsymbol{n})\boldsymbol{\tau} = \gamma(\boldsymbol{n}) > 0$ and $\boldsymbol{n}\cdot\boldsymbol{\xi} = \gamma(\boldsymbol{n})$, we obtain

$$0 \leq \boldsymbol{n}^T \boldsymbol{Z}_{k_0}(\boldsymbol{n})\boldsymbol{n} = k_0(\boldsymbol{n}) - \gamma(\boldsymbol{n}) \quad \Rightarrow \quad k_0(\boldsymbol{n}) \geq \gamma(\boldsymbol{n}) > 0, \quad \boldsymbol{n} \in \mathbb{S}^2. \tag{3.51}$$

To prove the existence of $k_0(\boldsymbol{n})$, for any given $\boldsymbol{n} \in \mathbb{S}^2$, we only need to show there exists a $k(\boldsymbol{n})$ sufficiently large such that $F_k(\boldsymbol{n},\boldsymbol{u},\boldsymbol{v}) \geq \gamma^2(\boldsymbol{u}\times\boldsymbol{v})$ for any $\boldsymbol{u},\boldsymbol{v} \in \mathbb{S}^2$.

Lemma 3.2. *Let $G(\boldsymbol{n},\boldsymbol{u},\boldsymbol{v})$ be an auxiliary function given by*

$$G(\boldsymbol{n},\boldsymbol{u},\boldsymbol{v}) := \gamma(\boldsymbol{n})\left[\gamma(\boldsymbol{n}) - 2(\boldsymbol{\xi}\cdot\boldsymbol{u})(\boldsymbol{n}\cdot\boldsymbol{u}) - 2(\boldsymbol{\xi}\cdot\boldsymbol{v})(\boldsymbol{n}\cdot\boldsymbol{v})\right], \quad \boldsymbol{n},\boldsymbol{u},\boldsymbol{v} \in \mathbb{S}^2, \tag{3.52}$$

then for any $k(\boldsymbol{n}) > 0$, the following inequality holds

$$F_k(\boldsymbol{n},\boldsymbol{u},\boldsymbol{v}) - G(\boldsymbol{n},\boldsymbol{u},\boldsymbol{v}) \geq \left[\gamma(\boldsymbol{n})k(\boldsymbol{n}) - 4|\boldsymbol{\xi}|^2\right]\left[(\boldsymbol{n}\cdot\boldsymbol{u})^2 + (\boldsymbol{n}\cdot\boldsymbol{v})^2\right]. \tag{3.53}$$

Proof. By direct computation and the arithmetic-geometric mean inequality, we obtain

$$\begin{aligned}
&F_k(\boldsymbol{n},\boldsymbol{u},\boldsymbol{v}) - G(\boldsymbol{n},\boldsymbol{u},\boldsymbol{v}) \\
&\geq \gamma(\boldsymbol{n})k(\boldsymbol{n})\left[(\boldsymbol{n}\cdot\boldsymbol{u})^2 + (\boldsymbol{n}\cdot\boldsymbol{v})^2\right] + k(\boldsymbol{n})^2(\boldsymbol{n}\cdot\boldsymbol{u})^2(\boldsymbol{n}\cdot\boldsymbol{v})^2 \\
&\quad - 4|\boldsymbol{\xi}|^2\left|(\boldsymbol{n}\cdot\boldsymbol{u})(\boldsymbol{n}\cdot\boldsymbol{v})\right| - 2|\boldsymbol{\xi}|\,k(\boldsymbol{n})\left|(\boldsymbol{n}\cdot\boldsymbol{u})(\boldsymbol{n}\cdot\boldsymbol{v})\right|\left(|\boldsymbol{n}\cdot\boldsymbol{u}| + |\boldsymbol{n}\cdot\boldsymbol{v}|\right) \\
&\geq \left[\gamma(\boldsymbol{n})k(\boldsymbol{n}) - 2|\boldsymbol{\xi}|^2\right]\left[(\boldsymbol{n}\cdot\boldsymbol{u})^2 + (\boldsymbol{n}\cdot\boldsymbol{v})^2\right] + k(\boldsymbol{n})^2(\boldsymbol{n}\cdot\boldsymbol{u})^2(\boldsymbol{n}\cdot\boldsymbol{v})^2 \\
&\quad - k(\boldsymbol{n})\,|\boldsymbol{\xi}|\left[(\boldsymbol{n}\cdot\boldsymbol{u})^2\left(\frac{2|\boldsymbol{\xi}|}{k(\boldsymbol{n})} + \frac{k(\boldsymbol{n})}{2|\boldsymbol{\xi}|}(\boldsymbol{n}\cdot\boldsymbol{v})^2\right) + (\boldsymbol{n}\cdot\boldsymbol{v})^2\left(\frac{2|\boldsymbol{\xi}|}{k(\boldsymbol{n})} + \frac{k(\boldsymbol{n})}{2|\boldsymbol{\xi}|}(\boldsymbol{n}\cdot\boldsymbol{u})^2\right)\right] \\
&= \left[\gamma(\boldsymbol{n})k(\boldsymbol{n}) - 4|\boldsymbol{\xi}|^2\right]\left[(\boldsymbol{n}\cdot\boldsymbol{u})^2 + (\boldsymbol{n}\cdot\boldsymbol{v})^2\right],
\end{aligned}$$

which is the desired inequality (3.53). □

Since $\gamma(\boldsymbol{p})$ is not differentiable at $\boldsymbol{0}$, in order to handle $\gamma^2(\boldsymbol{u}\times\boldsymbol{v})$, we first show the following lemma.

Lemma 3.3. *For any $\gamma(\boldsymbol{n})$ satisfying (3.2), then $\gamma^2(\boldsymbol{p})$ is continuous differentiable in $\mathbb{R}^3$. Moreover, there exists a constant C_1 defined by*

$$C_1 = \frac{1}{2}\sup_{\boldsymbol{n}\in\mathbb{S}^2} \|\mathbf{H}_{\gamma^2}(\boldsymbol{n})\|_2\,, \qquad \mathbf{H}_{\gamma^2}(\boldsymbol{n}) = \nabla\nabla\gamma^2(\boldsymbol{p})|_{\boldsymbol{p}=\boldsymbol{n}}. \tag{3.54}$$

where $\|\cdot\|_2$ is the spectral norm, such that

$$\gamma^2(\boldsymbol{p}) - \gamma^2(\boldsymbol{q}) \le \nabla(\gamma^2(\boldsymbol{q}))\cdot(\boldsymbol{p}-\boldsymbol{q}) + C_1|\boldsymbol{p}-\boldsymbol{q}|^2, \qquad \forall \boldsymbol{p},\boldsymbol{q}\in\mathbb{R}^3. \tag{3.55}$$

Proof. It is straightforward to check $\gamma^2(\boldsymbol{p}) \in C^1(\mathbb{R}^3)$ by definition.

To prove the inequality (3.55), we first consider the case that the line segment of $\boldsymbol{p},\boldsymbol{q}$ does not pass $\mathbf{0}$, i.e., $\lambda\boldsymbol{p} + (1-\lambda)\boldsymbol{q} \neq \mathbf{0}$ for all $0 \le \lambda \le 1$. Since $\gamma^2(\boldsymbol{p})$ is homogeneous of degree 2, we know that $\mathbf{H}_{\gamma^2}(\boldsymbol{p})$ is homogeneous of degree 0, which yields

$$\mathbf{H}_{\gamma^2}(\boldsymbol{\zeta}) = \mathbf{H}_{\gamma^2}\left(\boldsymbol{\zeta}/|\boldsymbol{\zeta}|\right), \qquad \forall \mathbf{0}\neq\boldsymbol{\zeta}\in\mathbb{R}^3. \tag{3.56}$$

By the mean value theorem, there exists a $\lambda_0 \in (0,1)$ and $\boldsymbol{\zeta} = \lambda_0\boldsymbol{p} + (1-\lambda_0)\boldsymbol{q} \neq \mathbf{0}$, such that

$$\gamma^2(\boldsymbol{p}) = \gamma^2(\boldsymbol{q}) + \nabla(\gamma^2(\boldsymbol{q}))\cdot(\boldsymbol{p}-\boldsymbol{q}) + \frac{1}{2}(\boldsymbol{p}-\boldsymbol{q})^T\mathbf{H}_{\gamma^2}(\boldsymbol{\zeta})(\boldsymbol{p}-\boldsymbol{q}). \tag{3.57}$$

Thus (3.55) holds for such $\boldsymbol{p},\boldsymbol{q}$.

If $\mathbf{0}$ is contained in line segment of $\boldsymbol{p},\boldsymbol{q}$, we can find a sequence $(\boldsymbol{p}_k,\boldsymbol{q}_k)\to(\boldsymbol{p},\boldsymbol{q})$ such that for each k, the line segment of $\boldsymbol{p}_k,\boldsymbol{q}_k$ does not pass $\mathbf{0}$. We know (3.55) holds for such $\boldsymbol{p}_k,\boldsymbol{q}_k$. By using the continuity of $\gamma^2(\boldsymbol{p})$ and $\nabla(\gamma^2(\boldsymbol{p}))$, we obtain that (3.55) is valid in this case by letting $k\to\infty$.

Thus the inequity (3.55) is established. □

Theorem 3.3. *Suppose $\gamma(\boldsymbol{n})$ satisfies the energy stability condition (3.2). Then there exists a constant $K(\boldsymbol{n}) < \infty$ only depends on $\gamma(\boldsymbol{n})$ given by*

$$K := K(\boldsymbol{n}) = \frac{6|\boldsymbol{\xi}(\boldsymbol{n})|^2 + 8\gamma(\boldsymbol{n})|\boldsymbol{\xi}(\boldsymbol{n})| + 16C_1}{\gamma(\boldsymbol{n})} < \infty, \qquad \forall \boldsymbol{n}\in\mathbb{S}^2, \tag{3.58}$$

such that $F_K(\boldsymbol{n},\boldsymbol{u},\boldsymbol{v}) \ge \gamma^2(\boldsymbol{u}\times\boldsymbol{v})$ for any $\boldsymbol{u},\boldsymbol{v}\in\mathbb{S}^2$.

Proof. It is convenient to first consider the special case $\boldsymbol{n} = (0,0,1)^T$. For any $\boldsymbol{u}, \boldsymbol{v} \in \mathbb{S}^2$, we write them in the spherical coordinates as

$$\boldsymbol{u} = (\cos\theta_1 \cos\phi_1, \sin\theta_1 \cos\phi_1, \sin\phi_1)^T, \qquad 0 \le \theta_1 < 2\pi, \quad -\frac{\pi}{2} \le \phi_1 \le \frac{\pi}{2}, \tag{3.59a}$$

$$\boldsymbol{v} = (\cos\theta_2 \cos\phi_2, \sin\theta_2 \cos\phi_2, \sin\phi_2)^T, \qquad 0 \le \theta_2 < 2\pi, \quad -\frac{\pi}{2} \le \phi_2 \le \frac{\pi}{2}, \tag{3.59b}$$

where in case when $\phi_1 = \pm\frac{\pi}{2}$, we choose $\theta_1 = 0$; and when $\phi_2 = \pm\frac{\pi}{2}$, we choose $\theta_2 = 0$. The cross product $\boldsymbol{u} \times \boldsymbol{v}$ is then represented as

$$\boldsymbol{u} \times \boldsymbol{v} = \cos\phi_2 \sin\phi_1 \, \hat{\boldsymbol{v}}_0 + \cos\phi_1 \sin\phi_2 \, \hat{\boldsymbol{u}}_0 + \cos\phi_1 \cos\phi_2 \, \hat{\boldsymbol{w}}_0, \tag{3.60}$$

where

$$\hat{\boldsymbol{u}}_0 = (\sin\theta_1, -\cos\theta_1, 0)^T, \qquad \hat{\boldsymbol{v}}_0 = (-\sin\theta_2, \cos\theta_2, 0)^T,$$
$$\hat{\boldsymbol{w}}_0 = (0, 0, \sin\theta_{21})^T, \qquad \text{with} \quad \theta_{21} = \theta_2 - \theta_1.$$

Since $\boldsymbol{u}, \boldsymbol{v}$ are symmetric in $F_K(\boldsymbol{n}, \boldsymbol{u}, \boldsymbol{v})$ and $\gamma^2(\boldsymbol{u} \times \boldsymbol{v})$. Without loss of generality, we can always assume $\sin\theta_{21} \ge 0$.

Denoting $\boldsymbol{u}_0, \boldsymbol{v}_0 \in \mathbb{S}^2$ as

$$\boldsymbol{u}_0 := (\cos\theta_1, \sin\theta_1, 0)^T, \quad \boldsymbol{v}_0 := (\cos\theta_2, \sin\theta_2, 0)^T, \tag{3.61}$$

we know that $|(\boldsymbol{u}-\boldsymbol{u}_0)\times\boldsymbol{v}| \le |\boldsymbol{u}-\boldsymbol{u}_0|, |\boldsymbol{u}\times(\boldsymbol{v}-\boldsymbol{v}_0)| \le |\boldsymbol{v}-\boldsymbol{v}_0|, |(\boldsymbol{u}-\boldsymbol{u}_0)\times(\boldsymbol{v}-\boldsymbol{v}_0)| \le |\boldsymbol{u}-\boldsymbol{u}_0| + |\boldsymbol{v}-\boldsymbol{v}_0|$ since $|\boldsymbol{u}|, |\boldsymbol{v}|, |\boldsymbol{u}_0|, |\boldsymbol{v}_0| = 1$. Thus we get

$$|\boldsymbol{u} \times \boldsymbol{v} - \boldsymbol{u}_0 \times \boldsymbol{v}_0|^2 \le 8\left(|\boldsymbol{u} - \boldsymbol{u}_0|^2 + |\boldsymbol{v} - \boldsymbol{v}_0|^2\right). \tag{3.62}$$

Taking $\boldsymbol{p} = \boldsymbol{u} \times \boldsymbol{v}, \boldsymbol{q} = \boldsymbol{u}_0 \times \boldsymbol{v}_0$ in (3.55), and noticing $\boldsymbol{u}_0 \times \boldsymbol{v}_0 = (\sin\theta_{21})\,\boldsymbol{n}$, we

obtain

$$
\begin{aligned}
&\gamma^2(\boldsymbol{u}\times\boldsymbol{v}) - (\sin\theta_{21})^2\gamma^2(\boldsymbol{n}) \\
&\le \sin\theta_{21}\,\nabla(\gamma^2(\boldsymbol{n}))\cdot(\boldsymbol{u}\times\boldsymbol{v}-\boldsymbol{u}_0\times\boldsymbol{v}_0) + C_1|\boldsymbol{u}\times\boldsymbol{v}-\boldsymbol{u}_0\times\boldsymbol{v}_0|^2 \\
&\le 2\gamma(\boldsymbol{n})\,\boldsymbol{\xi}\cdot(\sin\phi_1\,\hat{\boldsymbol{v}}_0+\sin\phi_2\,\hat{\boldsymbol{u}}_0)\sin\theta_{21} \\
&\quad + 2\gamma(\boldsymbol{n})\boldsymbol{\xi}\cdot((\cos\phi_2-1)\sin\phi_1\boldsymbol{v}_0+(\cos\phi_1-1)\sin\phi_2\boldsymbol{u}_0)\sin\theta_{21} \\
&\quad + 2\gamma(\boldsymbol{n})\boldsymbol{\xi}\cdot\hat{\boldsymbol{\omega}}_0(1-\cos\phi_1\cos\phi_2)\sin\theta_{21} + 8C_1(|\boldsymbol{u}-\boldsymbol{u}_0|^2+|\boldsymbol{v}-\boldsymbol{v}_0|^2) \\
&\le 2\gamma(\boldsymbol{n})\,\boldsymbol{\xi}\cdot[(\cos\theta_{21}\,\boldsymbol{v}_0-\boldsymbol{u}_0)\,(\boldsymbol{n}\cdot\boldsymbol{u})+(\cos\theta_{2,1}\,\boldsymbol{u}_0-\boldsymbol{v}_0)\,(\boldsymbol{n}\cdot\boldsymbol{v})] \\
&\quad + 4(\gamma(\boldsymbol{n})\,|\boldsymbol{\xi}|+4C_1)\left[(\boldsymbol{n}\cdot\boldsymbol{u})^2+(\boldsymbol{n}\cdot\boldsymbol{v})^2\right].
\end{aligned}
\tag{3.63}
$$

Here we use the facts $|\boldsymbol{u}-\boldsymbol{u}_0| = 2|\sin\frac{\phi_1}{2}|$, $|\boldsymbol{v}-\boldsymbol{v}_0| = 2|\sin\frac{\phi_2}{2}|$, $(\sin\phi)^2 \ge 2(\sin\frac{\phi}{2})^2 = 1-\cos\phi$ for all $-\frac{\pi}{2}\le\phi\le\frac{\pi}{2}$, and $0\le 1-\cos\phi_1\cos\phi_2\le(1-\cos\phi_1)+(1-\cos\phi_2)$.

To estimate $G(\boldsymbol{n},\boldsymbol{u},\boldsymbol{v})$, we observe the following inequalities

$$
\begin{aligned}
(\boldsymbol{\xi}\cdot\boldsymbol{u})(\boldsymbol{n}\cdot\boldsymbol{u}) &= (\boldsymbol{\xi}\cdot\boldsymbol{u}_0)(\boldsymbol{n}\cdot\boldsymbol{u}) + (\boldsymbol{\xi}\cdot(\boldsymbol{u}-\boldsymbol{u}_0))(\boldsymbol{n}\cdot(\boldsymbol{u}-\boldsymbol{u}_0)) \\
&\le (\boldsymbol{\xi}\cdot\boldsymbol{u}_0)(\boldsymbol{n}\cdot\boldsymbol{u}) + |\boldsymbol{\xi}||\boldsymbol{u}-\boldsymbol{u}_0|^2 \\
&\le (\boldsymbol{\xi}\cdot\boldsymbol{u}_0)(\boldsymbol{n}\cdot\boldsymbol{u}) + 2|\boldsymbol{\xi}|(\boldsymbol{n}\cdot\boldsymbol{u})^2,
\end{aligned}
\tag{3.64a}
$$

$$
(\boldsymbol{\xi}\cdot\boldsymbol{v})(\boldsymbol{n}\cdot\boldsymbol{v}) \le (\boldsymbol{\xi}\cdot\boldsymbol{v}_0)(\boldsymbol{n}\cdot\boldsymbol{v}) + 2|\boldsymbol{\xi}|(\boldsymbol{n}\cdot\boldsymbol{v})^2.
\tag{3.64b}
$$

Combining (3.52) and (3.64) yields

$$
\begin{aligned}
G(\boldsymbol{n},\boldsymbol{u},\boldsymbol{v}) &= \gamma^2(\boldsymbol{n}) - 2\gamma(\boldsymbol{n})\,[(\boldsymbol{\xi}\cdot\boldsymbol{u})(\boldsymbol{n}\cdot\boldsymbol{u})+(\boldsymbol{\xi}\cdot\boldsymbol{v})(\boldsymbol{n}\cdot\boldsymbol{v})] \\
&\ge \gamma^2(\boldsymbol{n}) - 2\gamma(\boldsymbol{n})\,[(\boldsymbol{\xi}\cdot\boldsymbol{u}_0)(\boldsymbol{n}\cdot\boldsymbol{u})+(\boldsymbol{\xi}\cdot\boldsymbol{u}_0)(\boldsymbol{n}\cdot\boldsymbol{u})] \\
&\quad - 4\gamma(\boldsymbol{n})|\boldsymbol{\xi}|\left[(\boldsymbol{n}\cdot\boldsymbol{u})^2+(\boldsymbol{n}\cdot\boldsymbol{v})^2\right].
\end{aligned}
\tag{3.65}
$$

Finally, by (3.53) in lemma 3.2, the estimate of $\gamma^2(\boldsymbol{u}\times\boldsymbol{v})$ in (3.63), and the

estimate of $G(\boldsymbol{n},\boldsymbol{u},\boldsymbol{v})$ in (3.65), we obtain

$$\begin{aligned}
&F_K(\boldsymbol{n},\boldsymbol{u},\boldsymbol{v})-\gamma^2(\boldsymbol{u}\times\boldsymbol{v})\\
&\geq \gamma(\boldsymbol{n})^2(\cos\theta_{21})^2-2\gamma(\boldsymbol{n})\cos\theta_{21}\ [(\boldsymbol{\xi}\cdot\boldsymbol{v}_0)(\boldsymbol{n}\cdot\boldsymbol{u})+(\boldsymbol{\xi}\cdot\boldsymbol{u}_0)(\boldsymbol{n}\cdot\boldsymbol{v})]\\
&\quad+\left[\gamma(\boldsymbol{n})K(\boldsymbol{n})-4|\boldsymbol{\xi}|^2-8\gamma(\boldsymbol{n})|\boldsymbol{\xi}|-16C_1\right]\left[(\boldsymbol{n}\cdot\boldsymbol{u})^2+(\boldsymbol{n}\cdot\boldsymbol{v})^2\right]\\
&\geq \gamma(\boldsymbol{n})^2(\cos\theta_{21})^2-2\gamma(\boldsymbol{n})|\cos\theta_{21}|\ |\boldsymbol{\xi}|\ [(\boldsymbol{n}\cdot\boldsymbol{u})+(\boldsymbol{n}\cdot\boldsymbol{v})]\\
&\quad+2|\boldsymbol{\xi}|^2\left[(\boldsymbol{n}\cdot\boldsymbol{u})^2+(\boldsymbol{n}\cdot\boldsymbol{v})^2\right]\\
&\geq 0.
\end{aligned}$$

Thus we have $F_K(\boldsymbol{n},\boldsymbol{u},\boldsymbol{v})\geq\gamma^2(\boldsymbol{u}\times\boldsymbol{v})$ for the special case $\boldsymbol{n}=(0,0,1)^T$.

Since the constant $K(\boldsymbol{n})$ only depends on $\gamma(\boldsymbol{n})$, thus the proof is valid for arbitrary $\boldsymbol{n}\in\mathbb{S}^2$ via a similar argument. The proof is completed. □

Theorem 3.3 indicates that the set $\left\{k(\boldsymbol{n})\middle|F_k(\boldsymbol{n},\boldsymbol{u},\boldsymbol{v})\geq\gamma^2(\boldsymbol{u}\times\boldsymbol{v}),\quad\forall\boldsymbol{u},\boldsymbol{v}\in\mathbb{S}^2\right\}$ contains at least an element $K(\boldsymbol{n})<\infty$, and thus it is not empty. This, together with the fact $k_0(\boldsymbol{n})\geq\gamma(\boldsymbol{n})$, yields the existence of the minimal stabilizing function $k_0(\boldsymbol{n})$.

Corollary 3.1 (existence of the minimal stabilizing function)**.** *Suppose the surface energy $\gamma(\boldsymbol{n})$ satisfying the energy stable condition (3.2). Then the minimal stabilizing function $k_0(\boldsymbol{n})$ in (3.49) is well-defined.*

Finally, we point out the minimal stabilizing function $k_0(\boldsymbol{n})$ is determined by $\gamma(\boldsymbol{n})$, and thus we can consider the mapping from $\gamma(\boldsymbol{n})$ to $k_0(\boldsymbol{n})$. Similar to the result in 2D in [8], the mapping is sub-linear.

Theorem 3.4 (positive homogeneity and subadditivity)**.** *Let $k_0(\boldsymbol{n})$, $k_1(\boldsymbol{n})$ and $k_2(\boldsymbol{n})$ be the minimal stabilizing functions of $\gamma(\boldsymbol{n})$, $\gamma_1(\boldsymbol{n})$ and $\gamma_2(\boldsymbol{n})$, respectively. Then we have*

(i) for any $c>0$, $ck_0(\boldsymbol{n})$ is the stabilizing function of $c\gamma(\boldsymbol{n})$; and

(ii) suppose $\gamma(\boldsymbol{n})=\gamma_1(\boldsymbol{n})+\gamma_2(\boldsymbol{n})$, then $k_0(\boldsymbol{n})\leq k_1(\boldsymbol{n})+k_2(\boldsymbol{n})$ for $\boldsymbol{n}\in\mathbb{S}^2$.

Proof. The proof of positive homogeneity in (i) is similar to the proof of Lemma 4.4 in [8], and thus details are omitted here for brevity.

To prove the subadditivity in (ii), we denote

$$\boldsymbol{\xi} := \nabla\gamma(\boldsymbol{p})\big|_{\boldsymbol{p}=\boldsymbol{n}}, \quad \boldsymbol{\xi}_1 := \nabla\gamma_1(\boldsymbol{p})\big|_{\boldsymbol{p}=\boldsymbol{n}}, \quad \boldsymbol{\xi}_2 := \nabla\gamma_2(\boldsymbol{p})\big|_{\boldsymbol{p}=\boldsymbol{n}}.$$

Since $k_1(\boldsymbol{n})$ is the minimal stabilizing function of $\gamma_1(\boldsymbol{n})$, for any $t \in \mathbb{R}$, we have

$$\begin{aligned}
&\frac{1}{2}\boldsymbol{u}^T \boldsymbol{Z}_{k_1}(\boldsymbol{n})\boldsymbol{u} + \frac{t^2}{2}\boldsymbol{v}^T \boldsymbol{Z}_{k_1}(\boldsymbol{n})\boldsymbol{v} - t\gamma_1(\boldsymbol{u}\times\boldsymbol{v}) \\
&\geq 2\sqrt{\frac{t^2}{4}F_{k_1}(\boldsymbol{n},\boldsymbol{u},\boldsymbol{v})} - t\gamma_1(\boldsymbol{u}\times\boldsymbol{v}) \\
&\geq 0, \qquad \forall \boldsymbol{n},\boldsymbol{u},\boldsymbol{v} \in \mathbb{S}^2.
\end{aligned} \tag{3.66}$$

A similar inequality is also true for $\gamma_2(\boldsymbol{n})$. Adding the two inequalities together and noticing $\boldsymbol{\xi} = \boldsymbol{\xi_1} + \boldsymbol{\xi_2}$, we obtain

$$\frac{1}{2}\boldsymbol{u}^T \boldsymbol{Z}_{k_1+k_2}(\boldsymbol{n})\boldsymbol{u} + \frac{t^2}{2}\boldsymbol{v}^T \boldsymbol{Z}_{k_1+k_2}(\boldsymbol{n})\boldsymbol{v} - t\gamma(\boldsymbol{u}\times\boldsymbol{v}) \geq 0, \qquad \forall t \in \mathbb{R}, \tag{3.67}$$

which means its discriminant $\gamma^2(\boldsymbol{u}\times\boldsymbol{v}) - F_{k_1+k_2}(\boldsymbol{n},\boldsymbol{u},\boldsymbol{v}) \leq 0$ for all $\boldsymbol{n},\boldsymbol{u},\boldsymbol{v} \in \mathbb{S}^2$. Then the subadditivity is a direct conclusion from the definition of the minimal stabilizing function (3.49). □

3.4.2 The proof

By establishing the existence of $k_0(\boldsymbol{n})$, we now have enough tools to prove (3.50b) in theorem 3.2. To simplify the proof, we first introduce the following alternative definition for the surface gradient operator ∇_Γ.

Lemma 3.4. *Suppose σ be a non-degenerated triangle with three ordered vertices $\{\boldsymbol{q}_1,\boldsymbol{q}_2,\boldsymbol{q}_3\}$ (cf. Fig. 3.2). Let f and $\boldsymbol{F}$ be scalar- and vector-valued functions in $\mathcal{P}^1(\sigma)/[\mathcal{P}^1(\sigma)]^3$, respectively, $\{\boldsymbol{n},\boldsymbol{\tau}_1,\boldsymbol{\tau}_2\}$ forms an orthonormal basis. Then the discretized surface gradient operator ∇_Γ in (3.44) satisfies*

$$\nabla_\Gamma f = (\partial_{\boldsymbol{\tau}_1} f)\,\boldsymbol{\tau}_1 + (\partial_{\boldsymbol{\tau}_2} f)\,\boldsymbol{\tau}_2, \qquad \nabla_\Gamma \boldsymbol{F} = (\partial_{\boldsymbol{\tau}_1}\boldsymbol{F})\,\boldsymbol{\tau}_1^T + (\partial_{\boldsymbol{\tau}_2}\boldsymbol{F})\,\boldsymbol{\tau}_2^T, \tag{3.68}$$

where $\partial_{\boldsymbol{\tau}} f$ denotes the directional derivative of f with respect to $\boldsymbol{\tau}$.

Proof. It suffices to prove the left equality in (3.68). Let $\boldsymbol{x} = \lambda_1\boldsymbol{q}_1 + \lambda_2\boldsymbol{q}_2 + \lambda_3\boldsymbol{q}_3$ with $0 \le \lambda_1, \lambda_2, \lambda_3 \le 1$ satisfying $\lambda_1 + \lambda_2 + \lambda_3 = 1$ be a point in σ. We observe that

$$\begin{aligned}[(\boldsymbol{q}_3 - \boldsymbol{q}_2) \times \boldsymbol{n}] \cdot (\boldsymbol{x} - \boldsymbol{q}_3) &= [(\boldsymbol{x} - \boldsymbol{q}_3) \times (\boldsymbol{q}_3 - \boldsymbol{q}_2)] \cdot \boldsymbol{n} \\ &= [(-\lambda_1(\boldsymbol{q}_3 - \boldsymbol{q}_1) - \lambda_2(\boldsymbol{q}_3 - \boldsymbol{q}_2)) \times (\boldsymbol{q}_3 - \boldsymbol{q}_2)] \cdot \boldsymbol{n} \\ &= -\lambda_1 [(\boldsymbol{q}_2 - \boldsymbol{q}_1 + \boldsymbol{q}_3 - \boldsymbol{q}_2) \times (\boldsymbol{q}_3 - \boldsymbol{q}_2)] \cdot \boldsymbol{n} \\ &= -\lambda_1 |\mathcal{J}\{\sigma\}|. \end{aligned} \tag{3.69}$$

Thus $\lambda_1 = \frac{(\boldsymbol{q}_2 - \boldsymbol{q}_3) \times \boldsymbol{n}}{|\mathcal{J}\{\sigma\}|} \cdot (\boldsymbol{x} - \boldsymbol{q}_3)$, and λ_2, λ_3 can be derived similarly.

By the definition of the directional derivative, we deduce that

$$\begin{aligned}\partial_{\boldsymbol{\tau}_1} f(\boldsymbol{x}) &= \lim_{h\to 0} \frac{f(\boldsymbol{x} + h\boldsymbol{\tau}_1) - f(\boldsymbol{x})}{h} \\ &= \lim_{h\to 0} \frac{1}{h} \left(f(\boldsymbol{q}_1) \frac{(\boldsymbol{q}_2 - \boldsymbol{q}_3) \times \boldsymbol{n}}{|\mathcal{J}\{\sigma\}|} \cdot (h\boldsymbol{\tau}_1) \right. \\ &\quad \left. + f(\boldsymbol{q}_2) \frac{(\boldsymbol{q}_3 - \boldsymbol{q}_1) \times \boldsymbol{n}}{|\mathcal{J}\{\sigma\}|} \cdot (h\boldsymbol{\tau}_1) + f(\boldsymbol{q}_3) \frac{(\boldsymbol{q}_1 - \boldsymbol{q}_2) \times \boldsymbol{n}}{|\mathcal{J}\{\sigma\}|} \cdot (h\boldsymbol{\tau}_1) \right) \\ &= \nabla_\Gamma f(\boldsymbol{x}) \cdot \boldsymbol{\tau}_1. \end{aligned} \tag{3.70}$$

Similarly, we have $\partial_{\boldsymbol{\tau}_2} f = \nabla_\Gamma f \cdot \boldsymbol{\tau}_2$. Since $\{\boldsymbol{n}, \boldsymbol{\tau}_1, \boldsymbol{\tau}_2\}$ forms an orthonormal basis, by vector decomposition and $\nabla_\Gamma f \cdot \boldsymbol{n} = 0$, we obtain

$$\begin{aligned}\nabla_\Gamma f &= (\nabla_\Gamma f \cdot \boldsymbol{n})\boldsymbol{n} + (\nabla_\Gamma f \cdot \boldsymbol{\tau}_1)\boldsymbol{\tau}_1 + (\nabla_\Gamma f \cdot \boldsymbol{\tau}_2)\boldsymbol{\tau}_2 \\ &= (\partial_{\boldsymbol{\tau}_1} f)\, \boldsymbol{\tau}_1 + (\partial_{\boldsymbol{\tau}_2} f)\, \boldsymbol{\tau}_2, \end{aligned} \tag{3.71}$$

which is the desired identity. □

With the help of (3.68), we can then give the following upper bound of the summand $\gamma(\boldsymbol{n})\,|\sigma|$ in the discretized energy W^m in (3.47b).

Lemma 3.5. *Suppose σ and $\bar{\sigma}$ are two non-degenerated triangles with ordered vertices $\{\boldsymbol{q}_1, \boldsymbol{q}_2, \boldsymbol{q}_3\}, \{\bar{\boldsymbol{q}}_1, \bar{\boldsymbol{q}}_2, \bar{\boldsymbol{q}}_3\}$, and outward unit normal vectors $\boldsymbol{n}$ and $\bar{\boldsymbol{n}}$, respectively (cf. Fig. 3.2). Let $\boldsymbol{X}$ be a vector-valued function in $[\mathcal{P}^1(\sigma)]^3$ satisfying $\boldsymbol{X}(\boldsymbol{q}_i) = \bar{\boldsymbol{q}}_i$ for $i = 1, 2, 3$. Then for any $k(\boldsymbol{n}) \ge k_0(\boldsymbol{n})$ for $\boldsymbol{n} \in \mathbb{S}^2$, the following inequality holds*

$$\frac{1}{6}|\sigma| \sum_{i=1}^{3} \left(\boldsymbol{Z}_k(\boldsymbol{n}) \nabla_\Gamma \boldsymbol{X}((\boldsymbol{q}_i)^-) \right) : \nabla_\Gamma \boldsymbol{X}((\boldsymbol{q}_i)^-) \ge \gamma(\bar{\boldsymbol{n}})\, |\bar{\sigma}|. \tag{3.72}$$

Proof. Since $\boldsymbol{X} \in [\mathcal{P}^1(\sigma)]^3$, its derivative $\nabla_\Gamma \boldsymbol{X}$ is a constant matrix in σ. Suppose $\{\boldsymbol{n}, \boldsymbol{\tau}_1, \boldsymbol{\tau}_2\}$ forms an orthonormal basis, by applying (3.68), we obtain

$$\nabla_\Gamma \boldsymbol{X}((\boldsymbol{q}_i)^-) = \left(\partial_{\boldsymbol{\tau}_1} \boldsymbol{X}((\boldsymbol{q}_i)^-)\right) \boldsymbol{\tau}_1^T + \left(\partial_{\boldsymbol{\tau}_2} \boldsymbol{X}((\boldsymbol{q}_i)^-)\right) \boldsymbol{\tau}_2^T, \qquad i = 1, 2, 3. \tag{3.73}$$

Let $\partial_{\boldsymbol{\tau}_1} \boldsymbol{X} = s\boldsymbol{u}$ and $\partial_{\boldsymbol{\tau}_2} \boldsymbol{X} = t\boldsymbol{v}$ with $s, t \geq 0$ and $\boldsymbol{u}, \boldsymbol{v} \in \mathbb{S}^2$. Substituding this and the definition of $Z_k(\boldsymbol{n})$ in (3.29) into the LHS of (3.72), we get

$$\begin{aligned}
&\frac{1}{6}|\sigma| \sum_{i=1}^{3} \left(\boldsymbol{Z}_k(\boldsymbol{n}) \nabla_\Gamma \boldsymbol{X}((\boldsymbol{q}_i)^-)\right) : \nabla_\Gamma \boldsymbol{X}((\boldsymbol{q}_i)^-) \\
&= \frac{1}{2}|\sigma| \left(\boldsymbol{Z}_k(\boldsymbol{n})(s\boldsymbol{u}\boldsymbol{\tau}_1^T + t\boldsymbol{v}\boldsymbol{\tau}_2^T)\right) : (s\boldsymbol{u}\boldsymbol{\tau}_1^T + t\boldsymbol{v}\boldsymbol{\tau}_2^T) \\
&= \frac{1}{2}|\sigma| \left(s^2(\boldsymbol{\tau}_1 \cdot \boldsymbol{\tau}_1)\boldsymbol{u}^T \boldsymbol{Z}_k(\boldsymbol{n})\boldsymbol{u} + t^2(\boldsymbol{\tau}_2 \cdot \boldsymbol{\tau}_2)\boldsymbol{v}^T \boldsymbol{Z}_k(\boldsymbol{n})\boldsymbol{v}\right) \\
&\geq st\,|\sigma| \sqrt{F_k(\boldsymbol{n}, \boldsymbol{u}, \boldsymbol{v})} \geq st\,|\sigma|\,\gamma(\boldsymbol{u} \times \boldsymbol{v}).
\end{aligned} \tag{3.74}$$

For the RHS of (3.72), since $\bar{\sigma} = \boldsymbol{X}(\sigma)$, it holds that

$$\gamma(\bar{\boldsymbol{n}})\,|\bar{\sigma}| = \gamma(\bar{\boldsymbol{n}}) \int_\sigma |(\partial_{\boldsymbol{\tau}_1} \boldsymbol{X}) \times (\partial_{\boldsymbol{\tau}_2} \boldsymbol{X})|\, dA = st\,|\sigma|\,\gamma(\bar{\boldsymbol{n}})\,|\boldsymbol{u} \times \boldsymbol{v}|. \tag{3.75}$$

Finally, since $\boldsymbol{X} \in [\mathcal{P}^1(\sigma)]^3$, for $\boldsymbol{p}$ and $\boldsymbol{p} + h\boldsymbol{\tau}_1$ in σ, we have $\boldsymbol{X}(\boldsymbol{p} + h\boldsymbol{\tau}_1)$ and $\boldsymbol{X}(\boldsymbol{p})$ in $\bar{\sigma}$. From the definition of directional derivative for functions in $[\mathcal{P}^1(\sigma)]^3$, we get

$$s\,\boldsymbol{u} \cdot \bar{\boldsymbol{n}} = (\partial_{\boldsymbol{\tau}_1} \boldsymbol{X}) \cdot \bar{\boldsymbol{n}} = \frac{\boldsymbol{X}(\boldsymbol{p} + h\boldsymbol{\tau}_1) - \boldsymbol{X}(\boldsymbol{p})}{h} \cdot \bar{\boldsymbol{n}} = 0, \tag{3.76}$$

and similarly $\boldsymbol{v} \cdot \bar{\boldsymbol{n}} = 0$, thus $\gamma(\boldsymbol{u} \times \boldsymbol{v}) = |\boldsymbol{u} \times \boldsymbol{v}|\,\gamma(\bar{\boldsymbol{n}})$. This equation, together with (3.74) and (3.75), yields the desired inequality (3.72). □

With the help of lemma (3.5), we can then prove the energy stability part (3.50b) in our main theorem 3.2.

Proof. First for any $\boldsymbol{p} \in \mathbb{S}^2$, since $k(\boldsymbol{n}) \geq k_0(\boldsymbol{n})$, we have

$$\boldsymbol{p}^T \boldsymbol{Z}_k(\boldsymbol{n})\boldsymbol{p} = \gamma(\boldsymbol{n}) - 2(\boldsymbol{\xi} \cdot \boldsymbol{p})(\boldsymbol{n} \cdot \boldsymbol{p}) + k(\boldsymbol{n})(\boldsymbol{n} \cdot \boldsymbol{p})^2 \geq 0, \tag{3.77}$$

thus $\boldsymbol{Z}_k(\boldsymbol{n})$ is positive definite. By Cauchy's inequality, it holds that

$$\begin{aligned}
&\langle \boldsymbol{Z}_k(\boldsymbol{n}^m)\nabla_\Gamma \boldsymbol{X}^{m+1}, \nabla_\Gamma(\boldsymbol{X}^{m+1}-\boldsymbol{X}^m)\rangle^h_{\Gamma^m} \\
&\geq \frac{1}{2}\langle \boldsymbol{Z}_k(\boldsymbol{n}^m)\nabla_\Gamma \boldsymbol{X}^{m+1}, \nabla_\Gamma \boldsymbol{X}^{m+1}\rangle^h_{\Gamma^m} - \frac{1}{2}\langle \boldsymbol{Z}_k(\boldsymbol{n}^m)\nabla_\Gamma \boldsymbol{X}^{m}, \nabla_\Gamma \boldsymbol{X}^{m}\rangle^h_{\Gamma^m}.
\end{aligned} \tag{3.78}$$

Suppose $\{\boldsymbol{n}_j^m, \boldsymbol{\tau}_{j,1}^m, \boldsymbol{\tau}_{j,2}^m\}$ $(1 \leq j \leq J)$ forms an orthonomal basis, by using (3.68), we obtain

$$\begin{aligned}
&\frac{1}{2}\langle \boldsymbol{Z}_k(\boldsymbol{n}^m)\nabla_\Gamma \boldsymbol{X}^{m}, \nabla_\Gamma \boldsymbol{X}^{m}\rangle^h_{\Gamma^m} \\
&= \frac{1}{6}\sum_{j=1}^{J}\sum_{i=1}^{3} |\sigma_j^m| \left(\boldsymbol{Z}_k(\boldsymbol{n}_j^m)\,\nabla_\Gamma \boldsymbol{X}^m\left((\boldsymbol{q}_{j_i}^m)^-\right)|_{\sigma_j^m}\right) : \left(\nabla_\Gamma \boldsymbol{X}^m\left((\boldsymbol{q}_{j_i}^m)^-\right)|_{\sigma_j^m}\right) \\
&= \frac{1}{2}\sum_{j=1}^{J} |\sigma_j^m| \left[(\boldsymbol{\tau}_{j,1}^m)^T \boldsymbol{Z}_k(\boldsymbol{n}_j^m)\boldsymbol{\tau}_{j,1}^m + (\boldsymbol{\tau}_{j,2}^m)^T Z_k(\boldsymbol{n}_j^m)\boldsymbol{\tau}_{j,2}^m\right] \\
&= \frac{1}{2}\sum_{j=1}^{J} |\sigma_j^m|\,\gamma(\boldsymbol{n}_j^m)\,\left(\boldsymbol{\tau}_{j,1}^m\cdot\boldsymbol{\tau}_{j,1}^m + \boldsymbol{\tau}_{j,2}^m\cdot\boldsymbol{\tau}_{j,2}^m\right) \\
&= \sum_{j=1}^{J} |\sigma_j^m|\,\gamma(\boldsymbol{n}_j^m) = W^m.
\end{aligned} \tag{3.79}$$

For $1 \leq j \leq J$, applying Lemma 3.5 with $\sigma = \sigma_j^m, \bar{\sigma} = \sigma_j^{m+1}$ and $\boldsymbol{X} = \boldsymbol{X}^{m+1}|_{\sigma_j^m}$, we get

$$\frac{1}{6}|\sigma_j^m|\sum_{j=1}^{3}\left(\boldsymbol{Z}_k(\boldsymbol{n}_j^m)\,\nabla_\Gamma \boldsymbol{X}^m\left((\boldsymbol{q}_{j_i}^m)^-\right)|_{\sigma_j^m}\right) : \left(\nabla_\Gamma \boldsymbol{X}^m\left((\boldsymbol{q}_{j_i}^m)^-\right)|_{\sigma_j^m}\right) \geq \gamma(\boldsymbol{n}_j^{m+1})|\,\sigma_j^{m+1}|. \tag{3.80}$$

Summing (3.80) for $j = 1, 2, \ldots, J$ and combining (3.78) and (3.79), we obtain

$$\begin{aligned}
&\langle \boldsymbol{Z}_k(\boldsymbol{n}^m)\nabla_\Gamma \boldsymbol{X}^{m+1}, \nabla_\Gamma(\boldsymbol{X}^{m+1}-\boldsymbol{X}^m)\rangle^h_{\Gamma^m} + W^m \\
&\geq \frac{1}{2}\langle \boldsymbol{Z}_k(\boldsymbol{n}^m)\nabla_\Gamma \boldsymbol{X}^{m+1}, \nabla_\Gamma \boldsymbol{X}^{m+1}\rangle^h_{\Gamma^m} \\
&\geq W^{m+1}, \quad m \geq 0.
\end{aligned} \tag{3.81}$$

Finally, choosing $\psi = \mu^{m+1}$ in (3.45a) and $\boldsymbol{\omega} = \boldsymbol{X}^{m+1}$ in (3.45b), noting (3.81), we have

$$W^{m+1} - W^m \leq \tau\left(\nabla_\Gamma \mu^{m+1}, \nabla_\Gamma \mu^{m+1}\right)^h_{\Gamma^m} \leq 0, \qquad m \geq 0, \tag{3.82}$$

which immediately implies the unconditional energy stability (3.50b) in Theorem 3.2. □

Remark 3.5. *We remark here, if in 2D, the inequality (3.81) is replaced by [8, (4.22)]*

$$\frac{1}{2}\langle \boldsymbol{Z}_k(\boldsymbol{n}^m)\nabla_\Gamma \boldsymbol{X}^{m+1}, \nabla_\Gamma \boldsymbol{X}^{m+1}\rangle^h_{\Gamma^m} + \frac{1}{2}W^m \geq W^{m+1}. \tag{3.83}$$

Due to the additional positive term $\frac{1}{2}W^m$ on the left hand side of the above inequality, the proof can much simplified and is straightforward by using the AM-GM inequality [8].

3.5 Numerical results

In this section, we first state the setup for solving the symmetrized SP-PFEM (3.45). Then we present several numerical computations, including the convergence test and the structure-preserving test. Finally, we apply (3.45) to simulate surface evolution for different anisotropic energies.

In our practical computations, the minimal stabilizing function $k_0(\boldsymbol{n})$ can be obtained via numerically solving (3.49). Then by taking a stabilizing function $k(\boldsymbol{n}) \geq k_0(\boldsymbol{n})$ for $\boldsymbol{n} \in \mathbb{S}^2$, we can determine the surface energy matrix $\boldsymbol{Z}_k(\boldsymbol{n})$, and thus the symmetrized SP-PFEM (3.45) is well-determined. At each time step, the weakly nonlinear system (3.45) is solved by Newton's method with a given tolerance at $\varepsilon_0 = 10^{-12}$ [13].

Given an initial closed surface Γ_0, we generate its approximation $\Gamma^0 := \Gamma_0^h = \cup_{j=1}^J \overline{\sigma_j^0}$ with J triangles $\{\sigma_j^0\}_{j=1}^J$ and I vertices $\{\boldsymbol{q}_i^0\}_{i=1}^I$ by using the Matlab toolbox called *CFDTool* [132] with a given parameter mesh size h. Given a time step size τ and a mesh size h, we denote $(\boldsymbol{X}_{h,\tau}^m, \mu_{h,\tau}^m)$ as the solution of (3.45) with the initial approximation Γ_0^h at the time $t = t_m$. We define $\boldsymbol{X}_{h,\tau}(t)$ by

$$\boldsymbol{X}_{h,\tau}(\cdot,t) = \frac{t-t_m}{\tau}\boldsymbol{X}_{h,\tau}^m(\cdot) + \frac{t_{m+1}-t}{\tau}\boldsymbol{X}_{h,\tau}^{m+1}(\cdot), \qquad \forall t \in [t_m, t_{m+1}], \quad m \geq 0, \tag{3.84}$$

(h,τ)	$e_{h,\tau}(\frac{1}{2})$ Case 1	order	$e_{h,\tau}(\frac{1}{2})$ Case 2	order	$e_{h,\tau}(\frac{1}{2})$ Case 3	order
(h_0,τ_0)	1.24E-1	-	1.47E-1	-	1.12E-1	-
$(\frac{h_0}{2},\ \frac{\tau_0}{4})$	3.06E-2	2.01	3.54E-2	2.05	2.82E-2	1.98
$(\frac{h_0}{2^2},\ \frac{\tau_0}{4^2})$	7.90E-3	1.96	8.74E-3	2.02	7.54E-3	1.90
(h,τ)	$e_{h,\tau}(\frac{1}{2})$ Case 4	order	$e_{h,\tau}(\frac{1}{2})$ Case 5	order	$e_{h,\tau}(\frac{1}{2})$ Case 6	order
(h_0,τ_0)	1.10E-1	-	1.12E-1	-	1.12E-1	-
$(\frac{h_0}{2},\ \frac{\tau_0}{4})$	2.83E-2	1.96	2.89E-2	1.96	3.09E-2	1.99
$(\frac{h_0}{2^2},\ \frac{\tau_0}{4^2})$	7.48E-3	1.92	7.58E-3	1.93	7.86E-3	1.97

(h,τ)	$e_{h,\tau}(1)$ Case 1	order	$e_{h,\tau}(1)$ Case 2	order	$e_{h,\tau}(1)$ Case 3	order
(h_0,τ_0)	1.46E-1	-	1.22E-1	-	1.11E-1	-
$(\frac{h_0}{2},\ \frac{\tau_0}{4})$	3.52E-2	2.05	3.01E-2	2.02	2.74E-2	2.02
$(\frac{h_0}{2^2},\ \frac{\tau_0}{4^2})$	8.67E-3	2.02	7.75E-3	1.96	7.21E-3	1.93
(h,τ)	$e_{h,\tau}(1)$ Case 4	order	$e_{h,\tau}(1)$ Case 5	order	$e_{h,\tau}(1)$ Case 6	order
(h_0,τ_0)	1.10E-1	-	1.10E-1	-	1.13E-1	-
$(\frac{h_0}{2},\ \frac{\tau_0}{4})$	2.76E-2	1.99	2.80E-2	1.97	2.90E-2	1.96
$(\frac{h_0}{2^2},\ \frac{\tau_0}{4^2})$	7.23E-3	1.93	7.36E-3	1.93	7.56E-3	1.94

Table 3.1: Numerical errors of $e_{h,\tau}(t = 0.5)$ and $e_{h,\tau}(t = 1)$ for Cases 1-6, while $h_0 := 2^{-1}$ and $\tau_0 := \frac{2^{-1}}{25}$ with 140 triangles and 72 vertices for the initial partition $\Gamma_0^{h_0}$, with 624 triangles and 314 vertices for the initial partition $\Gamma_0^{h_0/2}$, and with 2502 triangles and 1253 vertices for the initial partition $\Gamma_0^{h_0/4}$.

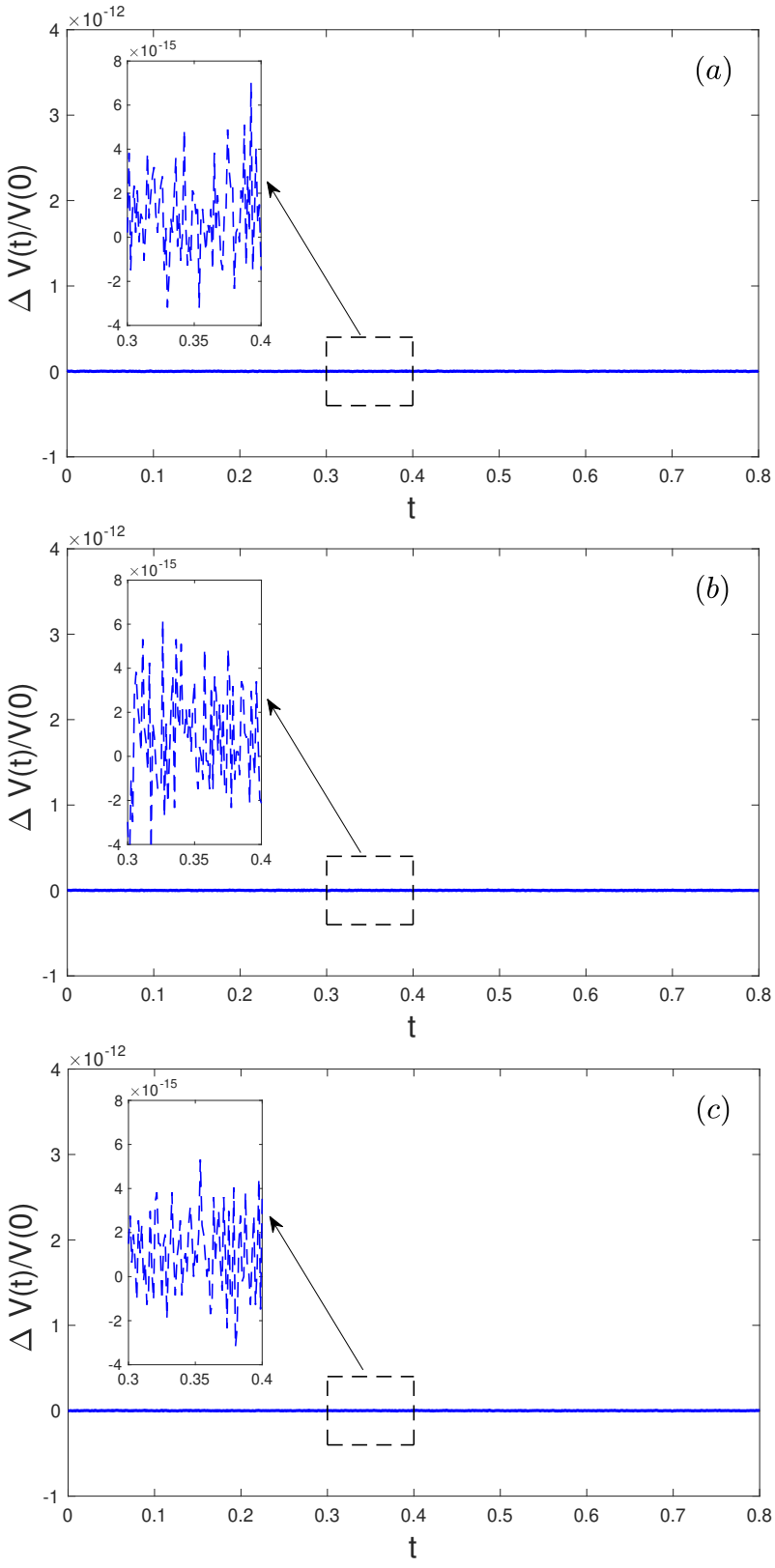

Figure 3.3: Plot of the normalized volume change $\frac{\Delta V(t)}{V(0)}$ for different cases: (a) for Case 1, (b) for Case 2, and (c) for Case 3.

and the surface $\Gamma_{h,\tau}(t)$ is represented by $\boldsymbol{X}_{h,\tau}(\cdot,t)$.

To test the convergence rate of (3.45), we adopt the manifold distance $M(\cdot,\cdot)$ to measure the difference between two closed surfaces Γ_1 and Γ_2, which is given by

$$M(\Gamma_1,\Gamma_2) := 2|\Omega_1 \cup \Omega_2| - |\Omega_1| - |\Omega_2|, \tag{3.85}$$

where Ω_1 and Ω_2 are the regions enclosed by Γ_1 and Γ_2, respectively, and $|\Omega|$ denotes the volume of the region Ω. Based on the manifold distance, the numerical error is defined as

$$e_{h,\tau}(t) := M(\Gamma_{h,\tau}(t),\Gamma(t)), \qquad t \geq 0. \tag{3.86}$$

In our practical computations, $\Gamma(t)$ is obtained numerically by taking $k(\boldsymbol{n}) = k_0(\boldsymbol{n})$ and with a very refined mesh size at $h = h_e = 2^{-4}$ and a very small time step at $\tau = \tau_e = \frac{2}{25}h_e^2$.

In the numerical experiments for testing convergence rates, the time step size and the mesh size are chosen as $\tau = \frac{2}{25}h^2$, the initial shape Γ_0 is chosen as a $2\times2\times1$ cuboid, and its finest partition is a polyhedron $\Gamma_0^{h_e}$ with 10718 triangles and 5361 vertices. We consider the following five cases of the anisotropic surface energy $\gamma(\boldsymbol{n})$ as well as the stabilizing function $k(\boldsymbol{n})$:

- Case 1: $\gamma(\boldsymbol{n}) = 1 + \frac{1}{4}(n_1^4 + n_2^4 + n_3^4)$, $k(\boldsymbol{n}) = k_0(\boldsymbol{n})$;
- Case 2: $\gamma(\boldsymbol{n}) = 1 + \frac{1}{2}(n_1^4 + n_2^4 + n_3^4)$, $k(\boldsymbol{n}) = k_0(\boldsymbol{n})$;
- Case 3: $\gamma(\boldsymbol{n}) = (n_1^4 + n_2^4 + n_3^4)^{\frac{1}{4}}$, $k(\boldsymbol{n}) = k_0(\boldsymbol{n})$;
- Case 4: $\gamma(\boldsymbol{n}) = (n_1^4 + n_2^4 + n_3^4)^{\frac{1}{4}}$, $k(\boldsymbol{n}) = k_0(\boldsymbol{n}) + 1$;
- Case 5: $\gamma(\boldsymbol{n}) = (n_1^4 + n_2^4 + n_3^4)^{\frac{1}{4}}$, $k(\boldsymbol{n}) = k_0(\boldsymbol{n}) + 2$;
- Case 6: $\gamma(\boldsymbol{n}) = (n_1^4 + n_2^4 + n_3^4)^{\frac{1}{4}}$, $k(\boldsymbol{n}) = k_0(\boldsymbol{n}) + 5$.

The numerical errors are listed in Table 3.1. We note that while $\gamma(\boldsymbol{n})$ and $k(\boldsymbol{n})$ are chosen differently in different cases, the convergence rates for this manifold error are all about second order in h. These results indicate that the proposed

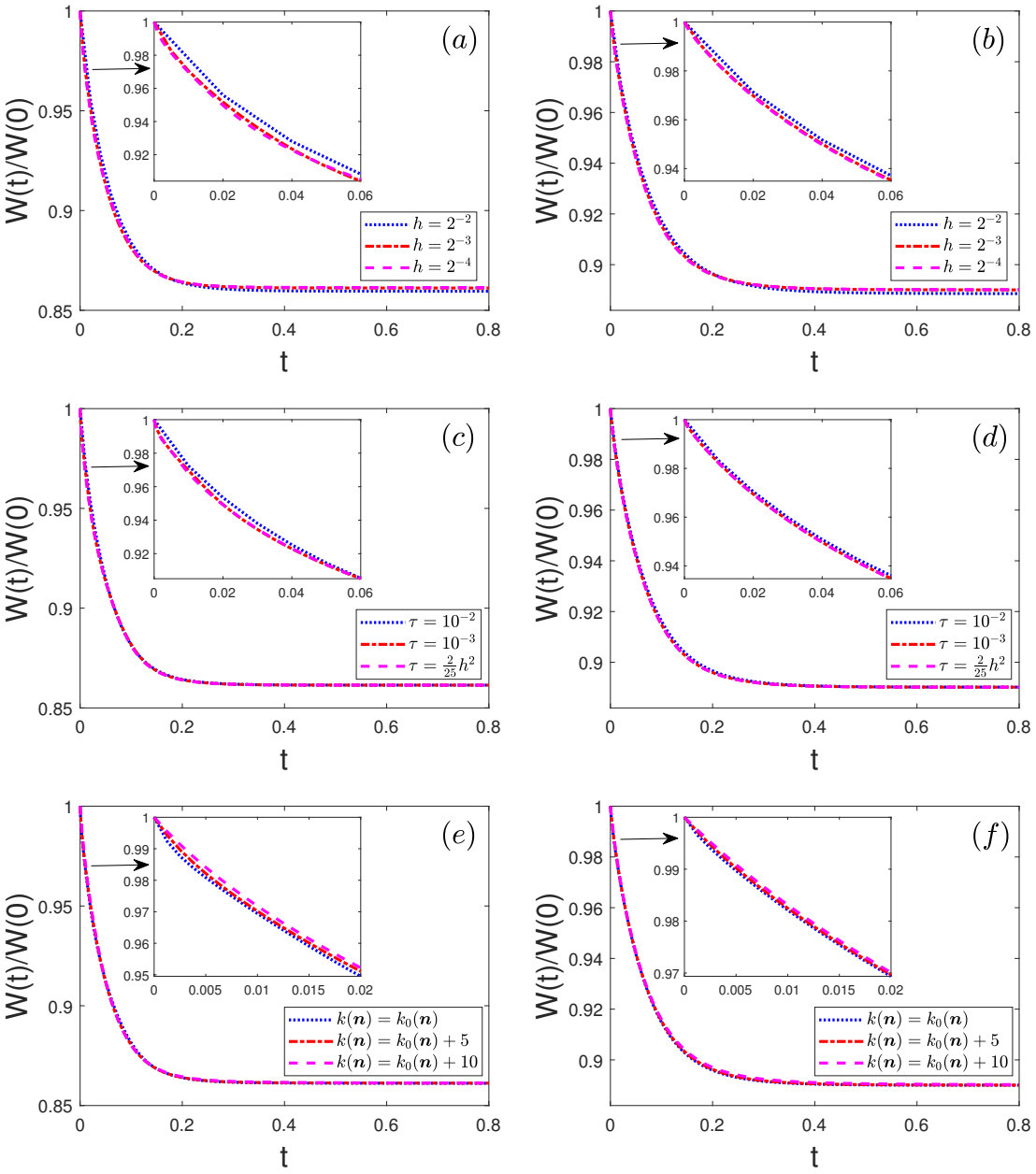

Figure 3.4: Plot of the normalized energy $\frac{W(t)}{W(0)}$ for weak anisotropy $\gamma(\boldsymbol{n}) = 1 + \frac{1}{4}(n_1^4 + n_2^4 + n_3^4)$ (left column) and strong anisotropy $\gamma(\boldsymbol{n}) = 1 + \frac{1}{2}(n_1^4 + n_2^4 + n_3^4)$ (right column) for: with fixed $k(\boldsymbol{n}) = k_0(\boldsymbol{n})$ for different h and τ (top row with (a) and (b)), and for fixed $h = 2^{-4}$ and different τ (middle row with (c) and (d)); and with fixed $h = 2^{-4}, \tau = \frac{2}{25}h^2$ for different $k(\boldsymbol{n})$ (bottom row with (e) and (f)).

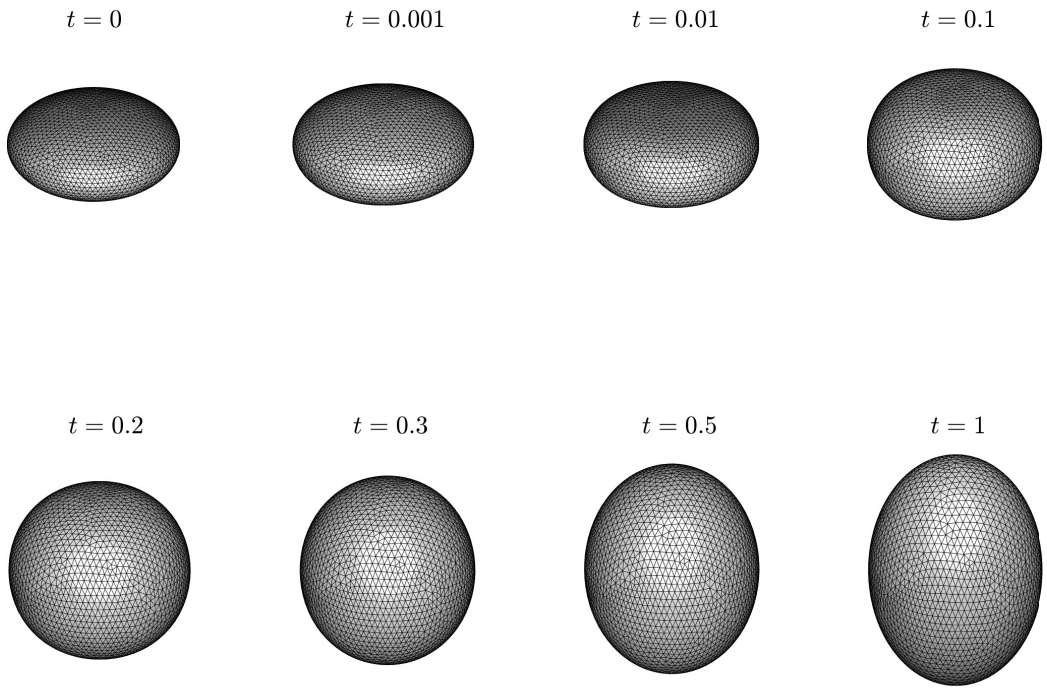

Figure 3.5: Evolution of a $2 \times 2 \times 1$ ellipsoid by anisotropic surface diffusion with a weak anisotropy $\gamma(\boldsymbol{n}) = \sqrt{n_1^2 + n_2^2 + 2n_3^2}$ and $k(\boldsymbol{n}) = k_0(\boldsymbol{n})$ at different times.

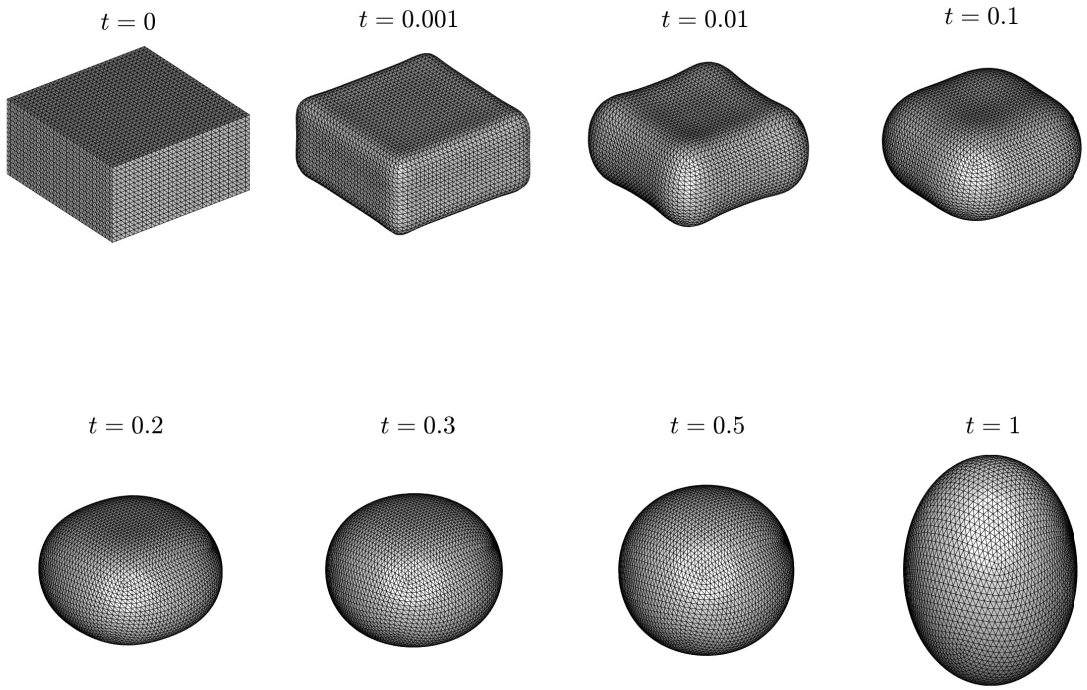

Figure 3.6: Evolution of a $2 \times 2 \times 1$ cuboid by anisotropic surface diffusion with a weak anisotropy $\gamma(\boldsymbol{n}) = \sqrt{n_1^2 + n_2^2 + 2n_3^2}$ and $k(\boldsymbol{n}) = k_0(\boldsymbol{n})$ at different times.

symmetrized SP-PFEM (3.45) has a good robustness in convergence rate, which is in general independent of $\gamma(\boldsymbol{n})$ and $k(\boldsymbol{n})$. Thus in practical computations, there is no need to choose $k(\boldsymbol{n})$ as the minimal stabilizing function $k_0(\boldsymbol{n})$.

To examine the volume conservation and unconditionally energy dissipation, we consider these two indicators: the normalized volume change $\frac{\Delta V(t)}{V(0)} := \frac{V(t)-V(0)}{V(0)}$ and the normalized energy $\frac{W(t)}{W(0)}$. The initial shape is taken as a $2\times2\times1$ ellipsoid. Figure 3.3 shows the normalized volume change $\frac{\Delta V(t)}{V(0)}$ for Cases 1–3 with fixed $h = 2^{-3}$ and $\tau = \frac{2}{25}h^2$. We find the order of magnitude of the volume change $\Delta V(t)$ is at around 10^{-15}, which is close to the machine epsilon at around 10^{-16}, and thus it confirms numerically volume conservation of the symmetrized SP-PFEM in Theorem (3.2). Figure 3.4 plots the normalized energy $\frac{W(t)}{W(0)}$ for different mesh size h with $\tau = \frac{2}{25}h^2$ and for different τ with a fixed mesh size $h = 2^{-4}$. We observe that the normalized energy $\frac{W(t)}{W(0)}$ is monotonically decreasing in time for all cases, which again confirms the unconditional energy stability of the symmetrized SP-PFEM in Theorem (3.2). Furthermore, our numerical results suggest that different stabilizing functions $k(\boldsymbol{n})$ do not pollute the energy too much, and thus we can choose a relatively large stabilizing function $k(\boldsymbol{n})$ in practical computations.

Finally, we use the symmetrized SP-PFEM (3.45) to investigate the motion by anisotropic surface diffusion with different anisotropies. We consider the weak anisotropy $\gamma(\boldsymbol{n}) = \sqrt{n_1^2 + n_2^2 + 2n_3^2}$ with $k(\boldsymbol{n}) = k_0(\boldsymbol{n})$. The evolutions of a smooth $2 \times 2 \times 1$ ellipsoid and a non-smooth $2 \times 2 \times 1$ cuboid are shown in figure 3.5 and figure 3.6, respectively. We choose the mesh size $h = 2^{-4}$ and the time step size $\tau = \frac{2}{25}h^2$, and the ellipsoid and the cuboid are initially approximated by 10718 triangles and 5361 vertices, and 32768 triangles and 16386 vertices, respectively. By comparing the two figures, we find the two numerical equilibriums are close in shape, which indicates our SP-PFEM (3.45) is robust in capturing the equilibrium shape for different initial shapes. We can see that the meshes are well distributed during the evolution, and there is no need to re-mesh during the evolution.

Then we show the evolution of a strong anisotropy $\gamma(\boldsymbol{n}) = 1 + \frac{1}{2}(n_1^4 + n_2^4 + n_3^4)$

from a $2 \times 2 \times 1$ cuboid, and the parameters are chosen the same as in previous weak anisotropy. As it can be seen from Figure 3.7, the large and flat facets may be broken into small facets, and the small facets may also merge into a large facet. Moreover, we note from Figure 3.7 that the triangulations become dense at the edges where the facets merge but become sparse at the other edges and at the interior of the facets where the weighted mean curvature μ is almost a constant. This indicates the meshes achieve the same 'stable fashion' as in the BGN scheme [19].

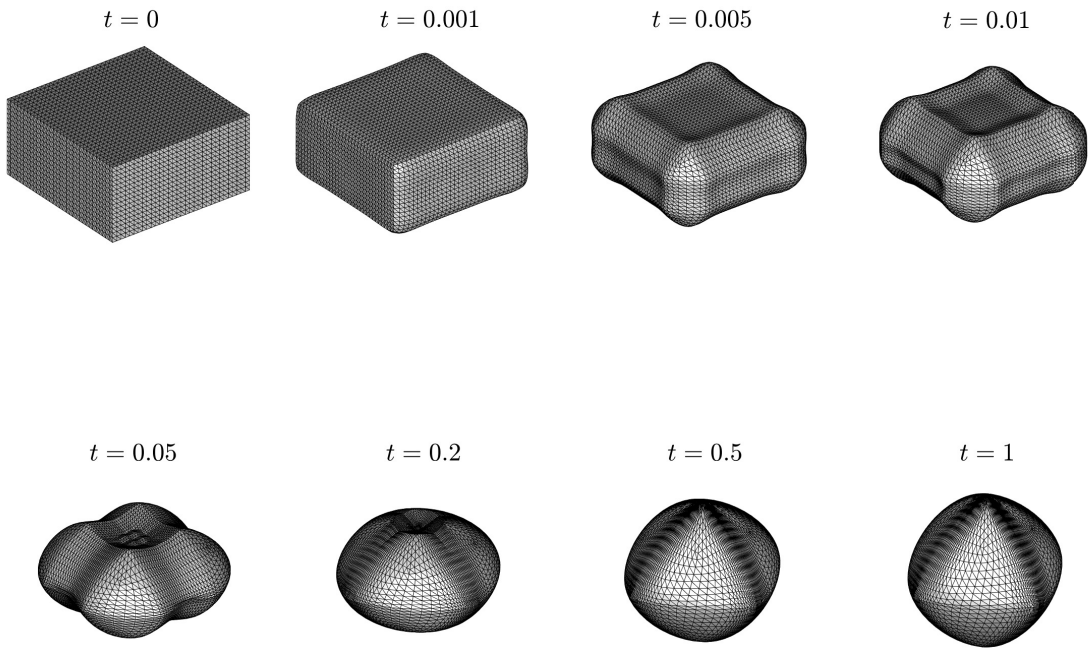

Figure 3.7: Evolution of a $2 \times 2 \times 1$ cuboid by anisotropic surface diffusion with a strong anisotropy $\gamma(\boldsymbol{n}) = 1 + \frac{1}{2}(n_1^4 + n_2^4 + n_3^4)$ and $k(\boldsymbol{n}) = k_0(\boldsymbol{n})$ at different times.

Chapter 4

A unified SP-PFEM for arbitrary surface energy

So far, for the symmetric anisotropy $\gamma(\boldsymbol{n}) = \gamma(-\boldsymbol{n})$, we have successfully proposed the symmetrized SP-PFEM for curves and surfaces, and developed the rigorous analysis for energy stability. Hence, it is a natural question that for the arbitrary anisotropic surface energy $\gamma(\boldsymbol{n})$, especially the non-symmetric $\gamma(-\boldsymbol{n}) \neq \gamma(\boldsymbol{n})$, how to establish a PFEM that can be proved to be structural-preserving. In fact, several important anisotropic surface energies do not satisfy the condition $\gamma(-\boldsymbol{n}) = \gamma(\boldsymbol{n})$, such as the 3-fold anisotropy, and the piecewisely Riemannian metric anisotropic surface energy. However, as mentioned in the Corollary 2.1, the symmetrized SP-PFEM can only work for symmetric anisotropy. Therefore, to include the arbitrary anisotropic surface energy, we need to develop an essentially different SP-PFEM.

Moreover, we also want the proposed SP-PFEM can be applied to both curves and surfaces. To overcome this difficulty, we need to compare the essential differences related to the dimension. First, the dimension of the tangential space is different, which leads to the difference between the definition of the minimal stabilizing function $k_0(\boldsymbol{n})$. Second, the proof of energy stability requires the estimate of $k_0(\boldsymbol{n})$, which relies on several dimensional-dependent inequalities. However, the two essential differences are related to the analysis of energy stability, which challenges

us to develop a new analysis framework!

In this Chapter, we design a novel unified SP-PFEM for arbitrary anisotropic surface energies that overcomes the two problems simultaneously – first, it can work for both 2D curves ($d = 2$) and 3D surfaces ($d = 3$); second, it enlarges the energy stability condition from $\gamma(-\boldsymbol{n}) = \gamma(\boldsymbol{n})$ to $\gamma(-\boldsymbol{n}) < (5-d)\gamma(\boldsymbol{n})$. To this end, we first recall the definition of global parameterization and the surface gradient operator. Then by introducing a unified surface energy matrix $\boldsymbol{G}_k(\boldsymbol{n})$, we derive a unified weak formulation for the weighted mean curvature μ as well as the conservative variational formulation for the anisotropic surface diffusion. After that, we adopt the PFEM to get its full discretization – the unified SP-PFEM. Next, we develop a new framework for the energy-stable analysis, including these three steps: First, we adopt the definition of the minimal stabilizing function $k_0(\boldsymbol{n})$ to derive the local estimate. Second, the local estimate is applied to prove the energy stability. Third, by several in-depth and careful calculations, we get the existence of the minimal stabilizing function $k_0(\boldsymbol{n})$. Finally, a large number of numerical experiments are shown to illustrate the efficiency and validate the energy stability of our unified SP-PFEM.

4.1 A unified weak formulation

4.1.1 Some general anisotropic surface energies and their $\boldsymbol{\xi}$-vectors

Here we list the commonly used non-symmetric $\gamma(\boldsymbol{n})$ with their $\boldsymbol{\xi}$-vector and Hessian as follows:

- the piecewisely Riemannian metric anisotropic surface energy [55]

$$\gamma(\boldsymbol{n}) = \sqrt{(a + b\ \mathrm{sgn}(n_1))\, n_1^2 + n_2^2}, \qquad \forall \boldsymbol{n} = (n_1, n_2)^T \in \mathbb{S}^1, \tag{4.1}$$

  where $a, a + b > 0$, sgn is the sign function. The $\boldsymbol{\xi}$-vector and the Hessian matrix are similar to the Riemannian metric anisotropy (2.4).

It can also be extended to 3D as

$$\gamma(\boldsymbol{n}) = \sqrt{(a + b\ \mathrm{sgn}(n_1))\, n_1^2 + n_2^2 + n_3^2}, \qquad \forall \boldsymbol{n} \in \mathbb{S}^2, \tag{4.2}$$

where $\boldsymbol{n} = (n_1, n_2, n_3)^T \in \mathbb{S}^2$.

- the 3-fold anisotropic surface energy [10, 96, 113, 145]

$$\gamma(\boldsymbol{n}) = 1 + \beta \cos(3(\theta - \theta_0)), \qquad \forall \boldsymbol{n} = (-\sin\theta, \cos\theta)^T \in \mathbb{S}^1, \tag{4.3}$$

where $\theta_0 \in [-\pi, \pi]$ is a constant, and $\beta \geq 0$ is a dimensionless anisotropic strength constant. When $\theta_0 = 0$, we have

$$\gamma(\boldsymbol{p}) = \left(p_1^2 + p_2^2\right)^{\frac{1}{2}} (1 + \beta \cos(3\theta)), \forall \boldsymbol{p} = |p|(-\sin\theta, \cos\theta)^T \in \mathbb{R}^2_*. \tag{4.4}$$

Plugging (4.4) into (1.3), we get

$$\boldsymbol{\xi} = \boldsymbol{\xi}(\boldsymbol{n}) = \boldsymbol{n} + \beta \cos(3\theta)\boldsymbol{n} + 3\beta \sin(3\theta)\boldsymbol{n}^{\perp}, \quad \boldsymbol{n} = (-\sin\theta, \cos\theta), \tag{4.5}$$

$$\lambda(\boldsymbol{n}) = 1 - 8\beta \cos(m\theta), \tag{4.6}$$

which indicates that it is weakly anisotropic if $0 \leq \beta \leq \frac{1}{8}$; otherwise, it is strongly anisotropic.

4.1.2 Mathematical formulation

Let $\Gamma_0 \subset \mathbb{R}^d$ be the initial orientable 2D curve/3D surface with the global parameterization $\boldsymbol{X}(\boldsymbol{\rho}, t)$ as

$$\boldsymbol{X}(\cdot, t) : \Gamma_0 \to \mathbb{R}^d,\ (\boldsymbol{\rho}, t) \mapsto \boldsymbol{X}(\boldsymbol{\rho}, t) := (X_1(\boldsymbol{\rho}, t), \ldots, X_d(\boldsymbol{\rho}, t))^T, \tag{4.7}$$

Let $\boldsymbol{n}$ be the outward unit vector of the closed orientable surface $\Gamma(t)$. By [33, Definition 25], the normal velocity V_n of $\Gamma(t)$ is thus given as

$$V_n = V_n(\boldsymbol{\rho}, t) = \partial_t \boldsymbol{X}(\boldsymbol{\rho}, t) \cdot \boldsymbol{n}. \tag{4.8}$$

For a differentiable scalar-valued function f defined in an open neighbourhood of Γ_0, the surface gradient operator $\nabla_{\Gamma(t)} f$ is defined by [12, 55]

$$\nabla_\Gamma f = \nabla_{\Gamma(t)} f := \nabla f - (\nabla f \cdot \boldsymbol{n})\boldsymbol{n} = (\underline{D}_1 f, \ldots, \underline{D}_d f)^T. \tag{4.9}$$

Similarly, the surface gradient/divergence for a vector-valued function $\boldsymbol{f} = (f_1, \ldots, f_d)^T$ are

$$\nabla_\Gamma \boldsymbol{f} = \nabla_{\Gamma(t)} \boldsymbol{f} := (\nabla_\Gamma f_1, \ldots, \nabla_\Gamma f_d)^T, \quad \nabla_\Gamma \cdot \boldsymbol{f} = \nabla_{\Gamma(t)} \cdot \boldsymbol{f} := \sum_{i=1}^{d} \underline{D}_i f_i. \tag{4.10}$$

The functional spaces $L^2(\Gamma_0)$ is given as follows

$$L^2(\Gamma_0) := \left\{ u : \Gamma_0 \to \mathbb{R} \mid \int_{\Gamma_0} |u|^2 \, dA < +\infty \right\}, \tag{4.11}$$

with the weighted inner product $(\cdot, \cdot)_{\Gamma(t)}$ with respect to $\Gamma(t)$ as

$$(u, v)_{\Gamma(t)} := \int_{\Gamma_0} u\, v \, \det(\boldsymbol{J}_{\boldsymbol{X}(\cdot,t)}) dA = \int_{\Gamma(t)} u\, v \, dA(t), \quad \forall u, v \in L^2(\Gamma_0). \tag{4.12}$$

where $dA, dA(t)$ is the area element of $\Gamma_0, \Gamma(t)$, respective. And $\boldsymbol{J}_{\boldsymbol{X}(\cdot,t)}$ is the Jacobian matrix given by $\boldsymbol{X}(\cdot, t)$. Similarly, we can define the functional spaces $[L^2(\Gamma_0)]^d$ and $[L^2(\Gamma_0)]^{d\times d}$. Moreover, the inner product for two matrix-valued functions $\boldsymbol{U}, \boldsymbol{V} \in [L^2(\Gamma_0)]^{d\times d}$ with respect to $\Gamma(t)$ is emphasized as

$$\langle \boldsymbol{U}, \boldsymbol{V} \rangle_{\Gamma(t)} := \int_{\Gamma_0} \boldsymbol{U} : \boldsymbol{V} \, \det(\boldsymbol{J}_{\boldsymbol{X}(\cdot,t)}) dA = \int_{\Gamma(t)} \boldsymbol{U} : \boldsymbol{V} \, dA(t), \tag{4.13}$$

here $\boldsymbol{U} : \boldsymbol{V} = \mathrm{Tr}(\boldsymbol{V}^T \boldsymbol{U})$ is the Frobenius inner product. The Sobolev spaces $H^1(\Gamma_0), [H^1(\Gamma_0)]^d$ are thus given as

$$H^1(\Gamma_0) := \left\{ u : \Gamma_0 \to \mathbb{R} \mid u \in L^2(\Gamma_0),\, \nabla_\Gamma u \in [L^2(\Gamma_0)]^d \right\}, \tag{4.14}$$

$$[H^1(\Gamma_0)]^d := \left\{ \boldsymbol{u} : \Gamma_0 \to \mathbb{R}^d \mid \boldsymbol{u} \in [L^2(\Gamma_0)]^d,\, \nabla_\Gamma \boldsymbol{u} \in [L^2(\Gamma_0)]^{d\times d} \right\}. \tag{4.15}$$

We recall that the motion of $\Gamma(t)$ under the anisotropic surface diffusion (1.21) can be reformulated as the PDE formulation

$$\begin{cases} \boldsymbol{n} \cdot \partial_t \boldsymbol{X} = \Delta_\Gamma \mu, & \text{(4.16a)} \\ \mu = \nabla_\Gamma \cdot \boldsymbol{\xi}, \quad \xi(\boldsymbol{n}) = \nabla \gamma(\boldsymbol{p})|_{\boldsymbol{p}=\boldsymbol{n}}. & \text{(4.16b)} \end{cases}$$

Let $V(t)$ be the enclosed volume and $W(t)$ be the total energy of the closed orientable evolving curve/surface $\Gamma(t)$, respectively. Based on this global parameterization, $V(t), W(t)$ are formally given by

$$V(t) := \frac{1}{d} \int_{\Gamma(t)} \boldsymbol{X} \cdot \boldsymbol{n} \, dA(t), \qquad W(t) := \int_{\Gamma(t)} \gamma(\boldsymbol{n}) \, dA(t). \tag{4.17}$$

From [33, 55] we know that the under the surface diffusion (4.16), the enclosed volume $V(t)$ is conserved, and the total energy $W(t)$ is decreasing.

Finally, our goal is to propose a unified SP-PFEM with the following energy-stable condition on $\gamma(\boldsymbol{p})$:

$$\gamma(-\boldsymbol{p}) < (5-d)\gamma(\boldsymbol{p}),\ \forall \boldsymbol{p} \in \mathbb{R}^d_*, \qquad \gamma(\boldsymbol{p}) \in C(\mathbb{R}^d) \cap C^2(\mathbb{R}^d_*). \tag{4.18}$$

Remark 4.1. *In fact, similar to the 2D paper [11], the regularity condition in (4.18) can be relaxed to piecewise C^2-anisotropies.*

4.1.3 A unified surface energy matrix

Define the unified surface energy matrix $\boldsymbol{G}_k(\boldsymbol{n})$ as

$$\boldsymbol{G}_k = \boldsymbol{G}_k(\boldsymbol{n}) = \gamma(\boldsymbol{n})I_d - \boldsymbol{n}\boldsymbol{\xi}^T + \boldsymbol{\xi}\boldsymbol{n}^T + k(\boldsymbol{n})\boldsymbol{n}\boldsymbol{n}^T, \tag{4.19}$$

where $k(\boldsymbol{n}) : \mathbb{S}^{d-1} \to \mathbb{R}_{\geq 0}$ is the stabilizing function. Denote its symmetric part as $\boldsymbol{G}_k^{(s)}$, and its anti-symmetric part as $\boldsymbol{G}^{(a)}$, i.e.,

$$\boldsymbol{G}_k^{(s)} := \gamma(\boldsymbol{n})I_d + k(\boldsymbol{n})\boldsymbol{n}\boldsymbol{n}^T,\ \boldsymbol{G}^{(a)} := -\boldsymbol{n}\boldsymbol{\xi}^T + \boldsymbol{\xi}\boldsymbol{n}^T,\ \boldsymbol{G}_k = \boldsymbol{G}_k^{(s)} + \boldsymbol{G}^{(a)}. \tag{4.20}$$

The importance of the proposed unified surface energy matrix $\boldsymbol{G}_k(\boldsymbol{n})$ can be seen from the following theorem.

Theorem 4.1. *Let Γ be a closed orientable C^2-curve/surface with the outward unit normal vector $\boldsymbol{n}$. For any $\boldsymbol{\omega} \in [H^1(\Gamma)]^d$, there holds the following equality*

$$(\mu\boldsymbol{n}, \boldsymbol{\omega})_\Gamma = \langle \boldsymbol{G}_k(\boldsymbol{n})\nabla_\Gamma \boldsymbol{X}, \nabla_\Gamma \boldsymbol{\omega}\rangle_\Gamma. \tag{4.21}$$

Proof. We first consider the 2D curve. Let s be the arc-length parameter for the closed orientable curve Γ, ∂_s be the arc-length derivative, and $\boldsymbol{\tau} = \partial_s \boldsymbol{X}$ be the unit tangential vector. From [11], we know that the left-hand side for (4.21) becomes

$$(\mu\boldsymbol{n}, \boldsymbol{\omega})_\Gamma = (\boldsymbol{G}_k(\boldsymbol{n})\partial_s \boldsymbol{X}, \partial_s \boldsymbol{\omega})_\Gamma\,. \tag{4.22}$$

On the other hand, [33, Definition 5] gives that

$$\nabla_\Gamma \boldsymbol{X} = \partial_s \boldsymbol{X} \boldsymbol{\tau}^T, \qquad \nabla_\Gamma \boldsymbol{\omega} = \partial_s \boldsymbol{\omega} \boldsymbol{\tau}^T. \tag{4.23}$$

Thus by applying the definition of the inner product for two matrix-valued functions (4.13), the right-hand side for (4.21) can be simplified as

$$\begin{aligned}
\langle \boldsymbol{G}_k(\boldsymbol{n}) \nabla_\Gamma \boldsymbol{X}, \nabla_\Gamma \boldsymbol{\omega} \rangle_\Gamma &= \int_\Gamma \mathrm{Tr}(\boldsymbol{\tau} (\partial_s \boldsymbol{\omega})^T \boldsymbol{G}_k(\boldsymbol{n}) \partial_s \boldsymbol{X} \boldsymbol{\tau}^T)\, dA \\
&= \int_\Gamma \mathrm{Tr}((\partial_s \boldsymbol{\omega})^T \boldsymbol{G}_k(\boldsymbol{n}) \partial_s \boldsymbol{X} (\boldsymbol{\tau}^T \boldsymbol{\tau}))\, dA \\
&= \int_\Gamma \mathrm{Tr}((\partial_s \boldsymbol{\omega})^T \boldsymbol{G}_k(\boldsymbol{n}) \partial_s \boldsymbol{X})\, dA \\
&= (\boldsymbol{G}_k(\boldsymbol{n}) \partial_s \boldsymbol{X}, \partial_s \boldsymbol{\omega})_\Gamma .
\end{aligned} \tag{4.24}$$

The desired equality (4.1) is the direct result of (4.22) and (4.24).

For the 3D case, from [12, Lemma 2.1] and (4.19), we have already known that

$$\begin{aligned}
(\mu \boldsymbol{n}, \boldsymbol{\omega})_\Gamma &= \langle (\gamma(\boldsymbol{n}) I_3 - \boldsymbol{n}\boldsymbol{\xi}^T - \boldsymbol{\xi}\boldsymbol{n}^T + k(\boldsymbol{n}) \boldsymbol{n}\boldsymbol{n}^T) \nabla_\Gamma \boldsymbol{X}, \nabla_\Gamma \boldsymbol{\omega} \rangle_\Gamma \\
&= \langle \boldsymbol{G}_k(\boldsymbol{n}) \nabla_\Gamma \boldsymbol{X}, \nabla_\Gamma \boldsymbol{\omega} \rangle_\Gamma - 2 \langle \boldsymbol{\xi}\boldsymbol{n}^T \nabla_\Gamma \boldsymbol{X}, \nabla_\Gamma \boldsymbol{\omega} \rangle_\Gamma .
\end{aligned} \tag{4.25}$$

From equation (24b) in [55], we obtain that

$$\nabla_\Gamma \boldsymbol{X} = I_3 - \boldsymbol{n}\boldsymbol{n}^T. \tag{4.26}$$

Thus by combining (4.25) and (4.26), we deduce that

$$\begin{aligned}
(\mu \boldsymbol{n}, \boldsymbol{\omega})_\Gamma &= \langle \boldsymbol{G}_k(\boldsymbol{n}) \nabla_\Gamma \boldsymbol{X}, \nabla_\Gamma \boldsymbol{\omega} \rangle_\Gamma - 2 \langle \boldsymbol{\xi}\boldsymbol{n}^T (I_3 - \boldsymbol{n}\boldsymbol{n}^T), \nabla_\Gamma \boldsymbol{\omega} \rangle_\Gamma \\
&= \langle \boldsymbol{G}_k(\boldsymbol{n}) \nabla_\Gamma \boldsymbol{X}, \nabla_\Gamma \boldsymbol{\omega} \rangle_\Gamma - 2 \langle \boldsymbol{\xi}\boldsymbol{0}^T, \nabla_\Gamma \boldsymbol{\omega} \rangle_\Gamma \\
&= \langle \boldsymbol{G}_k(\boldsymbol{n}) \nabla_\Gamma \boldsymbol{X}, \nabla_\Gamma \boldsymbol{\omega} \rangle_\Gamma .
\end{aligned} \tag{4.27}$$

Which validates (4.21) □

4.1.4 A weak formulation and its structure-preserving properties

By utilizing (4.1) and taking integration by parts, we then derive the following unified conservative weak formulation for (4.16): Let the initial closed and orientable

curve/surface be Γ_0 and the function $\boldsymbol{X}_0(\boldsymbol{\rho}) = \boldsymbol{\rho}, \forall \boldsymbol{\rho} \in \Gamma_0$. Find the solution $(\boldsymbol{X}(\cdot,t), \mu(\cdot,t)) \in [H^1(\Gamma_0)]^d \times H^1(\Gamma_0)$, such that $\boldsymbol{X}(\cdot,0) = \boldsymbol{X}_0(\cdot)$ and

$$(\partial_t \boldsymbol{X} \cdot \boldsymbol{n}, \phi)_{\Gamma(t)} + (\nabla_\Gamma \mu, \nabla_\Gamma \phi)_{\Gamma(t)} = 0, \quad \forall \phi \in H^1(\Gamma_0), \tag{4.28a}$$

$$(\mu \boldsymbol{n}, \boldsymbol{\omega})_{\Gamma(t)} - \langle \boldsymbol{G}_k(\boldsymbol{n}) \nabla_\Gamma \boldsymbol{X}, \nabla_\Gamma \boldsymbol{\omega} \rangle_{\Gamma(t)} = 0, \quad \forall \boldsymbol{\omega} \in [H^1(\Gamma_0)]^d. \tag{4.28b}$$

Here $\Gamma(t)$ is given by $\boldsymbol{X}(\Gamma_0, t)$.

For the unified conservative weak formulation (4.28), in the same way as Theorem 2.2 in [12], it can be shown that the two geometric properties are well preserved.

Theorem 4.2. *Let $\Gamma(t)$ be the solution of the unified conservative weak formulation, then the enclosed volume $V(t)$ is conserved, and the total energy $W(t)$ is dissipative:*

$$V(t) \equiv V(0), \qquad W(t) \leq W(t') \leq W(0), \quad \forall t \geq t' \geq 0. \tag{4.29}$$

4.2 The unified SP-PFEM

4.2.1 The unified discretization

To discretize the unified conservative weak formulation (4.28), we approximate the closed orientable curve/surface Γ with the closed orientable polygon curve/polyhedral surface Γ^h. For convenience, we assume that Γ^h is composed of a family of disjoint and open non-degenerate line segments/triangles

$$\Gamma^h := \cup_{j=1}^{J} \bar{\sigma}_j, \tag{4.30}$$

where the intersection of $\bar{\sigma}_i$ and $\bar{\sigma}_j$ is a k-simplex of both $\bar{\sigma}_i$ and $\bar{\sigma}_j$, where $k < d-1$. For each line segment σ_j, its two vertices $\{\boldsymbol{q}_{j_1}, \boldsymbol{q}_{j_2}\}$ are assigned an order such that the induced direction vector $\mathcal{J}\{\sigma\}$ given by

$$\mathcal{J}\{\sigma_j\} := -(\boldsymbol{q}_{j_2} - \boldsymbol{q}_{j_1})^\perp, \tag{4.31}$$

pointing the outside of the closed polygon curve Γ^h, where $(u_1, u_2)^\perp = (u_2, -u_1), \forall \boldsymbol{u} = (u_1, u_2) \in \mathbb{R}^2$. And for each triangle σ_j, its three vertices $\{\boldsymbol{q}_{j_1}, \boldsymbol{q}_{j_2}, \boldsymbol{q}_{j_3}\}$ are also assigned an order with the direction vector

$$\mathcal{J}\{\sigma_j\} := (\boldsymbol{q}_{j_2} - \boldsymbol{q}_{j_1}) \times (\boldsymbol{q}_{j_3} - \boldsymbol{q}_{j_2}), \tag{4.32}$$

see Figure. 4.1.

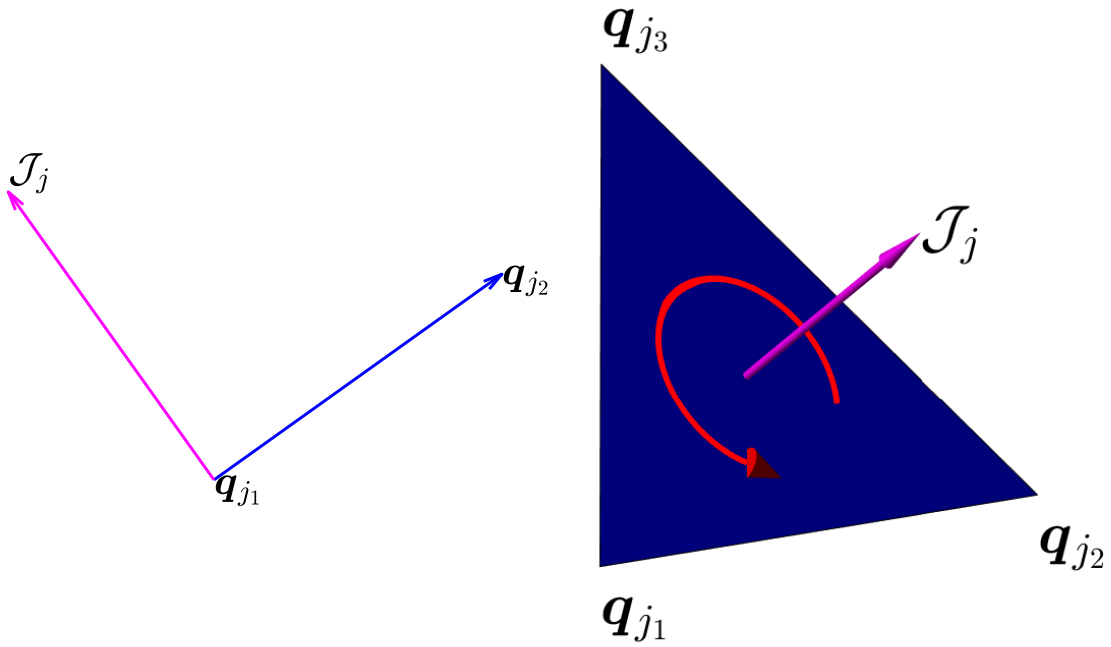

Figure 4.1: Plot of the direction vector $\mathcal{J}$, left is 2D and right is 3D.

By using the direction vector $\mathcal{J}\{\sigma_j\}$, we can thus denote the area $|\sigma_j|$ and the outward normal vector $\boldsymbol{n}_j$ of σ_j as follows

$$|\sigma_j| := \frac{1}{d-1}|\mathcal{J}\{\sigma_j\}|, \qquad \boldsymbol{n}_j := \frac{\mathcal{J}\{\sigma_j\}}{|\mathcal{J}\{\sigma_j\}|}. \tag{4.33}$$

The discretized surface gradient operator ∇_Γ in 2D becomes

$$\nabla_\Gamma f|_{\sigma_j} := \big(f(\boldsymbol{q}_{j_2}) - f(\boldsymbol{q}_{j_1})\big)\frac{\boldsymbol{q}_{j_2} - \boldsymbol{q}_{j_1}}{|\sigma_j|^2}. \tag{4.34}$$

And in 3D, it is

$$\begin{aligned}\nabla_\Gamma f|_{\sigma_j} := \big(&f(\boldsymbol{q}_{j_1})(\boldsymbol{q}_{j_2} - \boldsymbol{q}_{j_3}) + f(\boldsymbol{q}_{j_2})(\boldsymbol{q}_{j_3} - \boldsymbol{q}_{j_1}) \\ &+ f(\boldsymbol{q}_{j_3})(\boldsymbol{q}_{j_1} - \boldsymbol{q}_{j_2})\big) \times \frac{\boldsymbol{n}_j}{2|\sigma_j|}.\end{aligned} \tag{4.35}$$

Suppose the closed orientable C^2-evolving curve/surface $\Gamma(t)$ is approximated by the closed orientable evolving polygon curve/polyhedral surface $\Gamma^h(t) = \cup_{j=1}^J \bar{\sigma}_j(t)$ with the vertices $\boldsymbol{q}_i(t)$. And we denote $\Gamma_0^h := \Gamma^h(0), \sigma_{j,0} := \sigma_j(0)$, $\boldsymbol{q}_{i,0} := \boldsymbol{q}_i(0)$. The global parameterization $\boldsymbol{X}(\cdot, t)$ is approximated by $\boldsymbol{X}^h(\boldsymbol{q}_{i,0}, t) = \boldsymbol{q}_i(t)$ with $\boldsymbol{X}^h(\boldsymbol{q}_{i,0}, 0) = \boldsymbol{X}^h(\boldsymbol{q}_{i,0}) = \boldsymbol{q}_{i,0}$. Similarly, due to the one-to-one correspondence between the function on $\Gamma^h(t)$ and Γ_0^h, it suffices to restrict our interest to the functions on Γ_0^h.

Denote the approximation of $L^2(\Gamma_0)$ as $\mathbb{K}(\Gamma_0^h)$ given by

$$\mathbb{K}(\Gamma_0^h) := \left\{ u \in C(\Gamma_0^h) \,\middle|\, u|_{\sigma_{j,0}} \in \mathcal{P}^1(\sigma_{j,0}),\ \forall j \right\}, \tag{4.36}$$

here $\mathcal{P}^1(\sigma_{j,0})$ is the set of polynomials on $\sigma_{j,0}$ with degree no higher than 1. Suppose $u, v \in \mathbb{K}(\Gamma^h)$, the weighted inner product $(u, v)_{\Gamma(t)}$ is approximated by the weighted mass-lumped inner product $(u, v)^h_{\Gamma^h(t)}$ in the following way:

$$\begin{aligned}(u, v)^h_{\Gamma^h(t)} :&= \frac{1}{d} \sum_{j=1}^{J} \sum_{i=1}^{d} |\boldsymbol{X}^h(\sigma_{j,0}, t)|\, u((\boldsymbol{q}_{j_i,0})^-)\, v((\boldsymbol{q}_{j_i,0})^-) \\ &= \frac{1}{d} \sum_{j=1}^{J} \sum_{i=1}^{d} |\sigma_j(t)|\, u((\boldsymbol{q}_{j_i}(t))^-)\, v((\boldsymbol{q}_{j_i}(t))^-),\end{aligned} \tag{4.37}$$

where $u((\boldsymbol{q}_{j_i,0})^-) = \lim\limits_{\substack{\boldsymbol{q} \to \boldsymbol{q}_{j_i,0} \\ \boldsymbol{q} \in \sigma_{j,0}}} u(\boldsymbol{q})$. This definition holds true for $[\mathbb{K}(\Gamma_0^h)]^d, [\mathbb{K}(\Gamma_0^h)]^{d\times d}$, and applies to the piecewise continuous functions as well. We present the mass-lumped inner product for two matrix-valued functions $\boldsymbol{U}, \boldsymbol{V}$ as follows

$$\langle \boldsymbol{U}, \boldsymbol{V} \rangle^h_{\Gamma^h(t)} := \frac{1}{d} \sum_{j=1}^{J} \sum_{i=1}^{d} |\sigma_j(t)|\, \boldsymbol{U}((\boldsymbol{q}_{j_i}(t))^-) : \boldsymbol{V}((\boldsymbol{q}_{j_i}(t))^-). \tag{4.38}$$

To derive a unified full-discretization, we choose the uniform time step τ, and the discrete time levels become $t_m = m\tau$, $m = 0, 1, 2, \ldots$. Let $\Gamma^m = \cup_{j=1}^J \bar{\sigma}_j^m$ be an approximation of $\Gamma(t_m)$, and we use the notation $\mathbb{K}^h$ to refer to $\mathbb{K}(\Gamma^0)$. By adopting the backward-Euler method, the unified conservative weak formulation (4.28) can thus be discretized by a unified semi-implicit parametric finite element method as follows. Let $\Gamma^0 = \cup_{j=1}^J \bar{\sigma}_j^0$ be an approximation of Γ_0 with vertices $\boldsymbol{q}_i^0$. For each

$m = 0, 1, 2, \ldots$, find the solution $(\boldsymbol{X}^{m+1}, \mu^{m+1}) \in [\mathbb{K}^h]^d \times \mathbb{K}^h$ such that

$$\left(\frac{\boldsymbol{X}^{m+1} - \boldsymbol{X}^m}{\tau} \cdot \boldsymbol{n}^{m+\frac{1}{2}}, \phi\right)^h_{\Gamma^m} + \left(\nabla_\Gamma \mu^{m+1}, \nabla_\Gamma \phi\right)^h_{\Gamma^m} = 0, \quad \forall \phi \in \mathbb{K}^h \tag{4.39a}$$

$$\left(\mu^{m+1}\boldsymbol{n}^{m+\frac{1}{2}}, \boldsymbol{\omega}\right)^h_{\Gamma^m} - \langle \boldsymbol{G}_k(\boldsymbol{n}^m)\nabla_\Gamma \boldsymbol{X}^m, \nabla_\Gamma \boldsymbol{\omega}\rangle^h_{\Gamma^m} = 0, \quad \forall \boldsymbol{\omega} \in [\mathbb{K}^h]^d. \tag{4.39b}$$

And $\sigma_j^{m+1} = \boldsymbol{X}^{m+1}(\sigma_j^m)$ with the ordered vertices $\boldsymbol{q}_{j_i}^{m+1} = \boldsymbol{X}^{m+1}(\boldsymbol{q}_{j_i}^m)$, $\forall 1 \le j \le J$, $i = 1, \ldots, d$. Here $\boldsymbol{n}^{m+\frac{1}{2}}$ is defined by

$$\boldsymbol{n}^{m+\frac{1}{2}}|_{\sigma_j^m} := \begin{cases} \frac{1}{2}\frac{1}{|\sigma_j^m|}(\mathcal{J}\{\sigma_j^m\} + \mathcal{J}\{\sigma_j^{m+1}\}), & d = 2; \\ \frac{\mathcal{J}\{\sigma_j^m\} + 4\mathcal{J}\{\sigma_j^{m+\frac{1}{2}}\} + \mathcal{J}\{\sigma_j^{m+1}\}}{12|\sigma_j^m|}, & d = 3. \end{cases} \tag{4.40}$$

and $\sigma_j^{m+\frac{1}{2}} := \frac{1}{2}(\sigma_j^m + \sigma_j^{m+1})$.

Remark 4.2. *The only implicit term in (4.39) is the smart approximation $\boldsymbol{n}^{m+\frac{1}{2}}$ proposed by Bao and Zhao in [13], which preserves the enclosed volume exactly. Therefore a significant number of terms in the fully-implicit unified SP-PFEM (4.39) are given explicitly, especially the domain of integration Γ^m. The unified SP-PFEM (4.39) achieves good performance in terms of computation. In fact, by adopting Newton's method, only 2 or 3 iterations are needed for each time step for the isotropic surface diffusion [13], and the anisotropic surface diffusion with the even $\gamma(\boldsymbol{n})$ [8,12].*

4.2.2 The minimal stabilizing function

In 2d, the unit tangent vector $\boldsymbol{\tau}$ together with $\boldsymbol{n}$ form an orthonormal basis $\{\boldsymbol{\tau}, \boldsymbol{n}\}$. We thus define the auxiliary 2×2 symmetric matrix $\tilde{M}(O, \alpha)$ for any $O \in SO(2)$ and $\alpha \in \mathbb{R}_{\ge 0}$ as follows

$$\tilde{M}(O, \alpha) := \begin{bmatrix} \gamma(\boldsymbol{n}) + \alpha(O\boldsymbol{\tau} \cdot \boldsymbol{n})^2 & * \\ -\frac{1}{2}\left((O\boldsymbol{\tau} \cdot \boldsymbol{\tau})\gamma(\boldsymbol{n}) + (O\boldsymbol{\tau} \cdot \boldsymbol{n})(\boldsymbol{\tau} \cdot \boldsymbol{\xi}) + \gamma(O\boldsymbol{n})\right) & \gamma(\boldsymbol{n}) \end{bmatrix}, \tag{4.41}$$

here the entries above the main diagonal are abbreviated to $*$.

By utilizing $\tilde{M}(O, \alpha)$, we can define the minimal stabilizing function $k_0(\boldsymbol{n})$ as

$$k_0(\boldsymbol{n}) := \inf\left\{\alpha \,\middle|\, \tilde{M}(O, \alpha) \text{ is semi-positive definite} \quad \forall O \in SO(2)\right\}. \tag{4.42}$$

The existence of $k_0(\boldsymbol{n})$ is given by the following theorem.

Theorem 4.3. *For any $\gamma(\boldsymbol{n})$ satisfies (4.18), the minimal stabilizing function $k_0(\boldsymbol{n})$ given in (4.42) is well-defined.*

In 3d, for any $\boldsymbol{n} \in \mathbb{S}^2$, it can be assigned with two normal vectors $\boldsymbol{\tau}_1, \boldsymbol{\tau}_2 \in \mathbb{S}^2$, such that $\{\boldsymbol{\tau}_1, \boldsymbol{\tau}_2, \boldsymbol{n}\}$ form an orthornormal basis. We thus define the auxiliary 4×4 symmetric matrix $M(O,\alpha)$ for any $O \in SO(3)$ and $\alpha \in \mathbb{R}_{\geq 0}$ as follows

$$\begin{bmatrix} \gamma(\boldsymbol{n}) + \alpha(O\boldsymbol{\tau}_1 \cdot \boldsymbol{n})^2 & * & * & * \\ -\frac{1}{2}\gamma(O\boldsymbol{n}) & \gamma(\boldsymbol{n}) + \alpha(O\boldsymbol{\tau}_2 \cdot \boldsymbol{n})^2 & * & * \\ \alpha(O\boldsymbol{\tau}_1 \cdot \boldsymbol{n})(O\boldsymbol{\tau}_2 \cdot \boldsymbol{n}) & 0 & \gamma(\boldsymbol{n}) + \alpha(O\boldsymbol{\tau}_2 \cdot \boldsymbol{n})^2 & * \\ M_{41} & M_{42} & M_{43} & \gamma(\boldsymbol{n}) \end{bmatrix}, \tag{4.43}$$

and M_{41}, M_{42}, M_{43} are

$$M_{41} = -\frac{1}{2}(\gamma(\boldsymbol{n})(O\boldsymbol{\tau}_1 \cdot \boldsymbol{\tau}_1) + (O\boldsymbol{\tau}_1 \cdot \boldsymbol{n})(\boldsymbol{\tau}_1 \cdot \boldsymbol{\xi})), \tag{4.44a}$$

$$M_{42} = -\frac{1}{2}(\gamma(\boldsymbol{n})(O\boldsymbol{\tau}_2 \cdot \boldsymbol{\tau}_2) + (O\boldsymbol{\tau}_2 \cdot \boldsymbol{n})(\boldsymbol{\tau}_2 \cdot \boldsymbol{\xi})), \tag{4.44b}$$

$$M_{43} = -\frac{1}{2}(\gamma(\boldsymbol{n})(O\boldsymbol{\tau}_2 \cdot \boldsymbol{\tau}_1) + (O\boldsymbol{\tau}_2 \cdot \boldsymbol{n})(\boldsymbol{\tau}_1 \cdot \boldsymbol{\xi})). \tag{4.44c}$$

Similarly, the minimal stabilizing function $k_0(\boldsymbol{n})$ for 3d is given as

$$k_0(\boldsymbol{n}) := \inf\left\{\alpha \,\middle|\, M(O,\alpha) \text{ is semi-positive definite} \quad \forall O \in SO(3)\right\}. \tag{4.45}$$

And

Theorem 4.4. *For any $\gamma(\boldsymbol{n})$ satisfies (4.18), the minimal stabilizing function $k_0(\boldsymbol{n})$ given in (4.45) is well-defined.*

We give the proof for Theorem 4.3/4.4 in Section 4.4.

4.2.3 Structure-preserving properties

The minimal stabilizing function is critical in showing the energy stability in the unified SP-PFEM (4.39). Suppose the enclosed volume and surface energy for the

solution $\Gamma^m = \cup_{j=1}^J \bar{\sigma}_j^m$ of (4.39) to be V^m and W^m, respectively, which are given as

$$V^m := \frac{1}{d}(\boldsymbol{X}^m, \boldsymbol{n}^m)^h_{\Gamma^m} = \frac{1}{d^2}\sum_{j=1}^{J}\sum_{i=1}^{d} |\sigma_j^m|\, \boldsymbol{q}_{j_i}^m \cdot \boldsymbol{n}_j^m, \tag{4.46a}$$

$$W^m := (\gamma(\boldsymbol{n}^m), 1)^h_{\Gamma^m} = \sum_{j=1}^{J} |\sigma_j^m| \gamma(\boldsymbol{n}_j^m). \tag{4.46b}$$

And our main result is the structure-preserving property of unified SP-PFEM (4.39):

Theorem 4.5 (structure-preserving)**.** *Suppose the stabilizing function $k(\boldsymbol{n}) \geq k_0(\boldsymbol{n})$, then the unified SP-PFEM (4.39) is volume conservative and energy dissipative, i.e.*

$$V^{m+1} = V^m = \ldots = V^0, \tag{4.47a}$$

$$W^{m+1} \leq W^m \leq \ldots \leq W^0, \qquad \forall m = 0, 1, \ldots \tag{4.47b}$$

The proof of volume conservation for 2D/3D is similar to Theorem 2.1/3.2 in Chapter 2/Chapter 3, respectively. Thus it is omitted here for brevity. However, the proof of energy stability (4.47b) part requires in-depth analysis, thus we leave it to the next section.

4.3 Proof of energy dissipation

To prove (4.47b), it is quite useful to establish the following estimate of $W^{m+1} - W^m$

$$\langle \boldsymbol{G}_k(\boldsymbol{n}^m)\nabla_\Gamma \boldsymbol{X}^{m+1}, \nabla_\Gamma(\boldsymbol{X}^{m+1} - \boldsymbol{X}^m)\rangle^h_{\Gamma^m} \geq W^{m+1} - W^m. \tag{4.48}$$

Since the velocity by anisotropic surface diffusion (4.16) is locally determined, we can expect that for $d = 2, 3$, the local version of (4.48) on σ_j^m also holds, i.e.,

$$\begin{aligned}&\frac{1}{d}|\sigma_j^m| \sum_{i=1}^{d} \left(\boldsymbol{G}_k(\boldsymbol{n}_j^m)\nabla_\Gamma \boldsymbol{X}^{m+1}((\boldsymbol{q}_{j_i}^m)^-)\right) : (\nabla_\Gamma \boldsymbol{X}^{m+1}((\boldsymbol{q}_{j_i}^m)^-) - \nabla_\Gamma \boldsymbol{X}^m((\boldsymbol{q}_{j_i}^m)^-))\\ &\geq \gamma(\boldsymbol{n}_j^{m+1})|\sigma_j^{m+1}| - \gamma(\boldsymbol{n}_j^m)|\sigma_j^m|,\end{aligned} \tag{4.49}$$

should hold for all $1 \leq j \leq J$. The inequality (4.49) is called the *local estimate*.

4.3.1 Local estimate in 2D

To verify (4.49), a proper representation of $\nabla_\Gamma \boldsymbol{X}^{m+1}$ is required, which is given by the following lemma.

Lemma 4.1 (QR factorization)**.** *Let $\{\boldsymbol{\tau}, \boldsymbol{n}\}$ be an orthonormal basis of $\mathbb{R}^2$. Suppose $A \in \mathbb{R}^{2\times 2}$ satisfies $A\boldsymbol{\tau} \cdot A\boldsymbol{n} = 0$ and $\det(A) > 0$. Then there exists a matrix $O \in SO(2)$ and $p, q \in \mathbb{R}$, such that $p, q > 0$ and*

$$A\begin{bmatrix}\boldsymbol{\tau}, \boldsymbol{n}\end{bmatrix} = O\begin{bmatrix}\boldsymbol{\tau}, \boldsymbol{n}\end{bmatrix}\begin{bmatrix} p & 0 \\ 0 & q \end{bmatrix}. \tag{4.50}$$

Here $SO(d)$ stands for the special orthogonal group in dimension d. We refer the proof to the proof of lemma 4.3.

Lemma 4.2. *Suppose σ and $\bar{\sigma}$ are two non-degenerated line-segments with ordered vertices $\{\boldsymbol{q}_1, \boldsymbol{q}_2\}, \{\bar{\boldsymbol{q}}_1, \bar{\boldsymbol{q}}_2\}$, and outward unit normal vectors $\boldsymbol{n}$ and $\bar{\boldsymbol{n}}$, respectively. Let $\boldsymbol{X}$ be a vector-valued function in $[\mathcal{P}^1(\sigma)]^2$ satisfying $\boldsymbol{X}((\boldsymbol{q}_i)^-) = \bar{\boldsymbol{q}}_i$ for $i = 1, 2$. Then for any $k(\boldsymbol{n}) \geq k_0(\boldsymbol{n})$ for $\boldsymbol{n} \in \mathbb{S}^1$, the following inequality holds*

$$\begin{aligned}&\frac{1}{2}|\sigma| \sum_{i=1}^{2} \left(\boldsymbol{G}_k(\boldsymbol{n})\nabla_\Gamma \boldsymbol{X}((\boldsymbol{q}_i)^-)\right) : (\nabla_\Gamma \boldsymbol{X}((\boldsymbol{q}_i)^-) - \nabla_\Gamma \boldsymbol{id}((\boldsymbol{q}_i)^-)) \\ &\geq \gamma(\bar{\boldsymbol{n}})\,|\bar{\sigma}| - \gamma(\boldsymbol{n})|\sigma|.\end{aligned} \tag{4.51}$$

Here $\boldsymbol{id}(\boldsymbol{q}) = \boldsymbol{q}$, $\forall \boldsymbol{q} \in \mathbb{R}^2$.

Proof. Suppose $\{\boldsymbol{\tau}_1, \boldsymbol{n}\}$ forms an orthonormal basis. Let the matrix $A \in \mathbb{R}^{2\times 2}$ and $\boldsymbol{b} \in \mathbb{R}^2$ satisfy

$$\bar{\boldsymbol{q}}_i = A\boldsymbol{q}_i + \boldsymbol{b}, \quad i = 1, 2, \quad \bar{\boldsymbol{n}} = A\boldsymbol{n}. \tag{4.52}$$

It is easy to see such $\{\boldsymbol{\tau}, \boldsymbol{n}\}$ and A satisfy the condition in Lemma 4.1. Thus by applying Lemma 4.1, we deduce that there exists a matrix $O \in SO(2)$ and $p, q > 0$, such that

$$A\begin{bmatrix}\boldsymbol{\tau}, \boldsymbol{n}\end{bmatrix} = O\begin{bmatrix}\boldsymbol{\tau}, \boldsymbol{n}\end{bmatrix}\begin{bmatrix} p & 0 \\ 0 & q \end{bmatrix}. \tag{4.53}$$

We further notice that $1 = |\bar{\boldsymbol{n}}| = |A\boldsymbol{n}| = |qO\boldsymbol{n}| = |q|$. Together with $q > 0$, we deduce that $q = 1$.

Moreover, since $\boldsymbol{id}, \boldsymbol{X} \in [\mathcal{P}^1(\sigma)]^2$ and $\boldsymbol{id}(\boldsymbol{q}) = \boldsymbol{q}, \boldsymbol{X}(\boldsymbol{q}_i) = \bar{\boldsymbol{q}}_i = A\boldsymbol{q}_i + \boldsymbol{b}$. By applying Lemma 3.6 in [12], we obtain

$$\nabla_\Gamma \boldsymbol{id}((\boldsymbol{q}_i)^-) = \boldsymbol{\tau}\boldsymbol{\tau}^T, \qquad i = 1, 2. \tag{4.54}$$

And

$$\nabla_\Gamma \boldsymbol{X}((\boldsymbol{q}_i)^-) = (\partial_{\boldsymbol{\tau}} (A\boldsymbol{q} + \boldsymbol{b}))|_{(\boldsymbol{q}_i)^-} \boldsymbol{\tau}^T = A\boldsymbol{\tau}\boldsymbol{\tau}^T, \qquad i = 1, 2. \tag{4.55}$$

The left-hand side of (4.51) can be written as the summation of two parts. By applying (4.53), (4.55) and the definition of $\boldsymbol{G}_k(\boldsymbol{n})$ (4.19), and noticing (4.20) that $\boldsymbol{G}_k(\boldsymbol{n}) = \boldsymbol{G}_k^{(s)} + \boldsymbol{G}^{(a)}$, the first term can be written as

$$\begin{aligned}
&\frac{1}{2}|\sigma| \sum_{i=1}^{2} \left(\boldsymbol{G}_k(\boldsymbol{n}) \nabla_\Gamma \boldsymbol{X}((\boldsymbol{q}_i)^-)\right) : \nabla_\Gamma \boldsymbol{X}((\boldsymbol{q}_i)^-) \\
&= |\sigma| \left(\boldsymbol{G}_k^{(s)}(\boldsymbol{n})(A\boldsymbol{\tau}\boldsymbol{\tau}^T)\right) : (A\boldsymbol{\tau}\boldsymbol{\tau}^T) \\
&= |\sigma| \operatorname{Tr}\left[(\boldsymbol{\tau}\boldsymbol{\tau}^T A^T)(\gamma(\boldsymbol{n}) I_2 + k(\boldsymbol{n})\boldsymbol{n}\boldsymbol{n}^T)(A\boldsymbol{\tau}\boldsymbol{\tau}^T)\right] \\
&= |\sigma| \left[|A\boldsymbol{\tau}|^2 \gamma(\boldsymbol{n}) + k(\boldsymbol{n})(A\boldsymbol{\tau}\cdot\boldsymbol{n})^2\right] \\
&= |\sigma| \left[p^2 \gamma(\boldsymbol{n}) + k(\boldsymbol{n}) p^2 (O\boldsymbol{\tau}\cdot\boldsymbol{n})^2\right].
\end{aligned} \tag{4.56}$$

The second term can be written as

$$\begin{aligned}
&\frac{1}{2}|\sigma| \sum_{i=1}^{2} \left(\boldsymbol{G}_k(\boldsymbol{n}) \nabla_\Gamma \boldsymbol{X}((\boldsymbol{q}_i)^-)\right) : \nabla_\Gamma \boldsymbol{id}((\boldsymbol{q}_i)^-) \\
&= |\sigma| \operatorname{Tr}\left((\boldsymbol{\tau}\boldsymbol{\tau}^T)(\gamma(\boldsymbol{n}) I_2 - \boldsymbol{n}\boldsymbol{\xi}^T + \boldsymbol{\xi}\boldsymbol{n}^T + k(\boldsymbol{n})\boldsymbol{n}\boldsymbol{n}^T)(A\boldsymbol{\tau}\boldsymbol{\tau}^T)\right) \\
&= |\sigma| \left[(A\boldsymbol{\tau}\cdot\boldsymbol{\tau})\gamma(\boldsymbol{n}) + (A\boldsymbol{\tau}\cdot\boldsymbol{n})(\boldsymbol{\tau}\cdot\boldsymbol{\xi})\right] \\
&= |\sigma| \left[p(O\boldsymbol{\tau}\cdot\boldsymbol{\tau})\gamma(\boldsymbol{n}) + p(O\boldsymbol{\tau}\cdot\boldsymbol{n})(\boldsymbol{\tau}\cdot\boldsymbol{\xi})\right].
\end{aligned} \tag{4.57}$$

For the right-hand side of (4.51), by applying (4.53) again, and noticing $\bar{\sigma} = \boldsymbol{X}(\sigma)$, $\bar{\boldsymbol{n}} = A\boldsymbol{n}, q = 1$, we deduce that

$$\begin{aligned}
\gamma(\bar{\boldsymbol{n}})\,|\bar{\sigma}| &= \gamma(qO\boldsymbol{n}) \int_\sigma |(\partial_{\boldsymbol{\tau}} \boldsymbol{X})|\, dA = \gamma(O\boldsymbol{n}) \int_\sigma |A\boldsymbol{\tau}|\, dA \\
&= \gamma(O\boldsymbol{n}) \int_\sigma |pO\boldsymbol{\tau}|\, dA = p\,\gamma(O\boldsymbol{n})|\sigma|
\end{aligned} \tag{4.58}$$

By substituting (4.56), (4.57), (4.58) into (4.51), and noticing (4.41), we know the inequality (4.51) is equivalent to

$$|\sigma| \begin{bmatrix} p \\ 1 \end{bmatrix}^T \tilde{M}(O, k(\boldsymbol{n}))(\boldsymbol{n}) \begin{bmatrix} p \\ 1 \end{bmatrix} \geq 0. \tag{4.59}$$

By the definition of $k_0(\boldsymbol{n})$, we know $\tilde{M}(O, k(\boldsymbol{n}))(\boldsymbol{n})$ is semi-positive definite for all $O \in SO(2)$. Therefore the desired inequality (4.51) is validated. □

Proof of (4.49) *in 2D.* Suppose $\{\boldsymbol{\tau}_j^m, \boldsymbol{n}_j^m\}$ $(1 \leq j \leq J)$ forms an orthonomal basis. By applying Lemma 4.2 with $\sigma = \sigma_j^m, \bar{\sigma} = \sigma_j^{m+1}$ and $\boldsymbol{X} = \boldsymbol{X}^{m+1}|_{\sigma_j^m}$ for $1 \leq j \leq J$, we get

$$\begin{aligned} &\frac{1}{2}|\sigma_j^m| \sum_{i=1}^{2} \left(\boldsymbol{G}_k(\boldsymbol{n}_j^m) \nabla_\Gamma \boldsymbol{X}^{m+1}((\boldsymbol{q}_{j_i}^m)^-)\right) : (\nabla_\Gamma \boldsymbol{X}^{m+1}((\boldsymbol{q}_{j_i}^m)^-) - \nabla_\Gamma \boldsymbol{X}^m((\boldsymbol{q}_{j_i}^m)^-)) \\ &\geq \gamma(\boldsymbol{n}_j^{m+1})|\sigma_j^{m+1}| - \gamma(\boldsymbol{n}_j^m)|\sigma_j^m|, \ \forall 1 \leq j \leq J. \end{aligned} \tag{4.60}$$

which immediately implies the local estimate (4.49) in 2D. □

4.3.2 Local estimate in 3D

Similar to the proof in 2D, to represent $\nabla_\Gamma \boldsymbol{X}^{m+1}$, we need the following lemma.

Lemma 4.3 (QR factorization)**.** *Let* $\{\boldsymbol{\tau}_1, \boldsymbol{\tau}_2, \boldsymbol{n}\}$ *be an orthonormal basis of* $\mathbb{R}^3$*. Suppose* $A \in \mathbb{R}^{3\times 3}$ *satisfies* $A\boldsymbol{\tau}_1 \cdot A\boldsymbol{n} = 0, A\boldsymbol{\tau}_2 \cdot A\boldsymbol{n} = 0$ *and* $\det(A) > 0$*. Then there exists a matrix* $O \in SO(3)$ *and* $p, q, r, s \in \mathbb{R}$*, such that* $p, q, r > 0$ *and*

$$A\left[\boldsymbol{\tau}_1, \boldsymbol{\tau}_2, \boldsymbol{n}\right] = O\left[\boldsymbol{\tau}_1, \boldsymbol{\tau}_2, \boldsymbol{n}\right] \begin{bmatrix} p & 0 & 0 \\ s & q & 0 \\ 0 & 0 & r \end{bmatrix}. \tag{4.61}$$

Proof. By QR factorization, we have

$$A\left[\boldsymbol{\tau}_1, \boldsymbol{\tau}_2, \boldsymbol{n}\right] = QR = \left(Q\left[\boldsymbol{\tau}_1, \boldsymbol{\tau}_2, \boldsymbol{n}\right]^T\right)\left[\boldsymbol{\tau}_1, \boldsymbol{\tau}_2, \boldsymbol{n}\right] R, \tag{4.62}$$

where Q is orthogonal and $R = (r_{ij})$ is an lower trianglar matrix with $r_{ii} > 0$ and thus $\det R > 0$. Furthermore, since $A\boldsymbol{\tau}_1 \cdot A\boldsymbol{n} = 0$ and Q is orthogonal, we have

$$0 = A\boldsymbol{\tau}_1 \cdot A\boldsymbol{n} = \left(Q \begin{bmatrix} r_{11} \\ r_{21} \\ r_{31} \end{bmatrix} \right) \cdot \left(Q \begin{bmatrix} 0 \\ 0 \\ r_{33} \end{bmatrix} \right) = r_{31}\, r_{33}. \tag{4.63}$$

Thus $r_{31} = 0$, and similarly $r_{32} = 0$. We obtain

$$R = \begin{bmatrix} p & 0 & 0 \\ s & q & 0 \\ 0 & 0 & r \end{bmatrix}, \tag{4.64}$$

with $p, q, r > 0$.

On the other hand, We know $\{\boldsymbol{\tau}_1, \boldsymbol{\tau}_2, \boldsymbol{n}\}$ forms an orthonormal basis implies the matrix $\left[\boldsymbol{\tau}_1, \boldsymbol{\tau}_2, \boldsymbol{n}\right]$ is also orthogonal. Therefore $O := Q \left[\boldsymbol{\tau}_1, \boldsymbol{\tau}_2, \boldsymbol{n}\right]^T$ is orthogonal, and such O satisfies (4.61).

Finally, $\det(O) = \frac{\det(A)}{\det(R)} = \frac{\det(A)}{pqr} > 0$, thus $\det(O) = 1$ and $O \in SO(3)$. Which is the desired result. □

Lemma 4.4. *Suppose σ and $\bar{\sigma}$ are two non-degenerated triangles with ordered vertices $\{\boldsymbol{q}_1, \boldsymbol{q}_2, \boldsymbol{q}_3\}, \{\bar{\boldsymbol{q}}_1, \bar{\boldsymbol{q}}_2, \bar{\boldsymbol{q}}_3\}$, and outward unit normal vectors $\boldsymbol{n}$ and $\bar{\boldsymbol{n}}$, respectively. Let $\boldsymbol{X}$ be a vector-valued function in $[\mathcal{P}^1(\sigma)]^3$ satisfying $\boldsymbol{X}((\boldsymbol{q}_i)^-) = \bar{\boldsymbol{q}}_i$ for $i = 1, 2, 3$. Then for any $k(\boldsymbol{n}) \geq k_0(\boldsymbol{n})$ for $\boldsymbol{n} \in \mathbb{S}^2$, the following inequality holds*

$$\begin{aligned} &\frac{1}{3}|\sigma| \sum_{i=1}^{3} \left(\boldsymbol{G}_k(\boldsymbol{n}) \nabla_\Gamma \boldsymbol{X}((\boldsymbol{q}_i)^-) \right) : (\nabla_\Gamma \boldsymbol{X}((\boldsymbol{q}_i)^-) - \nabla_\Gamma \boldsymbol{id}((\boldsymbol{q}_i)^-)) \\ &\geq \gamma(\bar{\boldsymbol{n}})\, |\bar{\sigma}| - \gamma(\boldsymbol{n})|\sigma|. \end{aligned} \tag{4.65}$$

Here $\boldsymbol{id}(\boldsymbol{q}) = \boldsymbol{q}$, $\forall \boldsymbol{q} \in \mathbb{R}^3$.

Proof. Suppose $\{\boldsymbol{\tau}_1, \boldsymbol{\tau}_2, \boldsymbol{n}\}$ forms an orthonormal basis, where $\boldsymbol{\tau}_1, \boldsymbol{\tau}_2$ are determined by $\boldsymbol{n}$ as in $M(O, \alpha)(\boldsymbol{n})$. Let the matrix $A \in \mathbb{R}^{3\times 3}$ and $\boldsymbol{b} \in \mathbb{R}^3$ satisfy

$$\bar{\boldsymbol{q}}_i = A\boldsymbol{q}_i + \boldsymbol{b}, \quad i = 1, 2, 3, \quad \bar{\boldsymbol{n}} = A\boldsymbol{n}. \tag{4.66}$$

It is easy to see such $\{\boldsymbol{\tau}_1, \boldsymbol{\tau}_2, \boldsymbol{n}\}$ and A satisfy the condition in Lemma 4.3. Similarly, we know that there exists a matrix $O \in SO(3)$ and $p, q > 0, s \in \mathbb{R}$, such that

$$A\left[\boldsymbol{\tau}_1, \boldsymbol{\tau}_2, \boldsymbol{n}\right] = O\left[\boldsymbol{\tau}_1, \boldsymbol{\tau}_2, \boldsymbol{n}\right]\begin{bmatrix} p & 0 & 0 \\ s & q & 0 \\ 0 & 0 & 1 \end{bmatrix}. \tag{4.67}$$

By the same argument as in (4.54), (4.55), we have

$$\nabla_\Gamma \boldsymbol{id}((\boldsymbol{q}_i)^-) = \boldsymbol{\tau}_1\boldsymbol{\tau}_1^T + \boldsymbol{\tau}_2\boldsymbol{\tau}_2^T, \qquad i = 1, 2, 3. \tag{4.68}$$

$$\nabla_\Gamma \boldsymbol{X}((\boldsymbol{q}_i)^-) = A\boldsymbol{\tau}_1\boldsymbol{\tau}_1^T + A\boldsymbol{\tau}_2\boldsymbol{\tau}_2^T, \qquad i = 1, 2, 3. \tag{4.69}$$

For the left-hand side of (4.65), by applying lemma 4.3 and the calculations for (4.56), (4.57), we deduce that

$$\begin{aligned} &\frac{1}{3}|\sigma| \sum_{i=1}^{3} \left(\boldsymbol{G}_k(\boldsymbol{n})\nabla_\Gamma \boldsymbol{X}(\boldsymbol{q}_i^-)\right) : (\nabla_\Gamma \boldsymbol{X}((\boldsymbol{q}_i)^-) - \nabla_\Gamma \mathbf{id}((\boldsymbol{q}_i)^-)) \\ &= |\sigma| \left[(p^2 + s^2 + q^2)\gamma(\boldsymbol{n})\right] \\ &\quad + |\sigma| \left[k(\boldsymbol{n})(p^2(O\boldsymbol{\tau}_1 \cdot \boldsymbol{n})^2 + (s^2 + q^2)(O\boldsymbol{\tau}_2 \cdot \boldsymbol{n})^2 + 2ps(O\boldsymbol{\tau}_1 \cdot \boldsymbol{n})(O\boldsymbol{\tau}_2 \cdot \boldsymbol{n}))\right] \\ &\quad + 2|\sigma|(M_{41}p + M_{42}q + M_{43}s). \end{aligned} \tag{4.70}$$

For the right-hand side of (4.65), similar to (4.58), it holds that

$$\begin{aligned} \gamma(\bar{\boldsymbol{n}})\,|\bar{\sigma}| &= \gamma(A\boldsymbol{n}) \int_\sigma |(\partial_{\boldsymbol{\tau}_1}\boldsymbol{X}) \times (\partial_{\boldsymbol{\tau}_2}\boldsymbol{X})|\, dA = \gamma(O\boldsymbol{n}) \int_\sigma |(A\boldsymbol{\tau}_1) \times (A\boldsymbol{\tau}_2)|\, dA \\ &= \gamma(O\boldsymbol{n}) \int_\sigma |(pO\boldsymbol{\tau}_1 + sO\boldsymbol{\tau}_2) \times (qO\boldsymbol{\tau}_2)|\, dA = pq\,\gamma(O\boldsymbol{n})|\sigma| \end{aligned} \tag{4.71}$$

Finally, by substituting (4.70), (4.71) into (4.65), and noticing (4.43), we know the inequality (4.65) is equivalent to

$$|\sigma| \begin{bmatrix} p \\ q \\ s \\ 1 \end{bmatrix}^T M(O, k(\boldsymbol{n}))(\boldsymbol{n}) \begin{bmatrix} p \\ q \\ s \\ 1 \end{bmatrix} \geq 0. \tag{4.72}$$

By the definition of $k_0(\boldsymbol{n})$, we know $M(O, k(\boldsymbol{n}))(\boldsymbol{n})$ is semi-positive definite for all $O \in SO(3)$, which validates the desired inequality (4.65). □

The local estimate (4.49) in 3D is also a direct result of Lemma 4.4.

4.3.3 The proof

With the help of the local estimate (4.49), we are finally able to finish the proof energy stability part (4.47b) of the main theorem 4.5.

Proof of energy stability. By taking summation of (4.49) for j from 1 to J, and applying the mass-lumped inner product (4.38) and the definition for W^m (4.46b), we get

$$\begin{aligned}
&\langle \boldsymbol{G}_k(\boldsymbol{n}^m)\nabla_\Gamma \boldsymbol{X}^{m+1},\, \nabla_\Gamma(\boldsymbol{X}^{m+1}-\boldsymbol{X}^m)\rangle_{\Gamma^m}^h \\
&= \frac{1}{d}\sum_{j=1}^{J}|\sigma_j^m|\sum_{i=1}^{d}\left(\boldsymbol{G}_k(\boldsymbol{n}_j^m)\nabla_\Gamma \boldsymbol{X}^{m+1}((\boldsymbol{q}_{j_i}^m)^-)\right) : (\nabla_\Gamma \boldsymbol{X}^{m+1}((\boldsymbol{q}_{j_i}^m)^-) - \nabla_\Gamma \boldsymbol{X}^m((\boldsymbol{q}_{j_i}^m)^-)) \\
&\geq \sum_{j=1}^{J}\left(\gamma(\boldsymbol{n}_j^{m+1})|\sigma_j^{m+1}| - \gamma(\boldsymbol{n}_j^m)|\sigma_j^m|\right) = W^{m+1}-W^m, \qquad m\geq 0,
\end{aligned} \tag{4.73}$$

Choosing $\phi = \mu^{m+1}$ in (4.39a) and $\boldsymbol{\omega} = \boldsymbol{X}^{m+1}$ in (4.39b), together with (4.73) yields that

$$\begin{aligned}
W^{m+1}-W^m &\leq \langle \boldsymbol{G}_k(\boldsymbol{n}^m)\nabla_\Gamma \boldsymbol{X}^{m+1}, \nabla_\Gamma(\boldsymbol{X}^{m+1}-\boldsymbol{X}^m)\rangle_{\Gamma^m}^h \\
&= -\tau\left(\nabla_\Gamma \mu^{m+1}, \nabla_\Gamma \mu^{m+1}\right)_{\Gamma^m}^h \leq 0, \qquad m\geq 0,
\end{aligned} \tag{4.74}$$

which validates the unconditional energy stability (4.47b) in Theorem 4.5. □

4.4 Existence of minimal stabilizing function

4.4.1 Useful lemmas

In this section, we provide some useful lemmas in proving the semi-definiteness of $M(O,\alpha)$.

Lemma 4.5 (Sylvester's criterion)**.** *Let A be an $n\times n$ symmetric matrix with leading principle minors be $A_1, A_2, \ldots, A_n$. Denote $F_i = \det(A_i), i = 1,2,\ldots,n$, then*

$$A \text{ is positive definite} \iff F_i > 0, \quad \forall i = 1,2,\ldots,n. \tag{4.75}$$

Lemma 4.6 (Schur complement)**.** *Let A be an $n \times n$ symmetric matrix, A_{n-1} be its $n-1$th leading principle minor. If A_{n-1} is positive definite, and $\det(A) \geq 0$, then*

$$A \text{ is semi-positive definite.} \tag{4.76}$$

Proof. Denote the Schur complement for A_{n-1} as A/A_{n-1}, which can also be regarded as a real number. From the fact that A_{n-1} is positive definite, we know A_{n-1} is invertible with $\det(A_{n-1}) > 0$. From Appendix A.5.5 in [37], we know that

$$A \text{ is semi-positive definite} \iff A/A_{n-1} \text{ is semi-positive definite.} \tag{4.77}$$

On the other hand, the property of Schur complement indicates that

$$\det(A/A_{n-1}) = \frac{\det(A)}{\det(A_{n-1})} \geq 0. \tag{4.78}$$

Since A/A_{n-1} is a non-negative number, we know A/A_{n-1} is semi-positive definite. By (4.77), we know that A is semi-positive definite. □

Lemma 4.7. *Suppose the two $n \times n$ symmetric continuous matrices A, D defined in $SO(d) \times \mathbb{R}$ and $SO(d)$ satisfy*

$$A(O, \alpha) = A(O, 0) + \alpha D(O), \qquad D(O) \text{ is semi-positive definite.} \tag{4.79}$$

Let A_{n-1} be the $(n-1)$th leading principle minor of A. And there exists a $k_{n-1} \geq 0$, such that

$$A_{n-1}(O, \alpha) \text{ is positive definite,} \qquad \forall O \in SO(d), \alpha \geq k_{n-1}. \tag{4.80}$$

If for any $O \in SO(d)$, there exists a constant $k_{n,O} \geq k_{n-1}$ and an open neighbourhood $\mathcal{U}_O$ of O, such that

$$F_n(\tilde{O}, k_{n,O}) = \det(A(\tilde{O}, k_{n,O})) \geq 0, \qquad \forall \tilde{O} \in \mathcal{U}_O. \tag{4.81}$$

Then there exists a finite constant $k_n \geq k_{n-1}$, such that for any $O \in SO(d), \alpha \geq k_n$, it holds

$$A(O, \alpha) \text{ is semi-positive definite.} \tag{4.82}$$

Proof. For any $O \in SO(d)$ with the constant $k_{n,O} \geq k_{n-1}$ and neighbourhood $\mathcal{U}_O$, we know that for all $\tilde{O} \in \mathcal{U}_O$, $\det(A(\tilde{O}, k_{n,O})) \geq 0$ and $A_{n-1}(\tilde{O}, k_{n,O})$ is positive definite. Thus by Lemma 4.6, we know that $A(\tilde{O}, k_{n,O})$ is semi-positive definite.

For any $\alpha \geq k_{n,O}$, by (4.79), we know that

$$A(\tilde{O}, \alpha) = A(\tilde{O}, k_{n,O}) + (\alpha - k_{n,O})D(\tilde{O}). \tag{4.83}$$

Thus $A(\tilde{O}, \alpha)$ is semi-positive definite for all $\alpha \geq k_{n,O}, \tilde{O} \in \mathcal{U}_O$. And (4.82) is a direct result of the compactness of $SO(d)$ and the open cover theorem. □

Lemma 4.7 gives a simple approach to show the semi-positive definiteness of a symmetric continuous matrix $M_n(O, \alpha)$. The positive definiteness of M_{n-1} can be established by applying Lemma 4.5. To verify condition (4.81), if $F_n(O, k_{n,O}) > 0$ for some $k_{n,O} > 0$, then the existence of such neighbourhood $\mathcal{U}_O$ is ensured by the continuity of $F_n(\cdot, k_{n,O})$. The problem is when $F_n(O, k_{n,O}) = 0$, we need to show that O is a local minimum of $F_n(\cdot, k_{n,O})$, which requires to consider its Hessian matrix. Thus an elegant formulation for the Hessian matrix of a determinant (4.8) as well as a proper parameterization for $SO(d)$ (Lemma 4.9, 4.10) are important and highly demanded.

Lemma 4.8 (Jacobi's formula)**.** *Suppose $A = (a_{i,j})_{n\times n}$ be a matrix of functions, we have*

$$\frac{\partial \det(A)}{\partial \alpha} = \operatorname{tr}\left(\operatorname{adj}(A)\frac{\partial A}{\partial \alpha}\right). \tag{4.84}$$

$$\frac{\partial^2 \det(A)}{\partial \alpha \partial \beta} = \operatorname{tr}\left(\operatorname{adj}(A)\frac{\partial^2 A}{\partial \alpha \partial \beta}\right) + \sum_{i\neq j} \det \begin{bmatrix} a_{1,1} & a_{1,2} & \dots & a_{1,n} \\ \vdots & \vdots & \dots & \vdots \\ \frac{\partial a_{i,1}}{\partial \alpha} & \frac{\partial a_{i,2}}{\partial \alpha} & \dots & \frac{\partial a_{i,n}}{\partial \alpha} \\ \vdots & \vdots & \dots & \vdots \\ \frac{\partial a_{j,1}}{\partial \alpha} & \frac{\partial a_{j,2}}{\partial \alpha} & \dots & \frac{\partial a_{j,n}}{\partial \alpha} \\ \vdots & \vdots & \dots & \vdots \\ a_{n,1} & a_{n,2} & \dots & a_{n,n} \end{bmatrix}. \tag{4.85}$$

Here $\operatorname{adj}(A)$ *is the adjunct matrix of* A.

Lemma 4.9 (Euler angles, 2d). *For any $O \in SO(2)$, there exists θ, such that*

$$O\left[\boldsymbol{\tau}, \boldsymbol{n}\right] = \left[\boldsymbol{\tau}, \boldsymbol{n}\right] O(\theta), \tag{4.86}$$

where

$$O(\theta) = \begin{bmatrix} \cos\theta & \sin\theta \\ -\sin\theta & \cos\theta \end{bmatrix}.$$

Moreover, we have

$$O\Big|_{(0)} \left[\boldsymbol{\tau}, \boldsymbol{n}\right] = \left[\boldsymbol{\tau}, \boldsymbol{n}\right] I_2, \tag{4.87a}$$

$$\frac{dO}{d\theta}\Big|_{(0)} \left[\boldsymbol{\tau}, \boldsymbol{n}\right] = \left[\boldsymbol{\tau}, \boldsymbol{n}\right] \begin{bmatrix} 0 & 1 \\ -1 & 0 \end{bmatrix}, \tag{4.87b}$$

$$\frac{d^2O}{d\theta^2}\Big|_{(0)} \left[\boldsymbol{\tau}, \boldsymbol{n}\right] = \left[\boldsymbol{\tau}, \boldsymbol{n}\right] \begin{bmatrix} -1 & 0 \\ 0 & -1 \end{bmatrix}. \tag{4.87c}$$

Lemma 4.10 (Euler angles, 3d). *For any $O \in SO(3)$, there exists ϕ, θ, ψ, such that*

$$O\left[\boldsymbol{\tau}_1, \boldsymbol{\tau}_2, \boldsymbol{n}\right] = \left[\boldsymbol{\tau}_1, \boldsymbol{\tau}_2, \boldsymbol{n}\right] O(\phi, \theta, \psi), \tag{4.88}$$

where

$$O(\phi, \theta, \psi) = \begin{bmatrix} \cos\theta\cos\psi & -\cos\phi\sin\psi + \sin\phi\sin\theta\cos\psi & \sin\phi\sin\psi + \cos\phi\sin\theta\cos\psi \\ \cos\theta\sin\psi & \cos\phi\cos\psi + \sin\phi\sin\theta\sin\psi & -\sin\phi\cos\psi + \cos\phi\sin\theta\sin\psi \\ -\sin\theta & \sin\phi\cos\theta & \cos\phi\cos\theta \end{bmatrix}.$$

Moreover, for $\beta, \gamma \in \{\phi, \theta, \psi\}$*, we have*

$$O\Big|_{(0,0,0)} \Big[\boldsymbol{\tau}_1, \boldsymbol{\tau}_2, \boldsymbol{n}\Big] = \Big[\boldsymbol{\tau}_1, \boldsymbol{\tau}_2, \boldsymbol{n}\Big]\, I_3, \tag{4.89a}$$

$$\frac{\partial O}{\partial \phi}\Big|_{(0,0,0)} \Big[\boldsymbol{\tau}_1, \boldsymbol{\tau}_2, \boldsymbol{n}\Big] = \Big[\boldsymbol{\tau}_1, \boldsymbol{\tau}_2, \boldsymbol{n}\Big] \begin{bmatrix} 0 & 0 & 0 \\ 0 & 0 & -1 \\ 0 & 1 & 0 \end{bmatrix}, \tag{4.89b}$$

$$\frac{\partial O}{\partial \theta}\Big|_{(0,0,0)} \Big[\boldsymbol{\tau}_1, \boldsymbol{\tau}_2, \boldsymbol{n}\Big] = \Big[\boldsymbol{\tau}_1, \boldsymbol{\tau}_2, \boldsymbol{n}\Big] \begin{bmatrix} 0 & 0 & 1 \\ 0 & 0 & 0 \\ -1 & 0 & 0 \end{bmatrix}, \tag{4.89c}$$

$$\frac{\partial O}{\partial \psi}\Big|_{(0,0,0)} \Big[\boldsymbol{\tau}_1, \boldsymbol{\tau}_2, \boldsymbol{n}\Big] = \Big[\boldsymbol{\tau}_1, \boldsymbol{\tau}_2, \boldsymbol{n}\Big] \begin{bmatrix} 0 & -1 & 0 \\ 1 & 0 & 0 \\ 0 & 0 & 0 \end{bmatrix}, \tag{4.89d}$$

$$\frac{\partial^2 O}{\partial \psi^2}\Big|_{(0,0,0)} \Big[\boldsymbol{\tau}_1, \boldsymbol{\tau}_2, \boldsymbol{n}\Big] = \Big[\boldsymbol{\tau}_1, \boldsymbol{\tau}_2, \boldsymbol{n}\Big] \begin{bmatrix} -1 & 0 & 0 \\ 0 & -1 & 0 \\ 0 & 0 & 0 \end{bmatrix}, \tag{4.89e}$$

$$\frac{\partial^2}{\partial \beta \partial \gamma} \left(O\boldsymbol{\tau}_1 \cdot \boldsymbol{n}\right)^2 \Big|_{(0,0,0)} = 2\delta_{\beta\phi}\delta_{\gamma\phi}, \quad \frac{\partial^2}{\partial \beta \partial \gamma} \left(O\boldsymbol{\tau}_2 \cdot \boldsymbol{n}\right)^2 \Big|_{(0,0,0)} = 2\delta_{\beta\theta}\delta_{\gamma\theta}. \tag{4.89f}$$

4.4.2 For curves in 2D

In this section, our main aim is to prove that there exists a $k_0(\boldsymbol{n}) < \infty$, such that for any $\alpha \geq k_0(\boldsymbol{n})$, the matrix $\tilde{M}(O, \alpha)$ defined as follows

$$\tilde{M}(O, \alpha) := \begin{bmatrix} \gamma(\boldsymbol{n}) + \alpha(O\boldsymbol{\tau} \cdot \boldsymbol{n})^2 & * \\ -\frac{1}{2}\left((O\boldsymbol{\tau} \cdot \boldsymbol{\tau})\gamma(\boldsymbol{n}) + (O\boldsymbol{\tau} \cdot \boldsymbol{n})(\boldsymbol{\tau} \cdot \boldsymbol{\xi}) + \gamma(O\boldsymbol{n})\right) & \gamma(\boldsymbol{n}) \end{bmatrix}, \tag{4.90}$$

is semi-positive definite for any $O \in SO(2)$.

The leading principle minors of $\tilde{M}(O, \alpha)$ are denoted as $\tilde{M}_1(O, \alpha), \tilde{M}_2(O, \alpha)$, their determinants are named by $\tilde{F}_1(O, \alpha), \tilde{F}_2(O, \alpha)$, respectively.

Now we are going to prove the existence of $k_0(\boldsymbol{n})$ by applying Lemma 4.7.

Lemma 4.11. *For any $\gamma(\boldsymbol{n}) \in C^2$, there exists a $k_1 < \infty$, such that $\forall O \in SO(2), \alpha \geq k_1$, there holds*

$$\tilde{M}_1(O,\alpha) \text{ is positive definite.} \tag{4.91}$$

Proof. We choose $k_1 = 0$. It is easy to check $\tilde{F}_1(O,\alpha) = \gamma(\boldsymbol{n}) + \alpha(O\boldsymbol{\tau}\cdot\boldsymbol{n})^2 > 0$, and thus we know that $\tilde{M}_1(O,\alpha)$ is positive definite. □

Lemma 4.12. *For any $\gamma(\boldsymbol{n}) \in C^2$, there exists $k_1 \leq k_{2,(0)} < \infty$ with the open neighbourhood $\mathcal{U}$ of 0 such that*

$$\tilde{F}_2(O, k_{2,(0)}) \geq 0, \quad \forall\theta \in \mathcal{U}; \tag{4.92}$$

Proof. First by applying the chain rule, noticing $\nabla\gamma(\boldsymbol{p})|_{\boldsymbol{p}=\boldsymbol{n}} = \boldsymbol{\xi}(\boldsymbol{n}), \nabla\nabla\gamma(\boldsymbol{p})|_{\boldsymbol{p}=\boldsymbol{n}} = \mathbf{H}_\gamma(\boldsymbol{n})$, together with (4.87), we obtain that

$$\gamma(O\boldsymbol{n})\Big|_0 = \gamma(\boldsymbol{n}), \tag{4.93a}$$

$$\frac{d\gamma(O\boldsymbol{n})}{d\theta}\Big|_0 = \boldsymbol{\xi}\cdot\boldsymbol{\tau}, \tag{4.93b}$$

$$\begin{aligned}\frac{d^2\gamma(O\boldsymbol{n})}{d\theta^2}\Big|_0 &= \left(\frac{dO}{d\theta}\Big|_0\boldsymbol{n}\right)\cdot\mathbf{H}_\gamma(\boldsymbol{n})\cdot\left(\frac{dO}{d\theta}\Big|_0\boldsymbol{n}\right) + \boldsymbol{\xi}\cdot\left(\frac{d^2O}{d\theta^2}\Big|_0\boldsymbol{n}\right)\\ &= \boldsymbol{\tau}\cdot(\mathbf{H}_\gamma(\boldsymbol{n})\boldsymbol{\tau}) - \gamma(\boldsymbol{n}).\end{aligned} \tag{4.93c}$$

By definition of $\tilde{M}_2(O,\alpha)$, (4.87), (4.93), and the definition of adjunct matrix, we know that

$$\tilde{M}_2(O,\alpha)\Big|_0 = \gamma(\boldsymbol{n})\begin{bmatrix}1 & -1\\ -1 & 1\end{bmatrix}, \tag{4.94a}$$

$$\mathrm{adj}(\tilde{M}_2(O,\alpha))\Big|_0 = \gamma(\boldsymbol{n})\begin{bmatrix}1\\ 1\end{bmatrix}\begin{bmatrix}1 & 1\end{bmatrix}, \tag{4.94b}$$

$$\frac{d\tilde{M}_2(O,\alpha)}{d\theta}\Big|_0 = \begin{bmatrix}0 & 0\\ 0 & 0\end{bmatrix}, \tag{4.94c}$$

$$\frac{d^2\tilde{M}_2(O,\alpha)}{d\theta^2}\Big|_0 = \begin{bmatrix}2\alpha & *\\ -\frac{1}{2}(-2\gamma(\boldsymbol{n}) + \boldsymbol{\tau}\cdot(\mathbf{H}_\gamma(\boldsymbol{n})\boldsymbol{\tau})) & 0\end{bmatrix}. \tag{4.94d}$$

(4.84), (4.85) in Lemma 4.8 and (4.94a)-(4.94d) suggest that

$$\tilde{F}_2(O,\alpha)\Big|_0 = 0, \quad \frac{d\tilde{F}_2(O,\alpha)}{d\theta}\Big|_0 = 0, \tag{4.95}$$

and

$$\frac{d^2\tilde{F}_2(O,\alpha)}{d\theta^2}\Big|_0 = \gamma(\boldsymbol{n})\left(2\alpha + 2\gamma(\boldsymbol{n}) - \boldsymbol{\tau}\cdot(\mathbf{H}_\gamma(\boldsymbol{n})\boldsymbol{\tau})\right). \tag{4.96}$$

(4.96) implies that there exists a $k_1 \le k_{2,(0)} < \infty$, such that $\frac{d^2\tilde{F}_2(O,k_{2,(0)})}{d\theta^2}\Big|_0 > 0$. By the continuity of $\frac{d^2\tilde{F}_2(O,k_{2,(0)})}{d\theta^2}$, we know that there exists an open neighbourhood $\mathcal{U}$ of 0, such that $\frac{d^2\tilde{F}_2(O,k_{2,(0)})}{d\theta^2}|_\theta \ge 0, \forall\theta\in\mathcal{U}$. Thus by Taylor expansion and (4.95), we know that there exists a $\tilde{F}_2(O,k_{2,(0)}) \ge 0, \forall\theta\in\mathcal{U}$, which validates (4.92). □

Lemma 4.13. *For any $\gamma(\boldsymbol{n}) \in C^2$ with $\gamma(-\boldsymbol{n}) < 3\gamma(\boldsymbol{n})$, there exists a $k_2 < \infty$, such that $\forall O \in SO(2), \alpha \ge k_2$, there holds*

$$\tilde{M}_2(O,\alpha) \text{ is semi-positive definite.} \tag{4.97}$$

Proof. First from Lemma 4.11, we know that there exists a $\alpha \ge k_1 \ge 0$, such that $\tilde{M}_1(O,\alpha)$ is positive definite.

Suppose $(O_0\boldsymbol{\tau}\cdot\boldsymbol{n})^2 \ne 0$, we have

$$\tilde{F}_2(O_0,\alpha) = \gamma(\boldsymbol{n})(O_0\boldsymbol{\tau}\cdot\boldsymbol{n})^2\alpha + \mathcal{O}(1) \tag{4.98}$$

Thus for such O_0, there exists a $k_1 \le k_{2,O_0} < \infty$ and a neighborhood $\mathcal{U}_{O_0}$ of O_0, such that $\tilde{F}_2(O,k_{2,O_0}) \ge 0, \forall O\in\mathcal{U}_{O_0}$.

If $(O_1\boldsymbol{\tau}\cdot\boldsymbol{n})^2 = 0$, we know that $O_1\boldsymbol{n} = \pm\boldsymbol{n}$. First we assume that $O_1\boldsymbol{n} = \boldsymbol{n}$, i.e. $\theta = 0$. In this case, the open neighborhood and constant are given by Lemma 4.12.

The last case is $O_1\boldsymbol{n} = -\boldsymbol{n}$. From the fact $\gamma(-\boldsymbol{n}) < 3\gamma(\boldsymbol{n})$ and $O_1\boldsymbol{\tau} = -\boldsymbol{\tau}$, we have

$$\tilde{F}_2(O_1,\alpha) = \frac{3\gamma(\boldsymbol{n}) - \gamma(-\boldsymbol{n})}{4}(\gamma(\boldsymbol{n}) + \gamma(-\boldsymbol{n})) > 0. \tag{4.99}$$

Thus there is an open neighbourhood $\mathcal{U}_{O_1}$ of O_1 and a $k_1 = k_{2,O_1} < \infty$, such that $\forall O\in\mathcal{U}_{O_1}$, it holds $\tilde{F}_2(O,k_{2,O_1}) \ge 0$.

It is obvious that $\tilde{M}_2(O,\alpha) = \tilde{M}_2(O,0) + \alpha\tilde{D}$, where $\tilde{D} = \mathrm{diag}((O\boldsymbol{\tau}\cdot\boldsymbol{n})^2, 0)$ is semi-positive definite. By Lemma 4.7, we derive the desired result (4.117). □

The proof of the existence of $k_0(\boldsymbol{n})$ is almost done, and we make it clear as follows

Proof of Theorem 4.3. Lemma 4.13 shows that

$$k_2 < \infty \in \left\{\alpha \middle| \ \tilde{M}(O,\alpha) \text{ is semi-positive definite} \quad \forall O \in SO(2)\right\}. \tag{4.100}$$

Thus such a set is nonempty. On the other hand, let $O\boldsymbol{\tau}\cdot\boldsymbol{n} = 1$ and $\tilde{\alpha} = -2\gamma(\boldsymbol{n})$. We know that $\tilde{F}_1(O,\tilde{\alpha}) = \gamma(\boldsymbol{n}) + \tilde{\alpha}(O\boldsymbol{\tau}\cdot\boldsymbol{n})^2 = -\gamma(\boldsymbol{n}) < 0$, and the set is also bounded below. Therefore the set has a finite infimum $k_0(\boldsymbol{n})$. □

4.4.3 For surfaces in 3D

In this section, our main aim is to prove that there exists a $k_0(\boldsymbol{n}) < \infty$, such that for any $\alpha \geq k_0(\boldsymbol{n})$, the matrix $M(O,\alpha)$ defined as follows

$$\begin{bmatrix} \gamma(\boldsymbol{n}) + \alpha(O\boldsymbol{\tau}_1\cdot\boldsymbol{n})^2 & * & * & * \\ -\frac{1}{2}\gamma(O\boldsymbol{n}) & \gamma(\boldsymbol{n}) + \alpha(O\boldsymbol{\tau}_2\cdot\boldsymbol{n})^2 & * & * \\ \alpha(O\boldsymbol{\tau}_1\cdot\boldsymbol{n})(O\boldsymbol{\tau}_2\cdot\boldsymbol{n}) & 0 & \gamma(\boldsymbol{n}) + \alpha(O\boldsymbol{\tau}_2\cdot\boldsymbol{n})^2 & * \\ M_{41} & M_{42} & M_{43} & \gamma(\boldsymbol{n}) \end{bmatrix} \tag{4.101}$$

is semi-positive definite for any $O \in SO(3)$.

The leading principle minors of $M(O,\alpha)$ are denoted as $M_1(O,\alpha), M_2(O,\alpha), M_3(O,\alpha)$. And we also use $M_4(O,\alpha)$ to stand for $M(O,\alpha)$. Their determinants are named by $F_1(O,\alpha), F_2(O,\alpha), F_3(O,\alpha)$ and $F_4(O,\alpha)$, respectively.

To apply Lemma 4.7, we first need to show $M_3(O,\alpha)$ is positive definite for large enough α.

Lemma 4.14. *For any $\gamma(\boldsymbol{n}) \in C^2$ with $\gamma(-\boldsymbol{n}) < 2\gamma(\boldsymbol{n})$, there exists a $k_3 < \infty$, such that $\forall O \in SO(3), \alpha \geq k_3$, there holds*

$$M_3(O,\alpha) \text{ is positive definite.} \tag{4.102}$$

Proof. By Lemma 4.5, $M_3(O,\alpha)$ is positive definite if and only if $F_1, F_2, F_3 > 0$. It

is easy to verify that

$$F_1(O,\alpha) = \gamma(\boldsymbol{n}) + \alpha(O\boldsymbol{\tau}_1\cdot\boldsymbol{n})^2, \tag{4.103a}$$

$$F_2(O,\alpha) = \alpha^2(O\boldsymbol{\tau}_1\cdot\boldsymbol{n})^2(O\boldsymbol{\tau}_2\cdot\boldsymbol{n})^2 + \alpha((O\boldsymbol{\tau}_1\cdot\boldsymbol{n})^2 + (O\boldsymbol{\tau}_2\cdot\boldsymbol{n})^2)\gamma(\boldsymbol{n}) + \frac{4\gamma(\boldsymbol{n})^2 - \gamma(O\boldsymbol{n})^2}{4}, \tag{4.103b}$$

$$F_3(O,\alpha) = \left(\alpha((O\boldsymbol{\tau}_1\cdot\boldsymbol{n})^2 + (O\boldsymbol{\tau}_2\cdot\boldsymbol{n})^2)\gamma(\boldsymbol{n}) + \frac{4\gamma(\boldsymbol{n})^2 - \gamma(O\boldsymbol{n})^2}{4}\right) (\gamma(\boldsymbol{n}) + \alpha(O\boldsymbol{\tau}_2\cdot\boldsymbol{n})^2). \tag{4.103c}$$

Thus for $\alpha \geq 0$, we know $F_1(O,\alpha) > 0, \alpha^2(O\boldsymbol{\tau}_1\cdot\boldsymbol{n})^2(O\boldsymbol{\tau}_2\cdot\boldsymbol{n})^2 \geq 0$, and F_2, F_3 is nondecreasing with respect to α. Moreover, if $\alpha((O\boldsymbol{\tau}_1\cdot\boldsymbol{n})^2 + (O\boldsymbol{\tau}_2\cdot\boldsymbol{n})^2)\gamma(\boldsymbol{n}) + \frac{4\gamma(\boldsymbol{n})^2-\gamma(O\boldsymbol{n})^2}{4} > 0$, we can deduce that $F_2, F_3 > 0$.

Suppose $(O_1\boldsymbol{\tau}_1\cdot\boldsymbol{n})^2 + (O_1\boldsymbol{\tau}_2\cdot\boldsymbol{n})^2 > 0$. Then for such $O_1 \in SO(3)$, we know that there exists a $k_{3,O_1} \geq 0$ with an open neighbourhood $\mathcal{U}_{O_1}$ of O_1, such that

$$\alpha((\tilde{O}_1\boldsymbol{\tau}_1\cdot\boldsymbol{n})^2 + (\tilde{O}_1\boldsymbol{\tau}_2\cdot\boldsymbol{n})^2)\gamma(\boldsymbol{n}) + \frac{4\gamma(\boldsymbol{n})^2 - \gamma(\tilde{O}_1\boldsymbol{n})^2}{4} > 0, \quad \forall \tilde{O} \in \mathcal{U}_{O_1}, \alpha > k_{3,O_1}. \tag{4.104}$$

On the contrary, if both $O_2\boldsymbol{\tau}_1\cdot\boldsymbol{n} = 0$ and $O_2\boldsymbol{\tau}_2\cdot\boldsymbol{n} = 0$, we know that $O_2\boldsymbol{n} = \pm\boldsymbol{n}$. In this case, $\alpha((O\boldsymbol{\tau}_1\cdot\boldsymbol{n})^2 + (O\boldsymbol{\tau}_2\cdot\boldsymbol{n})^2)\gamma(\boldsymbol{n}) + \frac{4\gamma(\boldsymbol{n})^2-\gamma(O\boldsymbol{n})^2}{4}$ becomes

$$\frac{4\gamma(\boldsymbol{n})^2 - \gamma(O\boldsymbol{n})^2}{4} \geq \min\left\{\frac{3\gamma(\boldsymbol{n})^2}{4}, \frac{4\gamma(\boldsymbol{n})^2 - \gamma(-\boldsymbol{n})^2}{4}\right\} > 0. \tag{4.105}$$

And we can simply choose $k_{3,O_2} = 0$. By applying the open cover theorem and (4.104),(4.105), and the above analysis, we deduce the desired result. □

Lemma 4.15. *For any $\gamma(\boldsymbol{n}) \in C^2$ with $\gamma(-\boldsymbol{n}) < 2\gamma(\boldsymbol{n})$, there exists $k_3 \leq k_{4,(0,0,0)} < \infty, k_3 \leq k_{4,(0,0,\pi)} < \infty$ with the open neighbourhood $\mathcal{U}$ of $(0,0,0)$, $\mathcal{V}$ of $(0,0,\pi)$ such that*

$$F_4(O, k_{4,(0,0,0)}) \geq 0, \quad \forall(\phi,\theta,\psi) \in \mathcal{U}; \tag{4.106}$$

$$F_4(O, k_{4,(0,0,\pi)}) \geq 0, \quad \forall(\phi,\theta,\psi) \in \mathcal{V}. \tag{4.107}$$

Proof. First by applying the chain rule, noticing $\nabla\gamma(\boldsymbol{p})|_{\boldsymbol{p}=\boldsymbol{n}} = \boldsymbol{\xi}(\boldsymbol{n}), \nabla\nabla\gamma(\boldsymbol{p})|_{\boldsymbol{p}=\boldsymbol{n}} = \mathbf{H}_\gamma(\boldsymbol{n})$, together with (4.89), we obtain that

$$\gamma(O\boldsymbol{n})\Big|_{(0,0,0)} = \gamma(\boldsymbol{n}), \tag{4.108a}$$

$$\frac{\partial\gamma(O\boldsymbol{n})}{\partial\phi}\Big|_{(0,0,0)} = \nabla\gamma(O\boldsymbol{n})\Big|_{(0,0,0)} \cdot \left(\frac{\partial O}{\partial\phi}\Big|_{(0,0,0)}\boldsymbol{n}\right) = -\boldsymbol{\xi}\cdot\boldsymbol{\tau}_2, \tag{4.108b}$$

$$\frac{\partial\gamma(O\boldsymbol{n})}{\partial\theta}\Big|_{(0,0,0)} = \boldsymbol{\xi}\cdot\boldsymbol{\tau}_1, \tag{4.108c}$$

$$\frac{\partial\gamma(O\boldsymbol{n})}{\partial\psi}\Big|_{(0,0,0)} = \mathbf{0}, \tag{4.108d}$$

$$\begin{aligned}\frac{\partial^2\gamma(O\boldsymbol{n})}{\partial\psi^2}\Big|_{(0,0,0)} &= \left(\frac{\partial O}{\partial\psi}\Big|_{(0,0,0)}\boldsymbol{n}\right)\cdot\mathbf{H}_\gamma(\boldsymbol{n})\cdot\left(\frac{\partial O}{\partial\psi}\Big|_{(0,0,0)}\boldsymbol{n}\right)\\ &\quad + \boldsymbol{\xi}\cdot\left(\frac{\partial^2 O}{\partial\psi^2}\Big|_{(0,0,0)}\boldsymbol{n}\right)\\ &= \mathbf{0}\cdot(\mathbf{H}_\gamma(\boldsymbol{n})\mathbf{0}) + \boldsymbol{\xi}\cdot\mathbf{0} = \mathbf{0}.\end{aligned} \tag{4.108e}$$

By definition of $M_4(O,\alpha)$, (4.89), (4.108), and the definition of adjunct matrix,

we know that

$$M_4(O,\alpha)\Big|_{(0,0,0)} = \gamma(\boldsymbol{n}) \begin{bmatrix} 1 & -1/2 & 0 & -1/2 \\ -1/2 & 1 & 0 & -1/2 \\ 0 & 0 & 1 & 0 \\ -1/2 & -1/2 & 0 & 1 \end{bmatrix}, \tag{4.109a}$$

$$\mathrm{adj}(M_4(O,\alpha))\Big|_{(0,0,0)} = \frac{3}{4}\gamma(\boldsymbol{n})^3 \begin{bmatrix} 1 \\ 1 \\ 0 \\ 1 \end{bmatrix} \begin{bmatrix} 1 & 1 & 0 & 1 \end{bmatrix}, \tag{4.109b}$$

$$\frac{\partial M_4(O,\alpha)}{\partial \phi}\Big|_{(0,0,0)} = \frac{1}{2} \begin{bmatrix} 0 & \boldsymbol{\tau}_2\cdot\boldsymbol{\xi} & 0 & 0 \\ \boldsymbol{\tau}_2\cdot\boldsymbol{\xi} & 0 & 0 & -\boldsymbol{\tau}_2\cdot\boldsymbol{\xi} \\ 0 & 0 & 0 & -\boldsymbol{\tau}_1\cdot\boldsymbol{\xi} \\ 0 & -\boldsymbol{\tau}_2\cdot\boldsymbol{\xi} & -\boldsymbol{\tau}_1\cdot\boldsymbol{\xi} & 0 \end{bmatrix}, \tag{4.109c}$$

$$\frac{\partial M_4(O,\alpha)}{\partial \theta}\Big|_{(0,0,0)} = \frac{\boldsymbol{\tau}_1\cdot\boldsymbol{\xi}}{2} \begin{bmatrix} 0 & -1 & 0 & 1 \\ -1 & 0 & 0 & 0 \\ 0 & 0 & 0 & 0 \\ 1 & 0 & 0 & 0 \end{bmatrix}, \tag{4.109d}$$

$$\frac{\partial M_4(O,\alpha)}{\partial \psi}\Big|_{(0,0,0)} = \frac{\gamma(\boldsymbol{n})}{2} \begin{bmatrix} 0 & 0 & 0 & 0 \\ 0 & 0 & 0 & 0 \\ 0 & 0 & 0 & 1 \\ 0 & 0 & 1 & 0 \end{bmatrix}, \tag{4.109e}$$

$$\frac{\partial^2 M_4(O,\alpha)}{\partial \psi^2}\Big|_{(0,0,0)} = \frac{\gamma(\boldsymbol{n})}{2} \begin{bmatrix} 0 & 0 & 0 & 1 \\ 0 & 0 & 0 & 1 \\ 0 & 0 & 0 & 0 \\ 1 & 1 & 0 & 0 \end{bmatrix}. \tag{4.109f}$$

(4.84) in Lemma 4.8 and (4.109a)-(4.109e) suggest that

$$F_4(O,\alpha)\Big|_{(0,0,0)} = 0, \quad \frac{\partial F_4(O,\alpha)}{\partial \beta}\Big|_{(0,0,0)} = 0, \ \forall \beta \in \{\phi,\theta,\psi\}. \tag{4.110}$$

Obviously, $M_4(O,0)$ is independent of α. From (4.109), we observe that $M_4(O,\alpha)\Big|_{(0,0,0)}$, $\frac{\partial M_4(O,\alpha)}{\partial \beta}\Big|_{(0,0,0)}, \beta \in \{\phi,\theta,\psi\}$ are also independent of α. Thus for any $\beta,\varphi \in \{\phi,\theta,\psi\}$, we define the constant $C^1_{4,\beta,\varphi}, C^2_{4,\beta,\varphi}$ as follows

$$C^1_{4,\beta,\varphi} := \frac{3}{4}\gamma(\boldsymbol{n})^3 \begin{bmatrix} 1 \\ 1 \\ 0 \\ 1 \end{bmatrix}^T \frac{\partial^2 M_4(O,0)}{\partial\beta\partial\varphi}\Big|_{(0,0,0)} \begin{bmatrix} 1 \\ 1 \\ 0 \\ 1 \end{bmatrix}, \tag{4.111a}$$

$$C^2_{4,\beta,\varphi} := \sum_{i\neq j} \det \begin{bmatrix} M_{1,1} & M_{1,2} & M_{1,3} & M_{1,4} \\ \frac{\partial M_{i,1}}{\partial\beta} & \frac{\partial M_{i,2}}{\partial\beta} & \frac{\partial M_{i,3}}{\partial\beta} & \frac{\partial M_{i,3}}{\partial\beta} \\ \frac{\partial M_{j,1}}{\partial\varphi} & \frac{\partial M_{j,2}}{\partial\varphi} & \frac{\partial M_{j,3}}{\partial\varphi} & \frac{\partial M_{j,3}}{\partial\varphi} \\ M_{4,1} & M_{4,2} & M_{4,3} & M_{4,4} \end{bmatrix}. \tag{4.111b}$$

From the definition of $M(O,\alpha)$, we know that

$$\begin{aligned} M_4(O,\alpha) &:= M_4(O,0) + \alpha D(O) \\ &= M_4(O,0) + \alpha \begin{bmatrix} (O\boldsymbol{\tau}_1\cdot\boldsymbol{n})^2 & 0 & (O\boldsymbol{\tau}_1\cdot\boldsymbol{n})(O\boldsymbol{\tau}_2\cdot\boldsymbol{n}) & 0 \\ 0 & (O\boldsymbol{\tau}_2\cdot\boldsymbol{n})^2 & 0 & 0 \\ (O\boldsymbol{\tau}_1\cdot\boldsymbol{n})(O\boldsymbol{\tau}_2\cdot\boldsymbol{n}) & 0 & (O\boldsymbol{\tau}_2\cdot\boldsymbol{n})^2 & 0 \\ 0 & 0 & 0 & 0 \end{bmatrix}. \end{aligned} \tag{4.112}$$

Use (4.85) in Lemma 4.8, together with (4.109b), (4.89f), (4.111), (4.112), we

deduce for any $\beta, \varphi \in \{\phi, \theta, \psi\}$, the second order derivative of F_4 as follows

$$\begin{aligned}
&\frac{\partial^2 F_4(O,\alpha)}{\partial\beta\partial\varphi}\Big|_{(0,0,0)} \\
&= \mathrm{tr}\left(\mathrm{adj}(M_4(O,\alpha))\frac{\partial^2 M_4(O,\alpha)}{\partial\beta\partial\varphi}\right) + \sum_{i\neq j}\det\begin{bmatrix} M_{1,1} & M_{1,2} & M_{1,3} & M_{1,4} \\ \frac{\partial M_{i,1}}{\partial\beta} & \frac{\partial M_{i,2}}{\partial\beta} & \frac{\partial M_{i,3}}{\partial\beta} & \frac{\partial M_{i,3}}{\partial\beta} \\ \frac{\partial M_{j,1}}{\partial\varphi} & \frac{\partial M_{j,2}}{\partial\varphi} & \frac{\partial M_{j,3}}{\partial\varphi} & \frac{\partial M_{j,3}}{\partial\varphi} \\ M_{4,1} & M_{4,2} & M_{4,3} & M_{4,4} \end{bmatrix} \\
&= \frac{3}{4}\gamma(\boldsymbol{n})^3\begin{bmatrix}1\\1\\0\\1\end{bmatrix}\cdot\frac{\partial^2(M_4(O,0)+\alpha D(O))}{\partial\beta\partial\varphi}\Big|_{(0,0,0)}\begin{bmatrix}1\\1\\0\\1\end{bmatrix} + C^2_{4,\beta,\varphi} \\
&= C^1_{4,\beta,\varphi} + C^2_{4,\beta,\varphi} + \frac{3\alpha}{4}\gamma(\boldsymbol{n})^3(2\delta_{\beta\phi}\delta_{\varphi\phi} + 2\delta_{\beta\theta}\delta_{\varphi\theta}).
\end{aligned} \tag{4.113}$$

We note only $\frac{\partial^2 F_3(O,\alpha)}{\partial\phi^2}\Big|_{(0,0,0)}, \frac{\partial^2 F_3(O,\alpha)}{\partial\theta^2}\Big|_{(0,0,0)}$ depend on α. Hence the Hessian matrix $\mathbf{H}_{F_4(O,\alpha)}\Big|_{(0,0,0)}$ can be written as

$$\mathbf{H}_{F_4(O,\alpha)}\Big|_{(0,0,0)} = (C^1_{4,\beta,\varphi} + C^2_{4,\beta,\varphi})_{\beta,\varphi\in\{\phi,\theta,\psi\}} + \frac{3\alpha}{2}\gamma(\boldsymbol{n})^3\mathrm{diag}(1,1,0). \tag{4.114}$$

Moreover, by combining (4.109b), (4.109e), (4.109f), (4.111), (4.114) for $\frac{\partial^2 F_4(O,\alpha)}{\partial\psi^2}\Big|_{(0,0,0)}$, we have

$$\frac{\partial^2 F_4(O,\alpha)}{\partial\psi^2}\Big|_{(0,0,0)} = C^1_{4,\psi,\psi} + C^2_{4,\psi,\psi} = \frac{9}{8}\gamma(\boldsymbol{n})^4 > 0. \tag{4.115}$$

This together with (4.114) and Lemma 4.5 imply that there exists a $k_3 \leq k_{4,(0,0,0)} < \infty$, such that $\mathbf{H}_{F_4(O,k_{4,(0,0,0)})}\Big|_{(0,0,0)}$ is positive definite. By the continuity of $\mathbf{H}_{F_4(O,\alpha)}$, we know that there is an open neighbourhood $\mathcal{U}$ of $(0,0,0)$, such that $\forall(\phi,\theta,\psi)\in\mathcal{U}$, it holds

$$\mathbf{H}_{F_4(O,k_{4,(0,0,0)})}\Big|_{(\phi,\theta,\psi)} \text{ is semi-positive definite.} \tag{4.116}$$

Thus by Taylor expansion, we know that $F_4(O, k_{4,(0,0,0)}) \geq 0, \forall(\phi,\theta,\psi)\in\mathcal{U}$, which validates (4.106). And the proof of (4.107) is similar. □

Lemma 4.16. *For any $\gamma(\boldsymbol{n}) \in C^2$ with $\gamma(-\boldsymbol{n}) < 2\gamma(\boldsymbol{n})$, there exists a $k_4 < \infty$, such that $\forall O \in SO(3), \alpha \geq k_4$, there holds*

$$F_4(O,\alpha) \geq 0, \quad M_4(O,\alpha) \text{ is semi-positive definite.} \tag{4.117}$$

Proof. First from Lemma 4.14, we know that there exists a $\alpha \geq k_3 \geq 0$, such that $M_3(O,\alpha)$ is positive definite.

Suppose $(O_0\boldsymbol{\tau}_2 \cdot \boldsymbol{n})^2 \neq 0$, we have

$$\begin{aligned}
F_4(O_0,\alpha) &= (O_0\boldsymbol{\tau}_2 \cdot \boldsymbol{n})^2\gamma(\boldsymbol{n})^2 \left((O_0\boldsymbol{\tau}_1 \cdot \boldsymbol{n})^2 + (O_0\boldsymbol{\tau}_2 \cdot \boldsymbol{n})^2\right)\alpha^2 \\
&\quad - (O_0\boldsymbol{\tau}_2 \cdot \boldsymbol{n})^2 \left((O_0\boldsymbol{\tau}_1 \cdot \boldsymbol{n})M_{43} - (O_0\boldsymbol{\tau}_2 \cdot \boldsymbol{n})M_{41}\right)^2\alpha^2 + \mathcal{O}(\alpha) \\
&= (O_0\boldsymbol{\tau}_2 \cdot \boldsymbol{n})^2\gamma(\boldsymbol{n})^2 \left((O_0\boldsymbol{\tau}_1 \cdot \boldsymbol{n})^2 + (O_0\boldsymbol{\tau}_2 \cdot \boldsymbol{n})^2\right)\alpha^2 \\
&\quad - \frac{(O_0\boldsymbol{\tau}_2 \cdot \boldsymbol{n})^2\gamma(\boldsymbol{n})^2}{4}[(O_0\boldsymbol{\tau}_1 \cdot \boldsymbol{n})(O_0\boldsymbol{\tau}_2 \cdot \boldsymbol{\tau}_1) - (O_0\boldsymbol{\tau}_2 \cdot \boldsymbol{n})(O_0\boldsymbol{\tau}_1 \cdot \boldsymbol{\tau}_1)]^2\alpha^2 \\
&\quad + \mathcal{O}(\alpha) \\
&\geq \frac{(O_0\boldsymbol{\tau}_2 \cdot \boldsymbol{n})^2\gamma(\boldsymbol{n})^2}{2}\left((O_0\boldsymbol{\tau}_1 \cdot \boldsymbol{n})^2 + (O_0\boldsymbol{\tau}_2 \cdot \boldsymbol{n})^2\right)\alpha^2 + \mathcal{O}(\alpha)
\end{aligned}$$

Thus for such O_0, there exists a $k_3 \leq k_{4,O_0} < \infty$ and a neighborhood $\mathcal{U}_{O_0}$ of O_0, such that $F_4(O, k_{4,O_0}) \geq 0, \forall O \in \mathcal{U}_{O_0}$.

Next, suppose $(O_1\boldsymbol{\tau}_1 \cdot \boldsymbol{n})^2 \neq 0, (O_1\boldsymbol{\tau}_2 \cdot \boldsymbol{n})^2 = 0$, we have

$$\begin{aligned}
F_4(O_1,\alpha) &= \gamma(\boldsymbol{n})(O_1\boldsymbol{\tau}_1 \cdot \boldsymbol{n})^2\left(\gamma(\boldsymbol{n})^2 - M_{42}^2 - M_{43}^2\right)\alpha + \mathcal{O}(1) \\
&\geq \frac{1}{2}\gamma(\boldsymbol{n})^3(O_1\boldsymbol{\tau}_1 \cdot \boldsymbol{n})^2\alpha + \mathcal{O}(1)
\end{aligned}$$

By the same argument, we know that there exists a $k_3 \leq k_{4,O_1} < \infty$ and a neighborhood $\mathcal{U}_{O_1}$ of O_1, such that $F_4(O, k_{4,O_1}) \geq 0, \forall O \in \mathcal{U}_{O_1}$.

If both $(O_2\boldsymbol{\tau}_1 \cdot \boldsymbol{n})^2 = 0$ and $(O_2\boldsymbol{\tau}_2 \cdot \boldsymbol{n})^2 = 0$, we know that $O_2\boldsymbol{n} = \pm\boldsymbol{n}$. First we assume that $O_2\boldsymbol{n} = \boldsymbol{n}$, i.e. $\phi = \theta = 0$. In this case, from Lemma 4.10 and (4.88) we obtain

$$O_2\boldsymbol{\tau}_1 \cdot \boldsymbol{\tau}_1 = \cos\psi,\ O_2\boldsymbol{\tau}_1 \cdot \boldsymbol{\tau}_2 = \sin\psi,\ O_2\boldsymbol{\tau}_2 \cdot \boldsymbol{\tau}_2 = \cos\psi,\ O_2\boldsymbol{\tau}_2 \cdot \boldsymbol{\tau}_1 = -\sin\psi. \tag{4.118}$$

For any $\alpha \geq k_3$, by applying (4.118) we have

$$F_4(O_2,\alpha) = \frac{9\sin^2\psi}{16}\gamma(\boldsymbol{n})^4. \tag{4.119}$$

Thus if $\psi \neq 0, \pi$, we know that $F_4(O_2, k_3) > 0$. By the same argument, there exists such open neighbourhood $\mathcal{U}_{O_2}$ of O_2 and the $k_3 = k_{4,O_2} < \infty$. And if $\psi = 0$ or $\psi = \pi$, the open neighborhood and constant are given by Lemma 4.15.

The last case is $O_3\boldsymbol{n} = -\boldsymbol{n}$, we assume that $\phi = \pi, \theta = 0$. For any $\alpha > 0$, from the fact $\gamma(-\boldsymbol{n}) < 2\gamma(\boldsymbol{n})$ and Lemma 4.10, we have

$$F_4(O_3, \alpha) = \gamma(\boldsymbol{n})^2 \frac{2\gamma(\boldsymbol{n}) - \gamma(-\boldsymbol{n})}{32} \Big(\gamma(\boldsymbol{n})(10 - 2\cos(2\psi)) + \gamma(-\boldsymbol{n})(7 - 2\cos(2\psi)) \Big) > 0. \tag{4.120}$$

By the same argument, there is an open neighbourhood $\mathcal{U}_{O_3}$ of O_3 and a $k_3 = k_{4,O_3} < \infty$, such that $\forall O \in \mathcal{U}_{O_3}$, it holds $F_4(O, k_{4,O_3}) \geq 0$.

By Lemma 4.7 and (4.112), we derive the desired result (4.117). □

Similar to the proof of Theorem 4.3, Theorem 4.4 is also a direct result of Lemma 4.16.

4.5 Numerical results

In this section, we present numerical results for the proposed unified SP-PFEM (4.39) for surfaces in 3D. We demonstrate the efficiency of the method using a convergence test and verify the main result (4.5) with a conservation law test. And we also apply (4.39) to show the morphological evolution of several non-even anisotropic energies.

For the spatial discretization, the initial surface S_0 is approximated by the polyhedral mesh $\Gamma_{h,\tau}(0) = \Gamma^0 = \cup_{j=1}^{J} \sigma_j^0$ with the mesh size parameter h via the *CFDTool*. The time step τ corresponding to the mesh Γ^0 is chosen as $\tau = \frac{2}{25}h^2$. To solve the implicit unified SP-PFEM (4.39), we employ the Newton iteration proposed in [12], where the tolerance ε is chosen as 10^{-12}.

In the numerical tests, we consider the three anisotropic surface energies as follows

- Case I: $\gamma(\boldsymbol{n}) = 1 + \frac{1}{8}(n_1^3 + n_2^3 + n_3^3)$;
- Case II: $\gamma(\boldsymbol{n}) = 1 + \frac{1}{4}(n_1^3 + n_2^3 + n_3^3)$;
- Case III: $\gamma(\boldsymbol{n}) = \sqrt{(\frac{5}{2} + \frac{3}{2}\text{sign}(n_1))n_1^2 + n_2^2 + n_3^2}$.

The minimal stabilizing function $k_0(\boldsymbol{n})$ is determined numerically as follows: for the interpolation points $\boldsymbol{n}_{ij} = (\cos\theta_i \cos\phi_j, \cos\theta_i \sin\phi_j, \sin\theta_i)^T$ for $\theta_i = \frac{i\pi}{10}, \phi_j = -\frac{\pi}{2} + \frac{j-1}{10}\pi$, $i = 1, 2, \ldots, 20, j = 1, 2, \ldots, 21$, we solve the optimization problem (4.43) to determine $k_0(\boldsymbol{n}_{ij})$; and for the other points, $k_0(\boldsymbol{n})$ is given by the bilinear interpolation.

To test the convergence rate, the initial surface S_0 is chosen as a $2 \times 1 \times 1$ cuboid. We denote the numerical error between the numerical solution as $\Gamma_{h,\tau}(t)$ and the exact solution $\Gamma(t)$ as $e^h(t)$. The intermediate surface $\Gamma_{h,\tau}(t)$ is defined as

$$\Gamma_{h,\tau}(t) := \frac{t - t_m}{\tau}\Gamma_{h,\tau}(t_m) + \frac{t_{m+1} - t}{\tau}\Gamma_{h,\tau}(t_{m+1}), \qquad t_m \le t < t_{m+1}. \tag{4.121}$$

And the exact solution $\Gamma(t)$ is approximated by $S_{h_e,\tau_e}(t)$ with a small mesh size of $h_e = 2^{-4}$ and a time step of $\tau_e = \frac{2}{25}h_e^2$. We adopt the manifold distance $M(S_{h,\tau}(t), \Gamma(t))$ to quantify the numerical error $e^h(t)$, which is given as

$$e^h(t) = M(\Gamma_{h,\tau}(t), \Gamma(t)) := 2|\Omega_1 \cup \Omega_2| - |\Omega_1| - |\Omega_2|. \tag{4.122}$$

Here Ω_1, Ω_2 represents the enclosed region by $\Gamma_{h,\tau}(t), \Gamma(0)$, respectively.

The numerical errors for the anisotropic energies $\gamma(\boldsymbol{n})$ in Case I-III and the stabilizing functions $k(\boldsymbol{n}) = k_0(\boldsymbol{n})$ and $k(\boldsymbol{n}) = \sup_{\boldsymbol{n}\in\mathbb{S}^2} k_0(\boldsymbol{n})$ are presented in Table 4.1. Our results demonstrate that the order of convergence in h is approximately 2 for all configurations, which suggests that our unified SP-PFEM (4.39) is efficient. Additionally, we can reduce the bilinear interpolation cost by setting $k(\boldsymbol{n}) = \sup_{\boldsymbol{n}\in\mathbb{S}^2} k_0(\boldsymbol{n})$ but achieve the same performance of efficiency.

To validate the volume conservation and the energy dissipation, we consider the normalized volume change $\frac{\Delta V^h(t)}{V^h(0)}$ and the normalized energy $\frac{W^h(t)}{W^h(0)}$ as follows

$$\frac{\Delta V^h(t)}{V^h(0)}\Big|_{t=t_m} := \frac{V^m - V^0}{V^0}, \qquad \frac{W^h(t)}{W^h(0)}\Big|_{t=t_m} := \frac{W^m}{W^0}. \tag{4.123}$$

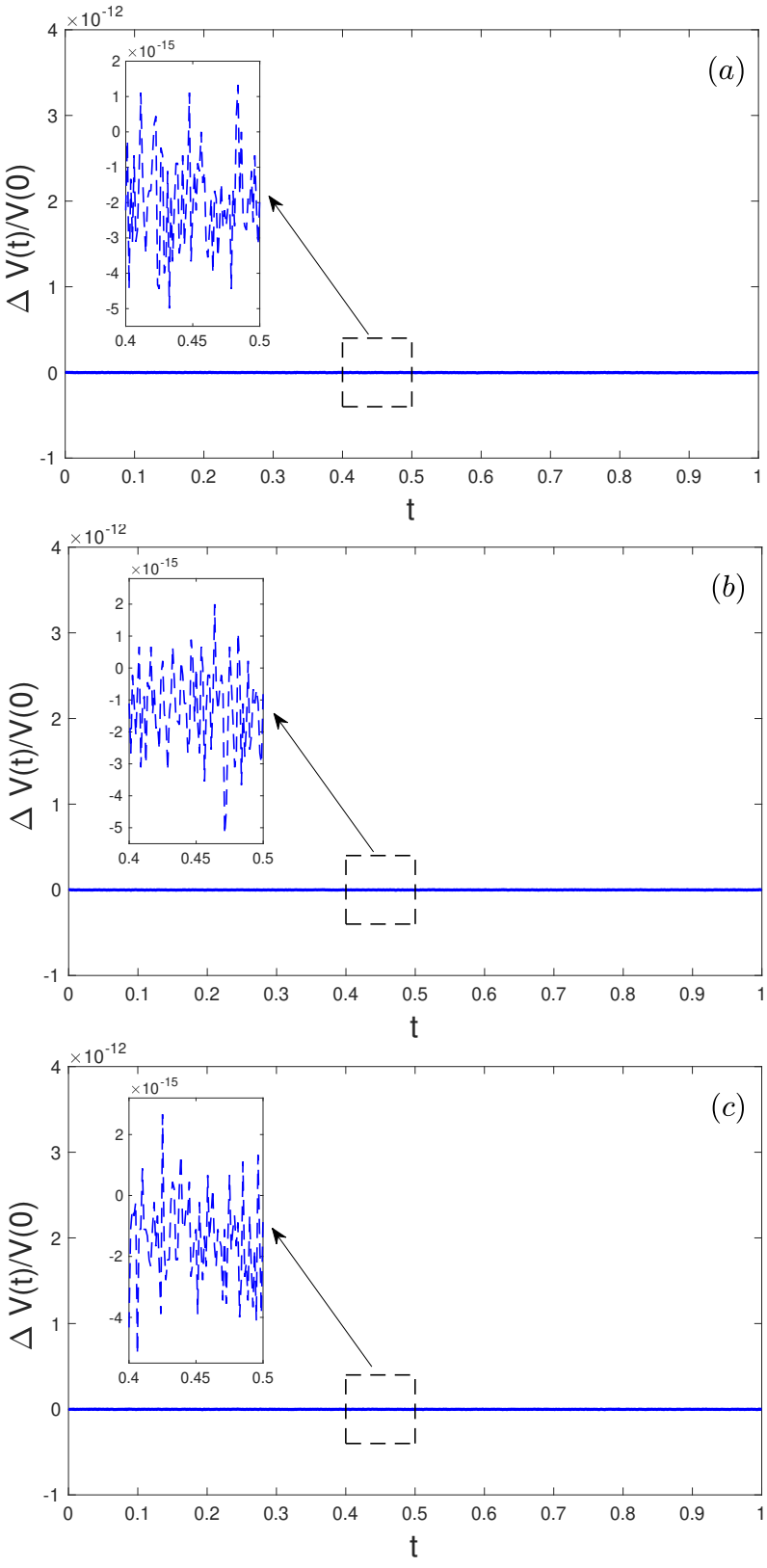

Figure 4.2: Plot of the normalized volume change $\frac{\Delta V(t)}{V(0)}$ for different cases: (a) for Case 1, (b) for Case 2, and (c) for Case 3.

(h,τ)	$e^h(1)$ Case 1	order	$e^h(1)$ Case 2	order	$e^h(1)$ Case 3	order
(h_0,τ_0)	1.48E-1	-	1.56E-1	-	1.63E-1	-
$(\frac{h_0}{2},\ \frac{\tau_0}{4})$	3.68E-2	2.01	3.87E-2	2.01	3.98E-2	2.03
$(\frac{h_0}{2^2},\ \frac{\tau_0}{4^2})$	8.95E-3	2.04	9.73E-3	1.99	9.53E-3	2.06
(h,τ)	$e^h(1)$ Case 1'	order	$e^h(1)$ Case 2'	order	$e^h(1)$ Case 3'	order
(h_0,τ_0)	1.63E-1	-	1.65E-1	-	1.66E-1	-
$(\frac{h_0}{2},\ \frac{\tau_0}{4})$	3.95E-2	2.04	4.23E-2	1.96	4.04E-2	2.04
$(\frac{h_0}{2^2},\ \frac{\tau_0}{4^2})$	9.66E-3	2.03	1.01E-2	2.07	9.76E-3	2.05

Table 4.1: Numerical errors of $e_{h,\tau}(t=1)$ with $k(\boldsymbol{n})=k_0(\boldsymbol{n})$ (the first row) and $k(\boldsymbol{n})=\sup_{\boldsymbol{n}\in\mathbb{S}^2}k_0(\boldsymbol{n})$ (the second row) for Cases 1-3, while $h_0:=2^{-1}$ and $\tau_0:=\frac{2^{-1}}{25}$. Here Case i/ Case i' means the anisotropic energy in Case i with $k(\boldsymbol{n})=k_0(\boldsymbol{n})/k(\boldsymbol{n})=\sup_{\boldsymbol{n}\in\mathbb{S}^2}k_0(\boldsymbol{n})$, respectively.

We investigate the anisotropic energies in Case I-III with the initial $2\times1\times1$ elliptic and fixed mesh size $h=2^{-4}$ and time step $\tau=\frac{2}{25}h^2$. Figure 4.2 shows the normalized volume changes with $k(\boldsymbol{n})=k_0(\boldsymbol{n})$, and Figure 4.3 illustrates the normalized energies with different $k(\boldsymbol{n})\geq k_0(\boldsymbol{n})$. It can be seen in Figure 4.2 that the normalized volume changes are in the same order of 10^{-15}, which is almost the machine epsilon. We also observe that the normalized energies are monotonically decreasing, as shown in Figure 4.3. In particular, the right column in Figure 4.3 indicates that the normalized energies are independent of $k(\boldsymbol{n})$.

The morphological evolutions of the $2\times2\times1$ cuboid under anisotropic surface diffusion are shown in Figure 4.4-4.6 for different anisotropies. We observe that the mesh points are well-behaved in each figure, and no mesh regularization is required. Moreover, by comparing the numerical equilibrium shapes in Figure 4.4 and 4.5, we can find the corners become sharper as the anisotropic effect increases from $\frac{1}{8}$ to $\frac{1}{4}$. Finally, we note that although the regularity of $\gamma(\boldsymbol{n})$ in Case III is not C^2, our

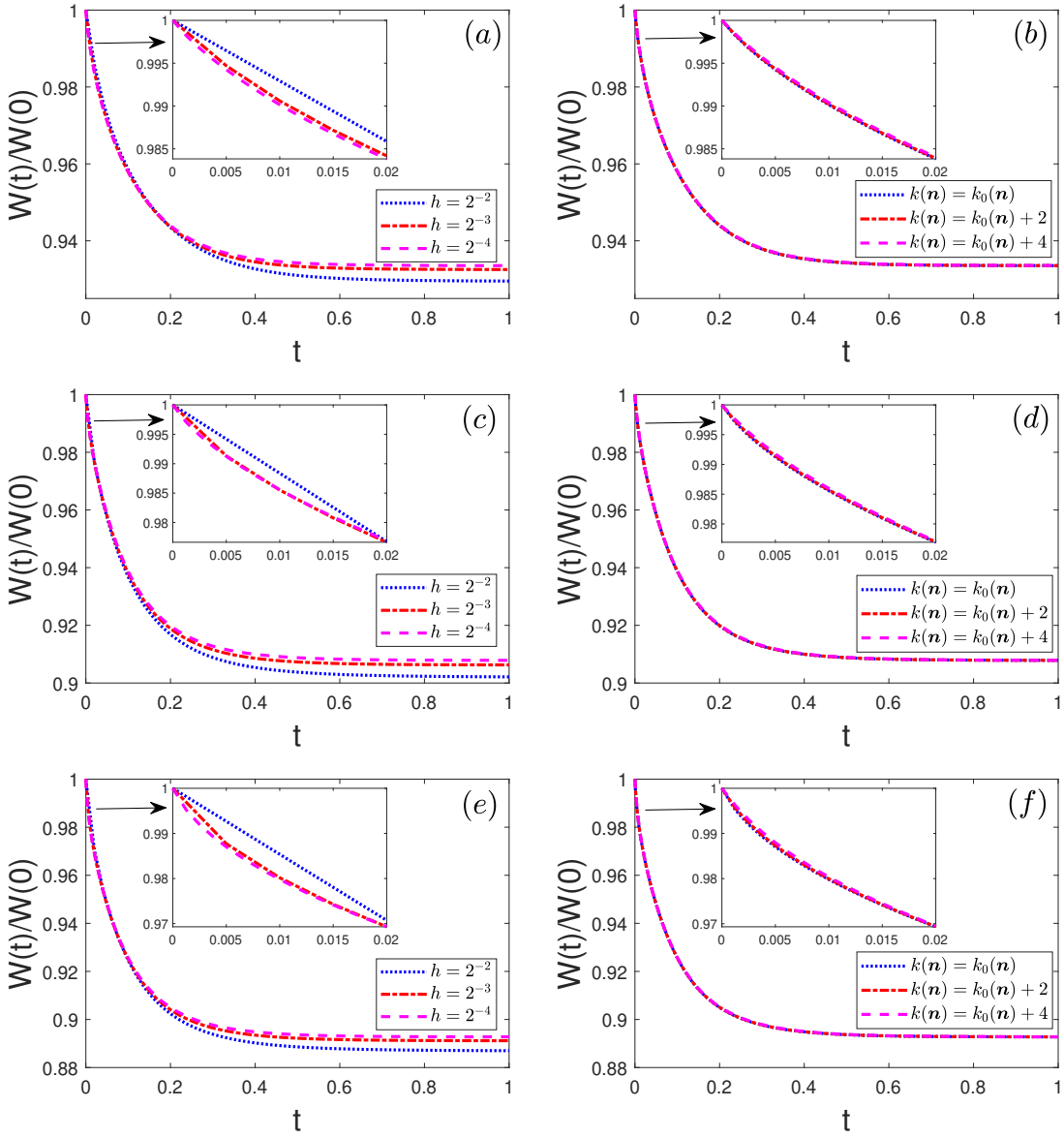

Figure 4.3: Plot of the normalized energy $\frac{W(t)}{W(0)}$ for anisotropic energies in Case I-III with the fixed $k(\boldsymbol{n}) = k_0(\boldsymbol{n})$ (left column) for different h and τ; or the fixed $h = 2^{-4}$ and $\tau = \frac{2}{25}h^2$ with different $k(\boldsymbol{n})$ (right column). The top, middle, and bottom rows correspond to the anisotropic energies in Case I-III, respectively.

unified SP-PFEM (4.39) works well for all the numerical tests, which validates our remark 4.1.

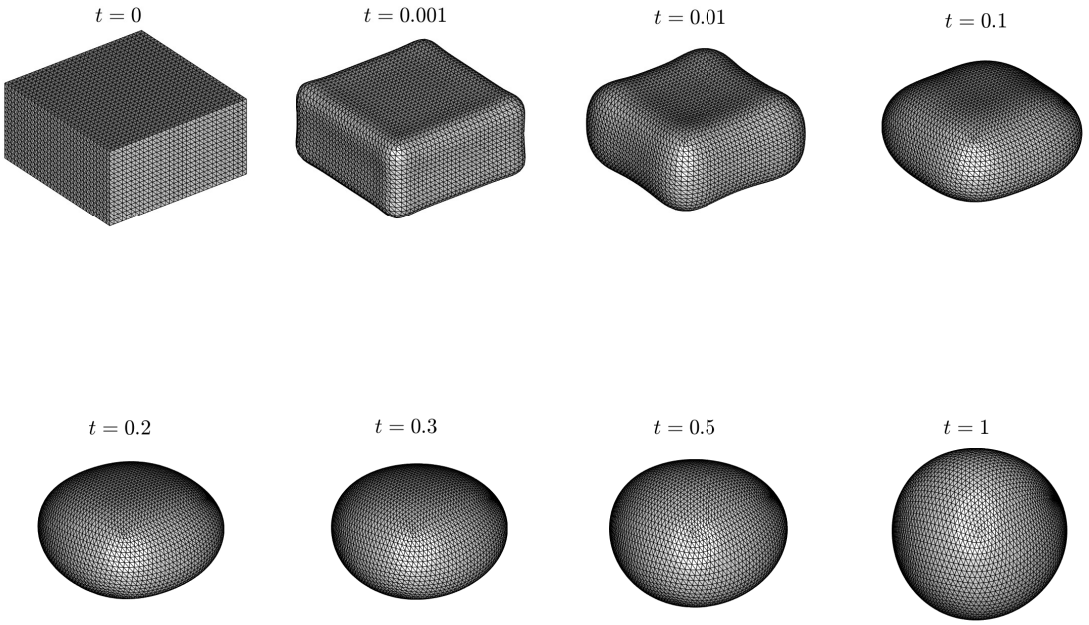

Figure 4.4: Evolution of a $2 \times 2 \times 1$ cuboid by anisotropic surface diffusion with a weak anisotropy $\gamma(\boldsymbol{n}) = 1 + \frac{1}{8}(n_1^3 + n_2^3 + n_3^3)$ and $k(\boldsymbol{n}) = k_0(\boldsymbol{n})$ at different times.

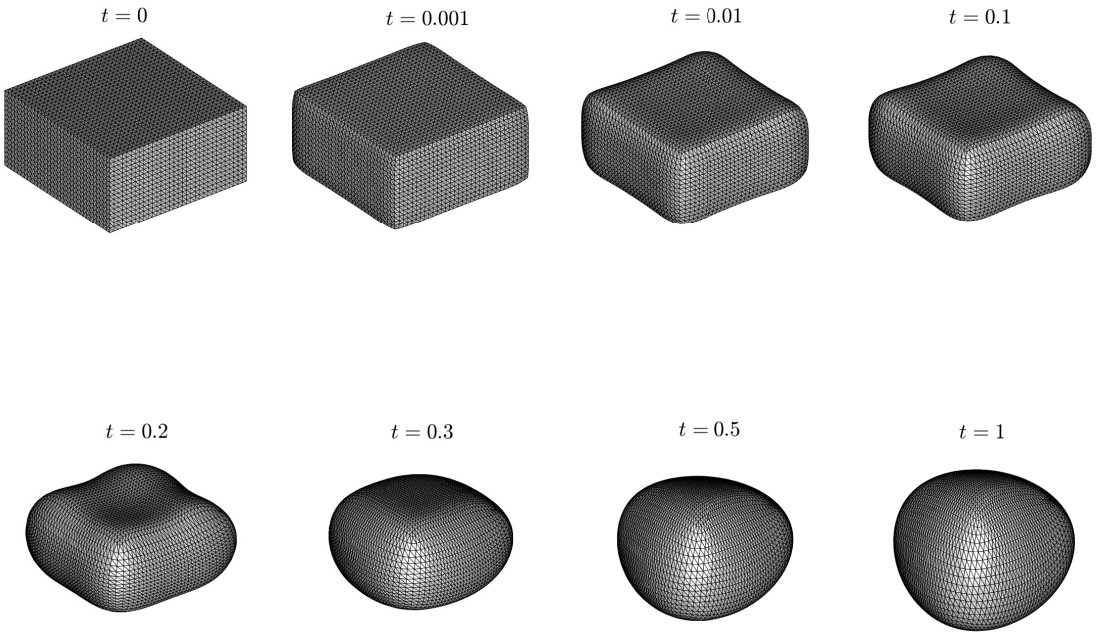

Figure 4.5: Evolution of a $2 \times 2 \times 1$ cuboid by anisotropic surface diffusion with a weak anisotropy $\gamma(\boldsymbol{n}) = 1 + \frac{1}{4}(n_1^3 + n_2^3 + n_3^3)$ and $k(\boldsymbol{n}) = k_0(\boldsymbol{n})$ at different times.

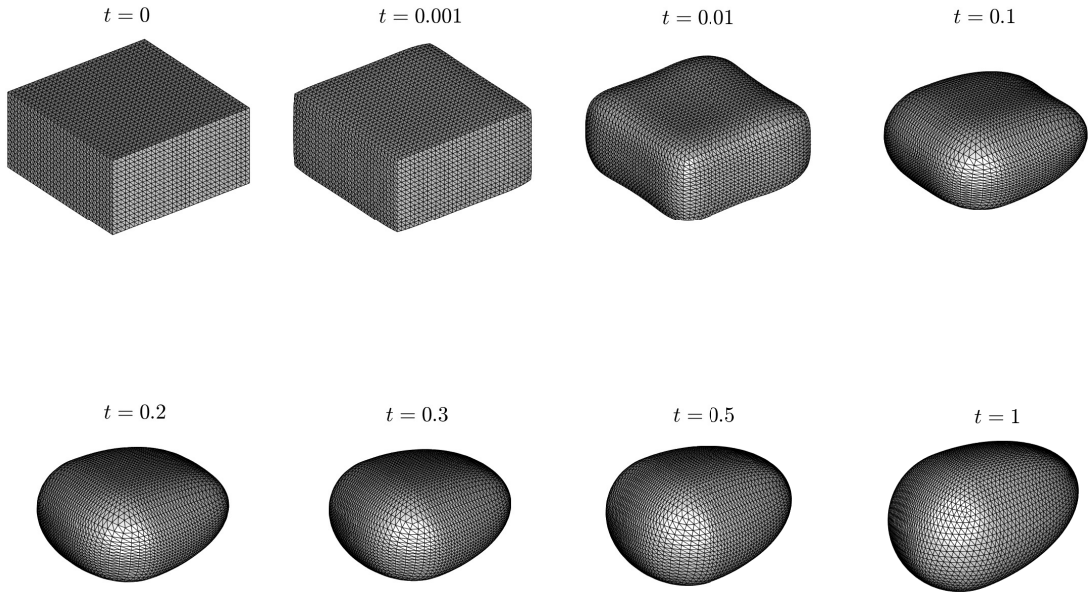

Figure 4.6: Evolution of a $2\times2\times1$ cuboid by anisotropic surface diffusion with a weak anisotropy $\gamma(\boldsymbol{n}) = \sqrt{(\frac{5}{2} + \frac{3}{2}\text{sign}(n_1))n_1^2 + n_2^2 + n_3^2}$ and $k(\boldsymbol{n}) = k_0(\boldsymbol{n})$ at different times.

Chapter 5

Extensions to other anisotropic geometric flows

This Chapter extends the unified SP-PFEM discussed in the previous Chapter to other anisotropic flows, including the anisotropic curvature flow and the anisotropic mass-conserved curvature flow. In fact, the energy stable condition on $\gamma(\boldsymbol{n})$ in (4.18), the definition of $\boldsymbol{G}_k(\boldsymbol{n})$ in (4.19), the alternative expression for μ in (4.21), and the definition of $k_0(\boldsymbol{n})$ in 2d (4.41) or in 3d (4.45) are independent of the anisotropic surface diffusion flow. Thus these definitions and the proof of energy stability can be directly applied to other anisotropic geometric flows after some minor modifications.

Unless otherwise specified, the notations used in this Chapter have the same meanings as those defined in Chapter 4.

5.1 For anisotropic curvature flow

5.1.1 Introduction

Curvature flow is a specific type of geometric flow, in which the normal velocity, V_n, of an interface, Γ, is dictated by the curvature, κ, such that $V_n = -\kappa$. It is another important model in the analysis of interface evolution within various multi-phase physical models [115]. Similar to surface diffusion, which is the H^{-1}-gradient

flow of surface energy, curvature flow also emerges in problems involving surface energy, and it can be interpreted as the L^2-gradient flow of the energy functional [139]. However, one key difference between curvature flow and surface diffusion is the conservation of mass. While surface diffusion preserves the total mass, mean curvature flow does not conserve mass, instead dissipating it at a specific rate. In addition to these two geometric properties, curvature flow possesses numerous other well-studied properties, including convexity preserving, and irregularities smoothing. We refer to [111] for a comprehensive overview.

The significance of the anisotropic surface energy for curvature flow is increasing across various scientific domains. This is particularly notable in the study of phase changes and phase separation within multiphase materials [1]. Such changes are integral to a multitude of physical phenomena and dictate the behavior of materials under different conditions. However, most studies on anisotropic curvature flow focus on the crystalline case [2, 44, 141]. By extending our unified SP-PFEM to anisotropic curvature flow, it can handle anisotropic mean curvature flow for a broader range of anisotropies. Therefore, we can model and analyze a more extensive physical phenomena, and contribute to the understanding of behavior in multiphase and crystalline materials.

5.1.2 The unified SP-PFEM

The normal velocity for the anisotropic curvature flow is $V_n = -\mu$. Similar to the anisotropic surface diffusion (1.21), for the anisotropic curvature flow, we have its geometric PDE formulation as

$$\begin{cases} \partial_t \boldsymbol{X} = -\mu \boldsymbol{n}, & \text{(5.1a)} \\ \mu = \nabla_\Gamma \cdot \boldsymbol{\xi}, \quad \xi(\boldsymbol{n}) = \nabla \gamma(\boldsymbol{p})|_{\boldsymbol{p}=\boldsymbol{n}}. & \text{(5.1b)} \end{cases}$$

By utilizing the surface energy matrix $\boldsymbol{G}_k(\boldsymbol{n})$ and the identity (4.21) in Theorem 4.1, we have the conservative weak formulation for the weighted mean curvature μ:

$$(\mu \boldsymbol{n}, \boldsymbol{\omega})_\Gamma = \langle \boldsymbol{G}_k(\boldsymbol{n}) \nabla_\Gamma \boldsymbol{X}, \nabla_\Gamma \boldsymbol{\omega} \rangle_\Gamma, \qquad \forall \boldsymbol{\omega} \in [H^1(\Gamma_0)]^d. \tag{5.2}$$

Suppose the initial curve $\boldsymbol{X}(\cdot,0)=(x(\cdot,0),y(\cdot,0))^T:=\Gamma_0\in[H^1(\Gamma_0)]^d$ and the initial weighted curvature $\mu(\cdot,0):=\mu_0(\cdot)\in H^1(\Gamma_0)$. Based on the conservative form (5.2), the variational formulation for anisotropic curvature flow is as follows: For any $t>0$, find the solution $(\boldsymbol{X}(\cdot,t),\mu(\cdot,t))\in[H^1(\Gamma_0)]^d\times H^1(\Gamma_0)$ satisfying

$$\Big(\boldsymbol{n}\cdot\partial_t\boldsymbol{X},\varphi\Big)_{\Gamma(t)}+\Big(\mu,\varphi\Big)_{\Gamma(t)}=0,\qquad\forall\varphi\in H^1(\Gamma_0),\tag{5.3a}$$

$$\Big(\mu\boldsymbol{n},\boldsymbol{\omega}\Big)_{\Gamma(t)}-\Big\langle\boldsymbol{G}_k(\boldsymbol{n})\nabla_\Gamma\boldsymbol{X},\nabla_\Gamma\boldsymbol{\omega}\Big\rangle_{\Gamma(t)}=0,\quad\forall\boldsymbol{\omega}\in[H^1(\Gamma_0)]^d.\tag{5.3b}$$

And the unified SP-PFEM for the anisotropic curvature flow (5.1) is as follows: Suppose the initial approximation $\Gamma^0(\cdot)\in[\mathbb{K}^h]^d$ is given by $\boldsymbol{X}^0(\rho_j)=\boldsymbol{X}_0(\rho_j),\forall j$, then for any $m=0,1,2,\ldots$, find the solution $(\boldsymbol{X}^m(\cdot),\mu^m(\cdot))\in[\mathbb{K}^h]^d\times\mathbb{K}^h$, such that

$$\Big(\boldsymbol{n}^{m+\frac12}\cdot\frac{\boldsymbol{X}^{m+1}-\boldsymbol{X}^m}{\tau},\varphi^h\Big)^h_{\Gamma^m}+\Big(\mu^{m+1},\varphi^h\Big)^h_{\Gamma^m}=0,\quad\forall\varphi^h\in\mathbb{K}^h,\tag{5.4a}$$

$$\Big(\mu^{m+1}\boldsymbol{n}^{m+\frac12},\boldsymbol{\omega}^h\Big)^h_{\Gamma^m}-\Big\langle\boldsymbol{G}_k(\boldsymbol{n}^m)\nabla_\Gamma\boldsymbol{X}^{m+1},\nabla_\Gamma\boldsymbol{\omega}^h\Big\rangle^h_{\Gamma^m}=0,\quad\forall\boldsymbol{\omega}^h\in[\mathbb{K}^h]^d.\tag{5.4b}$$

5.1.3 Main theorem

For the unified SP-PFEM (5.4), we have

Theorem 5.1 (structure-preserving)**.** *Suppose $\gamma(\boldsymbol{n})$ satisfies (4.18) and take a stabilizing function $k(\boldsymbol{n})\geq k_0(\boldsymbol{n})$, then the unified SP-PFEM (5.4) preserves mass decay rate and energy dissipation, i.e.,*

$$\frac{V^{m+1}-V^m}{\tau}=-\Big(\mu^{m+1},1\Big)^h_{\Gamma^m},\quad W^{m+1}\leq W^m\leq\ldots\leq W^0,\qquad\forall m\geq0.\tag{5.5}$$

Proof. From [13, Theorem 2.1], we know that

$$V^{m+1}-V^m=\Big(\boldsymbol{n}^{m+\frac12}\cdot(\boldsymbol{X}^{m+1}-\boldsymbol{X}^m),1\Big)^h_{\Gamma^m}.\tag{5.6}$$

Thus by taking $\varphi^h\equiv1\in\mathbb{K}^h$ in (5.4a), we know that

$$\frac{V^{m+1}-V^m}{\tau}=\Big(\boldsymbol{n}^{m+\frac12}\cdot\frac{\boldsymbol{X}^{m+1}-\boldsymbol{X}^m}{\tau},1\Big)^h_{\Gamma^m}=-\Big(\mu^{m+1},1\Big)^h_{\Gamma^m},\tag{5.7}$$

which is the desired decay rate in (5.5).

For energy dissipation, we have already known that the local energy estimates (4.49) is true. Taking $\varphi^h = \mu^{m+1}$ in (5.4a) and $\boldsymbol{\omega}^h = \boldsymbol{X}^{m+1} - \boldsymbol{X}^m$ in (5.4b), we know that

$$\begin{aligned} 0 &\geq -\tau\Big(\mu^{m+1}, \mu^{m+1}\Big)^h_{\Gamma^m} \\ &= \Big\langle \boldsymbol{G}_k(\boldsymbol{n}^m)\nabla_\Gamma \boldsymbol{X}^{m+1}, \nabla_\Gamma(\boldsymbol{X}^{m+1} - \boldsymbol{X}^m)\Big\rangle^h_{\Gamma^m} \geq W^{m+1} - W^m. \end{aligned}$$

Hence we complete the proof. □

5.1.4 Numerical results

We apply the proposed unified SP-PFEM to simulate the morphological evolution driven by the anisotropic curvature flow and anisotropic surface diffusion in 2D. Here we consider the following two anisotropic surface energies:

- Case I, the piecewisely Riemannian metric anisotropic surface energy (4.1) with $a = \frac{5}{2}$ and $b = \frac{3}{2}$,

$$\gamma(\boldsymbol{n}) = \sqrt{\left(\frac{5}{2} + \frac{3}{2}\mathrm{sgn}(n_1)\right) n_1^2 + n_2^2}, \qquad \forall \boldsymbol{n} \in \mathbb{S}^1. \tag{5.8}$$

- Case II, the 3-fold anisotropic surface energy (2.10) with $\theta_0 = 0$,

$$\gamma(\boldsymbol{n}) = 1 + \beta\cos(3\theta), \qquad \forall \boldsymbol{n} = (-\sin\theta, \cos\theta)^T \in \mathbb{S}^1. \tag{5.9}$$

Fig 5.1 and Fig 5.2 depict the anisotropic curvature flow and anisotropic surface diffusion at different times with anisotropy in case I and in case II with $\beta = 1/3$, respectively.

From Fig. 5.1-5.2, we can see that anisotropic curvature flow and anisotropic surface diffusion have the same equilibriums in shapes. While due to the different inertial geometric properties, they have different dynamics. The anisotropic curvature flow will first approach to the equilibrium shape, then shrink to a point; while the anisotropic surface diffusion approaches its equilibrium shape and remains stable.

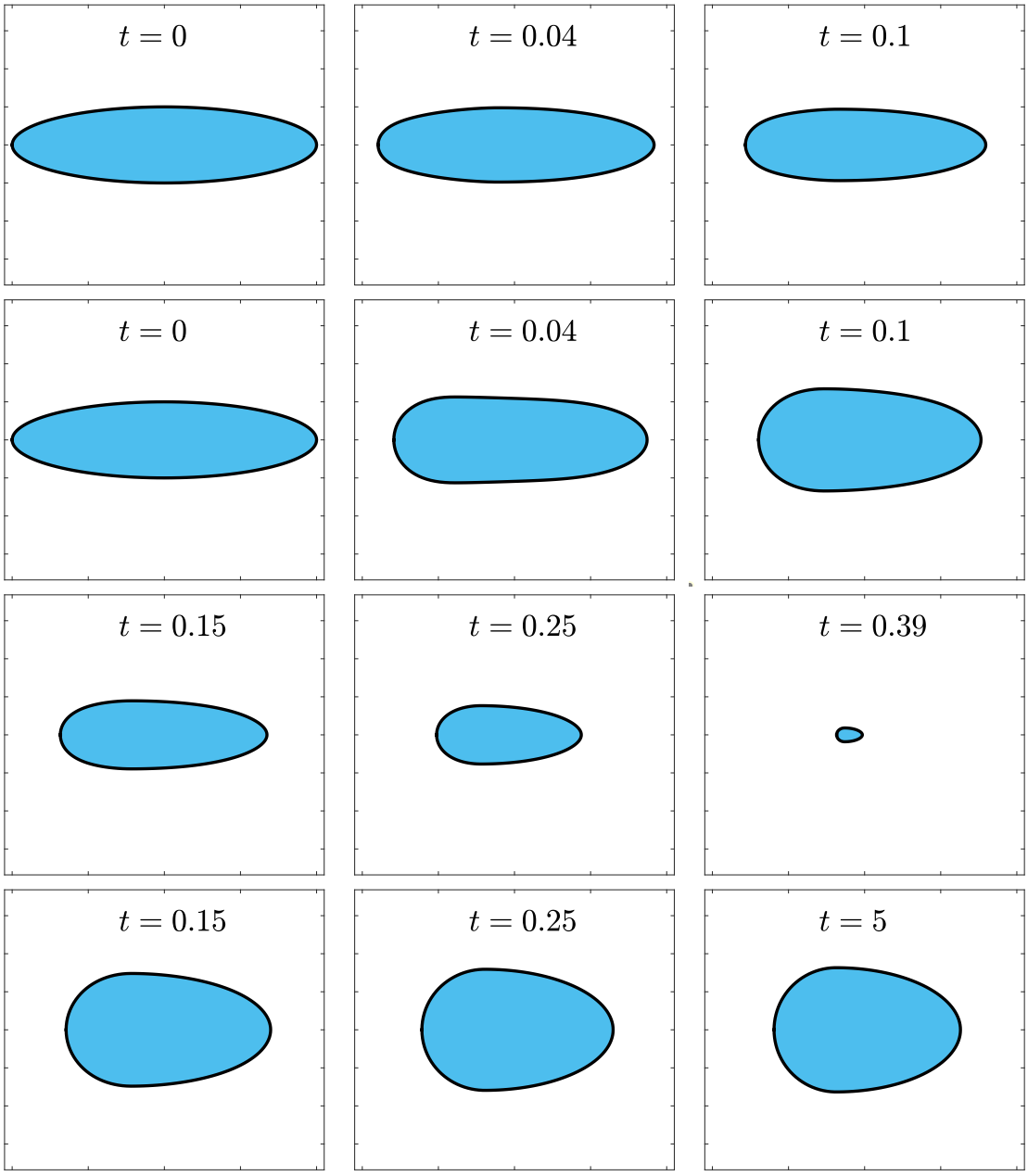

Figure 5.1: Morphological evolutions of a 4×1 ellipse under anisotropic curvature flow (first, third rows) and anisotropic surface diffusion (second, fourth rows) with the anisotropic surface energy in Case I at different times. The evolving curves and their enclosed regions are colored by blue and black. The mesh size and time step are taken as $h = 2^{-7}, \tau = 0.001$.

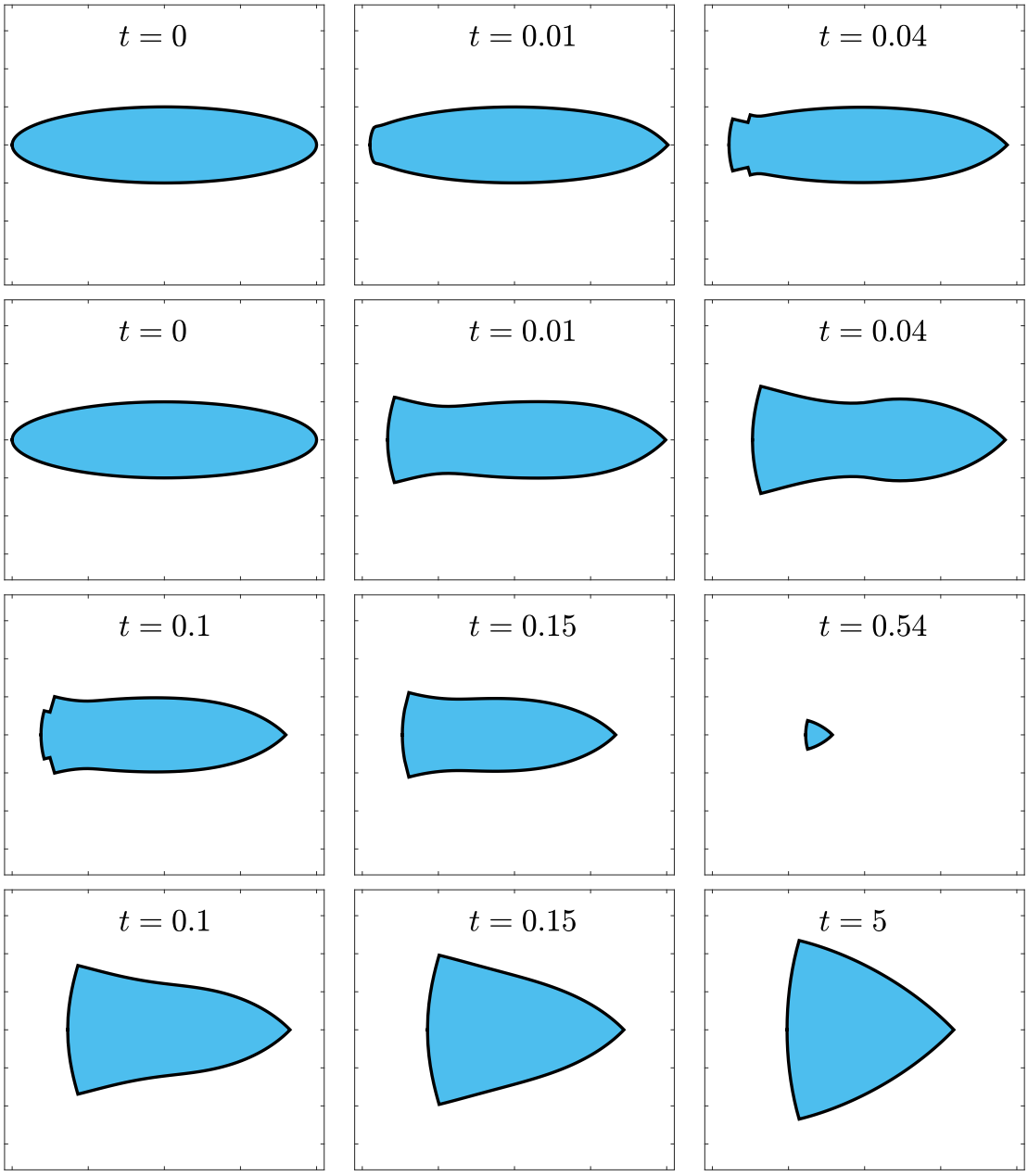

Figure 5.2: Morphological evolutions of a 4×1 ellipse under anisotropic curvature flow (first, third rows) and anisotropic surface diffusion (second, fourth rows) with the anisotropic surface energy in Case II with $\beta = 1/3$ at different times. The evolving curves and their enclosed regions are colored by blue and black. The mesh size and time step are taken as $h = 2^{-7}, \tau = 0.001$.

5.2 For anisotropic mass-conserved curvature flow

5.2.1 Introduction

A notable challenge in the anisotropic curvature flow lies in the mass dissipation that results in eventual contraction to a singular point. To balance the contraction, a force term $\lambda(t)$ depends on the evolving interface $\Gamma(t)$ in normal direction is introduced. More precisely, if $\lambda(t)$ satisfies the following equation

$$\lambda(t) = \frac{\int_{\Gamma(t)} \mu \, dA}{\int_{\Gamma(t)} 1 \, dA}, \tag{5.10}$$

the resulting regularized anisotropic curvature flow, i.e.,

$$\begin{cases} \partial_t \boldsymbol{X} = (-\mu + \lambda(t))\boldsymbol{n}, & \text{(5.11a)} \\ \mu = \nabla_\Gamma \cdot \boldsymbol{\xi}, \quad \xi(\boldsymbol{n}) = \nabla\gamma(\boldsymbol{p})|_{\boldsymbol{p}=\boldsymbol{n}}. & \text{(5.11b)} \end{cases}$$

will conserve its total mass. This alteration leads to a new variant of the anisotropic curvature flow, known as the anisotropic mass-conserved curvature flow, which preserves mass while maintaining the desired anisotropic properties.

5.2.2 The unified SP-PFEM

For the anisotropic mass-conserved curvature flow $V_n = -\mu + \lambda(t)$ with $\lambda(t) = \frac{\int_{\Gamma(t)} \mu \, dA}{\int_{\Gamma(t)} 1 \, dA}$, the geometric PDE is given as

$$\begin{cases} \boldsymbol{n} \cdot \partial_t \boldsymbol{X} = -\mu + \lambda(t), & \text{(5.12a)} \\ \mu = \nabla_\Gamma \cdot \boldsymbol{\xi}, \quad \xi(\boldsymbol{n}) = \nabla\gamma(\boldsymbol{p})|_{\boldsymbol{p}=\boldsymbol{n}}. & \text{(5.12b)} \end{cases}$$

and the variational formulation can be derived in a similar way.

In order to design a unified structure-preserving full discretization, we need to properly discretize $\lambda(t)$. Denote $\lambda^{m+\frac{1}{2}}$ with respect to Γ^m as

$$\lambda^{m+\frac{1}{2}} := \frac{(\mu^{m+1}, 1)^h_{\Gamma^m}}{(1, 1)^h_{\Gamma^m}}. \tag{5.13}$$

By adopting this $\lambda^{m+\frac{1}{2}}$, the unified SP-PFEM for the anisotropic mass-conserved curvature flow in (5.12) is as follows: Suppose the initial approximation $\Gamma^0(\cdot) \in [\mathbb{K}^h]^d$ is given by $\boldsymbol{X}^0(\rho_j) = \boldsymbol{X}_0(\rho_j), \forall j$; for any $m = 0, 1, 2, \ldots$, find the solution $(\boldsymbol{X}^m(\cdot), \mu^m(\cdot)) \in [\mathbb{K}^h]^d \times \mathbb{K}^h$, such that

$$\left(\boldsymbol{n}^m \cdot \frac{\boldsymbol{X}^{m+1} - \boldsymbol{X}^m}{\tau}, \varphi^h\right)_{\Gamma^m}^h + \left(\mu^{m+1} - \lambda^{m+\frac{1}{2}}, \varphi^h\right)_{\Gamma^m}^h = 0, \quad \forall \varphi^h \in \mathbb{K}^h, \tag{5.14a}$$

$$\left(\mu^{m+1}\boldsymbol{n}^m, \boldsymbol{\omega}^h\right)_{\Gamma^m}^h - \left\langle \boldsymbol{G}_k(\boldsymbol{n}^m)\nabla_\Gamma \boldsymbol{X}^{m+1}, \nabla_\Gamma \boldsymbol{\omega}^h\right\rangle_{\Gamma^m}^h = 0, \quad \forall \boldsymbol{\omega}^h \in [\mathbb{K}^h]^d. \tag{5.14b}$$

5.2.3 Main theorem

For the above unified SP-PFEM (5.14), we have

Theorem 5.2 (structure-preserving)**.** *Suppose $\gamma(\boldsymbol{n})$ satisfies (4.18) and take a finite stabilizing function $k(\boldsymbol{n}) \geq k_0(\boldsymbol{n})$, then the unified SP-PFEM (5.4) is structure-preserving, i.e.,*

$$V^{m+1} \equiv V^0, \quad W^{m+1} \leq W^m \leq \ldots \leq W^0, \qquad \forall m \geq 0. \tag{5.15}$$

Proof. For the mass conservation, taking $\varphi^h \equiv 1$ in (5.14a) yields that

$$\begin{aligned}
\left(\boldsymbol{n}^{m+\frac{1}{2}} \cdot (\boldsymbol{X}^{m+1} - \boldsymbol{X}^m), 1\right)_{\Gamma^m}^h &= -\tau\left(\mu^{m+1} - \lambda^{m+\frac{1}{2}}, 1\right)_{\Gamma^m}^h \\
&= -\tau\left(\mu^{m+1}, 1\right)_{\Gamma^m}^h + \tau\lambda^{m+\frac{1}{2}}\left(1, 1\right)_{\Gamma^m}^h \\
&= -\tau\left(\mu^{m+1}, 1\right)_{\Gamma^m}^h + \tau\frac{(\mu^{m+1}, 1)_{\Gamma^m}^h}{(1, 1)_{\Gamma^m}^h}\left(1, 1\right)_{\Gamma^m}^h \\
&= 0, \qquad m \geq 0.
\end{aligned}$$

By noting (5.5), we deduce that $V^{m+1} - V^m = 0$, which shows mass conservation.

For energy dissipation, by Cauchy-Schwarz inequality, we have

$$\begin{aligned}
\left(\lambda^{m+\frac{1}{2}}, \mu^{m+1}\right)_{\Gamma^m}^h &= \lambda^{m+\frac{1}{2}}\left(1, \mu^{m+1}\right)_{\Gamma^m}^h \\
&= \frac{1}{(1, 1)_{\Gamma^m}^h}\left(\left(1, \mu^{m+1}\right)_{\Gamma^m}^h\right)^2 \\
&\leq \frac{1}{(1, 1)_{\Gamma^m}^h}\left(1, 1\right)_{\Gamma^m}^h \left(\mu^{m+1}, \mu^{m+1}\right)_{\Gamma^m}^h \\
&= \left(\mu^{m+1}, \mu^{m+1}\right)_{\Gamma^m}^h, \qquad m \geq 0.
\end{aligned}$$

Taking $\varphi^h = \mu^{m+1}$ in (5.14a) and $\boldsymbol{\omega}^h = \boldsymbol{X}^{m+1} - \boldsymbol{X}^m$ in (5.14b), and adopting the local energy estimates (4.49) yields that

$$W^{m+1} - W^m \leq -\tau\Big(\mu^{m+1} - \lambda^{m+\frac{1}{2}}, \mu^{m+1}\Big)^h_{\Gamma^m} \leq 0, \qquad m \geq 0, \tag{5.16}$$

which implies the energy dissipation in (5.15). □

5.2.4 Numerical results

Here we adopt the unified SP-PFEM to simulate the morphological evolution driven by the anisotropic mass-conserved curvature flow and anisotropic surface diffusion in 2D. The anisotropic surface energies are the same as those in the previous section.

As shown in Fig. 5.3 (b)-(d), the edges emerge during the evolution and corners become sharper as the strength β increases. In contrast, there are no edges or corners in the morphological evolutions with anisotropy in Case I. This suggests that even if it is not a C^2-function, it is more like weak anisotropy!

From Fig. 5.4-5.5, we can see that the anisotropic surface diffusion and the anisotropic mass-conserved curvature flow have the same equilibriums in shapes, while they have different dynamics, i.e., the equilibriums are different in positions, and the anisotropic surface diffusion evolves faster than the anisotropic mass-conserved curvature flow.

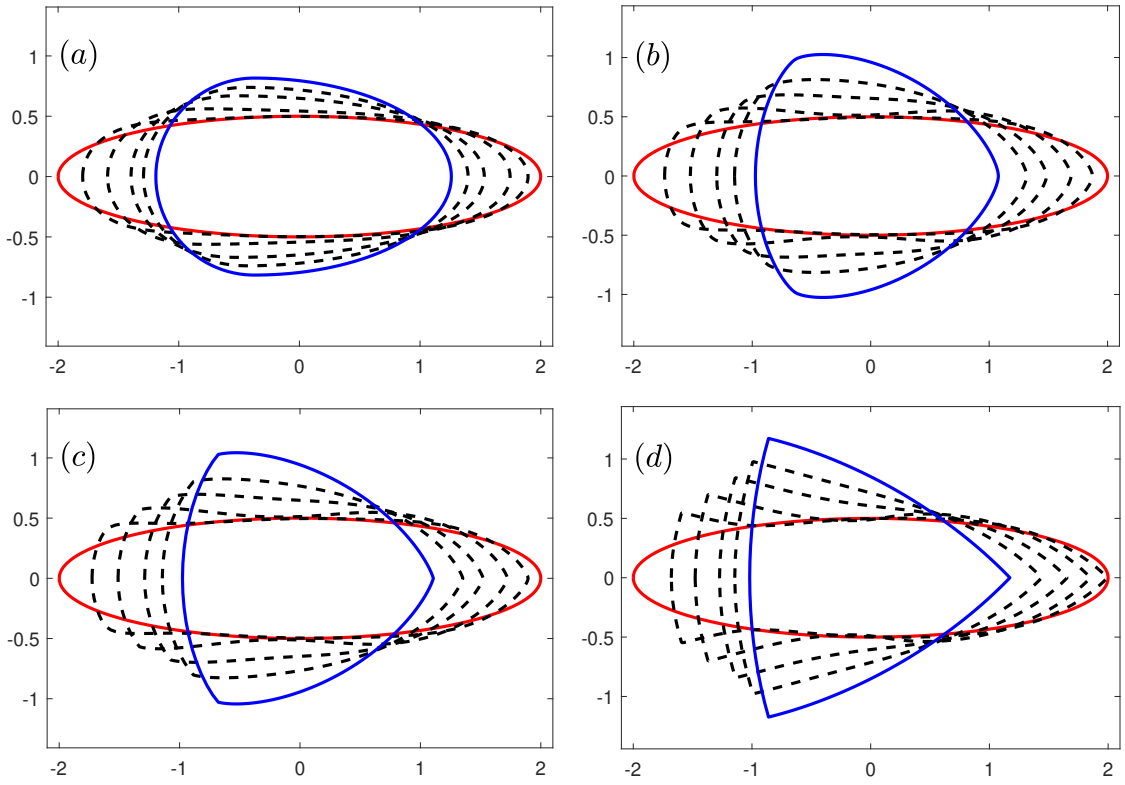

Figure 5.3: Morphological evolutions of a 4×1 ellipse under anisotropic mass-conserved curvature flow with four different anisotropic energies: (a) anisotropy in Case I; (b)-(d) anisotropies in case II with $\beta = 1/9, 1/7, 1/3$, respectively. The red and blue lines represent the initial curve and the numerical equilibrium, respectively; and the black dashed lines represent the intermediate curves. The mesh size and time step are taken as $h = 2^{-7}, \tau = h^2$.

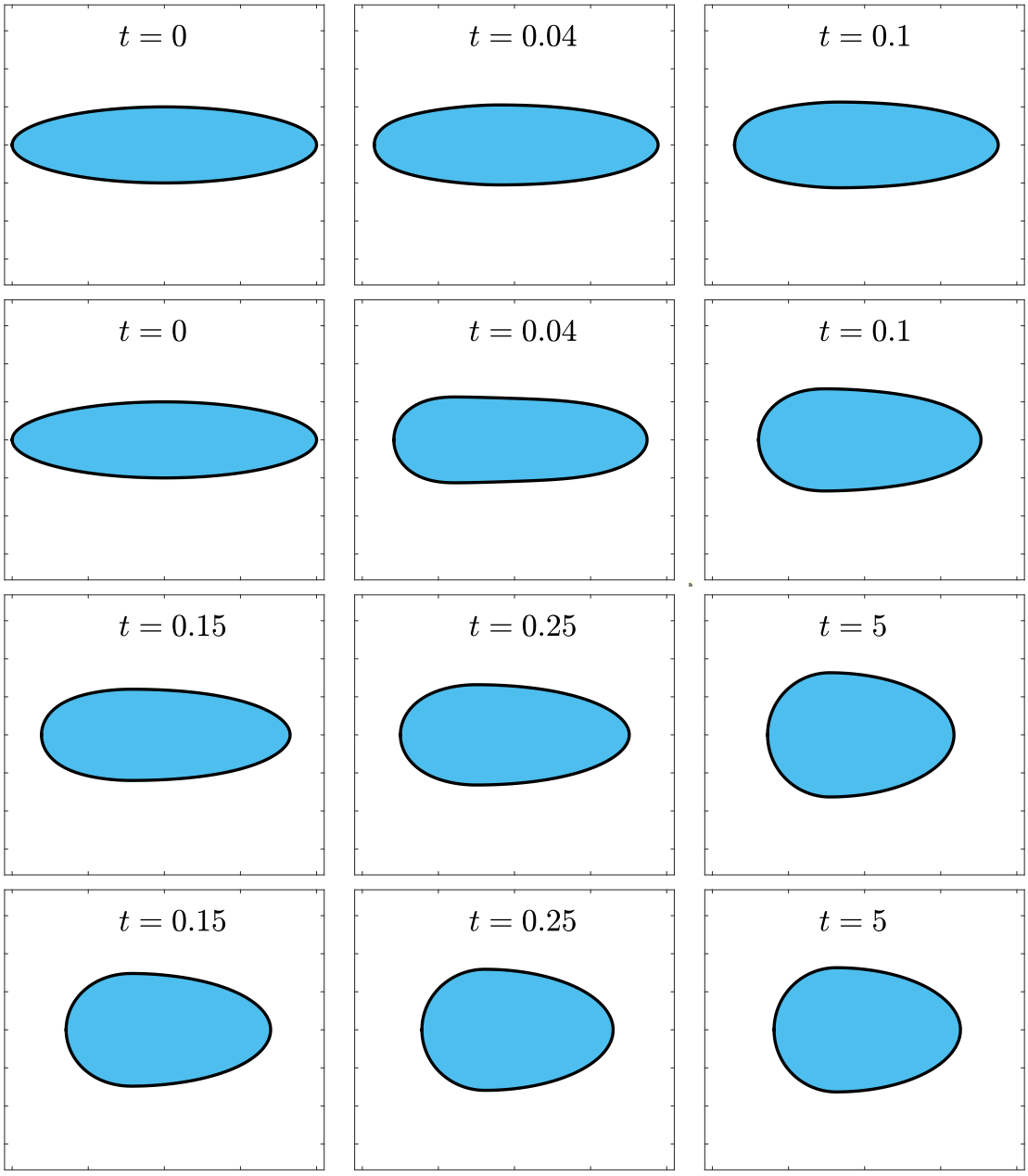

Figure 5.4: Morphological evolutions of a 4×1 ellipse under anisotropic mass-conserved curvature flow (first, third rows) and anisotropic surface diffusion (second, fourth rows) with the anisotropic surface energy in Case I at different times. The evolving curves and their enclosed regions are colored by blue and black. The mesh size and time step are taken as $h = 2^{-7}, \tau = 0.001$.

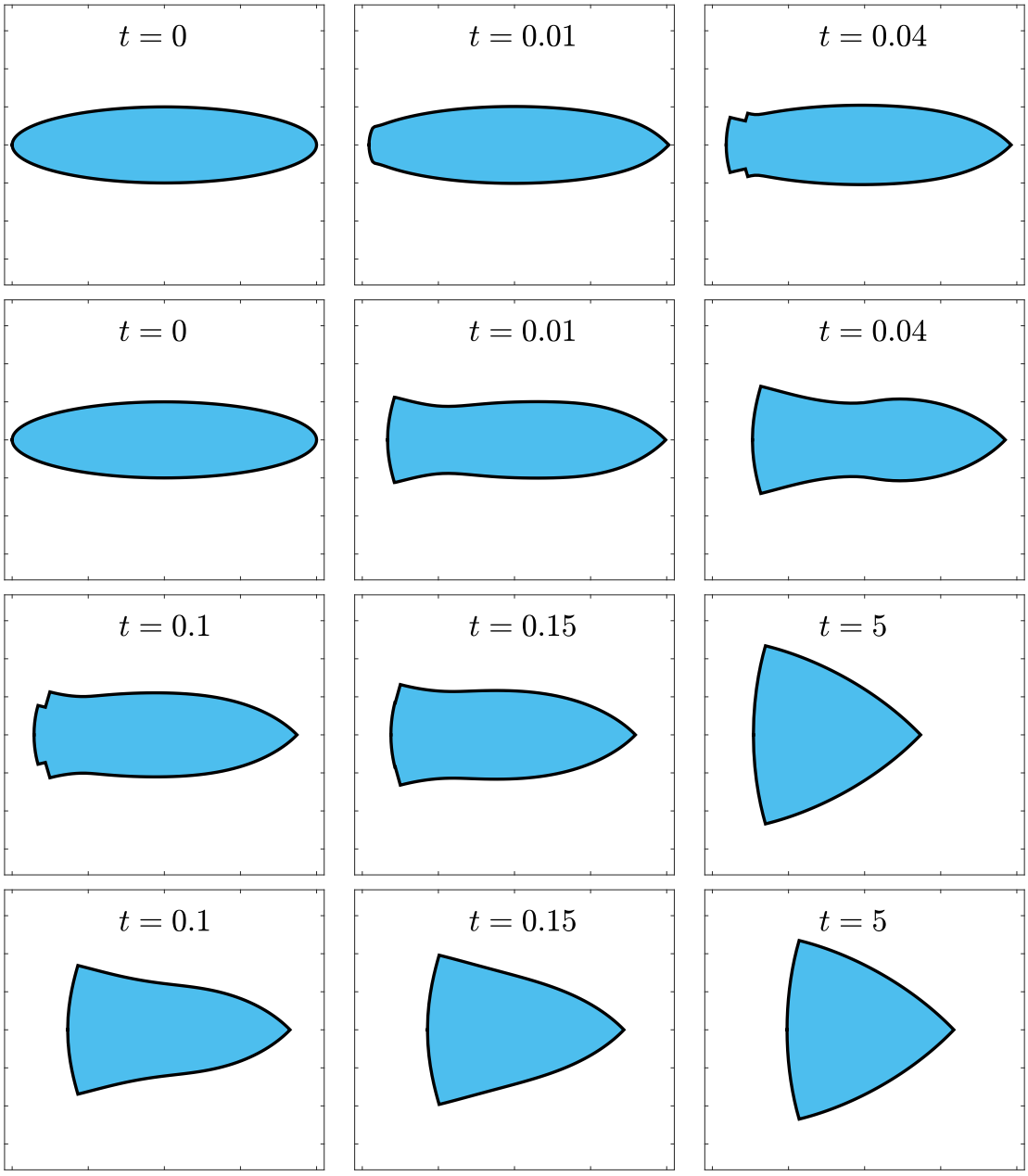

Figure 5.5: Morphological evolutions of a 4×1 ellipse under anisotropic mass-conserved curvature flow (first, third rows) and anisotropic surface diffusion (second, fourth rows) with the anisotropic surface energy in Case II with $\beta = 1/3$ at different times. The evolving curves and their enclosed regions are colored by blue and black. The mesh size and time step are taken as $h = 2^{-7}, \tau = 0.001$.

Chapter 6

Conclusion and Future Works

This thesis is focusing on the design of structure-preserving parametric finite element methods for anisotropic surface diffusion of 2d curves and 3d surfaces with arbitrary anisotropic surface energies. For the symmetric anisotropy $\gamma(-\boldsymbol{n}) = \gamma(\boldsymbol{n})$, based on the newly proposed symmetric surface energy matrix $\boldsymbol{Z}_k(\boldsymbol{n})$, we have proposed the novel symmetrized SP-PFEMs of curves and surfaces. For the general anisotropy, we introduced a unified SP-PFEM by adopting the surface energy matrix $\boldsymbol{G}_k(\boldsymbol{n})$. The energy stability condition on $\gamma(\boldsymbol{n})$ has been improved drastically to all the C^2 anisotropies with $\gamma(-\boldsymbol{n}) < (5-d)\gamma(\boldsymbol{n})$ for general $\gamma(\boldsymbol{n})$. This mild and simple condition makes our SP-PFEMs applicable for almost all the commonly-used anisotropic surface energies. Moreover, the framework developed in this thesis can also be extended to other geometric flows with the anisotropic effect.

In Chapter 2, for anisotropic surface diffusion in 2D with symmetric anisotropy, we proposed a symmetric positive definite surface energy matrix $\boldsymbol{Z}_k(\boldsymbol{n})$ and a stabilizing function $k(\boldsymbol{n})$. By utilizing $\boldsymbol{Z}_k(\boldsymbol{n})$, we reformulated the anisotropic surface diffusion equation into a novel symmetrized form and derived a new variational formulation. We discretized the variational problem in space by the PFEM. For temporal discretization, we proposed a fully implicit symmetrized SP-PFEM, which can rigorously preserve the total area up to machine precision. Then we rigorously proved that the proposed symmetrized SP-PFEM is unconditionally energy-stable

by showing the existence of the minimal stabilizing function $k_0(\boldsymbol{n})$. For several commonly-used symmetric anisotropies, we also gave the analytic formulation for the minimal stabilizing function $k_0(\boldsymbol{n})$. Furthermore, in Chapter 3, by introducing the surface gradient operator, we extended the symmetrized SP-PFEM to the evolution of a closed and orientable surface in 3D. We generalized the novel symmetric positive definite surface energy matrix $\boldsymbol{Z}_k(\boldsymbol{n})$ and thus derived a new symmetrized variational formulation for anisotropic surface diffusion in 3D with weakly or strongly anisotropic surface energy as well as the full discretization by symmetrized SP-PFEM. Compared to the 2D symmetrized SP-PFEM, we developed an essentially different approach to show that the 3D symmetrized SP-PFEM is unconditionally energy-stable for almost all anisotropic surface energies $\gamma(\boldsymbol{n})$ arising in practical applications.

In Chapter 4, for the arbitrary anisotropic surface energy $\gamma(\boldsymbol{n})$, we propose a unified SP-PFEM for anisotropic surface diffusion in both two and three dimensions ($d = 2, 3$). The proposed unified SP-PFEM is based on the unified surface energy matrix $\boldsymbol{G}_k(\boldsymbol{n})$, which is a sum of a symmetric positive definite matrix $\boldsymbol{G}_k^{(s)}(\boldsymbol{n})$ and an anti-symmetric matrix $\boldsymbol{G}^{(a)}(\boldsymbol{n})$, and the unified weak formulation of the chemical potential μ. The main challenge and contribution are establishing a unified framework to prove energy stability under the simple conditions $\gamma(\boldsymbol{p}) \in C^2(\mathbb{R}^d_*), \gamma(-\boldsymbol{n}) < (5-d)\gamma(\boldsymbol{n})$, which rely on the insight of the local energy estimates and the existence of $k_0(\boldsymbol{n})$.

Finally, in Chapter 5, we extended the unified SP-PFEM to other geometric flows with an anisotropic effect. We proposed SP-PFEMs for the evolution of a close curve under the anisotropic curvature flow and anisotropic mass-conserved curvature flow.

In each Chapter, we provided a large number of numerical simulations, and the numerical results indicate that the SP-PFEMs are second-order accurate in space, first-order in time, unconditionally energy-stable, and enjoy very good mesh quality during the evolution, and no mesh redistribution procedure is needed even for strongly anisotropic cases. Moreover, our SP-PFEMs work well for the piecewise

C^2 anisotropy, which is a significant achievement compared with other PFEMs.

A few notable future research prospects include the following:

- By selecting an appropriate $k(\boldsymbol{n})$, our 2D symmetrized SP-PFEM can reduce to the BGN's PFEM as described in [17] (see Remark 2.5). However, in 3D, our symmetrized SP-PFEM is essentially different from their PFEM. This suggests the possible existence of a more generalized PFEM that could serve as an extension of both.

- The minimal stabilizing function $k_0(\boldsymbol{n})$ is given explicitly only for a few symmetric anisotropies in 2D, and deriving its explicit formulation is quite complicated. For numerical implementation, it is desirable to find an estimate of the upper bound of $k_0(\boldsymbol{n})$.

- Since both the symmetrized SP-PFEM and the unified SP-PFEM are applicable to symmetric anisotropy, it is important to know which method is more accurate and efficient.

- The energy stability still requires the anisotropic surface energy $\gamma(\boldsymbol{p})$ to be piecewise $C^2(\mathbb{R}^d)$ and satisfy the condition $\gamma(-\boldsymbol{n}) < (5-d)\gamma(\boldsymbol{n})$. The regularity condition relies on the existence of $k_0(\boldsymbol{n})$, and the constant $5-d$ comes from the local error estimates, and the two conditions both can not be improved in our newly developed analysis framework. It is important but difficult to develop a "global" analysis framework that can relax the regularity condition to piecewise C^1 and improve the constant $5-d$.

- The convergence tests show that the convergence rate is rather robust. However, due to the tangential motion, the error analysis of the proposed PFEMs is still unknown.

- The global parameterization $\boldsymbol{X}$ assumes that there is a diffeomorphism between the initial interface Γ_0 and the interface $\Gamma(t)$ at time t, which makes our SP-PFEMs difficult to handle the topological change. We may explore

the concept of "surgery" from the mean curvature flow, or use the phase-field model to capture the topological change.

- It will be interesting to generalize the SP-PFEMs to other anisotropic geometric flows and free boundary problems.

Bibliography

[1] S. M. Allen and J. W. Cahn, *A microscopic theory for antiphase boundary motion and its application to antiphase domain coarsening*, Acta Metall., 27 (1979), pp. 1085–1095.

[2] F. Almgren and J. E. Taylor, *Flat flow is motion by crystalline curvature for curves with crystalline energies*, J. Differ. Geom., 42 (1995), pp. 1–22.

[3] S. Angenent, *Parabolic equations for curves on surfaces part i. curves with p-integrable curvature*, Ann. Math., (1990), pp. 451–483.

[4] S. Angenent and M. E. Gurtin, *Multiphase thermomechanics with interfacial structure 2. evolution of an isothermal interface*, Arch. Rational Mech. Anal., 108 (1989), pp. 323–391.

[5] E. Bänsch, P. Morin, and R. H. Nochetto, *Surface diffusion of graphs: variational formulation, error analysis, and simulation*, SIAM J. Numer. Anal., 42 (2004), pp. 773–799.

[6] W. Bao, H. Garcke, R. Nürnberg, and Q. Zhao, *Volume-preserving parametric finite element methods for axisymmetric geometric evolution equations*, J. Comput. Phys., 460 (2022), article 111180.

[7] ——, *A structure-preserving finite element approximation of surface diffusion for curve networks and surface clusters*, Numer. Methods Partial Differ. Equ., 39 (2023), pp. 759–794.

[8] W. Bao, W. Jiang, and Y. Li, *A symmetrized parametric finite element method for anisotropic surface diffusion of closed curves*, SIAM J. Numer. Anal., 61 (2023), pp. 617–641.

[9] W. Bao, W. Jiang, D. J. Srolovitz, and Y. Wang, *Stable equilibria of anisotropic particles on substrates: a generalized Winterbottom construction*, SIAM J. Appl. Math., 77 (2017), pp. 2093–2118.

[10] W. Bao, W. Jiang, Y. Wang, and Q. Zhao, *A parametric finite element method for solid-state dewetting problems with anisotropic surface energies*, J. Comput. Phys., 330 (2017), pp. 380–400.

[11] W. Bao and Y. Li, *A structure-preserving parametric finite element method for geometric flows with anisotropic surface energy*, arXiv preprint arXiv: 2211.00297, (2022).

[12] ——, *A symmetrized parametric finite element method for anisotropic surface diffusion ii. three dimensions*, SIAM J. Sci. Comput., 45 (2023), pp. A1438–A1461.

[13] W. Bao and Q. Zhao, *A structure-preserving parametric finite element method for surface diffusion*, SIAM J. Numer. Anal., 59 (2021), pp. 2775–2799.

[14] ——, *An energy-stable parametric finite element method for simulating solid-state dewetting problems in three dimensions*, J. Comput. Math., 41 (2023), pp. 771–796.

[15] J. W. Barrett, H. Garcke, and R. Nürnberg, *On the variational approximation of combined second and fourth order geometric evolution equations*, SIAM J. Sci. Comput., 29 (2007), pp. 1006–1041.

[16] ——, *A parametric finite element method for fourth order geometric evolution equations*, J. Comput. Phys., 222 (2007), pp. 441–467.

[17] ——, *Numerical approximation of anisotropic geometric evolution equations in the plane*, IMA J. Numer. Anal., 28 (2008), pp. 292–330.

[18] ——, *Parametric approximation of Willmore flow and related geometric evolution equations*, SIAM J. Sci. Comput., 31 (2008), pp. 225–253.

[19] ——, *A variational formulation of anisotropic geometric evolution equations in higher dimensions*, Numer. Math., 109 (2008), pp. 1–44.

[20] ——, *Finite-element approximation of coupled surface and grain boundary motion with applications to thermal grooving and sintering*, Eur. J. Appl. Math., 21 (2010), pp. 519–556.

[21] ——, *Numerical approximation of gradient flows for closed curves in* $\mathbb{R}^d$, IMA J. Numer. Anal., 30 (2010), pp. 4–60.

[22] ——, *On stable parametric finite element methods for the Stefan problem and the Mullins–Sekerka problem with applications to dendritic growth*, J. Comput. Phys., 229 (2010), pp. 6270–6299.

[23] ——, *The approximation of planar curve evolutions by stable fully implicit finite element schemes that equidistribute*, Numer. Methods Partial Differ. Equ., 27 (2011), pp. 1–30.

[24] ——, *Eliminating spurious velocities with a stable approximation of viscous incompressible two-phase Stokes flow*, Comput. Methods Appl. Mech. Eng., 267 (2013), pp. 511–530.

[25] ——, *Finite-element approximation of one-sided Stefan problems with anisotropic, approximately crystalline, Gibbs–Thomson law*, Adv. Differential Equations, 18 (2013), pp. 383 – 432.

[26] ——, *A stable parametric finite element discretization of two-phase Navier–Stokes flow*, J. Sci. Comput., 63 (2015), pp. 78–117.

[27] ——, *Computational parametric Willmore flow with spontaneous curvature and area difference elasticity effects*, SIAM J. Numer. Anal., 54 (2016), pp. 1732–1762.

[28] ——, *A stable numerical method for the dynamics of fluidic membranes*, Numer. Math., 134 (2016), pp. 783–822.

[29] ——, *Finite element approximation for the dynamics of fluidic two-phase biomembranes*, ESAIM: Math. Model. Numer., 51 (2017), pp. 2319–2366.

[30] ——, *Stable variational approximations of boundary value problems for willmore flow with gaussian curvature*, IMA J. Numer. Anal., 37 (2017), pp. 1657–1709.

[31] ——, *Gradient flow dynamics of two-phase biomembranes: sharp interface variational formulation and finite element approximation*, SMAI J. Comput. Math., 4 (2018), pp. 151–195.

[32] ——, *Finite element methods for fourth order axisymmetric geometric evolution equations*, J. Comput. Phys., 376 (2019), pp. 733–766.

[33] ——, *Parametric finite element approximations of curvature-driven interface evolutions*, in Handb. Numer. Anal., vol. 21, Elsevier, 2020, pp. 275–423.

[34] O. Bekhtereva, Y. L. Gavrilyuk, V. Lifshits, and B. Churusov, *Indium surface phase formation on Si (111) surface and their role in diffusion and desorption*, Poverkhnost'. Physika, Khimiia i Mekhanika, 8 (1988), article 54.

[35] G. Bellettini, M. Novaga, and M. Paolini, *Facet-breaking for three-dimensional crystals evolving by mean curvature*, Interfaces Free Bound., 1 (1999), pp. 39–55.

[36] G. Bellettini and M. Paolini, *Anisotropic motion by mean curvature in the context of Finsler geometry*, Hokkaido Math. J., 25 (1996), pp. 537–566.

[37] S. Boyd and L. Vandenberghe, *Convex Optimization*, Cambridge university press, 2004.

[38] J. E. Brothers and F. Morgan, *The isoperimetric theorem for general integrands.*, Mich. Math. J., 41 (1994), pp. 419–431.

[39] M. Burger, F. Hausser, C. Stöcker, and A. Voigt, *A level set approach to anisotropic flows with curvature regularization*, J. Comput. Phys., 225 (2007), pp. 183–205.

[40] J. Cahn, *Stability, microstructural evolution, grain growth, and coarsening in a two-dimensional two-phase microstructure*, Acta Metall. Mater., 39 (1991), pp. 2189–2199.

[41] J. Cahn and S. Allen, *A microscopic theory for domain wall motion and its experimental verification in Fe-Al alloy domain growth kinetics*, Journal de physique. Colloque, 38 (1977), pp. C7–51.

[42] J. Cahn and D. Hoffman, *A vector thermodlnamics for anisotropic surfaces—ii. curved and faceted surfaces*, Acta Mater., 22 (1974), pp. 1205–1214.

[43] J. W. Cahn and J. E. Taylor, *Overview no. 113 surface motion by surface diffusion*, Acta Metall. Mater., 42 (1994), pp. 1045–1063.

[44] W. C. Carter, A. Roosen, J. W. Cahn, and J. E. Taylor, *Shape evolution by surface diffusion and surface attachment limited kinetics on completely faceted surfaces*, Acta Metall. Mater., 43 (1995), pp. 4309–4323.

[45] L.-S. Chang, E. Rabkin, B. Straumal, B. Baretzky, and W. Gust, *Thermodynamic aspects of the grain boundary segregation in Cu (Bi) alloys*, Acta Materialia, 47 (1999), pp. 4041–4046.

[46] Y. G. Chen, Y. Giga, and S. Goto, *Uniqueness and existence of viscosity solutions of generalized mean curvature flow equations*, J. Differ. Geom., 33 (1991), pp. 749–786.

[47] U. Clarenz, U. Diewald, and M. Rumpf, *Anisotropic Geometric Diffusion in Surface Processing*, IEEE, 2000.

[48] U. Clarenz, F. Hausser, M. Rumpf, A. Voigt, and U. Weikard, *On level set formulations for anisotropic mean curvature flow and surface diffusion*, in Multiscale Modeling in Epitaxial Growth: Mini-Workshop at Mathematisches Forschungsinstitut Oberwolfach January 18–24, 2004, Springer, 2005, pp. 227–237.

[49] B. D. Coleman, R. S. Falk, and M. Moakher, *Stability of cylindrical bodies in the theory of surface diffusion*, Phys. D, 89 (1995), pp. 123–135.

[50] M. G. Crandall and P.-L. Lions, *Convergent difference schemes for nonlinear parabolic equations and mean curvature motion*, Numer. Math., 75 (1996), pp. 17–41.

[51] F. B. de Mongeot, W. Zhu, A. Molle, R. Buzio, C. Boragno, U. Valbusa, E. Wang, and Z. Zhang, *Nanocrystal formation and faceting instability in Al (110) homoepitaxy: True upward adatom diffusion at step edges and island corners*, Phys. Rev. Lett., 91 (2003), article 016102.

[52] K. Deckelnick and G. Dziuk, *A fully discrete numerical scheme for weighted mean curvature flow*, Numer. Math., 91 (2002), pp. 423–452.

[53] ——, *Error analysis for the elastic flow of parametrized curves*, Math. Comput., 78 (2009), pp. 645–671.

[54] K. Deckelnick, G. Dziuk, and C. M. Elliott, *Error analysis of a semidiscrete numerical scheme for diffusion in axially symmetric surfaces*, SIAM J. Numer. Anal., 41 (2003), pp. 2161–2179.

[55] ——, *Computation of geometric partial differential equations and mean curvature flow*, Acta Numer., 14 (2005), pp. 139–232.

[56] ——, *Fully discrete finite element approximation for anisotropic surface diffusion of graphs*, SIAM J. Numer. Anal., 43 (2005), pp. 1112–1138.

[57] K. Deckelnick and R. Nürnberg, *A novel finite element approximation of anisotropic curve shortening flow*, arXiv preprint arXiv: 2110.04605, (2021).

[58] M. P. do Carmo, *Differential geometry of curves and surfaces*, Englewood Cliffs, New Jersey, (1976).

[59] I. C. Dolcetta, S. F. Vita, and R. March, *Area-preserving curve-shortening flows: from phase separation to image processing*, Interfaces Free Bound., 4 (2002), pp. 325–343.

[60] P. Du, M. Khenner, and H. Wong, *A tangent-plane marker-particle method for the computation of three-dimensional solid surfaces evolving by surface diffusion on a substrate*, J. Comput. Phys., 229 (2010), pp. 813–827.

[61] G. Dziuk, *An algorithm for evolutionary surfaces*, Numer. Math., 58 (1990), pp. 603–611.

[62] G. Dziuk, *Numerical schemes for the mean curvature flow of graphs*, Solid Mech. Appl., 66 (1999), pp. 63–70.

[63] G. Dziuk, *Computational parametric Willmore flow*, Numer. Math., 111 (2008), pp. 55–80.

[64] M. Dziwnik, A. Münch, and B. Wagner, *A phase-field model for solid-state dewetting and its sharp-interface limit*, tech. rep., Berlin: Weierstraß-Institut für Angewandte Analysis und Stochastik, 2014.

[65] J. J. Eggleston, G. B. McFadden, and P. W. Voorhees, *A phase-field model for highly anisotropic interfacial energy*, Phys. D, 150 (2001), pp. 91–103.

[66] C. M. Elliott and H. Garcke, *Existence results for diffusive surface motion laws*, vol. 7, 1994.

[67] J. Escher, U. F. Mayer, and G. Simonett, *The surface diffusion flow for immersed hypersurfaces*, SIAM J. Math. Anal., 29 (1998), pp. 1419–1433.

[68] I. Fonseca, A. Pratelli, and B. Zwicknagl, *Shapes of epitaxially grown quantum dots*, Arch. Rational Mech. Anal., 214 (2014), pp. 359–401.

[69] F. Frank, *Metal surfaces*, ASM, Cleveland, OH, (1963).

[70] S. Gallot, D. Hulin, and J. Lafontaine, *Riemannian Geometry*, vol. 2, Springer, 1990.

[71] H. Garcke, R. Nürnberg, and J. W. Barrett, *Parametric approximation of surface clusters driven by isotropic and anisotropic surface energies*, Interfaces Free Bound., 12 (2010), pp. 187–234.

[72] J. W. Gibbs, *The Collected Works of J. Willard Gibbs.*, 1948.

[73] M.-H. Giga and Y. Giga, *Crystalline surface diffusion flow for graph-like curves*, Hokkaido Math. J., 1142 (2022), pp. 1–35.

[74] Y. Giga, *Surface evolution equations: a level set method*, J. Fac. Sci., Hokkaido Univ., Ser., 71 (2002), article 1.

[75] ——, *Surface Evolution Equations*, Springer, 2006.

[76] Y. Giga and K. Ito, *On pinching of curves moved by surface diffusion*, J. Fac. Sci., Hokkaido Univ., Ser., 379 (1997), pp. 1–12.

[77] D. Gilbarg, N. S. Trudinger, D. Gilbarg, and N. Trudinger, *Elliptic Partial Differential Equations of Second Order*, vol. 224, Springer, 1977.

[78] P. M. Girão and R. V. Kohn, *The crystalline algorithm for computing motion by curvature*, in Variational Methods for Discontinuous Structures: Applications to image segmentation, continuum mechanics, homogenization Villa Olmo, Como, 8–10 September 1994, Springer, 1996, pp. 7–18.

[79] F. Golightly, F. Stott, and G. Wood, *The relationship between oxide grain morphology and growth mechanisms for Fe-Cr-Al and Fe-Cr-Al-Y alloys*, J. Electrochem. Soc., 126 (1979), article 6.

[80] A. Golovin, S. Davis, and A. Nepomnyashchy, *Model for faceting in a kinetically controlled crystal growth*, Phys. Rev. E, 59 (1999), p. 803.

[81] A. Golovin, S. H. Davis, and P. W. Voorhees, *Self-organization of quantum dots in epitaxially strained solid films*, Phys. Rev. E, 68 (2003), article 056203.

[82] A. Golovin, M. Levine, T. Savina, and S. Davis, *Faceting instability in the presence of wetting interactions: A mechanism for the formation of quantum dots*, Phys. Rev. B, 70 (2004), p. 235342.

[83] K. F. Gurski and G. B. McFadden, *The effect of anisotropic surface energy on the Rayleigh instability*, Proceedings of the Royal Society of London. Series A: Mathematical, Physical and Engineering Sciences, 459 (2003), pp. 2575–2598.

[84] M. E. Gurtin, *Thermomechanics of Evolving Phase Boundaries in the Plane*, Clarendon Press, 1993.

[85] M. E. Gurtin and M. E. Jabbour, *Interface evolution in three dimensions with curvature-dependent energy and surface diffusion: Interface-controlled evolution, phase transitions, epitaxial growth of elastic films*, Arch. Rational Mech. Anal., 163 (2002), pp. 171–208.

[86] Y. Han, B. Unal, F. Qin, D. Jing, C. J. Jenks, D.-J. Liu, P. Thiel, and J. Evans, *Kinetics of facile bilayer island formation at low temperature: Ag/NiAl (110)*, Phys. Rev. Lett., 100 (2008), article 116105.

[87] F. Hausser and A. Voigt, *A discrete scheme for parametric anisotropic surface diffusion*, J. Sci. Comput., 30 (2007), pp. 223–235.

[88] C. Herring, *Some theorems on the free energies of crystal surfaces*, Phys. Rev., 82 (1951), p. 87.

[89] D. W. Hoffman and J. W. Cahn, *A vector thermodynamics for anisotropic surfaces: I. fundamentals and application to plane surface junctions*, Surf. Sci., 31 (1972), pp. 368–388.

[90] W. Huang, W. Jiang, and Y. Wang, *A θ-L approach for solving solid-state dewetting problems*, J. Comput. Math., 40 (2022), p. 275.

[91] W. Huang, W. Jiang, and Q. Zhao, *A θ-L formulation-based finite element method for solving axisymmetric solid-state dewetting problems*, East Asian J. Appl. Math., 11 (2021), pp. 389–405.

[92] C. Jahan, O. Faynot, L. Tosti, and J.-M. Hartmann, *Agglomeration control during the selective epitaxial growth of Si raised sources and drains on ultra-thin silicon-on-insulator substrates*, J. Cryst. Growth, 280 (2005), pp. 530–538.

[93] W. Jiang, W. Bao, C. V. Thompson, and D. J. Srolovitz, *Phase field approach for simulating solid-state dewetting problems*, Acta Mater., 60 (2012), pp. 5578–5592.

[94] W. Jiang and B. Li, *A perimeter-decreasing and area-conserving algorithm for surface diffusion flow of curves*, J. Comput. Phys., 443 (2021), article 110531.

[95] W. Jiang, Y. Wang, D. J. Srolovitz, and W. Bao, *Solid-state dewetting on curved substrates*, Phys. Rev. Mater., 2 (2018), article 113401.

[96] W. Jiang, Y. Wang, Q. Zhao, D. J. Srolovitz, and W. Bao, *Solid-state dewetting and island morphologies in strongly anisotropic materials*, Scr. Mater., 115 (2016), pp. 123–127.

[97] W. Jiang and Q. Zhao, *Sharp-interface approach for simulating solid-state dewetting in two dimensions: A Cahn–Hoffman ξ-vector formulation*, Phys. D, 390 (2019), pp. 69–83.

[98] W. Jiang, Q. Zhao, and W. Bao, *Sharp-interface model for simulating solid-state dewetting in three dimensions*, SIAM J. Appl. Math., 80 (2020), pp. 1654–1677.

[99] E. Jiran and C. Thompson, *Capillary instabilities in thin films*, J. Electron. Mater., 19 (1990), pp. 1153–1160.

[100] ——, *Capillary instabilities in thin, continuous films*, Thin Solid Films, 208 (1992), pp. 23–28.

[101] D. A. Kessler and H. Levine, *Growth velocity of three-dimensional dendritic crystals*, Phys. Rev. A, 36 (1987), pp. 4123–4126.

[102] ——, *Pattern selection in three dimensional dendritic growth*, Acta Mater., 36 (1988), pp. 2693–2706.

[103] L. Klinger, D. Amram, and E. Rabkin, *Kinetics of a retracting solid film edge: The case of high surface anisotropy*, Scr. Mater., 64 (2011), pp. 962–965.

[104] E. M. Kolahdouz and D. Salac, *A semi-implicit gradient augmented level set method*, SIAM J. Sci. Comput., 35 (2013), pp. A231–A254.

[105] B. Kovács, B. Li, and C. Lubich, *A convergent algorithm for forced mean curvature flow driven by diffusion on the surface*, Interfaces Free Bound., 22 (2020), pp. 443–464.

[106] ——, *A convergent evolving finite element algorithm for Willmore flow of closed surfaces*, Numer. Math., 149 (2021), pp. 595–643.

[107] W. Kühnel, *Differential Geometry: Curves-Surfaces-Manifolds*, vol. 16, American Mathematical Society Providence, 2005.

[108] F. Leroy, F. Cheynis, T. Passanante, and P. Müller, *Influence of facets on solid state dewetting mechanisms: Comparison between Ge and Si on SiO2*, Phys. Rev. B, 88 (2013), article 035306.

[109] Y. Li and W. Bao, *An energy-stable parametric finite element method for anisotropic surface diffusion*, J. Comput. Phys., 446 (2021), article 110658.

[110] Z. Li, H. Zhao, and H. Gao, *A numerical study of electro-migration voiding by evolving level set functions on a fixed cartesian grid*, J. Comput. Phys., 152 (1999), pp. 281–304.

[111] C. Mantegazza, *Lecture Notes on Mean Curvature Flow*, vol. 290, Springer Science & Business Media, 2011.

[112] U. F. Mayer and G. Simonett, *Self-intersections for the surface diffusion and the volume-preserving mean curvature flow*, Differ. Integral Equ., 13 (2000), pp. 1189 – 1199.

[113] G. McFadden, S. Coriell, and R. Sekerka, *Effect of surface tension anisotropy on cellular morphologies*, J. Cryst. Growth, 91 (1988), pp. 180–198.

[114] M. Meyyappan, *Catalyzed chemical vapor deposition of one-dimensional nanostructures and their applications*, Prog. Cryst., 55 (2009), pp. 1–21.

[115] W. W. Mullins, *Two-dimensional motion of idealized grain boundaries*, Journal of Applied Physics, 27 (1956), pp. 900–904.

[116] ——, *Theory of thermal grooving*, J. Appl. Phys., 28 (1957), pp. 333–339.

[117] ——, *Proof that the two-dimensional shape of minimum surface free energy is convex*, J. Math. Phys., 3 (1962), pp. 754–759.

[118] F. Nichols, *Surface-(interface-) and volume-diffusion contributions to morphological changes driven by capillarity*, Trans. Aime, 233 (1965), pp. 1840–1848.

[119] W. J. Niessen, B. M. T. H. Romeny, L. M. Florack, and M. A. Viergever, *A general framework for geometry-driven evolution equations*, Int. J. Comput. Vis., 21 (1997), pp. 187–205.

[120] R. Nuryadi, Y. Ishikawa, and M. Tabe, *Formation and ordering of self-assembled Si islands by ultrahigh vacuum annealing of ultrathin bonded silicon-on-insulator structure*, Appl. Surf. Sci., 159 (2000), pp. 121–126.

[121] S. Osher and R. P. Fedkiw, *Level set methods: an overview and some recent results*, J. Comput. Phys., 169 (2001), pp. 463–502.

[122] K. Oura, V. Lifshits, A. Saranin, A. Zotov, and M. Katayama, *Surface Science: an Introduction*, Springer Science & Business Media, 2013.

[123] M. Plateau, *Xxvii. on the recent theories of the constitution of jets of liquid issuing from circular orifices*, Lond. Edinb. Dublin philos. Mag. J. Sci., 12 (1856), pp. 286–297.

[124] T. V. Savina, A. A. Golovin, S. H. Davis, A. A. Nepomnyashchy, and P. W. Voorhees, *Faceting of a growing crystal surface by surface diffusion*, Phys. Rev. E, 67 (2003), article 021606.

[125] R. I. Saye and J. A. Sethian, *A review of level set methods to model interfaces moving under complex physics: recent challenges and advances*, Handb. Numer. Anal., 21 (2020), pp. 509–554.

[126] L. A. Segel, *The non-linear interaction of a finite number of disturbances to a layer of fluid heated from below*, J. Fluid Mech., 21 (1965), pp. 359–384.

[127] R. F. Sekerka, *Thermal Physics: Thermodynamics and Statistical Mechanics for Scientists and Engineers*, Elsevier, 2015.

[128] J. A. Sethian and D. Chopp, *Motion by intrinsic laplacian of curvature*, Interfaces Free Bound., 1 (1999), pp. 107–123.

[129] H. Shen, S. Nutt, and D. Hull, *Direct observation and measurement of fiber architecture in short fiber-polymer composite foam through micro-CT imaging*, Compos. Sci. Technol., 64 (2004), pp. 2113–2120.

[130] E. Shustorovich, *Metal-Surface Reaction Energetics. Theory and Applications to Heterogeneous Catalysis, Chemisorption, and Surface Diffusion*, VCH Weinheim, New York, 1991.

[131] M. Siegel, M. Miksis, and P. Voorhees, *Evolution of material voids for highly anisotropic surface energy*, J. Mech. Phys. Solids., 52 (2004), pp. 1319–1353.

[132] P. Simulation, *Cfdtool - matlab cfd simulation gui & toolbox, github.* https://github.com/precise-simulation/cfdtool/releases/tag/1.9.2, 2022.

[133] P. Smereka, *Semi-implicit level set methods for curvature and surface diffusion motion*, J. Sci. Comp., 19 (2003), pp. 439–456.

[134] H. M. Soner, *Motion of a set by the curvature of its boundary*, J. Differ. Equ., 101 (1993), pp. 313–372.

[135] D. Srolovitz and S. Safran, *Capillary instabilities in thin films. ii. kinetics*, J. Appl. Phys., 60 (1986), pp. 255–260.

[136] D. J. Srolovitz, *On the stability of surfaces of stressed solids*, Acta Mater., 37 (1989), pp. 621–625.

[137] A. P. Sutton and R. W. Balluffi, *Interfaces in Crystalline Materials*, Clarendon Press, 1995.

[138] J. Taylor, *Existence and structure of solutions to a class of nonelliptic variational problems*, in Symposia Mathematica, vol. 14, 1974, pp. 499–508.

[139] J. E. Taylor, *Mean curvature and weighted mean curvature*, Acta Metall. Mater., 40 (1992), pp. 1475–1485.

[140] J. E. Taylor and J. W. Cahn, *Linking anisotropic sharp and diffuse surface motion laws via gradient flows*, J. Stat. Phys., 77 (1994), pp. 183–197.

[141] J. E. Taylor, J. W. Cahn, and C. A. Handwerker, *Overview no. 98 i—geometric models of crystal growth*, Acta Metall. Mater., 40 (1992), pp. 1443–1474.

[142] C. V. Thompson, *Solid-state dewetting of thin films*, Annu. Rev. Mater. Res., 42 (2012), pp. 399–434.

[143] K.-N. Tu, *Interdiffusion in thin films*, Annu. Rev. Mater. Sci., 15 (1985), pp. 147–176.

[144] P. Voorhees, S. Coriell, G. McFadden, and R. Sekerka, *The effect of anisotropic crystal-melt surface tension on grain boundary groove morphology*, J. Cryst. Growth, 67 (1984), pp. 425–440.

[145] Y. Wang, W. Jiang, W. Bao, and D. J. Srolovitz, *Sharp interface model for solid-state dewetting problems with weakly anisotropic surface energies*, Phys. Rev. B, 91 (2015), article 045303.

[146] S. Wise, J. Kim, and J. Lowengrub, *Solving the regularized, strongly anisotropic Cahn–Hilliard equation by an adaptive nonlinear multigrid method*, J. Comput. Phys., 226 (2007), pp. 414–446.

[147] H. Wong, P. Voorhees, M. Miksis, and S. Davis, *Periodic mass shedding of a retracting solid film step*, Acta Mater., 48 (2000), pp. 1719–1728.

[148] G. Wulff, *Zur frage der geschwindigkeit des wachstums und der auflösung der krystallflächen*, Z. Kristallogr, 34 (1901), pp. 449–530.

[149] Y. Xu and C.-W. Shu, *Local discontinuous Galerkin method for surface diffusion and Willmore flow of graphs*, J. Sci. Comput., 40 (2009), pp. 375–390.

[150] J. Ye and C. V. Thompson, *Mechanisms of complex morphological evolution during solid-state dewetting of single-crystal nickel thin films*, Appl. Phys. Lett., 97 (2010), article 071904.

[151] ——, *Anisotropic edge retraction and hole growth during solid-state dewetting of single crystal nickel thin films*, Acta Mater., 59 (2011), pp. 582–589.

[152] ——, *Templated solid-state dewetting to controllably produce complex patterns*, Adv. Mater., 23 (2011), pp. 1567–1571.

[153] Q. Zhao, *A sharp-interface model and its numerical approximation for solid-state dewetting with axisymmetric geometry*, J. Comput. Appl. Math., 361 (2019), pp. 144–156.

[154] Q. Zhao, W. Jiang, and W. Bao, *A parametric finite element method for solid-state dewetting problems in three dimensions*, SIAM J. Sci. Comput., 42 (2020), pp. B327–B352.

[155] ——, *An energy-stable parametric finite element method for simulating solid-state dewetting*, IMA J. Num. Anal., 41 (2021), pp. 2026–2055.

List of Publications

[1] *An energy-stable parametric finite element method for anisotropic surface diffusion* (with W. Bao), J. Comput. Phys., Vol. 446 (2021), article 110658.

[2] *A symmetrized parametric finite element method for anisotropic surface diffusion of closed curves* (with W. Bao and W. Jiang), SIAM J. Numer. Anal., Vol. 61 (2023), pp. 617–641.

[3] *A structure-preserving parametric finite element method for area-conserved generalized curvature flow* (with L. Pei), J. Sci. Comput., Vol. 96 (2023), article 6.

[4] *A symmetrized parametric finite element method for anisotropic surface diffusion in 3D* (with W. Bao), SIAM J. Sci. Comput., Vol. 45 (2023), pp. A1438–A1461.

[5] *A symmetrized parametric finite element method for simulating solid-state dewetting problems* (with M. Li and L. Pei), Appl. Math. Model., Vol. 121 (2023), pp. 731–750.

[6] *A structure-preserving parametric finite element method for geometric flows with anisotropic surface energy* (with W. Bao), preprint (arXiv: 2211.00297).

[7] *A unified structure-preserving parametric finite element method for anisotropic surface diffusion* (with W. Bao), in preparation.

A STRUCTURE-PRESERVING PARAMETRIC FINITE ELEMENT METHOD FOR ANISOTROPIC SURFACE DIFFUSION

LI YIFEI

NATIONAL UNIVERSITY OF SINGAPORE

2023

A Structure-Preserving Parametric Finite Element Method for Anisotropic Surface Diffusion Li Yifei 2023